INEEL/EXT-04-02564

Fluidized Bed Steam Reforming of INEEL SBW Using THOR^{sm} Mineralizing Technology

Arlin L. Olson
Nicholas R. Soelberg
Douglas W. Marshall
Gary L. Anderson

December 2004

Idaho National Engineering and Environmental Laboratory
Bechtel BWXT Idaho, LLC

INEEL/EXT-04-02564

Fluidized Bed Steam Reforming of INEEL SBW Using THOR^{sm} Mineralizing Technology

Arlin L. Olson
Nicholas R. Soelberg
Douglas W. Marshall
Gary L. Anderson

December 2004

Idaho National Engineering and Environmental Laboratory
Environmental R&D Laboratory
Idaho Falls, Idaho 83415

Prepared for the
U.S. Department of Energy
Assistant Secretary for Environmental Management
Under DOE Idaho Operations Office
Contract DE-AC07-99ID13727

ABSTRACT

Sodium-bearing waste (SBW) disposition is one of the U.S. Department of Energy (DOE) Idaho Operation Office's (NE-ID) and State of Idaho's top priorities at the Idaho National Engineering and Environmental Laboratory (INEEL). Many studies have resulted in the identification of five treatment alternatives that form a short list of perhaps the most appropriate technologies from which the DOE may select. The alternatives are (a) calcination with maximum achievable control technology (MACT) upgrade, (b) steam reforming, (c) cesium ion exchange (CsIX) with immobilization, (d) direct evaporation, and (e) vitrification. Each alternative has undergone some degree of applied technical development and preliminary process design over the past four years.

DOE desired further experimental data, with regard to steam reforming technology, to make informed decisions concerning selection of treatment technology for SBW. Mineralizing steam reforming technology, offered by THOR Treatment Technologies, LLC would produce a denitrated, granular mineral waste form using a high-temperature fluidized bed process. A pilot scale demonstration of the technology was performed in a 15-cm-diameter reactor vessel September 27 through October 1, 2004. The pilot scale equipment is owned by the DOE, and located at the Science and Technology Applications Research (STAR) Center in Idaho Falls, ID. Flowsheet chemistry and operational parameters were defined through a collaborative effort involving Idaho National Engineering and Environmental Laboratory, Savannah River National Laboratory (SRNL), and THOR Treatment Technologies personnel. Personnel from Science Applications International Corporation, owners of the STAR Center, operated the pilot plant.

The pilot scale test was terminated as planned after achieving a total of 100 hrs of cumulative/continuous processing operation. About 278 kg of SBW simulant mixed with clay additive were processed that resulted in about 88 kg of solid product that included starting bed material and unreacted carbon. The process achieved about a 90% turnover of the starting bed. Samples of mineralized solid product materials were analyzed for chemical/physical properties and processing data were collected for operational analyses. Results of product performance testing conducted by SRNL will be reported separately by SRNL.

EXECUTIVE SUMMARY

The US Department of Energy (DOE) desired further experimental data, with regard to fluidized bed steam reforming (FBSR) technology, to make informed decisions concerning the selection of treatment technology for Idaho National Engineering and Environmental Laboratory (INEEL) sodium-bearing waste (SBW). Experimental data from tests using actual radioactive waste were desired to provide the most beneficial information to DOE. It was recognized that there was not an experimental fluidized bed test system/facility available to generate experimental radioactive data in the desired time frame. Therefore, a collaboration involving laboratory work at Savannah River National Laboratory (SRNL) and pilot scale work at the INEEL was initiated to provide the information.

The INEEL's pilot scale fluidized bed test system at the Science Applications International Corporation's (SAIC) Science and Technology Applications Research (STAR) facility was successfully operated during the last week of September 2004 to conduct a continuous processing test of THORSM Treatment Technology's (TTT) mineralized FBSR process technology with simulated waste materials representative of SBW. This report documents the experiments performed with SBW simulants, performance of the fluidized bed system, physical characteristics of the mineralized products, and mass balances. Assessment of the product performance with regard to leach resistance and durability (e.g., the Product Consistency Test) are to be reported separately by SRNL.

The pilot scale test generated a large amount of process/system conditions data real time and process materials sampling data. These data have been compiled and have undergone considerable analysis leading to the test results presented herein. Considerable further analyses are possible, however, to generate increased understanding of the technology and response to changes in key process parameters and hardware design.

The pilot scale test successfully achieved the planned total of 100 hours of cumulative/continuous stable processing operations, at an average feed rate of 2 L/hr. A sufficient quantity of mineralized product material was produced under stable process conditions for performance and durability testing. The process achieved about 90% bed turnover (replacement of the starting bed with mineralized product solids) and operated essentially within desired process conditions. This met the desired test objective of operating for 100 hours, but was slightly short of the test objective average feed rate of >3 L/hr.

The pilot scale test produced a significant quantity of representative FBSR mineralized solid product materials, samples of which have been analyzed for chemical/physical properties, and can be used to compare/validate equivalency with small lab-scale batch equilibrium mineralizing chemistry studies/tests by SRNL. The total amount of simulated SBW feed and additives processed was approximately 354 kg and the total output solid mass collected was approximately 88 kg. These data result in a total mass reduction by the process of 266 kg, or about 75%. The total input of solids included 58 kg of carbon, 18 kg of alumina starting bed, and about 47 kg clay. The total solids output included 18 kg of starting bed alumina and 6 kg of unreacted carbon. Therefore, about 231 kg of SBW surrogate processed resulted in about 64 kg of mineralized solid product, a mass reduction of about 72%. An overall solids mass balance closure of near 98% was achieved. The net solid waste product material mass

and volume are, of course, interesting for any subsequent processing or direct handling and disposal activities. The bed product to fines collected mass ratio ranged from 0.6 to 1.3. This value did not achieve the desired value of 3.5 to 1 as stated in the test objectives, and further optimization and/or development is needed to achieve this objective.

The mineralized steam reforming process is intended to immobilize the metal-nitrates in the SBW liquid waste feed solution into a stable product solid consisting largely of sodium/potassium-alumina-silicate target mineral phases of various structures. The mineral phases are formed as a result of the clay (aluminosilicate) additive and are intended to capture and retain (stabilize) the alkali metals (Na, K), target radionuclides (Tc and Cs), hazardous metals and anions. Test results show that nitrates in the liquid waste feed were essentially destroyed and that the bed and fines products largely consisted of desired target mineral phases. The major phase found in the bed product was nepheline (a cage structured sodium aluminosilicate), with minor amounts of corundum (from alumina starting bed) and combeite (sodium calcium silicate), and trace amounts of sodalite (a cage structured sodium aluminosilicate). The fines consisted of the major phase sodium aluminum silicate (unspecified name), with lesser amounts of nepheline and anatase (titanium dioxide).

Elemental analyses of the products indicate that sulfur, rhenium (surrogate for technetium), cesium, chlorine, magnesium, and phosphorous partitioned more to the fines than to the bed product. Conversely, nickel partitioned more to the bed product. The primary constituents (aluminum, sodium, and silicon), calcium, chromium, copper, iron, potassium, and manganese distributed nearly equally between the bed product and fines. Iodine was in too small a quantity to be detected in product samples. Mercury was quantitatively volatilized into the off-gas and collected on the granular activated carbon bed.

The majority (estimated >95 wt%) of the total mass of mineralized product solids was of a form expected during stable, steady mineralized process operations. These consisted of small (typically 0.2 – 0.3 mm), generally granular solids in the bed product or much smaller (typically 0.01 – 0.02 mm) granular solids in the elutriated fines captured in a heated filter downstream of the cyclone. Elutriated fines that were captured in the cyclone and recycled to the fluidized bed averaged about 0.04 mm in diameter. Only a small amount of the total product in the bed was undesirable larger solid pieces, typically the nozzle deposit/accretion agglomerations with dimensions from 10 to 40 mm.

NO_X was satisfactorily destroyed throughout the demonstration. NO_X destruction in the steam reforming process (upstream of the thermal oxidizer) averaged 97%, surpassing the test objective of greater than 80% destruction. Response of NO_X generation/destruction in the steam reforming process was as expected, being directly proportional to carbon feed rate/inventory changes which drive the attendant proportional production of H_2 and CO that are thought to participate in NO_X reduction reactions.

ACKNOWLEDGMENTS

Personnel from several organizations contributed to the performance of this technology demonstration activity. Overall direction was provided by the Department of Energy (Joel Case and Bill Owca).

The collaborative technical team consisted of THOR Treatment Technologies, LLC (Brad Mason, Kevin Ryan, and Brad Eldredge), Savannah River National Laboratory (Jim Marra and Carol Jantzen), and the authors from the Idaho National Engineering and Environmental Laboratory (INEEL).

Science Applications International Corporation (SAIC) modified and operated the DOE-owned fluidized bed test facility at the Science and Technology Research (STAR) Center under direction from the INEEL. The SAIC team was led by Tim Hertzler. This demonstrational activity could not have been accomplished without the intensity and diligence with which SAIC personnel performed their work, the innovation they used to solve problems and issues, and the overall quality of the tasks performed.

Significant changes were also made to the process logic controller interfaces, software, and data acquisition/data archive system. A team led by Curtis St Michel with the support of Havlovick Engineering (John Yadon) performed this activity.

The authors wish to acknowledge and thank all those involved.

CONTENTS

FIGURES

TABLES

ACRONYMS

ASTM	American Society for Testing and Materials
CAI	California Analytical Instruments
CEMS	continuous emissions monitoring system
COT	continuous operating time
DOE	Department of Energy
DP	differential pressure
DUV	dispersive ultraviolet
FBSR	fluidized bed steam reforming
GAC	granular activated carbon
HMPD	harmonic mean particle diameter
HWC	hazardous waste combustor
ID	inside diameter
INEEL	Idaho National Engineering & Environmental Laboratory
LAW	low-activity waste
LOI	Loss on Ignition
MACT	maximum achievable control technology
MMD	mass mean diameter
MMPD	mass mean particle diameter
NAR	nozzle atomizing ratio
NAS	sodium aluminosilicate
NDIR	nondispersive infrared
NE-ID	DOE Idaho Operations Office
NSNCR	non-selective, non-catalytic reduction
OD	outside diameter
P/F	product to fines ratio
PCT	Product Consistency Test
PDF	Powder Diffraction File
PLC	programmable logic controller
PSD	particle size distribution
SAIC	Science Applications International Corporation
SBW	Sodium-bearing waste
SEM	scanning electron micrograph
SPFT	single pass flow through test
SRNL	Savannah River National Laboratory
SRS	Savannah River Site

STAR	Science and Technology Applications Research
TCLP	Toxicity Characteristic Leach Procedure
TGA	thermal gravimetric analysis
THC	total hydrocarbons

of nitrates, nitrites, and sodium tetraphenyl borate (NaTPB). Destruction of the nitrates, nitrites, and organics was desired to reduce impacts of these species, while generating a solidified product, before vitrification at the Defense Waste Processing Facility. Fluidized bed steam reforming was considered a candidate technology for this task. The INEEL was tasked to perform a proof-of-concept steam reforming test to evaluate the technical feasibility for pretreating the Tank 48H waste [Soelberg, 2003]. Crucible bench scale tests were also conducted at the SRNL to optimize and augment the parameters tested at the pilot scale at INEEL [Jantzen, 2003]. The bench and pilot-scale tests were designed to evaluate producing sodium carbonate and sodium silicate products, rather than a mineralized sodium aluminosilicate product. Results of these tests provided the basis for correlating laboratory and pilot scale experiments.

A third demonstrational experiment was performed in November 2003, using the FBSR pilot scale system at the SAIC STAR Center, to produce a sodium aluminosilicate product with a surrogate of INEEL's sodium-bearing waste. The results of this experimental demonstration were also considered promising and have been published [Soelberg, et. al., 2004b].

A fourth series of related experimental demonstrations were performed during 2004. These tests were performed to prepare the FBSR test facility for operation and evaluate specific operating conditions for the SBW mineralization test that is the subject of this report. It was originally planned to perform pilot scale FBSR mineralizing demonstrations after laboratory efforts to select appropriate reductants and optimize the mineralizing chemistry had been completed. However, schedule and funding limitations precluded this approach and necessitated parallel laboratory and pilot scale efforts. The first pilot scale FBSR demonstration with SBW simulant was planned for early July, after desired modification and maintenance activities had been performed. Two functional equipment checkout activities were performed earlier however, one in May and one in June.

The May functional equipment test was performed to assess system performance after the FBSR system had been re-configured to a steam reforming operational mode from a calcination operational mode. Several equipment changes were required to achieve the desired FBSR test system configuration. The functional test scope was not focused on any evaluations of the performance of steam reforming technology. However, best engineering judgment was used to select additives and operating parameters, based on investigations performed through May, that were anticipated to be used in the SBW demonstration.

A slurry of Troy clay in water was fed through a SprayCo® pneumatic atomizing nozzle located in the FBSR wall 4 inches above the distributor in the May functional test. This is the same location as was used in prior FBSR tests for the SBW feed nozzle [Soelberg, 2004a and 2004b]. The SBW simulant was fed through a separate N_2-atomized nozzle located in the FBSR wall 9 inches above the clay slurry nozzle. Preliminary laboratory investigations indicated that Troy clay, with an Si:Al mole ratio of 1.21 and slurried in water at 33.3 wt% clay, matched with the excess Al in the simulant so that the target mineralized product would have an alkali, aluminum, and silicon mole ratio of near 1:1:1 (e.g., nepheline).

The SprayCo® feed nozzle used in the May test was the anti-bearding design to reduce the growth of accretions of dried feed on the face of the nozzle during the 7-hour operating period. No accretions were found on this nozzle during post-test inspection. This was the first time that no indications of simulant feed nozzle accretions were found during or after an FBSR test, so the anti-bearding design appeared to function well. However, about 50 separate nozzle accretions formed on the clay slurry nozzle, which did not have an anti-bearding design. The anti-bearding nozzle design was not available from the vendor in a size that prevented restrictions due to the slurry rheology. The accretions eventually

broke off of the nozzle. Some of these accretions were larger than 1 inch in diameter, and most of the accretions that were not fragmented had a visible hole through which the clay slurry had sprayed. The solid nozzle accretions tended to float on top of the bed rather than sink to the bottom, so they did not impair fluidization during the 7-hour test. However, many of these pieces were too large to fit through the bed drain/sample tubes, and would probably have eventually caused defluidization under continued operation unless the fluidized bed action could have broken the pieces up into small enough particles for removal.

The May test revealed some deficiencies in the waste feed/clay injection system, the carbon injection system, and a failed valve in the cyclone product recycle line. The results initiated some further individual system tests to optimize the system. The physical properties of the waste feeds (density, viscosity of waste/clay mixtures) were measured and feed injection nozzle experiments performed to determine the most efficient method for injecting the waste/clay mixture to the FBSR reactor. It was determined that a uniaxial-tube Bernoulli effect (UTB) nozzle entering the reactor through the bottom receiver, with waste/clay slurried together, was the preferred method. The previous nozzle entry at the 4-inch level above the fluidizing gas distributor remained as a backup. More details of this testing are located in Appendix B.

Fluidization visualization tests were performed using the reactor bottom receiver and a plexiglass mockup of the reactor vessel (discussed in Appendix A). These tests were performed using a Froude number correlation to match normal operating conditions with the test conditions. The objective was to determine the appropriate fluidizing gas distributor type to use during the SBW demonstration and to observe the effects of nozzle placement during operation. It was observed that fluidizing gas distributor type did not affect fluidizing conditions 6 inches above the distributor. A THOR ^{SM} proprietary distributor was selected.

A second, integrated functional test of the system at temperature was performed June 24 to validate system operation after repairs and modifications for the SBW demonstration. Again, the functional test scope was not focused on any evaluations of the performance of steam reforming technology, but laboratory data from SRNL activities were used to select the most desirable raw material additives that would be used in the SBW demonstration. Operational parameters anticipated for the FBSR during the SBW demonstration were also selected. Specific items that were to be addressed included: 1) Demonstrate feeding clay slurry through the uniaxial-tube Bernoulli-effect (UTB) nozzle, 2) Demonstrate the effectiveness of a reduced nozzle atomizing ratio (NAR) in producing bed product and reducing product fines generation, 3) Demonstrate cyclone catch recycle to the bed, and 4) Demonstrate the ability to reliably feed carbon to the bed.

The June functional test was terminated after 5½ hours of operation due to defluidization caused by an agglomerated monolith that had formed in the lower portion of the fluidized bed ranging about 2 – 7 inches above the distributor. The monolith had approximately three loose contact points with the reactor walls and internals. The monolith was physically located above the cyclone catch return port, above the tip of the UTB, and about 3 inches above the distributor. Several nozzle accretions were also observed in the bottom of the reformer that had dimensions that were generally less than one inch in length or diameter.

Observations during the June functional test indicated that the UTB nozzle successfully fed SBW-clay slurry without the slurry orifice or atomizing gas annulus becoming restricted. Some clay accumulated on the outer surface of the tube defining the gas annulus, which appears to be a consequence of the surface temperature being lower than that of the bed. The rate at which slurry was added may have contributed to the formation of the monolith, and the selected NAR for the test apparently may not have

satisfactorily atomized the feed. Recycle of cyclone catch fines was not demonstrated because of mechanical failure of the high-temperature valves purchased for this purpose. The system was to be modified to enable using the high-temperature valves, which had been previously used in the system, for the SBW demonstration. Demonstration of the carbon feed system was successful after a loose funnel that caused a problem with the load cells, and a Programmable Logic Controller (PLC) carbon feed rate control system issue, were resolved. The product that was formed appeared to be primarily nepheline with minor amounts of sodium aluminates and silica deficient sodium aluminosilicates based on XRD analyses performed at SRNL.

The first SBW demonstration was performed from July 7 through July 14, 2004, during two 3-day periods. The first test was performed July 7-9 and the second July 12-14, 2004. Both runs were terminated prematurely due to equipment problems. The first run suffered from bed defluidization due to the build up of accretions/agglomerates in the bed, most of which appeared to have formed from feed nozzle accretions that broke off of the feed nozzle during the test. The second test was terminated when the feed nozzle restricted and could not be cleared. The second run also encountered nozzle accretions that built up and threatened to defluidize the bed. However, by draining portions of the bed, screening out the large agglomerated particles, and returning the -20 mesh fraction to the bed, the test was able to continue until the irrecoverable nozzle restriction terminated operations.

This SBW demonstration was conducted with 293 gm Troy clay mixed with one liter of SBW simulant as feed to the FBSR. The slurry feed rate to the FBSR was initiated at 2.0 kg/hr and increased to 5 kg/hr over the course of the first test. The slurry feed rate was initiated at 2.0 kg/hr for the second test, increased to 4.0 kg/hr, and then maintained at 4.0 kg/hr for the duration of the test. Two different feed injection nozzles were used during the tests. For the first run, the vertical axial UTB nozzle was used. The UTB nozzle consists of three concentric tubes; an inner liquid tube, a middle atomizing gas tube, and an outer cooling shroud gas tube. This nozzle was tested prior to the run to determine the NAR that would give “good” atomization of the simulated SBW/clay slurry. In general, “good” atomization is achieved when the droplets are smaller than the bed particles. The nozzle performed well at atomizing the slurry into the bed. However, the cooling shroud gas kept the last centimeter of the nozzle tube relatively cool, which allowed the liquid slurry feed to wet the nozzle and form accretions that grew until they were broken off by the action of the bed and settled into the bottom of the bed. The largest accretions were ~3 cm wide and ~5 cm long. Many small accretions were also generated that were 0.5 to 0.7 cm wide and 1 to 2 cm long. Some of the accretions formed a tube or sleeve around the nozzle and retained this shape after breaking off. The mass of accretions in the final bed was 0.3 kg out of a total bed mass of 9.1 kg. However, the density of the accretions was fairly low because they were very porous, and the volume of the accretions was sufficient to fill the bottom ~10 cm of the FBSR vessel. The duration of this first test was 26.5 hours.

The second test used a SprayCo® pneumatic atomizing nozzle mounted in port I of the reactor vessel (see Figure 3.2-2), delivering waste feed horizontally across the fluidized bed about 4 inches above the fluidizing gas distributor. The nozzle performance was observed prior to the test to determine the NAR that would give “good” atomization of the simulated SBW/clay slurry. At the end of the test the nozzle was examined for evidence of nozzle accretions. As with the UTB nozzle, the area around the air cap was covered with a tenacious layer of reacted product solids from the feed that was approximately 0.1 to 0.15 cm thick. There were no other deposits on any other surfaces in the FBSR vessel. Since the air cap is constantly cooled by the atomizing gas flow, it was hypothesized that keeping the feed nozzle hot could be key to keeping nozzle accretions from forming. This led to the development of a modified nozzle that would be tested during the Hanford low activity waste (LAW) mineralization tests that were to be performed in August [Olson, 2004].

The starting bed for the second run was the final bed from the first run after it had been screened to remove the agglomerates. At approximately 20 hours after feed was introduced into the bed, it was apparent that the bed was again beginning to defluidize due to the build up of agglomerates. Several of the nozzle accretions had been removed during the routine bed drains and the bed thermocouples were starting to diverge. A method was devised to remove these agglomerates from the bed by draining the bed, sieving out the large agglomerates, and returning the -20 mesh material to the bed. This procedure was repeated about every 30-45 minutes until the number of large particles in the bed was observed to decrease. The bed was drained, screened, and recycled a total of 10 times before the run was terminated. This method proved to be effective at removing the large nozzle accretions that had caused the shutdown of the first run and the appearance of the bed seemed to show an improving trend over several hours (i.e., fewer accretions and better overall particle size distribution).

The second demonstrational test was terminated, after a total of about 27 hours of operating time, due to a feed nozzle restriction that could not be cleared. During the course of the second test, the feed nozzle was observed to have worked loose, which allowed some of the atomizing gas to leak into the annulus between the FBSR vessel and the feed nozzle retaining pipe. It is not known if this caused the nozzle to perform inadequately. However, the buildup of the nozzle accretions almost surely interfered with the nozzle spray pattern and atomization effectiveness, thereby encouraging undesirable bed particle growth. This was likely an ongoing issue throughout both runs.

The tests were successful at producing approximately 17.0 kg of granular product and 38.9 kg of filter fines for analysis. Chemical and physical analyses showed that the major products in the granular product were nepheline and carnegieite, sodium aluminum oxide, and other sodium aluminosilicates. In spite of the involuntary shutdowns experienced in these tests, they were successful at demonstrating that particle size control was possible, if large agglomerates can be removed preferentially from the bed (by sieving and recycling the bed material). Optimization of the nozzle geometry and performance was expected to essentially eliminate the generation of the unwanted nozzle accretions. A new reformer vessel bottom receiver (described in Section 3.2) was designed and fabricated for the Hanford LAW demonstration, allowing for more efficient removal of nozzle accretions if they were to occur. All other mechanical systems including the off-gas treatment system, continuous emissions monitoring system (CEMS), thermal oxidizer, and carbon bed performed very well during both tests. NO_X destruction, as noted by CEMS data, was generally greater than 90%.

Post-demonstration investigations provided further insight to waste feed injection and bed defluidization issues. It was discovered that, due to a calculation error, the Troy clay addition quantity to the SBW simulant should have been 223 g/L rather than the 293 g/L that was used for slurry feed. This error would have a significant affect on the mineralizing product formation chemistry.

The fifth test related to the work reported here was the test performed with the INEEL's pilot scale FBSR system in August 2004 to produce a sodium aluminosilicate product with a surrogate of Hanford's LAW [Olson, 2004]. The results of this demonstration provided additional insight for planning and performing the work reported here.

A DOE programmatic decision, providing additional funds, allowed for the performance of a second SBW demonstration, but it was not to be performed until further laboratory experimental data was available from SRNL. Detailed chemical and physical analyses of the products generated during the July SBW test were not performed. The second SBW mineralization test was performed in September 2004, based on additional experimental data from SRNL. The remainder of this report describes the detailed results of the September SBW mineralization test.

1.2 Scope

The scope of the collaborative work performed by the SRNL and INEEL included:

- Performance of laboratory scale simulated FBSR experiments at SRNL that would optimize steam reforming raw materials selection and mineralization chemistry.
- Performance of pilot scale FBSR experiments at INEEL with simulants that produced a mineralized product to which the products of the laboratory scale tests could be compared.
- Characterization of products via chemical assays, x-ray diffraction, and scanning electron microscopy.
- Product durability measured via Toxic Characteristic Leach Procedure (TCLP), and Product Consistency Test (PCT) measurements; performance will be measured by the single pass flow through (SPFT) testing.
- Determine, based on comparisons to the products of the pilot-scale tests, if the laboratory tests produce steam reforming conditions and mineralized products that are representative of actual fluidized bed steam reforming.

This report documents the tests of the mineralizing steam reforming technology for SBW conducted in the INEEL pilot-scale fluidized bed steam reformer (FBSR). Results from the FBSR test operations, physical characteristics of the mineralized SBW products, and process mass balances are provided. Assessment of the product performance with regard to leach resistance and durability are to be reported by SRNL separately.

2. THEORY/APPROACH

Mineralizing steam reforming technology is being considered by the Department of Energy as a treatment and immobilization method for liquid radioactive wastes being managed by the Department. In addition to being radioactive, these liquid wastes also contain large quantities of alkali metals and nitrates, and lesser quantities of hazardous metals and anions such as fluoride, chloride, and sulfate. Classical steam reforming is a versatile process that decomposes organic materials through reaction with steam. Steam reforming has been used on a large scale by the petrochemical industry to produce hydrogen for at least 65 years. If the material being reformed contains halogens, phosphorus, or sulfur, mineral acids are also formed (e.g., hydrochloric acid, phosphorous acid, phosphoric acid, and hydrogen sulfide) unless inorganic materials capable of scavenging these species are present in the waste or additives [Nimlos, 1990, 1992]. Organic nitrogen is converted to N_2 and organic oxygen is converted to CO or CO_2.

It is desired to immobilize radioactive components of the waste into a form that is quite durable (i.e., leach resistant) for hundreds or thousands of years. More recently, steam reforming has been proposed, along with the use of mineralizing additives, to immobilize liquid radioactive wastes into forms that meet durability criteria required at a wide variety of disposal sites.

2.1 Mineral Waste Forms

Previous development work has shown that sodium aluminosilicate (NAS) minerals provide host phases to accommodate radionuclide species. Waste forms of aluminosilicate based crystalline assemblages of mutually compatible, refractory, and leach-resistant solid solution phases have been proposed for the incorporation of radionuclide species of concern [Rusin, 1979]. An assemblage of silicate mineral phases (supercalcine ceramics) such as apatite (host for lanthanides), pollucite (host for Cs), and other oxide host phases for Sr, Ba, U, Zr, etc. seem appropriate [McCarthy, 1976 and Rusin 1979]. If the waste contains considerable Na and Si, then phases such as nepheline may form while wastes enriched in Al may form high temperature phases such as Al_2O_3 and magnetoplumbite aluminate species [Morgan, 1981 and Jantzen 1982]. The feldspathoid sodalite is a mineral phase found to incorporate Cs, Sr and Mo into the cage-like structure, e.g. Mo as $(NaAlSiO_4)_6(NaMoO_4)$ [Brookins, 1984]. A more detailed discussion of this subject can be found in Jantzen, 2002.

The NAS mineral phase assemblage(s) are anhydrous feldspathoid phases such as sodalite that are unique because they have cage-like structures formed of aluminosilicate tetrahedra (Figure 2.1-1). The remaining feldspathoid minerals, such as nepheline, have a silica “stuffed derivative” ring type structure. The cage structures are typical of sodalite and/or nosean phases where the cavities in the cage structure retain anions and/or radionuclides that are ionically bonded to the aluminosilicate tetrahdra and to sodium. The cage structured feldspathoid system of minerals has the basic structural framework formula $Na_6[Al_6Si_6O_{24}]$and an alumina:silica ratio of 1:1.

The nomenclature of the feldspathoid series of mineral species is governed by the species that occupy the cavities in the aluminosilicate framework and whether or not the resulting crystals have cubic or hexagonal crystal structures. Sodalite has the formula $Na_8[Al_6Si_6O_{24}](Cl_2)$. The cage is occupied by two sodium and two chlorine ions in natural sodalites [Deer, 1963]. The formula can also be written as $Na_6[Al_6Si_6O_{24}]\cdot(2NaCl)$ to indicate that two NaCl molecules are chemically bonded in the cavities of the cage structure while the remaining Na:Si:Al have a 1:1:1 stoichiometry [Deer, 1963]. When the sodium chloride molecules are replaced by Na_2SO_4, Na_2CO_3, $2NaNO_3$, and/or 2NaOH, the mineral and/or chemical names are as given in Table 2.1-1.

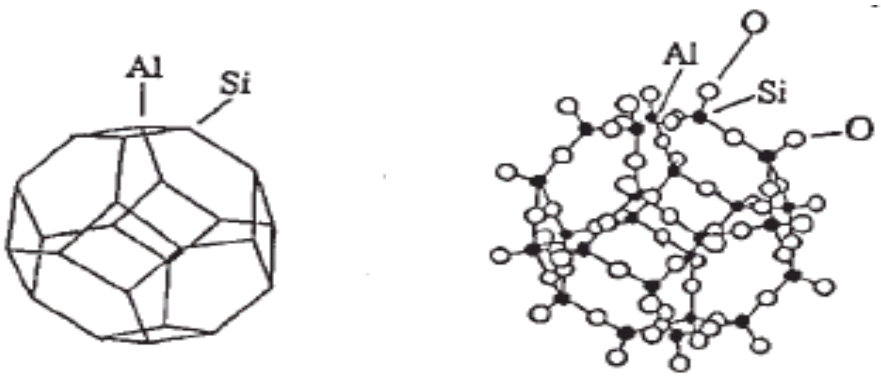

Figure 2.1-1. Part of the aluminosilicate framework in the structure of the feldspathoid sodalite [Deer, 1963].

One of the feldspathoid cage structured minerals is nosean, $Na_6[Al_6Si_6O_{24}](Na_2SO_4)$, with Na_2SO_4 bonded in the sodalite cage-like structure. Since the Cl^-, SO_4=, and/or S_2 are bonded inside the sodalite cage structure, these species do not readily leach out of the respective waste form mineral phases. A second feldspathoid mineral is nepheline ($NaAlSiO_4$) [Berry, 1959]. Nepheline is a hexagonal structured feldspathoid mineral. The ring structured aluminosilicate framework of nepheline forms cavities within the framework. There are eight large (nine-fold oxygen) coordination sites and six smaller (8-fold oxygen) coordination sites [Deer, 1963]. The larger nine-fold sites can hold large cations such as Cs, K, and Ca while the smaller sites accommodate the Na. The K analogue is known as leucite ($KAlSi_2O_6$). In nature, the nepheline structure is known to accommodate Fe, Ti and Mg as well.

A sodium rich cubic structured nepheline derivative $(Na_2O)_{0.33}Na[AlSiO_4]$ (PDF#39-0101) is also known to form. This nepheline derivative structure has large (twelve-fold oxygen) cage like voids in

the structure [Klingenberg, 1986]. This cage-structured nepheline is not known to occur in nature but the large cage-like voids should be capable of retaining large radionuclides, especially monovalent radionuclides such as Cs.

Τηε οβφεχτιωε οφ τηισ ωορκ ηασ βεεν το χρεατε τηε τψπεσ οφ μινεραλσ τηατ ωουλδ προωιδε λεαχη ρεσισταντ (δυραβλε) ωαστε φορμσ φορ τηε ιμμοβιλιζατιον οφ ΙΝΕΕΛ□σ σοδιυμ–βεαρινγ ωαστε (ΣΒΩ). Τηισ ηασ βεεν αππροαχηεδ βψ σελεχτινγ α χλαψ τψπε ωιτη τηε αππροπριατε Αλ:Σι μολε ρατιο τηατ ωουλδ συιταβλψ ρεαχτ ωιτη τηε Να, Κ, οτηερ μεταλσ ανδ ανιονσ ιν τηε ΣΒΩ. Α τερναρψ πηασε διαγραμ (Φιγυρε 2.1–2) σηοωσ τηε ταργετ ρεγιον οφ χομποσιτιονσ τηατ αρε τηουγητ το βε μοστ φαωοραβλε φορ προδυχινγ τηε δεσιρεδ μινεραλ προδυχτσ. Τηε μοστ φαωοραβλε ατομιχ ρατιοσ τηατ ωould produce the desired nepheline and sodalite products are thought to be M/Si = 1-1.33, M/Al = 1-1.33, Al/Si ≥ 1, and M/(Al+Si) = 0.5-0.67, where M represents an alkali metal, mostly Na in this case [Jantzen, 2004]. The acceptable composition region is not necessarily as small as indicated by the shaded region in Figure 2.1-2, it be could anywhere in the valley that points to the nepheline melting region. The atomic ratios provide guidelines because there may be significant substitution of different alkali and alkaline earths, and some Fe for Al, in these feldspathoid minerals.

Fluidized Bed Steam Reforming of INEEL SBW Using THOR^{sm} Mineralizing Technology

1. INTRODUCTION

Sodium-bearing waste (SBW) disposition is one of the U.S. Department of Energy (DOE) Idaho Operation Office's (NE-ID) and State of Idaho's top priorities at the Idaho National Engineering and Environmental Laboratory (INEEL). The INEEL has been working over the past several years to identify a treatment technology that meets NE-ID and regulatory treatment requirements, including consideration of stakeholder input. Many studies have resulted in the identification of five treatment alternatives that form a short list of perhaps the most appropriate technologies from which the DOE may select. The alternatives are (a) calcination with maximum achievable control technology (MACT) upgrade, (b) steam reforming, (c) cesium ion exchange (CsIX) with immobilization, (d) direct evaporation, and (e) vitrification. Each alternative has undergone some degree of applied technical development and preliminary process design over the past four years.

DOE identified the need in January 2004 for further experimental data, with regard to steam reforming technology, to make informed decisions concerning selection of treatment technology for SBW. Experimental data from tests using actual radioactive waste were desired to provide the most beneficial information to DOE. It was recognized that there was not an experimental fluidized bed test system/facility available to generate experimental radioactive data in the desired time frame. Therefore, a plan was conceived that would provide the technical information that was desired.

The basis for the plan was that a correlation between laboratory and pilot scale results existed and would need to be validated such that radioactive laboratory experiments performed in hot cells would provide the desired information. A collaboration involving laboratory work at Savannah River National Laboratory (SRNL) and pilot scale work at INEEL was initiated to validate the correlation. This report documents the results of the pilot scale experiments performed with SBW simulant during the last week of September 2004.

1.1 Background

Several demonstrations of fluidized bed steam reforming (FBSR) technology as applied to simulated radioactive liquid waste streams have been performed in the last two years. Five separate experiments that are specifically related to the work reported here were performed earlier. The first, conducted at the Hazen Research facility in Colorado in 2001, pertained to generating a sodium aluminosilicate (mineralized) product from Hanford low-activity waste (LAW). The results of this experiment were considered promising and characteristics of the product have been published [Jantzen, 2002].

The second demonstration, using the Idaho National Engineering and Environmental Laboratory's (INEEL) pilot scale FBSR system, was performed in 2003. The INEEL's pilot scale FBSR system is located at the Science Applications International Corporation's (SAIC) Science and Technology Applications Research (STAR) Center, in Idaho Falls, ID. The Savannah River Site (SRS) desired to make space in the SRS tank farm by removing/processing the Tank 48H waste. Tank 48H waste consists

Table 2.1-1. Structurally related zeolite and feldspathoid (sodalite and cancrinite) group mineral phases [Jantzen, 2002].

Substitution In Cage Structure	Chemical Formula	Common Mineral Name	Density (g/cm3)	Crystal Type	Ref.
Precursor					
NONE	$Na_{12}[Al_{12}Si_{12}O_{48}] \cdot 27H_2O$	Zeolite-A	1.99‡	Cubic	Kirk-Othmer, 1995
Sodalite Group (Anhydrous)					
2NaCl	$Na_6[Al_6Si_6O_{24}](2NaCl)$	Sodalite	2.31*	Cubic*	Deer, 1963
2NaOH	$Na_6[Al_6Si_6O_{24}](2NaOH) \cdot 1.5H_2O$	Basic Sodalite or Hydroxysodalite	2.215**	Cubic**	Barrer, 1959
$2NaNO_3$	$Na_6[Al_6Si_6O_{24}](2NaNO_3)$	Nitrated Sodalite	2.342	Cubic	PDF#50-0248
Na_2SO_4	$Na_6[Al_6Si_6O_{24}] (Na_2SO_4)$	Nosean	2.21tt	Cubictt	Dana, 1932
1-2(Ca,Na)SO_4	$(Na)_6[Al_6Si_6O_{24}]$ ((Ca,Na)(S,SO_4)1-2)t	Hauyne	2.4t	Cubict	Deer, 1963
x(Ca,Na)(S,SO_4 ,Cl)	$(Ca,Na)_6[Al_6Si_6O_{24}]$((Ca,Na)S,$SO_4$,Cl)Xt	Lazurite	2.43	Cubic	PDF #17-749
Cancrinite Group (Anhydrous)					
$2NaNO_3$	$Na_6[Al_6Si_6O_{24}](2NaNO_3) \cdot 4H_2O$	Nitrated Cancrinite	2.51	Hexagonal	PDF #38-513
$(Na,Ca,K)_2CO_3$	$(Na,Ca,K)_6$ $[Al_6Si_6O_{24}]$ $((Na,Ca,K)_2$ $CO_3)_{1.6} \cdot 2.1H_2O$	Cancrinite	2.60	Hexagonal	PDF #25-776
2(Na, K)Cl	$(Na,Ca,K)_6[Al_6Si_6O_{24}]$ (2(Na,K)Cl) 2-3	Microsommite	2.34	Hexagonal	PDF #20-743
2(Na, K)Cl	$(Na,Ca,K)_6[Al_6Si_6O_{24}]$ ((Na,K)2SO_4 ,Cl)3	Davyne	2.46	Hexagonal	PDF #20-379
Na_2CO_3	$Na_6[Al_6Si_6O_{24}] (Na_2CO_3)$	Natrodavyne	Not given	Hexagonal	PDF #15-794

t PDF #20-1087 * PDF # 20-495 ‡ PDF #11-0590 and #38-241
tt PDF #17-538 ** PDF #11-401 PDF – Powder Diffraction File

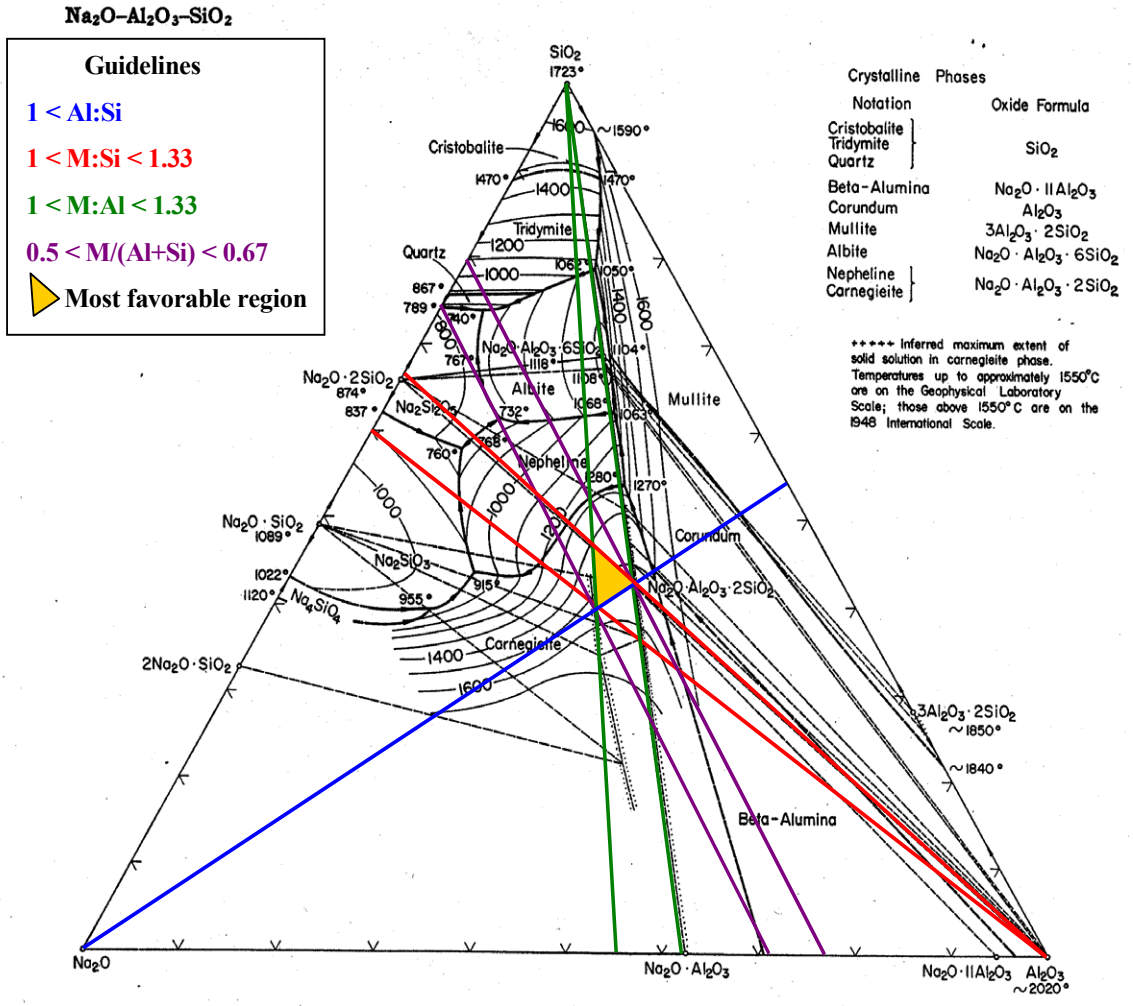

System Na_2O–Al_2O_3–SiO_2; composite.

E. F. Osborn and Arnulf Muan, revised and redrawn "Phase Equilibrium Diagrams of Oxide Systems," Plate 4, published by the American Ceramic Society and the Edward Orton, Jr., Ceramic Foundation, 1960.

Principal References

G. W. Morey and N. L. Bowen, *J. Phys. Chem.*, **28**, 1167–79 (1924).
F. C. Kracek, *J. Phys. Chem.*, **34**, 1583–98 (1930).
N. L. Bowen and J. W. Greig, *J. Am. Ceram. Soc.*, **7**, 238–54 (1924); corrections, ibid., 410.
N. A. Toropov and F. Ya. Galakhov, *Voprosy Petrogr. i Mineralog., Akad. Nauk S.S.S.R.*, **2**, 245–55 (1953).
Shigeo Aramaki and Rustum Roy, *Nature*, **184**, 631–32 (1959).
J. F. Schairer and N. L. Bowen, *Am. J. Sci.*, **254**, 129–95 (1956).
Liberto De Pablo-Galan and Wilfred R. Foster, *J. Am. Ceram. Soc.*, **42**, 491–98 (1959).

Figure 2.1-2. Most favorable composition region on the Na_2O – Al_2O_3 – SiO_2 ternary phase diagram.

2.2

2.3 Steam Reforming Chemistry

Fluidized bed steam reforming (FBSR) for treating liquid radioactive wastes involves (a) a bed of particles fluidized by an upward flowing gas (steam in the THOR^{sm} steam reforming process) into which the liquid waste is sprayed, and (b) a reductant that is reformed by reactions with steam to produce reformed products and intermediate products that create a reactive, reducing environment to destroy nitrates and nitrites in the feed to produce environmentally benign N_2, H_2O, and CO_2. A reductant, such as carbon, is steam reformed at elevated temperatures, exemplified by the following simple reaction:

$$C + H_2O \rightarrow CO + H_2 \qquad (1)$$

CO reacts further with both steam and H_2:

$$CO + H_2O \rightarrow CO_2 + H_2 \qquad (2)$$

$$CO + 3\,H_2 \rightarrow CH_4 + H_2O \qquad (3)$$

Consumption of CO and H_2 (such as through reactions with NO_x in a steam reformer, in addition to reactions (2) and (3) drives reaction (1) to produce more CO and H_2. Reaction (1) is endothermic, so added heat is required to enable this reaction to proceed. If air or oxygen is included in the reaction mixture, the process can be autothermal. That is, exothermic reactions of carbon and the reduced gas species H_2 and CH_4 with oxygen, to produce more oxidized species CO and CO_2. Heat from the exothermic oxidation reactions provides the heat needed for the steam reforming reactions. A tendency for steam reforming reactions to form more complex hydrocarbon species is suppressed by operating with a moderate excess of steam.

In principle, all organic compounds can be steam-reformed. The process has been demonstrated on a number of organic liquids (e.g., simple hydrocarbons, alcohols, ketones, and chlorocarbons), a variety of polymeric organic materials (paint residues, caulks, shredded paper, plastics, and wood products; organics adsorbed on soils, debris, activated carbon and ash), and even coal [Elliott, 1981] and cellulosic wastes [Antal, 1979].

Nitrate salts will thermally decompose, even in the absence of reducing agents, at elevated temperatures (see below). The complete thermal decomposition of $NaNO_3$ is not well understood. Rapid heating to very high temperatures (2,200 °C) results primarily in the formation of N_2 and O_2, which are thermodynamically and kinetically favored over NO_x gas species at such high temperatures. However, at more moderate temperatures, in the absence of a reductant that participates in the thermal decomposition process to tie up oxygen, the decomposition of nitrate salts favors NO_x as the primary product [Meile, 1984].

There is general agreement in the literature that at lower temperatures the first reaction in the thermal decomposition of $NaNO_3$ is the loss of oxygen to form $NaNO_2$.

$$2\,NaNO_3 \rightarrow 2\,NaNO_2 + O_2 \qquad (4)$$

In fact, at typical steam reforming temperatures (600-750 °C), the equilibrium between $NaNO_3$, $NaNO_2$, and O_2 (without the presence of a reductant) has been studied and quantified [Freeman, 1956].

Following the initial decomposition of $NaNO_3$ to $NaNO_2$ and O_2, the mechanism of interest is the decomposition of $NaNO_2$. The decomposition of $NaNO_2$ has been reported as probably first producing NO_x [Addison, 1964].

$$2\ NaNO_2 \rightarrow Na_2O + N_2O_3 \qquad (5)$$

$$N_2O_3 \rightarrow NO_2 + NO \qquad (6)$$

Many other reactions, some involving the direct conversion of $NaNO_3$ to products other than $NaNO_2$, have been postulated in the literature [Kramer, 1983]. N_2O has also occasionally been reported as being a product of nitrate decomposition [Bartos, 1956, Brown, 1975]. Although reaction mechanisms were not reported, N_2O can be produced from NO_x, especially in the presence of a catalyst or a reducing agent such as SO_2 [Hayhurst, 1992]. Additional products encountered in prior tests include both NH_3 and HCN [Soelberg, 2003].

The reactions above illustrate one possible route for $NaNO_3$ decomposition. In reality, it is likely that many of the above reactions occur in parallel with others such as the decomposition of nitrogen dioxide to nitric oxide and oxygen.

$$2\ NO_2 \leftrightarrow 2\ NO + O_2 \qquad (7)$$

Ultimately, the final mix of gaseous products from the thermal decomposition of nitrate, i.e., the ratio of NO_x to N_2 in the product stream, depends on a number of chemical and physical factors, such as catalyzing metals, residence times, reductant:oxidant stoichiometry, temperature, and flow patterns in the reaction vessel.

Reacting nitrates with reducing agents is a more direct and efficient route to producing N_2 rather than NO_x as a final decomposition product. A large number of chemical reducing agents have been examined for the denitrification of aqueous solutions. These chemicals include iron metal, Fe^{2+}, N_2H_2, glucose, CO, formaldehyde [Gunderloy, 1968, 1970], formic acid [Bradley, 1972], sugar [Bray, 1963], glycolic acid [Seymour, 1995], starch [Ryan, 1995], and urea [Cox, 1994]. Nitrate ions can be reduced to ammonia (and sometimes N_2) with aluminum [Murphy, 1991; Mattus, 1993] or iron [Cheng, 1997] powder, depending on the pH of the solution. Thermochemical reduction has also been applied to dry nitrate wastes. Ammonia and ammonium compounds have been reported to reduce nitrates directly to N_2 at temperatures of 300-600°C [Dotson, 1975]. Coke (carbon) has also been successfully used to directly reduce nitrates to N_2 although higher temperatures were required [Meile, 1984]. The reaction of sodium nitrate and coke is representative of the thermochemical processes.

$$2\ NaNO_3 + 4\ C \rightarrow Na_2CO_3 + N_2 + 3\ CO \qquad (8)$$

Carbonaceous reductants fed to the reformer provide chemically reducing conditions in the reformer via the kinds of reactions described above. The higher the reducing conditions of the reformer, the more effectively nitrates in the feed are chemically reduced to N_2.

A summary of potential reaction mechanisms (not all inclusive) is given in Table 2.2-1.

Table 2.2-1. Various potential chemical reactions under steam reforming conditions.

Process Step	General Reaction Examples	Comments
Solution evaporation/particles drying	Waste sol'n (liquid) → H_2O (gas) + $NaNO_3$, $Al(NO_3)_3$, etc.	Commences in liquid droplet, continues in particle film, except at high temperatures/high heating rates when evaporation occurs above the solid-gas boundary layer. Rapid evaporation of spray droplets results in sub-micron-size particles.
Solid salt thermal dissociation/ decomposition	2 $Al(NO_3)_3$ (s) → Al_2O_3 (s) + 6 NO_2 (g) + 1½O_2 (g) 2$NaNO_3$ (s) → Na_2O (s) + 2 NO_2 (g) + ½O_2 (g) Na_2CO_3 (s) ↔ Na_2O (s) + CO_2 (g) Na_2CO_3 (s) + H_2O (g) ↔ 2 NaOH (l) + CO_2 (g)	Transition metal nitrates typically rapidly dissociate below 400°C. Alkali metal nitrates typically denitrate slowly and can persist to temperatures up to 600°C. Molten alkali hydroxides can lead to dissolution of other salts and bed agglomeration, which is not desirable in a fluidized bed.
Organic compound depolymerization/ devolatilization/ char formation	C_mH_n (s) → char (s) + tars/oils, C_xH_y (g) $C_lH_mO_n$ → char (s) + tars/oils, C_xH_y (g) + H_2, OH', H_2O (g) $C_{12}H_{22}O_{11}$ (s) → 12 C (s) + 11H_2O (g)	Organic evolution rates and speciation depends on hydrocarbon functional groups, particle heating rates, reactor temperature, and particle residence time. Light gases and tars evolve competitively.
Solid state organic REDOX reactions	2 $NaNO_3$ (s) + C(s) or carbon source (s) → Na_2CO_3 (s) + N_2 (g) @ solid waste–char or carbon particle boundary [or] @ solid waste–organic compound/char in dehydrated droplets or solid layer on an existing particle.	Nitrate-organic reduction occurs spontaneously at 250–350°C and the reaction zone rapidly propagates through the remaining unreacted solid reactant mixture.
Solid state inorganic reactions	2 $NaNO_3$ (s) + Al_2O_3 (s) → 2 $NaAlO_2$ (s) + 2 NO_2 (g) + 1½ O_2 (g) Na_2O (s) + Al_2O_3 (s) → 2 $NaAlO_2$ (s) Na_2O (s) + SiO_2 (s) → Na_2SiO_3 (l) Na_2O (s) + $Al_2Si_2O_7 \cdot 2H_2O$ (s) → 2 $NaAlSiO_4$ (s) + 2 H_2O (g)	Silica is present as a contaminant in the makeup water and in the simulated heel solids. Aluminum nitrate is present in the SBW and decomposes to Al_2O_3, unless mineralizing additives are present. Alkali silicates may be molten at process temperatures. Clay can be added to the simulant to form alkali aluminosilicates.
Heterogeneous carbon gasification reactions	H_2O (g) + C (s) → CO (g) + H_2 (g) CO_2 (g) + C (s) → 2 CO (g) O_2 (g) + 2 C (s) → 2 CO (g) NO_2 (g) + C (s) → CO (g) + NO (g)	Gasification to CO is typically endothermic. NO_2-C char reactions are slower than other char reactions and may not be significant. Oxides and carbonates in the solids can catalyze char reactions.
Heterogeneous inorganic reactions	Na_2O (s) + NO_2 (g) + NO (g) ↔ 2 $NaNO_3$ (s) Na_2O (s) + CO_2 (g) → Na_2CO_3 (s) Na_2O (s) + H_2O (g) → 2 NaOH (l) Na_2O (s) + 2 HCl (g) → 2 NaCl (s) + H_2O (g) CaO (s) + 2 HCl (g) → $CaCl_2$ (s) + H_2O (g) 2 NaOH (l) + Al_2O_3 (s) → 2 $NaAlO_2$ (s) + H_2O (g) 2 NaOH (l) + SiO_2 (s) → Na_2SiO_3 (l) + H_2O (g) 2 NaOH (l) + $Al_2Si_2O_7 \cdot 2H_2O$ (s) → 2 $NaAlSiO_4$ (s) + 3 H_2O (g)	Product nitration, carbonate formation, and hydration are all possible. Nitration occurs at T< 400°C. Carbonate formation occurs at T< 800° C. Hydration produces a molten phase of alkali hydroxides capable of dissolving other product solids and causing agglomerations. Formation of alkali silicates is undesirable due to molten silicate phases that can cause agglomeration. Mineralizing additives (e.g., clay) can be added to form alkali aluminosilicates, which are insoluble and do not melt at process temperatures.

2.4

Gaseous hydrocarbon chemistry	$CO + H_2O \leftrightarrow CO_2 + H_2$ (water-gas shift reaction) $CO + 3\ H_2 \leftrightarrow CH_4 + H_2O$ (methanation reaction) $H_2O \leftrightarrow H\cdot + OH\cdot$ $CO + OH\cdot \rightarrow CO_2 + H\cdot$ $H_2 \leftrightarrow 2H\cdot$ $H\cdot + H_2O \leftrightarrow H_2 + OH\cdot$ $CO_2 \leftrightarrow CO + \frac{1}{2}\ O_2$ $CH_3\cdot + H\cdot \leftrightarrow CH_4$ $2\ CH_3\cdot + H2 \rightarrow 2\ CH_4$	The water-gas shift reaction is significant at T>600-625°C. Methanation is generally low. Hydrogen and carbon give rise to highly reactive hydrogen, hydroxide, peroxide, and oxygen radicals through the reducing zone. Such reactions promote ring opening, chain breaking, hydrogen extraction/substitution reaction, etc. These reactions are very fast at T>600-650°C and lead to chain propagation. Below 600°C, many radicals terminate and continued reaction is driven by OH· radical.
Gaseous nitrogen chemistry	$CH_4 + 4\ NO_2 \rightarrow 4\ NO + CO_2 + 2\ H_2O$ $CH_3\cdot + NO \rightarrow HCN + H2O$ $CH_3\cdot + NO_2 \rightarrow CH_3O\cdot + NO$ $CH_2\cdot + NO \rightarrow HCN + OH\cdot$ $CH\cdot + NO \rightarrow HCN + O\cdot$ $HCN + OH\cdot \rightarrow HNCO + H\cdot$ $HCNO + H\cdot \rightarrow \ldots\ NH_{i=1,2,3}$ $NH_2 + NO \rightarrow N_2 + H_2O$ $2\ CO + 2\ NO \rightarrow N_2 + 2\ CO_2$ $NO + H_2 \rightarrow NH\cdot + OH\cdot$ $NH_{i=0,1,2} + H\cdot \rightarrow NH_{j=1,2,3}$ $2\ NO_2 \leftrightarrow 2\ NO + O_2$	Nitrogen oxides are reduced mainly to nitrogen with minor amounts of ammonia and cyanides in the reducing atmosphere. Upward of 100 significant elementary-step reactions may beimportant. The reactions between the methyl radical and NO_x species are thought to be important mechanisms for NO_x destruction under these reforming conditions, especially for NO_2, based on prior tests conducted by the INEEL.
Overall C-NO_3 REDOX Reactions	$5\ C + 4\ MNO_3 \rightarrow 2\ M2CO_3 + 2\ N_2 + 3\ CO_2$ $5\ C + 4\ MNO_3 + 2\ Al_2Si_2O_7{\cdot}2H_2O \rightarrow 4\ MAlSiO_4 + 2\ N_2 + 5\ CO_2 + 4\ H_2O$ $3C + 4\ MNO_2 \rightarrow 2M_2CO_3 + 2N_2 + CO_2$ $3C + 4\ MNO_2 \rightarrow 2M_2O + 2N_2 + 3CO_2$	The most efficient C: MNO_3 and C:MNO_2 REDOX reactions produce N_2 and no CO, H_2, or C char. The most efficient C:NO_3 mole ratio is 1.25 to 1. The most efficient C:NO_2 mole ratio is 0.75 to 1. Numerous REDOX reactions can be written that produce various proportions of reduced or incompletely oxidized products including NO, N_2O, HCN, NH_3, H_2, CO, or C. These are all less efficient or summed with water-gas reactions. When incompletely reduced or oxidized species are included in the reaction products, the C:NO_3 mole ratio is higher than 1.25 to 1 and the C:NO_2 ratio is higher than 0.75:1, because the carbon is less efficiently utilized to convert NO_x to N_2.

2.5 Fluidized Bed Dynamics

Prior fluidized bed research programs at the INEEL have investigated fluidized bed particle dynamics theory. The following discussion is largely extracted from Boardman, 2004.

2.5.1 Particle Dynamics

Stable fluidized bed particle dynamics requires a balance between the production of fines and control of particle growth in the fluidized bed. However, excessive particle growth can lead to defluidizing agglomerations. The production of particles small enough to be elutriated with the upward moving gases must be minimized while producing a sufficient amount of small "seed" particles to provide nuclei for particle growth. Uniform feed deposition on the particles requires a uniform nozzle spray pattern and thorough mixing of the bed while the product is continually drawn from the bed to maintain a constant bed height. Buildup of particle agglomerates (caking) in the bed, on the vessel walls, on the vessel appurtenances, or on the feed nozzles must be avoided. The combined processes that affect the particle size distribution are illustrated in Figure 2.3-1. In order to maintain steady bed particle fluidization and dynamics, a target mean particle diameter must be achieved while the bed is withdrawn at the same rate as it is generated. This requires a balance between building the bed (increasing the particle diameters) and generating seed particles. If an excessive amount of fines are generated, or if the diameters of the fines are too small, then the fines will be elutriated from the bed, causing excessive loading on the off-gas cleanup equipment and possibly resulting in a product that is difficult to pneumatically transport. It is desired to maintain bed media particle sizes within the area marked "size interval" in Figure 2.3-1.

Fines generation is accomplished by two mechanisms: particle attrition and flash vaporization. The product to fines ratio (P/F) is a measure of the mass ratio of the product and fines generated during a test.

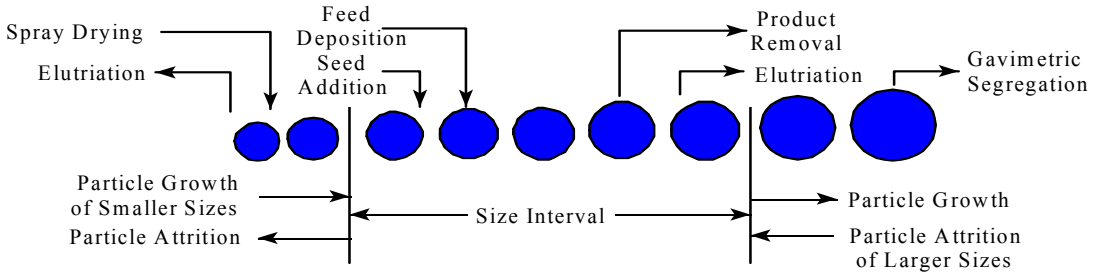

Figure 2.3-1. Processes that affect the particle size distribution during fluidized bed operation.

The mass of product includes bed that was built (or lost) during the test; therefore, the P/F can be determined by the following equation:

$$P/F = (P + FB - (SB - COT\ 0\ P\&F))/F$$

where

P/F = product-to-fines ratio

P = mass of product collected during the test (excluding COT 0)

FB = mass of the final bed

SB = mass of the starting bed

COT 0 P&F = mass of product and fines collected at COT 0 hr

F = mass of fines collected during the test (excluding COT 0).

The gas atomizing the feed is believed to control the particle size through jet grinding and control of feed droplet size. Increasing the velocity of the atomizing gas increases the momentum of the feed spray, until sonic velocity is reached. This increases the intensity of the particle-particle collisions in the vicinity of the feed nozzle, resulting in collisions that cause particle fracturing (attrition). The fluidizing air circulates the bed and causes particle collisions, but the fraction of fines attributed to the fluidizing air is considered minor compared to the feed nozzle atomizing gas. A separate jet grinder is sometimes used to control particle growth in order to conserve feed conditions and to prevent feed nozzle wear. Sufficient atomizing gas is necessary to avoid excessively large droplets from being introduced to the fluidized bed that may lead to localized overcooled granules and possible formation of larger agglomerations of bed particles that could cause defluidization of the bed and failure of the operation. Conversely, increased atomizing gas rate and velocity can produce a finer distribution of spray over the bed region; but if excessive, this may lead to undesirable fine particles that elutriate from the bed.

Particle elutriation is affected by the fluidizing gas velocity at the top of the bed and by bubble eruption at the bed surface. As the gas bubbles burst at the surface, both large and small particles are ejected up into the particle disengaging section. The fines that are entrained in the gas stream can be carried into the off-gas system unless they lose momentum and disengage from the off-gas in the freeboard section above the calciner bed. Most of the larger particles fall back to the bed; however, some of the fines remain entrained and are carried over into the off-gas cleanup train. Particles that have a terminal velocity that is lower than the gas velocity in the disengaging section ("freeboard") of the fluidized-bed will tend to be carried out with the off-gas, while particles that have a terminal velocity higher than the gas velocity in the disengaging section of the fluidized bed will tend to be disentrained and fall back into the reactor. It is therefore instructive to understand the relationship between bed fluidizing velocity and particle terminal velocity to bound operating conditions that will result in excess fines carryover.

Figures 2.3-2 and 2.3-3 illustrate the concept of the minimum calculated bed fluidization velocity and particle terminal velocity as a function of particle diameter for various particle densities. Both charts indicate the fluidizing gas velocity of approximately 0.59 m/s at the bed "surface," which is the approximate gas velocity for this test based on the total flow rates of fluidizing gas, vaporized water in the feed, atomizing gases, and instrument purges. The corresponding terminal velocity plot indicates that all particles of diameter less than about 80 μm can be lost or elutriated from the bed, with all other considerations—such as ejection of particles from bed turbulence as gas bubbles erupt at the bed surface, particle-particle collisions, particle-wall collisions, and localized gas velocity variations due to bed turbulence or variations in local temperatures and pressures—not being taken into consideration. In reality, some smaller particles are not elutriated, and some larger particles are elutriated, because these other considerations can be significant.

The particle size distribution (PSD) and average particle size are indicators as to whether agglomeration of the bed is occurring. Two common methods of determining the "average" particle sizes are the mass-mean particle diameter (MMPD) and the harmonic mass mean diameter (HMPD). The

MMPD signifies the mass-mean particle diameter where half of the mass is attributed to particles of lesser diameters and the other half to particles of larger diameters. The HMPD is the size of the particle that has

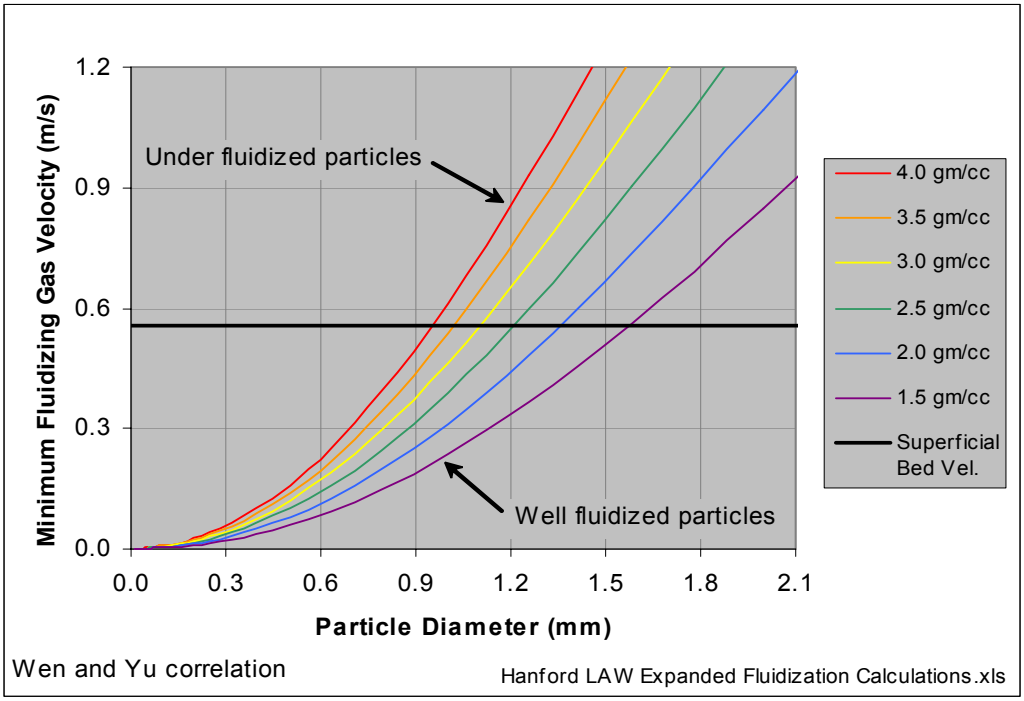

Figure 2.3-2. Minimum theoretical fluidization velocity as a function of particle diameter and density.

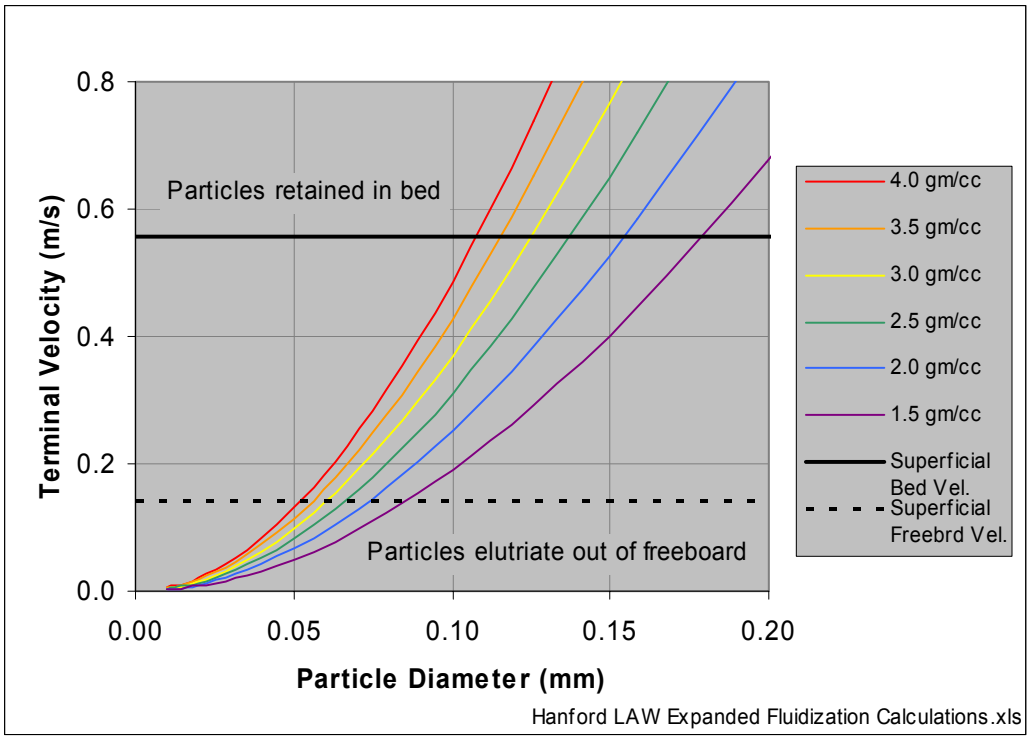

Figure 2.3-3. Theoretical particle terminal velocity as a function of particle diameter and density.

the same surface-area to volume ratio as the average of the entire bed. The MMPD is readily skewed toward the larger particles because the mass of the particles is proportional to the cube of the particle diameter (assuming nearly spherical particles). The HMPD is more sensitive to the smaller particles because they have a higher surface-area to volume ratio. The HMPD is used when calculating pressure drop through the bed (i.e., Ergun equation) and minimum fluidizing gas velocity. Close agreement between the MMPD and HMPD indicates a narrow particle size distribution. Divergence between the MMPD and HMPD indicates a wide particle size distribution or the presence of extreme particle sizes (e.g., significant quantities of coarse agglomerates or fine "flour") that differ from the particle sizes in the bulk media. Although the HMPD is used for calculating fluidizing gas velocity requirements, both numbers have value in monitoring dynamic changes in the bed particle size distribution.

The PSD, if plotted as the cumulative percent less than the screened particle size as a function of the particle size, usually forms an s-shaped curve. A PSD with very little size variation, as is normally the case with the starting bed, is indicated by a very steep center section of the curve. A gradual slope in the center section indicates a wider variation in particle size. Departure from an s-shaped curve indicates two or more dominant chemical or physical mechanisms controlling particle growth. For example, bed agglomeration results in a bi-modal particle distribution with a particle accumulation at a high particle diameter channel. Severe bed attrition can result in small particle (fines) buildup. Ideally, particle growth will be balanced by particle attrition, resulting in a steady state MMPD and HMPD.

2.5.2 Feed Droplet Evaporation

Fine particles are generated by flash evaporation of the liquid droplets before and after adhering to the bed particles. Some liquid droplets sprayed into a slugging fluidized bed, such as in the pilot-scale

FBSR tests, might not immediately impact bed particles, as the atomizing gas and flux of evaporated feed gases may tend to push bed particles away from the droplets. This may be most prevalent at the instant in time when a gas bubble, with few entrained particles, passes in front of the feed nozzle. A theoretical analysis has been done (Boardman, 2004) to bound the distance that atomized feed droplets of certain sizes might go before they are fully evaporated, assuming they do not contact any bed particles prior to evaporation. This distance has been a concern because (a) the formation of very fine particles is not desired, as they might easily elutriate from the bed, and (b) if the distance is far enough, then there is a chance that liquid feed droplets might impact on the vessel wall opposite to the feed nozzle, resulting in a buildup of solid material at that location.

The current feed nozzle design produces a finely divided mist in order to enhance uniform deposition on the bed particles. The atomized feed droplets, if they do not contact any solid surface including bed particles, evaporate according to the "d-squared" evaporation law [Kuo, 1986]:

$$d^2 = d_o^2 - [8 \frac{\rho_{air} D_{H_2O,gas}}{\rho_l} ln(1 + B)]t$$

where B is the Spaulding transfer number calculated from the following relationship,

$$B = C_{p,l} \frac{(T_\infty - T_s)}{\Delta H_v}$$

(with standard convention for all symbols). The longest possible droplet life, when droplets do not contact any bed particles, is thus a direct function of the properties of the gas, the temperature difference between the droplet surface and the surroundings, and, most importantly, the initial diameter of the feed droplets size. Hence, the feed droplet size can be increased to offset enhanced flash evaporation at elevated bed temperatures. However, droplets that are too large can impinge on the far wall of the fluidized bed if they do not first impinge on bed particles. This impingement can occur during slugs of fluidizing gas in a slugging fluidized bed. Larger droplets can also result in single particle quenching when they do hit a bed particle, which can give rise to possible particle-particle sticking (agglomeration) when the excessive liquid dries on the particle.

Figure 2.3-4 shows a plot of the theoretical extinction time for a droplet of water in a humid nitrogen gas stream at 600 and 700°C, respectively. The droplet life accounts for particle heating by conduction to the droplet, assuming that the velocity of the droplet is equivalent to the velocity of the surrounding gas. This assumption is a reasonable approximation for droplets that are atomized by the co-flowing atomizing gas. *These calculations assume that the atomizing gas is already at the bed temperature*. In reality, the atomizing gas must first be heated to the bed temperature; hence, the actual time of flight in non-obstructed space exceeds the correlation shown in Figure 2.3-4. This chart reveals, for example, that a 0.050-mm (or 50-micron particle) will be flash dried in 0.018 s (or 18 milliseconds).

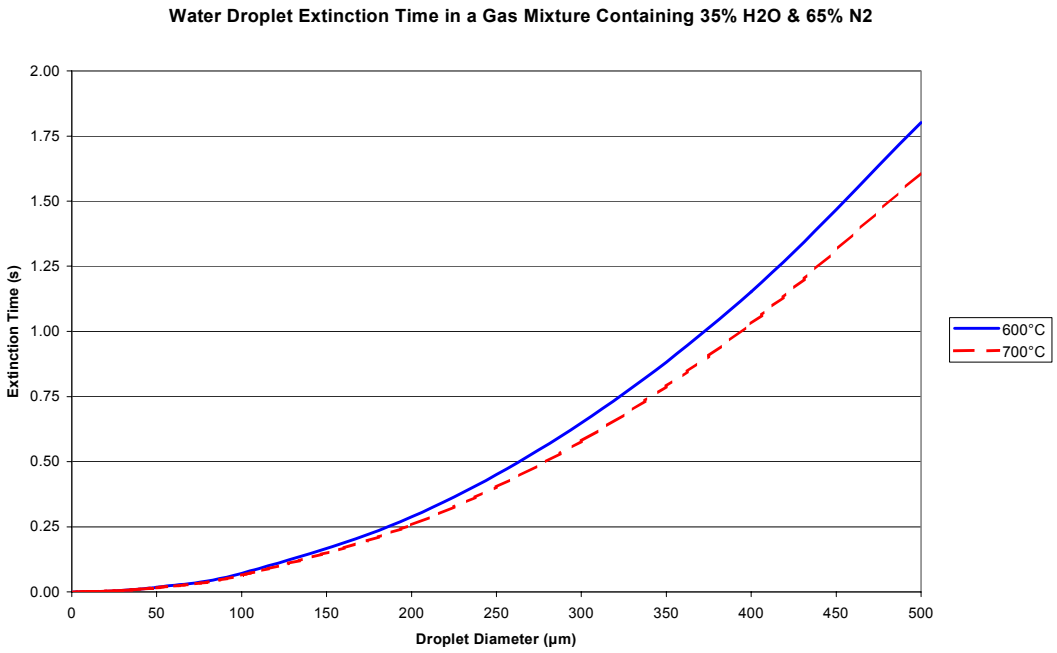

Figure 2.3-4. Comparison of droplet extinction time in a gas stream of 600 and 700°C (0 to 500 mm diameter particle size range).

Consider the following example:

Assumptions:

- *Spraying Systems nozzle*. 40/100 liquid cap, 120 air cap
- *Gas orifice surface area*. 2.2 mm^2
- *Liquid injection rate*. 6 $L \cdot hr^{-1}$
- *Nozzle atomizing air volumetric flow*. 3000 $L \cdot hr^{-1}$ (NAR = 500)
- *Gas temperature*. 600°C.

Then, using 2.3-4 and the gas velocity, the calculated extinction distance for a given water droplet is:

- *0.100 mm droplet*. 27 mm
- *0.200 mm droplet*. 80 mm

- *0.250 mm droplet*. 104 mm.

This example illustrates that a 0.250 mm particle leaving the nozzle at a spray angle of 35 degrees will impinge on the near side of a 150-mm diameter reactor (~91 mm actual distance to the wall) before it is fully evaporated, unless it impacts bed particles first. In order to minimize feed deposit on the wall, three conditions must be avoided; bed slugging (that periodically allows large gas bubbles to pass in front of the feed nozzle, providing an open path for atomized spray to the wall at that instant), "cold" surfaces in the reformer, and coarse atomization of the feed (that allows the formation of larger spray droplets). Nozzle spray testing with water and simulant feeds should be performed to determine the minimum NAR necessary to fully nebulize the waste feeds. The formation of nozzle accretions or restrictions in the nozzle, however, may disrupt the°spray pattern, resulting in large droplet formation that will likely exacerbate bed agglomeration and feed deposition on the wall or vessel appurtenances. Maintaining vessel wall and surface temperatures heated well above 400°C helps to prevent accretions from building on the surfaces because radiant heat transfer is sufficient to cause "film" boiling and the steam expelled from the droplets provide a protective gas barrier that prevents the droplets from physically contacting and wetting the surfaces.

°he calculations also show that the affect of temperature increase from 600 to 700 °C does not greatly affect droplet evaporation times. Thus, spray drying of droplets is more dependent on initial particle size.

Evaporation by film boiling on the surface of the particles increases at higher temperatures, resulting in the formation of small satellite particles that are easily ejected from the surface of the host particles. Film boiling results when the rate of heat transfer from the bed particles is high enough to cause rapid evaporation, which consequently prevents the droplets from wetting and adhering to a particle surface. Once the moisture is evaporated in the film layer above the particle, there may be insufficient adhesion of the residual solid to the surface of the particle, resulting in excessive production of fines.

Depending on the viscosity and surface tension of the feed and heat capacity of the solids, film boiling is observed at bed temperatures in excess of 600 °C. Above 700°C, film boiling has been considered severe for some fluidized bed operations, and, in fact, resulted in quantitative conversion of liquid feed to fines (i.e., P/F ratio of 0.05–0.1 observed at 700 °C in comparison to 0.5–0.75 at 625 °C). This phenomenon thus limits the bed operating temperature when feed is being atomized and the objective is to minimize fines generation.

2.5.3 Bed Turnover

Bed turnover plays a significant role in determining the fluidized bed operating characteristics and product quality when initiating the activity with a starting bed of significantly different composition than the material to be fed to the bed. It is defined as the mass fraction of the bed that represents the feed composition as compared to the starting bed composition. A bed turnover of greater than 90% is generally needed to ensure that the feed and bed material are indicative of the new product versus the behavior and characteristics of the starting bed.

Bed turnover at a particular time for an experiment is defined as:

$$TO = (1 - e^{-[P/W]})*100$$

where:

TO ≡ bed turnover percentage (%)

P ≡ cumulative net product mass (kg) [$P = Mass_{out} - Mass_{in} + W$]

$Mass_{out}$ ≡ mass of bed material harvested from the process (excluding the cyclone sample and filter catch)

$Mass_{in}$ ≡ mass of bed material added to the reactor [$Mass_{in} = Mass_0 + Mass_{augmentation}$]

$Mass_0$ ≡ mass of the initial bed charge

$Mass_{augmentation}$ ≡ mass of seed particles, catalysts, and recycled bed media added to the bed.

W ≡ bed mass including the unfluidized heel (kg) [$W = Mass_{fluidized} * (Mass_0 \div Mass_{0,\,fluidized})$].

$Mass_{fluidized}$ ≡ mass of the fluidized bed as seen by the instrumentation

The cumulative mass of removed product is *not* equal to the cumulative net product mass (P). This is because the mass of bed is changing over time as the bed density changes. Instead, the net product must account for the change in bed mass as well as the amount of product.

The bed mass (W) used in this equation is the total bed mass and not just the fluidized bed mass. For example, some amount of the bed resides in the bottom receiver of the reactor vessel. Since this material is not fluidized, it does not show up in the bed mass as indicated by the bed pressure drop or density measurements. However, the mass of this material must be included in the total bed mass when calculating the bed turnover.

3. EXPERIMENTAL SETUP/APPROACH

Mineralizing steam reforming process technology, offered by THOR^{SM} Treatment Technologies (TTT), LLC, under U.S. Patent No. 6280694, provided the basis for process materials and conditions utilized in this experimental program. The performing team consisted of personnel from INEEL, TTT, and SAIC. The mineralizing steam reforming process technology tests were performed by the team in the INEEL's pilot scale fluidized bed test system located at the SAIC STAR Center in Idaho Falls. The test system/equipment is briefly described in Section 3.2. The test data collection system/methods for process monitoring/control and the process/product materials sample collection and analyses methods utilized are described in section 3.3. The process specific input materials selected and utilized for the mineralizing steam reforming test are described in Section 3.4. Section 3.5 details the startup conditions and operational parameters that were planned.

3.1 Test Objectives

The overall objectives of the pilot-scale SBW tests were to 1) produce a mineralized product for use in validating and further developing correlations with laboratory scale experiments and product chemical/physical properties, 2) generate data that validates the operability of fluidized bed steam reforming with the appropriate waste mineralizing chemistry, 3) provide fundamental understanding of the chemistry and mineralization of waste forms in containing and holding radionuclide surrogates and hazardous contaminants, and 4) provide information about the longer term performance/durability of the mineralized product.

The pilot-scale tests were configured to provide data to satisfy the above objectives. They are summarized, prioritized in order of their perceived importance, in Table 3.1-1.

Table 3.1-1. Pilot scale mineralizing, steam reforming test objectives.

Objective Statement	Quantifiable Objective Target or Criteria	Measurable Parameters and Test Methods
Generate a product that incorporates sodium into the mineral forms of nepheline, sodalite, and nosean. Determine if product generated is leach resistant and durable. Determine the fate of radionuclides and surrogates (I, Cs, Re for Tc) and hazardous metal components (Cr, Ni, Hg, etc). [Note: For the most part, the product performance measurements will be conducted by SRNL, and reported separately.]	• <3 wt% soluble Na in bed product relative to product mass • <1 wt% soluble nitrate in bed product and fines particles. • <3 wt% carbonate in bed product • <1 wt% organic in bed product, exclusive of carbon added as reductant • Passes TCLP for hazardous metals • Results of PCT are comparable to EA glass • Performance is comparable to EA glass	• XRD/SEM analysis of product • Chemical analysis of product per sample analysis plan • Perform PCT and TCLP measurements for durability • Perform single pass flow through (SPFT) testing to measure performance
Produce a non-agglomerating bed product and fines fraction. Determine product bulk and true density. Maximize product to fines ratio.	• <10 wt% particle agglomeration/clustering relative to bed mass • P/F mass ratio >3.5 desirable to maximize the density (minimize the volume) of blended product	• Bed and fines size particle distribution and density trends • Product to fines ratio as calculated from measurement of product and fines cumulative masses
Determine suitable fluidized-bed operating parameters for treating the simulated SBW that will minimize carryover of unreacted carbon and clay additives in the filter product	• 80 hrs continuous operation at a feed rate of >3 L/hr blended feed • Uniform temperature distribution in bed with no greater than ±10ºC axial temperature variation in the bed • Bed height, as measured by bed pressure drop and bed density, to be maintained between 25 -28 inches. • Approach a controllable steady-state bed particle size distribution	• System flow meters, temperature indicators and pressure transducers • Gravimetric measurement of 8-hr bed samples and fines samples • MMPD and HMPD of 4-hr bed and fines samples density, agglomeration, etc.
Demonstrate acceptable material balance closure for major and minor constituents	• Material balance closure of ±10% for simulant constituents (Al, Na, K, Cl, F, NO_3, Cr, Re, I, etc.).	• Chemical analysis and mass measurements of FBSR products • Off-gas analysis with the continuous emissions monitoring instrumentation (CO, CO_2, Cl, etc.)
Demonstrate decomposition of nitrates, nitrites, and NO_X	• Achieve >80% destruction of NO_X off-gas emissions relative to nitrates and nitrites in the feed.	• Measurement of residual nitrate and nitrite in the FBSR solid products, and CEM NO_X measurements.

3.2

3.3 Test System Equipment

This section provides a summary description of the INEEL's pilot scale fluidized bed test system in the steam reforming processing configuration utilized for the SBW mineralizing tests reported herein. An overview of the FBSR test system is provided along with further description of selected key components/equipment of particular interest for this test.

The fluidized bed test system has been utilized to date to provide for a variety of fluidized bed steam reforming and calcination/oxidation process test conditions on various waste simulant materials for several potential liquid radioactive/mixed waste applications. The different tests have employed somewhat varied and evolving components and configurations appropriate to the particular process and waste application of interest, but most of the test system/components have remained the same.

3.3.1 FBSR Test System Overview

A simplified process flow and instrumentation diagram for the FBSR mineralizing process test system is shown in Figure 3.2-1. The fluidized bed section of the test system has a six-inch nominal inside diameter. Experience at the INEEL with pilot scale fluidized beds, ranging in diameters from as small as 3 inches up to 12 inches, has shown that a 6-inch diameter bed is typically the smallest size that still provides product bed particle attrition and growth dynamics that approach those of larger reactor beds. Even with a 6-inch bed diameter, the bed operates in an axial slugging mode for the fluidizing gas rates of interest, rather than the bubbling mode that would be more typical of larger-diameter, full-scale reactor beds. The axial slugging mode, however, provides the vigorous bed solids/gas mixing and large interface area for gas/solids contacting necessary for effective representation of the process thermal and chemical reaction conditions expected in a full scale fluidized bed reactor system. The 6-inch diameter bed is a reasonable compromise between a bed large enough to provide representative processing test data and a system small enough to control experimental parameters and minimize test permitting, operations, and waste disposal costs.

The FBSR test system/equipment consists of several primary subsystems including: 1) feed systems/equipment for gases, liquids/slurry, and small solids, 2) the fluidized bed reactor vessel consisting of the bed bottom receiver and fluidizing gas distributor section, the fluidized bed section, the upper larger diameter freeboard (bed particulate disengaging) section, and the vessel wall external heating system, 3) the process product/solids collection and management systems, 4) the off-gas treatment/emissions-control systems, and 5) the process monitoring and control system.

The FBSR test system occupies a space approximately 40 feet by 40 feet in area and 20 feet in height. All wetted components are constructed from corrosion resistant materials. Equipment and piping are fabricated from 300-series stainless steel except for the reformer vessel, which is fabricated from Inconel 800H. The system can be manually controlled or automatically controlled using a Process Logic Controller (PLC) system with multiple human-machine interface (HMI) stations. The STAR Center provides for all necessary test system utilities and support services including electrical power, water, compressed air, nitrogen, oxygen, various specialty calibration gases for continuous emissions monitoring systems, test system operations, permits, and materials/wastes management.

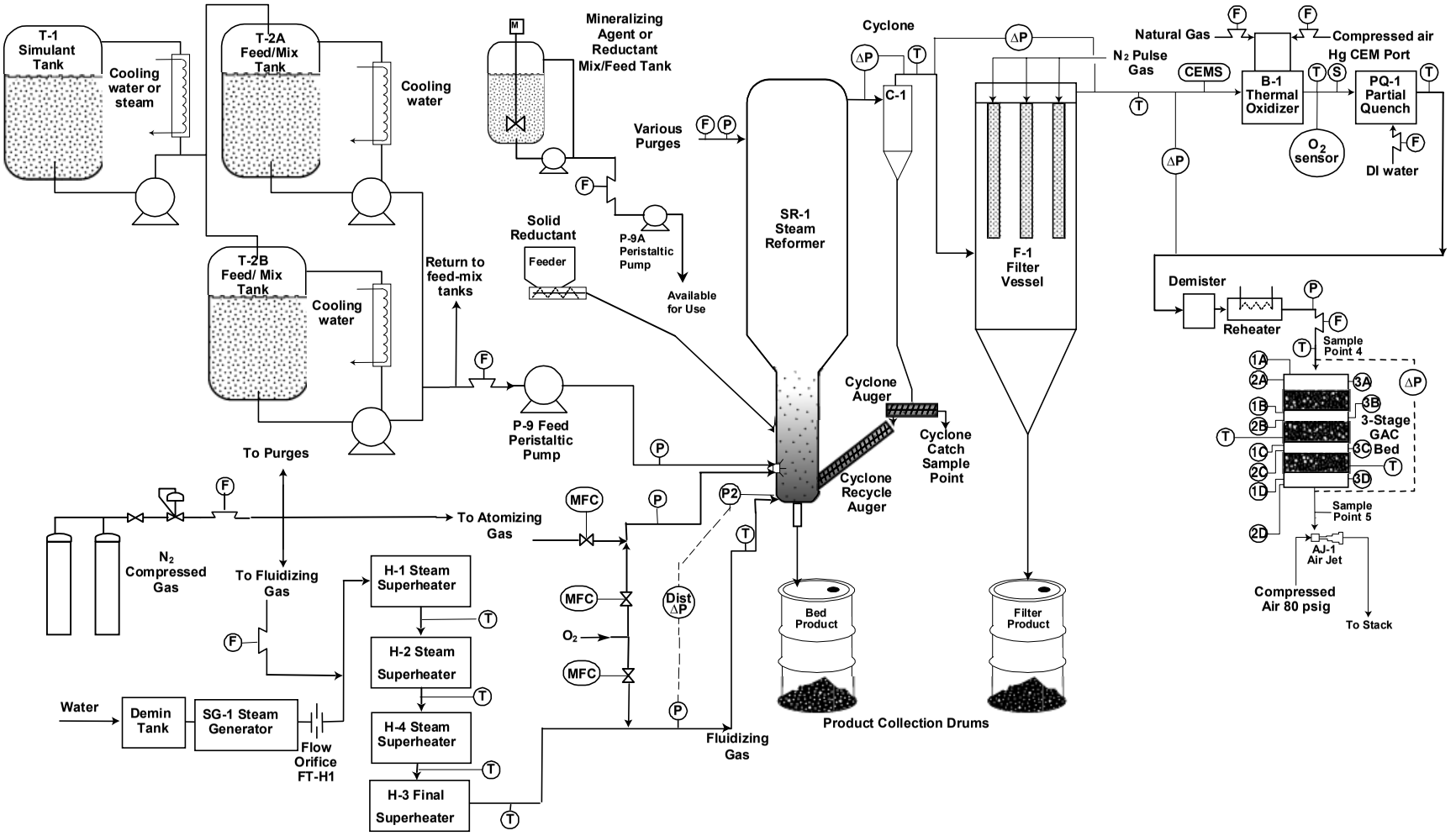
T-1 Simulant Tank
Cooling water or steam
T-2A Feed/Mix Tank
Cooling water
T-2B Feed/ Mix Tank
Cooling water
Return to feed-mix tanks
Mineralizing Agent or Reductant Mix/Feed Tank
Various Purges
Solid Reductant
Feeder
P-9A Peristaltic Pump
Available for Use
P-9 Feed Peristaltic Pump
SR-1 Steam Reformer
Cyclone
C-1
Cyclone Auger
Cyclone Catch Sample Point
Cyclone Recycle Auger
F-1 Filter Vessel
Natural Gas
N2 Pulse Gas
CEMS
B-1 Thermal Oxidizer
O2 sensor
PQ-1 Partial Quench
Compressed air
Hg CEM Port
DI water
Demister
Reheater
Sample Point 4
3-Stage GAC Bed
Sample Point 5
AJ-1 Air Jet
Compressed Air 80 psig
To Stack
To Purges
To Atomizing Gas
N2 Compressed Gas
To Fluidizing Gas
MFC
O2
Dist ΔP
Fluidizing Gas
H-1 Steam Superheater
H-2 Steam Superheater
H-4 Steam Superheater
H-3 Final Superheater
Water
Demin Tank
SG-1 Steam Generator
Flow Orifice FT-H1
Bed Product
Filter Product
Product Collection Drums

Figure 3.2-1. Process flow diagram for the fluidized bed mineralizing steam reforming demonstration.

3.3.2 **Fluidized Bed Reactor Vessel**

The fluidized-bed reactor vessel (shown in Figure 3.2-2) is made of Inconel 800H pipe to tolerate operating conditions, including temperatures that could reach 800 ^{O}C, oxidizing or reducing conditions, and the presence of corrosive or hazardous materials. The main features of the fluidized bed vessel are the fluidized-bed section and the freeboard (particle disengaging) section. The stainless steel bottom bed receiver and gas distributor section (shown in Figure 3.2-3) provides the reactor bottom vessel closure and entry/distribution for the fluidizing gas.

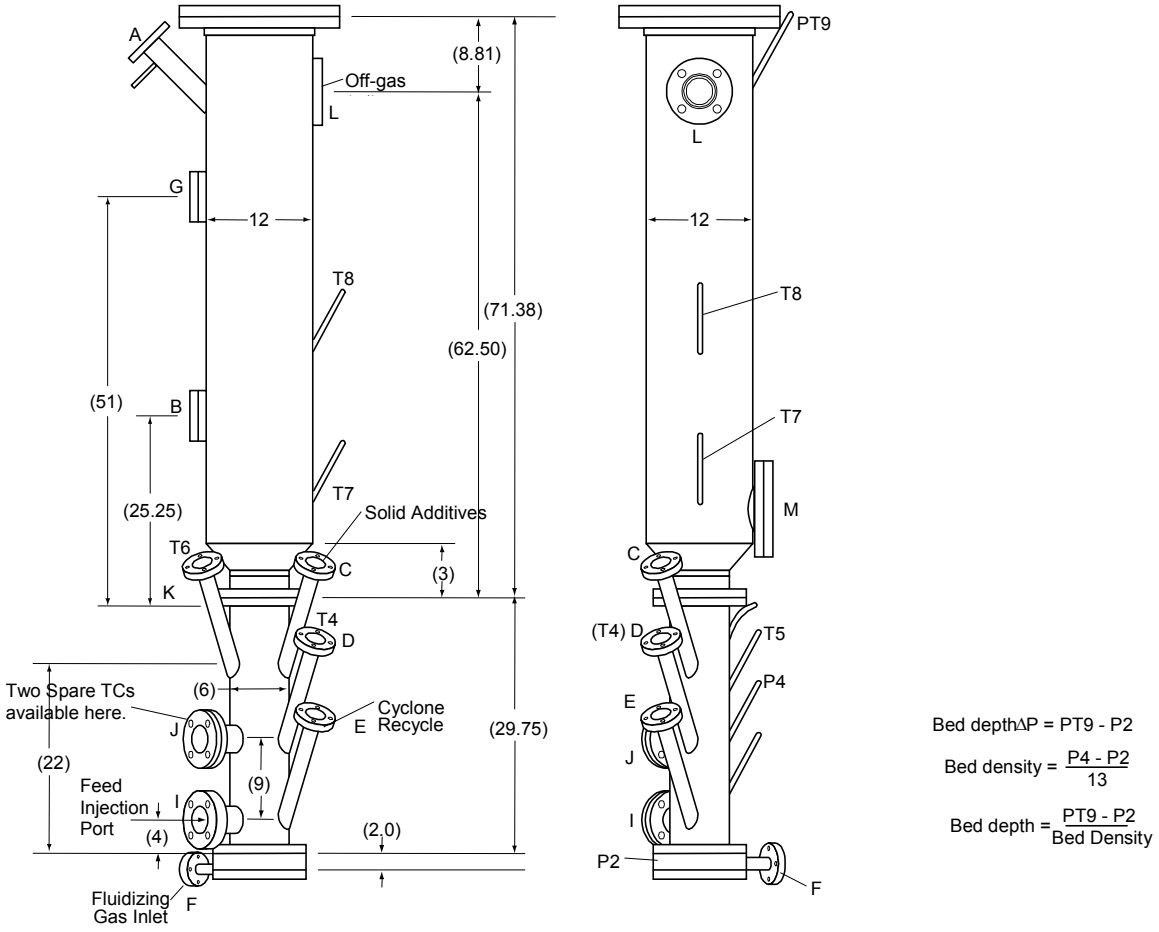

Figure 3.2-2. Fluidized bed reactor vessel.

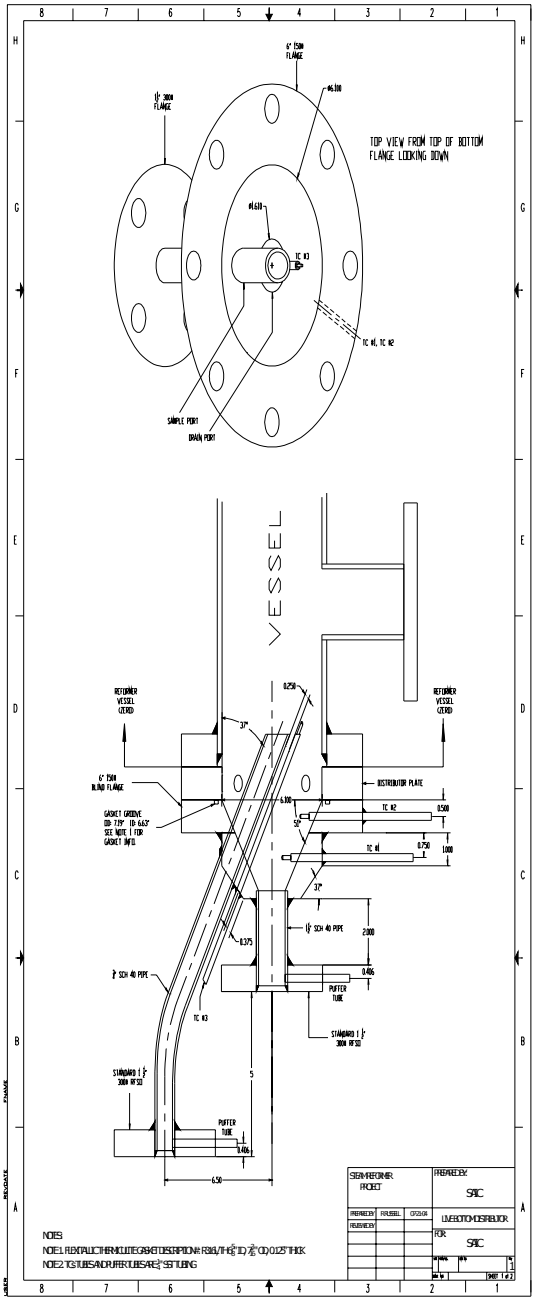

Figure 3.2-3. Reactor/reformer vessel bottom receiver.

The vessel bottom receiver consists of 6-inch, 150# flange and flat stock machined and welded to provide a conical type bottom that will collect static bed materials and facilitate the in-process removal/draining of product bed, agglomerates, and nozzle accretions through a standard 1 ½ -inch drain pipe. The bottom receiver also provides for a ¾-inch sample tube/riser for fluid bed sample collection and three thermocouples for bottom bed region temperature measurement. One thermocouple (TC3) extends into the fluid bed along with the sample tube and the other two (TC1 and TC2) extend into the conical bottom bed region. Small purge/pulse gas ports are also provided both in the bed sample and drain port flanges/receivers to loosen, if necessary, collected/static product bed granules or larger agglomerates for in-process sampling/draining.

Locations of process inputs and outputs, and of pressure and temperature sensors, are shown in Table 3.2-1. The simulant feed is fed through a gas-atomized nozzle in Port I, located four inches above the top of the distributor flange.

Table 3.2-1. FBSR vessel process inputs, process outputs, and sensors.

Item	Location	Axial distance above top of distributor flange, inches	Radial distance from inner wall, inches
Distributor	Distributor flange	~-0.5	---
Simulant feed nozzle	Port I	4	Air cap is flush with wall; liquid nozzle penetrates $1/16^{th}$ inch past the air cap
Cyclone recycle	Port E	4	0
Carbon reductant addition	Port C	22	0
T1	Bottom of bottom receiver	-2.75	0.5
T2	Top of bottom receiver	-1.5	0.5
T3	Coaxial with the bed sample tube	1.5	1.0
T4	Port D	12	1.0
T5	Port T5	17	1.5
T6	Port K	21	0.5
P2	Distributor flange	-0.5	0
P4	Port P4	13	1.0

The fluidizing gas distributor bolts in between the reactor vessel flange and the bottom receiver flange. A pressure measurement port is provided through the side of the distributor flange for measuring local static pressure in the bed/vessel at the distributor elevation and for use in determining tot al bed height and bed density from differential pressures. The pressure drop of fluidizing gas flow across the distributor is designed to be sufficient ($\Delta P_{dist} \geq 14$"WC) for the range of bed fluidization gas flows/velocities needed to properly fluidize bot h the starting bed and later product bed materials, which

can be of different particle density and size, and to prevent backflow of particulate into the distributor.

Various fluidizing gas distributor types are possible and several different designs have been utilized and described in earlier test reports. The fluidizing gas distributor utilized for this mineralizing steam reforming test was a THOR^{SM} Treatment Technologies, LLC proprietary design.

Direct observations of the fluidized bed flow convection cells and fluidization mode cannot be made in the 6-inch steam reformer reactor vessel during processing test operations. Prior to the mineralized steam reforming tests the FBSR vessel bed section was modeled using a Plexiglas tube and suitable bed material, so that a visible representation of the likely bed fluidization/flow patterns could be obtained and photographically recorded in comparative cold flow tests of the INEEL ring distributor [Soelberg, 2004b] and the THOR^{SM} distributor. The objective was to obtain a qualitative visual comparison of the fluidization of bed material and flow patterns resulting from the gas injection points and differing distributor geometries, rather than to evaluate distributor pressure drop. The distributors utilized were from existing available stock and selected to have similar pressure-drop values during operation. Hydraulic similitude was considered in establishing the cold flow test conditions.

These ambient temperature hydraulic similarity tests showed that both the THORSM and INEEL distributor designs adequately fluidize the bed. The emulsion phase was observed to be in motion at all points in the bed and around the bottom flange at the elevation of the distributor. The bubbles emanating from the THOR^{SM} distributor were visible near the edge of the supporting flange, but not along the reactor wall farthest away from the distributor. The ring distributor bubbles were seen at the reactor wall around most of the reactor circumference. By all appearances, the ring distributor seemed to distribute the gases more uniformly in the immediate vicinity of the distributor than the THOR^{SM} distributor. The movement of the emulsion phase appeared to be independent of the distributor type and configuration at the elevation of side port I in the reformer vessel (location of the liquid/slurry feed atomization nozzle).

3.3.3 Solids/Fines Collection

Solid and gaseous materials are produced during the fluidized bed reactor processing of simulated wastes and additive feed materials. The solid particles of sufficient mass remain fluidized within the bed and are sampled/drained into containers as appropriate through manually operated valves and piping that comprise interlock sections located beneath both the bed sample tube and the bed bottom receiver drain tube ports in the reactor bottom receiver assembly. The gases and smaller entrained solids (fines) exit the fluidized bed reactor vessel freeboard section and flow through a 6-inch diameter cyclone separator designed to remove >98% of 5 μm or larger solid particles when operating at design flow conditions. The off-gas exiting the cyclone is subsequently further filtered for remaining very small entrained particulate in a “hot candle filter”. This “hot filter” consists of a stainless vessel containing seven 2.5-inch-diameter, 24-inch-long, sintered-metal filters with a nominal pore size of 2 μm.

The solids collected in the cyclone (cyclone catch) during this steam reforming process were continuously drained and recycled to the fluidized bed through a series of two augers. The first auger can be operated in either a forward or reverse rotation. With the forward rotation, the cyclone catch is fed into the second auger, which pushes the product through port E (Fig 3.2-2) into the bottom of the fluidized bed section of the reactor vessel. When the first auger is operated in reverse, the cyclone catch is drained and subsequently collected in a sample container, which is located below two valves in the drainpipe in order to provide for process pressure isolation and minimize air in-leakage during sampling. With the exception of the cyclone solids collected during sampling events, the cyclone catch was

continuously recycled to the fluidized bed.

The hot filter particulate catch is collected continuously and drained into a filter fines/product container located below the filter vessel. The product container is periodically emptied and weighed for material balance closure and to obtain samples for analyses.

3.3.4 Process Feed Systems

Various materials in the form of liquids, solids, and gases are provided through several feed subsystems in order to obtain desired process materials and conditions in the fluidized bed reactor. For the mineralizing steam reforming process the primary liquid feed is a slurry consisting of the liquid waste simulant solution mixed with selected amounts of an insoluble powdered solid (clay) as a mineralizing additive. The primary dry solid feed materials are granular carbon and initial starting bed media (alumina grit). Process feed gases consist of fluidizing gas (superheated steam), atomizing gas (nitrogen and oxygen), and minor purge gas (nitrogen).

3.3.4.1 *Liquid Feed System*

The liquid feed system consists of three tanks equipped with variable speed agitators and a recirculation/transfer pump to ensure that solutions are fully mixed and that insoluble solids remain suspended and uniformly blended (e.g., clay additive solids in the mineralizing process waste feed/slurry).

The liquid waste (SBW) simulant from the simulant solution tank is mixed with the powdered clay additive in the feed mixing tanks and the resulting slurry mixture is continually recirculated through the feed/mix tanks with recirculation pumps. A peristaltic pump provides a slipstream of this slurry to the fluidized bed. A coriolis mass flow meter in this slipstream line is used for measurement and control of the liquid/slurry flow to the fluidized bed. The liquid/slurry waste simulant feed enters the fluid bed as an atomized spray via an atomizing nozzle located in Port I of the reactor vessel (see Figure 3.2-2).

Several different, and readily available, liquid feed atomization nozzle types and sizes had been previously evaluated over a range of potential slurry mixtures of clay and liquid waste simulants (SBW and LAW) prior to the SBW Sagger clay FBSR test [Olson, 2004]. These evaluations were performed in an initial effort to understand and improve longer-term atomization performance with slurry feed, including efforts to minimize the formation of nozzle deposits and accretions which could contribute to forming bed defluidizing agglomerations during FBSR operation.

The evaluations led to design, selection, and utilization of a variation of the SprayCo® nozzle design, designated the Marshall/Eldredge nozzle design, with unique modifications to prevent or minimize the formation of process solid deposits on the nozzle surfaces exposed to the fluidized bed. Based on the prior nozzle evaluations and test activities, and acceptable performance in the subsequent Hanford LAW tests, a version of the Marshall/Eldredge nozzle design was further adapted and utilized for the SBW Sagger clay FBSR test. The basic design features and configuration of the Marshall/Eldredge nozzle remained the same, but various atomizing gas orifice dimensions were reduced to increase the atomizing gas velocity at the atomizing gas flow rate used in the FBSR test.

A brief set of cold slurry feed atomization tests was conducted using two different sized nozzles, just prior to the SBW-Sagger clay FBSR test, to (a) verify atomization performance and flow control parameters and (b) select which of the two nozzles to use. These ambient temperature atomization tests, and associated SBW slurry viscosity evaluations, are reported in Appendix B.

The nozzles essentially consist of two concentric tubes, an inner liquid flow tube and an outer

concentric gas flow tube. Liquid/slurry flows within the inner tube, while an atomization gas flows in the concentric gap formed between the ID of the larger outer tube (the gas flow tube) and the OD of the inner tube (the liquid flow tube). The larger nozzle's dimensions were 0.100-inch ID and 0.150-inch OD liquid tube and a 0.170-inch ID air tube which yields a 0.010-inch concentric gap for atomizing gas flow and an atomizing gas cross sectional area of 0.0050 in^2, consistent with the original SprayCo® nozzle dimensions. The smaller nozzle used smaller diameter concentric tubes with liquid tube dimensions of 0.071-inch ID and 0.120-inch OD and a 0.141-inch ID air tube; which yields a 0.011-inch concentric gap for atomizing gas flow and atomizing gas cross sectional area of 0.0043 in^2. The smaller nozzle dimensions were designed to accommodate a range of anticipated lower SBW slurry flow rates while providing for similar or higher atomization gas flow rates and relatively higher gas velocities. A higher gas velocity provides increased atomization energy for a given gas flow rate. A sonic exit gas velocity is desired, if possible, to avoid vessel/bed pressure pulses from influencing atomizing gas velocity/flow. The smaller nozzle was selected for use during the FBSR test based on results of the cold slurry nozzle atomizing tests (Appendix B).

The nozzle atomization tests were performed using a less hazardous SBW lite simulant. The SBW lite was prepared with the main constituents of the SBW simulant (HNO_3, $NaNO_3$, $Al(NO_3)_3$, and water) without the minor constituents and hazardous metals. This lite simulant was shown to have essentially the same density and viscosity as the SBW simulant. Two different slurry mixtures (217 and 250 g Sagger clay (as received) per liter of SBW lite were tested. Both nozzles atomized the 217 g/L slurry to 0.1 – 0.2 mm MMPD when the slurry flow rate ranged from 2-5 kg/hr, the atomizing gas ranged from 1.5 – 3 kg/hr, and the NAR was about 1,100. The smaller nozzle provided better atomization at NARs below 1000, achieving atomization between 0.1 – 0.2 mm at NARs as low as 700. Both nozzles could atomize the slurry to less than 0.1 mm at NARs above 1,000 and atomizing gas flow rates above 3 kg/hr for slurry flow rate between 2-5 kg/hr. The large nozzle was not tested with the 250 g/L slurry. The smaller nozzle atomized the 250 g/L slurry to 0.1 – 0.2 mm MMPD when the slurry flow rate was 4 kg/hr, the atomizing gas ranged from 2 – 3 kg/hr, and the NAR was 700 – 1,000. The 250 g/L slurry at 4 kg/hr was atomized using the smaller nozzle almost as well as the 217 g/L slurry at the same flow rate.

As expected, better atomization (smaller atomized droplets) was achieved at higher NARs and higher atomizing gas flow rates. Lower slurry flow rates required higher NARs and higher atomizing gas flow rates to achieve the same degree of atomization that lower NARs and lower atomizing gas flow rates achieved for higher slurry flow rates. The nozzle with the smaller atomizing gas cross section area (providing a higher atomizing gas velocity) achieved better atomization (smaller droplets) without plugging than did the larger nozzle. Both nozzles achieved better atomization than did nozzles used in prior FBSR tests at higher concentrations of clay with either SBW or Hanford LAW simulants. The smaller nozzle was selected for the SBW FBSR test since it appeared to provide the best performance for the SBW slurry simulant.

A minimum NAR of 800 (for the small nozzle) and 1,000 (for the large nozzle), and a minimum atomizing gas rate of 2 kg/hr (for the small nozzle) and 3 kg/hr (for the large nozzle) were recommended operating limits for the SBW FBSR test. These values were recommended in order to best control the atomized particle size at average sizes near or below the bed particle size.

Liquid atomization depends on, among other factors, the liquid viscosity. In conjunction with the nozzle atomization tests, relative viscosity measurements were made for the SBW simulant and compared to measured viscosities for water and Hanford LAW simulant, with and without slurried clay. The viscosity measurements are also summarized in Appendix B.

3.3.4.2 *Solid Feed Systems*

Solid carbon utilized as a reductant material in the steam reforming reaction process is metered into the process by a vibratory feeder. The hopper of the vibratory ramp feeder is manually charged with a batch of carbon that is then fed via a controlled vibratory ramp to a small weigh hopper/funnel mounted on a load cell. The weigh hopper records and discharges a small feed batch to a feed pipe lock hopper section bounded on the inlet and outlet by two ball valves that operate sequentially to form the lock hopper. Nitrogen gas purges in the lock hopper/pipe keep atmospheric air from entering the process with the carbon feed and provide minor motive force to loosen and inject the low density carbon granules into the bed. This system is calibrated for the specific carbon that is used, and the PLC controls the carbon feed rate near the desired value.

Starting bed solid granular material (e.g. alumina grit) and any similar subsequent solid additions to the bed are made by simple manual batch feed and gravity drain through vessel port C (Figure 3.2-2). The two-valve lock hopper prevents process pressure disturbance and air in-leakage. Materials of sufficient density subside into the fluidized bed without further assistance. Other granular solid additions to the bed can also be made via the carbon feed/funnel system.

3.3.4.3 *Gas Injection Systems*

Process gases supplied to the fluidized bed include the reactor bed fluidizing gas and the atomizing nozzle gas. The fluidizing gas used for this steam reforming process was superheated steam. Nitrogen, along with a small amount of oxygen, was used as the atomizing nozzle gas. Moving the necessary small oxygen injection to be a part of the atomizing gas flow rather than a part of the fluidizing gas was a small, but important change that is further discussed below. Nitrogen was also used for a variety of small instrument and feed line purges, hot filter pulse gas, etc. Air was utilized as the oxidizing gas in the off-gas system thermal oxidizer.

Compressed air is utilized in various other portions of the system for functions external to the process, such as pilot valve operations and the facility gas eductor pump. The system is configured to provide compressed air from a diesel-powered compressor.

Small amounts of various bottled specialty gases are also utilized in periodic calibration of the off-gas monitoring instruments (CEMs), but do not enter the process flow.

The fluidizing steam is generated by the test system in a small steam generator/boiler and super-heated in electrical resistance Inconel tube heaters, which include customized 303 stainless steel mesh internals for improved heat transfer to the fluidizing gas at low flow rates. The superheater element (pipe) temperatures are maintained just below a maximum operating temperature limit of 1,100°C. The maximum fluidizing gas temperatures achievable at the super-heaters' exit may vary as a function of the fluidizing gas properties and mass flow rates, but is generally close to the operating bed temperature. Supply lines from the super-heaters to the vessel fluidizing gas distributor are insulated to maintain temperatures as high as possible.

Small amounts of oxygen necessary for desired exothermic reactions that provide internal heat generation for the FBSR process were previously introduced as a part of the fluidizing gas (steam) in earlier FBSR tests. Based upon previous operational experience the pilot scale system was modified for the SBW mineralizing tests, such that oxygen was introduced as a part of the nozzle atomizing gas. Adding necessary process oxygen with the atomizing gas, rather than the fluidizing steam, was expected to have several benefits all of which improve the capability to provide additional sensible heat energy to the reactor bed.

When cold oxygen was commingled with the superheated fluidizing steam in previous tests, the

temperature of the fluidizing gas mixture dropped 50 – 80°C below that of the steam alone, dependent on the flow/concentration of the oxygen in the resulting stream. The cold oxygen flow displaced some of the potential superheated steam in the total flow of fluidizing gas. The flow of fluidizing gas necessary for fluidization of the small product particles in the mineralizing process was already low, and displacement of steam with oxygen further reduced the steam flow rate required from the superheaters, leading to reduced heat transfer in the steam superheater and lower steam temperature/superheat. Injecting the oxygen as part of the atomizing gas, instead of with the fluidizing steam, eliminates these cooling effects associated with displacement of a portion of the high temperature steam as the fluidizing gas.

Furthermore, oxygen added to the atomizing gas displaced nitrogen, which was simply an inert and cold gas diluent in the process. Displacing some of the atomizing nitrogen with the oxygen reduced the total mass flow rate of the off-gas, provided for a longer gas residence time in the reformer and increased concentrations of gas-phase reactants (steam, CO, H_2, NO_x, etc) which may have improved process reactions, e.g. NO_x-reducing reactions. Necessary process heat from exothermic reactions of the added oxygen with carbon reductant was generated in the bed where it was most needed, in the locally cooler region of the atomized feed spray. Increased heat generation in the feed spray zone probably helped to reduce the local temperature depression in this zone of the reactor bed and consequently may have increased the kinetics of feed dehydration, nitrate decomposition, and alkali-clay reaction. The capability was present in the test system to inject oxygen either with the fluidizing gas, the atomizing gas, or both if desired. During the test, however, oxygen was injected only via the atomizing gas.

3.3.5 Off-Gas Treatment System

The off-gas treatment system, down-stream of the cyclone and hot filters, consists of a natural gas-fired thermal oxidizer, partial quench vessel, demister, re-heater, and a three-stage granular activated carbon filter bed. The process gases exiting the hot filter pass into the natural gas-fired thermal oxidizer (typically operated at 1,000°C), where they are combined with air to oxidize the hydrogen, carbon monoxide, methane, and other hydrocarbons resulting from the steam reforming process. The oxidized gases are then partially quenched with water spray to a temperature of 130°C. Although the partially quenched gases are not over quenched during normal operation, and remain above the dew-point temperature (no entrained mist), the off-gas is still passed through a demister and a re-heater to assure desired gas conditions entering the granular activated carbon filter/sorption column. The carbon captures Hg, trace concentrations of halogen gases, SO_2, NO_x, and trace hydrocarbons.

3.4 Test Data Collection and Sampling

Diagnostics performed during the FBSR tests included (a) continuous process measurements including key process flow rates, temperatures, and pressures, (b) continuous off-gas composition measurements, and (c) sample collection for laboratory analysis. These diagnostic activities provided data for controlling the process within test acceptance limits and for mass balance calculations to determine the fate of feed constituents.

3.4.1 Process Measurements

The fluidized bed test system data acquisition and control system (DACS) uses Allen Bradley programmable logic controllers (PLCs) for control and data acquisition. The PLC uses Rockwell hardware and software to monitor and control operation of the process from two or more human-machine interface (HMI) personal computer workstations, located in the vicinity of the process equipment. Additional workstations are available, one for use at the CEMS panels, and one for monitoring only (no

control allowed) located in an office area for non-operating personnel.

The process control functions include automated control of valve and pump sequences for the feed system, automated control of all total gas flow rates, selectable input temperature control for the fluidized bed vessel, vacuum control of the system based on the pressure in the reformer, and limited control of the CEMS. The graphical user interface (GUI) for the system shows the status of the components, provides a control interface for the operator, and displays readings from all the instrumentation in numeric and graphical trend form.

The data acquisition system utilizes Rockwell software (RSSql) integrated Sequel databases for electronically archiving data as it is monitored. Each record in the database includes the tag name for the data-point, the description, the value, the units, and a time-stamp. Analog values from the system are archived once per second, and discrete values are archived on change of state. Table 3.3-1 lists key process data recorded during the SBW FBSR demonstration. Hundreds of other parameters and calculations, including the CEMS data, were logged automatically by the PLC, and other parameters such as purge gas flow rates, measured using rotameters, were logged manually.

The process monitoring workstation in the office area was equipped with a Web interface to the database for access to the archived data during the test. The Web interface provides data access from the database and averages at user-defined intervals in Microsoft Excel spreadsheets.

Process data that was not electronically logged by the PLC system was recorded manually on operator data sheets. Manual control of many process parameters was also done according to operator discretion, the test plan, and steam reformer system operating instructions. The measured data are provided in subsequent sections of this report.

Table 3.3-1. Key process data that was electronically or manually logged.

Parameter	Units	Instrument	PLC tag name	Manual log frequency	Comments
Simulant feed rate	kg/hr	Micro Motion CFM010M 0-15 kg/hr coriolis mass flow meter	SR1_F1A_VAL	1/hr	
	liters/hr		SR1_F1A_VFR	Not logged manually	Local readout
Simulant density	gm/ml		SR1_D1_VAL	1/hr	
Simulant composition	---	---	---	Each feed mix	Determined at time of simulant preparation from recipe, including any organic or inorganic additives; verified by post-test sample analysis
Composition of each simulant additive	---	---	---	Each additive	Use vendor-provided composition or sample analysis
Atomizing N_2 flow rate	kg/hr	Brooks SLA 5850 0-100 SLM mass flow meter	SR1_F1B_KGH	1/hr	
Atomizing O_2 flow rate	kg/hr	Brooks SLA 5850 0-30 SLM mass flow controller	SR1_F3_KGH	1/hr	
Solid reductant feed rate	kg/hr	Pioneer Feeder model 1.5 cu.ft.	LF2_FD_RATE	1/hr	Calibrated vibratory feeder with load cell for active feed rate control
Solid reductant cumulative mass fed	kg		LF2_TOTAL2	---	The cumulative mass fed is calculated by the PLC from the feed rate and the time fed
		Weigh scale	---	1/hr	The mass of carbon added to the feed hopper is weighed, totaled, and recorded manually

Solid reductant composition, density, and particle size	---	---	---	Each additive	Use vendor-provided composition or sample analysis
Starting bed media mass	kg	Weigh scale	---	At test start	
Starting bed media composition, density, and particle size	---	---	---	Each additive	Use vendor-provided composition or sample analysis
Fluidizing gas 1 (steam) flow rate	kg/hr	Rosemount 1195/3095 Pro-Plate Tri-Loop orifice plate	H1_F_PV	1/hr	
Fluidizing gas temperature at distributor	^{o}C	K-Type TC	SR1_T14_VAL	1/hr	Measured steam temperature at the distributor
Fluidizing gas temperature (below distributor plate)	^{o}C	K-Type TC	H2_T_VAL	1/hr	Measured upstream of the steam distributor and upstream of where the fluidizing O_2 mixes with the steam
Fluidizing gas velocity ratio (U_{mf}, ratio to minimum velocity)	---	---	---	1/hr	Calculation from fluidizing gas flow rate and minimum velocity
Fluidizing gas velocity	m/s	---	FLUIDIZING_FV	1/hr	Calculation from fluidizing gas flow rate
Total N_2 flow rate	kg/hr	Kurz 504FT thermal meter	V1_F1_VAL	1/hr	Total N_2 flow rate is the sum of the atomizing N_2 flow rate and purge N_2 flow rates
Fluidized bed lower wall temperature	^{o}C	K-Type TCs	SR1_T20_VAL	---	
Fluidized bed upper wall temperature			SR1_T19_VAL	1/hr	
Disengage section lower wall temperature			SR1_T13_VAL	---	
Disengage section upper wall temperature			SR1_T11_VAL	1/hr	
Distributor plate dP	inches water	Rosemount 0305RC5/2024D 0-100 in. H_2O	SR1_PD1_VAL	1/hr	
Fluidized bed lower 12 in. dP			SR1_PD2_Averaged	1/hr	
Fluidized bed dP			SR1_PD3_Averaged	1/hr	
Bed temperature 1 in. below distributor	^{o}C	K-type TCs	SR1_T2_VAL	1/hr	
Bed temperature 1 in. above distributor			SR1_T3_VAL	1/hr	
Bed temperature 11 in. above distributor			SR1_T4_VAL	1/hr	
Bed temperature 17 in. above distributor			SR1_T5_VAL	1/hr	
Bed temperature 21 in. above distributor			SR1_T6_VAL	1/hr	
Disengage section lower off-gas temperature			SR1_T7_VAL	1/hr	
Disengage section mid off-gas temperature			SR1_T8_VAL	1/hr	
Disengage section upper off-gas temperature			SR1_T9_VAL	1/hr	
Cyclone dP	inches water	Rosemount 2024D 0-100 in. H_2O	C1_PD_VAL	1/hr	
Cyclone exit off-gas temperature	^{o}C	K-type TC	C1_T3_VAL	---	

Filter dP	inches water	Rosemount 2024D 0-100 in. H_2O	F1_PD_VAL	1/hr	
Filter exit off-gas temperature	^oC	K-type TC	F1_T2_VAL	1/hr	
Filter outlet off-gas flow rate	kg/hr	---	TOTAL_KGH_BEFORE_OXI	1/hr	Calculated from the input flow rates, gas generation in the FBSR, and gas mole weight
Oxidizer gas temperatures, stages 1, 2, and 3	^oC	K-type TCs	B1_T1_VAL B1_T1_VAL B1_T1_VAL	1/hr --- ---	
Partial quench off-gas temperature	^oC	K-type TC	PQ1_T1_VAL	1/hr	
Reheater outlet (carbon bed inlet) off-gas temperature	^oC	K-type TC	T-AJ-1	1/hr	
Reheater outlet (carbon bed inlet) off-gas pressure	psig	Rosemount 2088A	AJ1_P2_VAL	1/hr	
Reheater outlet (carbon bed inlet) off-gas flow rate	kg/hr	Micro Motion CFM200M 0-250 kg/hr coriolis mass flow meter	AJ1_F_VAL	1/hr	
Mass of bed product, cyclone samples, and filter fines	kg	Weigh scale	---	Each collection	Weights obtained manually every time bed product, cyclone samples, or filter fines are collected, and recorded on sample bags and data sheets
All parameters with a PLC tag name are electronically automatically logged under that tag name. Any parameters that do not have a PLC tag name are not electronically logged. Manual logs were maintained by both SAIC and INEEL personnel. At times, the manual log frequency varied from the typical listed frequencies.					

3.4.2 Continuous Off-gas Composition Monitoring

A continuous emissions monitoring system (CEMS) provided on-line off-gas composition measurements for process control, safety, air emissions measurements, and determining the fate of feed constituents that were converted to gaseous compounds. The off-gas composition was measured at two locations in the off-gas system. CEMS 1 was used to measure the off-gas composition at the outlet of the heated filter (upstream of the thermal oxidizer), to characterize the composition of the FBSR off-gas. CEMS 2 was used to measure the off-gas composition at operator-selectable locations at the inlet of the carbon bed or the outlet of any of the three stages of the carbon bed. CEMS-2 sampled only from the location at the inlet to the carbon bed during the SBW test, providing data that characterizes the off-gas downstream of the oxidizer and upstream of the carbon bed. This location is also downstream of the partial quench and reheater.

Each sampling and conditioning system includes:

- A heated probe through which off-gas is sampled
- A heated filter to remove particulate matter
- Heated sample line to transport hot, filtered sample gas from the heated filter to the chiller system
- An electrical refrigerated chiller system to cool the sample gas, condense water moisture from the sample gas, and separate the condensate with minimal scrubbing of water-soluble gases

- A sample pump
- A backup filter
- Flow monitoring and control manifold with control valves to deliver the cooled, dried, and filtered sample gas to the continuous monitors
- For CEMS 1 only, a carbon filter is located upstream of the flow control manifold, to remove residual condensable hydrocarbons that otherwise foul the analyzers and interfere with CEMS measurements. The THC analyzer withdraws sample gas upstream of the carbon filter in order to most representatively sample these hydrocarbons before they are removed by the carbon filter.

Figures 3.3-1 and 3.3-2 show the physical configurations of the two CEMSs.

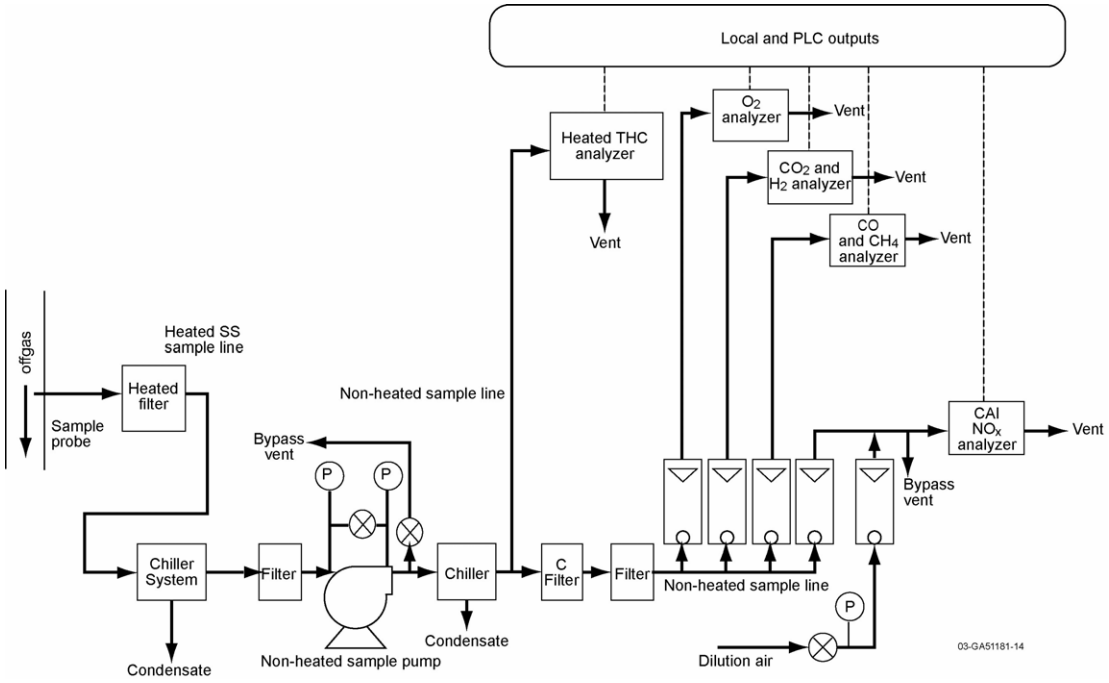

Figure 3.3-1. CEMS 1 for steam reformer off-gas measurements at the filter outlet sample location, upstream of the thermal oxidizer.

Figure 3.3-2. CEMS 2 for steam reformer off-gas measurements upstream of the carbon bed.

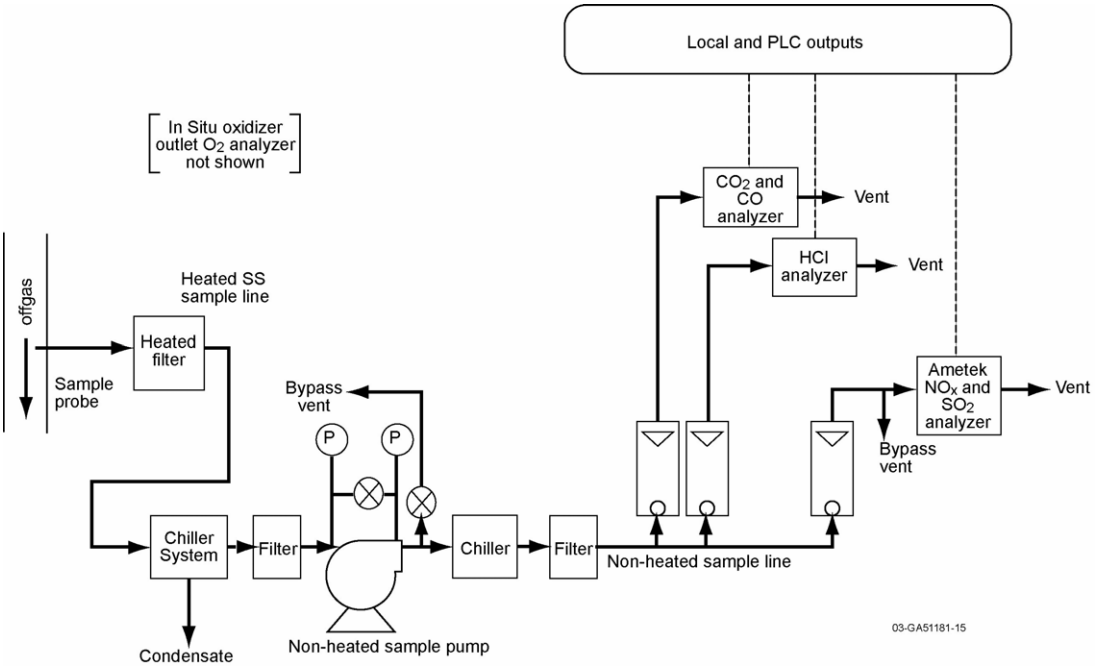

Specifications for the gas analyzers are shown in Table 3.3-2.

Table 3.3-2. Off-gas analyzer specifications.

Gas species	Instrument	Detection principle	Instrument range	Acceptance limits, % FS				Reference Method
				Calibration	Drift	Linearity	Bias	
O_2	Servomex 1440 CEMS 1)	Paramagnetism	0-25%	2	3	4	5	40 CFR 60 App. A Method 3A
	In situ ZrO_2 probe (CEMS 2)	Electrochemical						
CO_2	Nova 4230 RM (CEMS 1) CAI (CEMS 2)	Nondispersive infrared (NDIR)	0-40% 0-100%					
H_2	Nova 4230 RM (CEMS 1)	Thermal conductivity	0-5%	---	---	---	---	---
CO	CAI 200 (CEMS 1) CAI (CEMS 2)	NDIR	0-1% 0-2% (CEMS 1) 0-500 ppm 0-2,500 ppm (CEMS 2)	5	10	2	---	40 CFR 60 App. A Method 10
CH_4	CAI 200 (CEMS 1)		0-0.5% 0-1%	---	---	---	---	---
NO, NO_x	Ametek M922 (CEMS 2)	Dispersive ultraviolet (DUV)	0-5,000 ppm	2	3	4	5	40 CFR 60 App. A Method 7E
	Ecophysics CLD 70E (CEMS 1)	Chemiluminescence	0-5,000 ppm					
THC	CAI 300 HFID (CEMS 2)	Flame ionization detection (FID)	0-3% C_1	5	3	---	---	40 CFR 60 App. A Method 25A
HCl	Thermo 15C (CEMS 2)	NDIR with gas filter correlation (GFC)	0-100 ppm to 0-5,000 ppm	---	---	---	---	---
SO_2	Ametek M922 (CEMS 2)	Dispersive ultraviolet (DUV)	0-10 ppm to 0-25,000 ppm	2	3	4	5	40 CFR 60 App. A Method 6C

The analyzers were calibrated with calibration gases daily during the test series. Past experience has shown that CEMS calibrations once per day or even less frequently are usually adequate. During each calibration, the following activities were generally performed:

- The system was leak-checked two ways (a) by checking the response of the O_2 analyzer (a significant O_2 response would indicate a significant amount of air in-leakage upstream of the sample pump), and (b) by running the sample pump with the CEMS inlet plugged and demonstrating no sample gas flow.

- Analyzer zero responses were determined using a zero gas (N_2).

- Analyzer span responses were determined using a calibration gas with the specified gas concentration.

- Interferences of gas species on the detection of other gas species were determined by recording all analyzer responses for each of the calibration gases. With internal corrections for such interferences (such as the interference of CO_2 on the H_2 measurement) no post-test CEMS

interference corrections were needed after the test series.

- Calibration data generated prior to any analyzer adjustments applied to CEMS data during the time period prior to the calibration; calibration data generated after analyzer adjustments applied to CEMS data during the time period following that calibration.

- Calibration data was used to generate a composite correction factor for both air dilution and span calibration for the CEMS 1 NO_X analyzer, which requires air dilution for operation.

The calibrations showed that the average calibration, drift, linearity, and bias for each test period were within the intended acceptance limits.

3.4.3 Process Sample Collection

Process sample collection and analysis was performed to determine the fate of feed constituents, determine process mass balances, and evaluate the properties of the solid products. Some sample analyses were performed for process monitoring and control during the test series. Selected samples were also delivered for more comprehensive post-test laboratory analysis at SRNL. Table 3.3-3 shows the samples that were shipped to SRNL and the analyses that were performed. The sample selection matrix was designed to generate samples of feed and product materials sufficient to characterize those materials, perform key mass balances, and determine the fate of feed constituents in the steam reforming process. Test samples were identified with unique sample labels, and sample information was recorded on a sample log.

The scope of onsite analysis included:

- All bed samples were analyzed for particle size distribution (ASTM D 6913, "Standard Test Methods for Particle-Size Distribution (Gradation) of Soil using Sieve Analysis") bulk density (ASTM B 527, "Standard Test Method for Determination of Tap Density of Metallic Powders and Compounds"), and particle density (ASTM C 128, "Standard Test Method for Density, Relative Density (Specific Gravity), and Absorption of Fine Aggregate").

- All bed product, cyclone samples, and filter fines were weighed.

- Selected bed product, cyclone samples, and filter fines were also evaluated using onsite optical microscopy.

Table 3.3-3. Laboratory sample analysis matrix performed at SRNL.

Sample number	Sample date	Sample description	Analyses Performed															Remarks
									Elemental composition									
			Bulk density	Total calcine	SEM	SEM/ EDS	XRD	pH	Organic carbon	Cations	Anions	PSD	Redox	PCT	SPFT	PUF	TCLP	
1154	27-Sep	SBW simulant		X						X	X							To verify the mixture recipe
1156	27-Sep	SBW/KT Sagger slurry, 1st batch		X						X	X							
1162	29-Sep	SBW/KT Sagger slurry, last batch		X						X	X							T2A
1171	28-Sep	Bed product COT 31				X	X		X	X	X							1640 Unscreened dynamic bed sample
1172	30-Sep	Bed product COT 71					X		X	X	X							Unscreened dynamic bed drain
1173	1-Oct	Bed product COT 100				X	X		X	X	X		X	X			X	1630 Unscreened dynamic bed drain
1174	28-Sep	Cyclone fines COT 31			X		X		X	X	X	X						1640
1175	30-Sep	Cyclone fines COT 73					X		X	X	X	X						1335
1176	1-Oct	Cyclone fines COT 98	X			X	X		X	X	X	X						1430
1177	28-Sep	Filter fines COT 33			X		X		X	X	X	X						1840
1178	30-Sep	Filter fines 73					X		X	X	X	X						1330
1179	4-Oct	Filter fines 100+	X			X	X		X	X	X	X					X	1630+
1163	29-Sep	CEMS 1 condensate 1710						X			X							
1164	29-Sep	CEMS 2 condensate 1710						X			X							
1166	30-Sep	CEMS 1 condensate 1840						X			X							
1167	30-Sep	CEMS 2 condensate 1840						X			X							
1169	1-Oct	CEMS 1 condensate 1630						X	X	X	X							
1170	1-Oct	CEMS 2 condensate 1630						X	X	X	X							
1180	5-Oct	Carbon bed top of top layer								Hg							X	
1181	5-Oct	Carbon bed top of middle layer								Hg								
1182	5-Oct	Carbon bed top of bottom layer								Hg								
1183	5-Oct	C bed bottom of bottom layer								Hg								

1. Desired information from analyses is (a) determine degree of mineralization, types of mineralization and mineralized phases, and leachability of the FBSR bed and fines products, (b) characterize different bed constituents, and (c) elemental analyses.

2. Total calcine by loss on ignition (LOI) at 750°C, consistent with ASTM D3174.

3. Scanning electron micrograph (SEM) analysis of cyclone catch and filter fines to provide photos of these particles at high enough magnification (up to 5,000-20,000x) to discriminate ~0.1 μm particles.

4. SEM-energy dispersive Spectroscopy (SEM-EDS) to determine composition differences of different sectioned particles. For example, to determine if cores of bed particles are unreacted clay.

5. X-ray diffraction (XRD) analysis to determine different mineral phases.

6. Organic carbon content by LOI at 750°C consistent with ASTM D3174, except for the CEMS condensate samples. For those samples, use a liquid total organic carbon (TOC) procedure.

7. Cation analysis preceded by lithium tetraborate (Li borate) fusion at 1,000°C, followed by uptake (dissolution) in 2% HNO3 and HCl on a hotplate. Most samples dissolve well in the dilute HNO3; HCl is added to help dissolve high Fe samples and to provide added assurance of total dissolution of the sample matrix.

8. Cations Al, B, Ca, Cr, Fe, Pb, Mg, Mn, Ni, K, and Si, by inductively coupled plasma emission spectroscopy (ICP-ES); Cations Cs and Re by ICP-mass spectroscopy (ICP-MS) for better detection limits. The carbon used for Hg capture may require multiple extractions for Hg, for quantitative Hg recovery.

9. Anions analysis preceded by sodium peroxide (Na Per) fusion followed by water uptake to dissolve all anions.

10. Anions CO_3 (inorganic C), Cl, F, NO_2, NO_3, PO_4, and SO_4 by ion chromatography (IC). Iodine by ICP-MS. For best results, anion detection limits need be about 0.01 wt% (for solid samples) and about 0.1 mg/L (for liquid samples).

11. Particle size distribution (PSD) by Microtrak to determine size distributions of small particles. The PSD for bed media has already beenwas determined by sieve tray analysis (ASTM D 6913-04 C92 - 95) during the test.

12. The extent of oxidation is indicated by the ratio of Fe^{+2} to Fe (total) (REDOX test).

13. Product Consistency Test (PCT).

14. Single Pass-Through Flow Test (SPFT). Cannot do SPFT on filter fines.

15. Pressurized Unsaturated Flow (PUF) test.

3.5 Process Input Materials (Selection and Composition)

The TTT mineralizing steam reforming technology for the treatment of SBW in a fluidized bed reactor involves converting the liquid waste into an insoluble, mineralized product. Overall, water is evaporated, nitrates and nitrites converted mostly to N_2 and sodium is converted to sodium aluminosilicate. A mineralizing additive, clay, must be used in addition to a reducing additive (carbon) to achieve this. Clay powder/particulate is added to provide sufficient reactive Al and Si in a form suitable to combine with alkali elements (primarily Na and K) in the feed to produce nepheline and other aluminosilicate mineral phases as solid product granules/particles in the reformer. Toxic metals and radionuclides are expected to be immobilized in the solid product matrix, either by forming an incorporated mineral phase or by microencapsulation. Carbon was added to provide for some internal heat generation in the bed, and to form reducing conditions for NO_x destruction. The use of a dense, inert starting material, such as alumina, in a fluidized bed reactor operated at about 725 °C facilitates the conversion.

3.5.1 Starting Bed Media

Selection of the starting bed media is important for the operability and stability of a fluidized-bed process. Ideally, the starting bed material would be readily available, inexpensive, non-hazardous, durable (thermally stable, attrition resistant, chemically inert), and have similar particle size, density, thermal conductivity, and heat capacity as the expected product. For the purposes of completing a mass balance and tracking bed changeover to product material, it is also helpful if the starting bed is distinguishable from the product.

Fluidized bed steam reforming tests conducted by the INEEL at the SAIC STAR Center have generally used sintered bauxite or white alumina as the starting bed medium. Various other ceramic grit and engineered forms were considered, such as boron nitride, Extendospheres® (PQ Corp), and Macrolite® ceramic spheres (Kinetico, Inc.), etc., because the particle densities of these materials more closely matched that of the expected product material. Uncertainties about the durability of these alternative media with acidic SBW feed constituents in the aggressive steam reforming environment, and positive experience with alumina from earlier tests, led to the decision to use white alumina as the starting bed medium.

Experience has shown that alumina is attrition resistant, chemically inert, physically and chemically distinguishable from the mineralized product, has very good thermal conductivity, and has high heat capacity. The high thermal conductivity and heat capacity facilitate heat transfer to the atomized feed, while maintaining a relatively high bed temperature and reducing the potential for over-quenching the bed in the slurry feed zone. Experience in earlier FBSR tests has shown that hot alumina is also not readily coated by the mineralized product, perhaps due in part to the Leidenfrost (film boiling) effect, and in part to the relative inertness of the alumina. This aids in visually distinguishing the product material from the starting bed alumina via solids samples inspection as the experiment proceeds and the starting bed material is replaced by mineralized product. The primary disadvantages of using alumina are that the particle density is more than double the expected particle density of the expected products and the thermal conductivity and heat capacity are considerably higher than the product. This requires some compensation or adjustment in fluidizing parameters and process conditions (primarily slurry feed rate) as the experiment proceeds from starting bed to steady product bed conditions.

Compensation for the higher starting bed density, with regard to bed fluidization, can largely be achieved by decreasing the mean particle size of the starting bed so that fluidizing parameters will be similar to those of the expected lower density product. Expecting that the mean product bed particle size

(d_p) would be near 0.2 mm with a particle density (ρ_p) of about 1.8 gm/cc, 100-grit white alumina was selected as the starting bed ($\rho_p \approx 3.8$ gm/cc, $d_p \approx 0.140$ mm).

3.5.2 Carbon Reductant Additive

Carbon reductant additives are fed to the FBSR to produce the reducing environment necessary to effectively destroy NO_x species and to provide sensible heat to promote the endothermic reactions. The selected carbon needs to have good reactivity with steam and contain low concentrations of constituents that can lead to formation of a glassy phase, especially glass fluxing agents (boron, phosphorus, etc.). Berger Brothers pyrolyzed wood carbon (size P6) was selected based on its availability and performance during the Hanford LAW mineralization run [Olson, 2004].

Nine different carbon types were investigated for use as a reductant in the experimental program. Characteristics measured on carbon samples were reactivity (thermogravimetric analysis), particle size distribution, attrition resistance, moisture content, loss on ignition, and ash compositional analysis. Appendix C gives details on selection criterion used and rankings of carbons evaluated. A wood-based carbon and a coal-based carbon were selected for use in the pilot scale activities. Initial functional tests performed in July confirmed that the wood based carbon, supplied by Berger Brothers, performed the most efficiently and was selected for use in the initial experiments. A summary of the carbon reductant properties is shown in Table 3.4-1. Further property information about the Berger Brothers carbon can be found in Jantzen, 2004.

Table 3.4-1. Carbon reductant properties.

Supplier	Berger Brothers, Chicago, IL
Type/Size	Wood base, -0.371”, +0.185”
Moisture (% of Sample)	3.13
Ash at 650°C (% of Dried Sample)	5.38
Ash at 750°C (% of Dried Sample)	5.14
Loss on Ignition (% Loss of Undried Sample)	95.0

3.5.3 Mineralizing Additive

The function of the mineralizing additive in the mineralizing steam reforming process technology is to provide aluminosilicates to chemically bond with the alkali in the waste to form insoluble alkali (Na and K) aluminosilicates. Selection of a mineralizing agent (clay) followed an approach of investigating several potential candidate clay materials. Four clays (SnoBrite, OptikasT, Troy, and K-T Sagger XX) were investigated. Characteristics measured included phase analysis (X-ray diffraction), particle size distribution, whole element chemistry, and slurry rheological properties.

It is important to select a clay type with a Si:Al mole ratio that is in a favorable range, when reacted with the liquid waste, for producing the desired durable mineral product phases. Therefore the approach using the Na_2O-Al_2O_3-SiO_2 ternary phase diagram and atomic ratio guidelines, as discussed earlier in Section 2.1, led to identification of Troy or Sagger clays as best suited for mineralizing the SBW

composition. These had higher silica to alumina ratios. Particle size distribution is also important, with finely divided clays (high surface area) preferred such that as much of the clay mass as possible combines with and reacts with the liquid waste. All the clay types appeared to have acceptable and somewhat similar particle size distributions. Clay constituents that do not support generation of desirable mineral phases (e.g., quartz) should be minimized. Data obtained from laboratory analyses to support the clay raw material selection is documented [Jantzen, 2004]. The rheological properties of the clay slurry are important since the clay and waste must be combined, pumped, and injected via an atomization nozzle into the reactor with a minimum expenditure of energy. The slurry viscosity and atomization characteristics were briefly investigated as a part of slurry mixing, pumping, and nozzle atomization tests (Appendix B).

Troy clay was selected and used for the initial demonstration experiment conducted in July with SBW surrogate material. Although generally successful, the July 2004 test was terminated early due to bed agglomerations. During the immediate post test analyses a calculation error was identified, however, indicating the Troy clay addition quantity to the SBW simulant should have been 223 g/L rather than the 293 g/L that was actually used. This error could have had a significant affect on the mineralizing product formation chemistry. It was further noted that, since the atomic ratio of alkali, aluminum, and silicon in the desired product (i.e., nepheline) is near 1:1:1, and because the SBW contains a significant quantity of aluminum nitrate, the Troy clay did not have sufficient silica present to compensate for all of the aluminum nitrate in the SBW.

It was recommended, after further team analysis of clay properties and additional laboratory scale data, that 230 gm of as-received K-T Sagger ball clay should be added for every liter of simulated SBW for conduct of the September SBW experiment. Table 3.4-2 shows the properties of the Troy and Sagger XX clays. The quantity of clay to be mixed with the SBW simulant was selected such that the expected product composition was within the desired shaded region of the ternary phase diagram (Figure 3.4-1). An operating line can be drawn from the plotted location of the normalized SBW oxide composition, on the Na_2O-Al_2O_3-SiO_2 phase diagram (Figure 3.4-1), to that of the clay additive. The line represents the average composition of product mixtures based on the relative quantities SBW and clay used. Sagger XX ball clay has a Si:Al atomic ratio of 1.69:1 and appears to provide the most favorable product composition as noted by the desired product region and the target product composition. The Sagger XX clay also has an acceptable particle size distribution with a mass-mean diameter of 6.6 µm.

Table 3.4-2. Properties of candidate clays.

Clay	Troy	K-T Sagger XX
Major phases ($Al_2O_3 \cdot 2SiO_2 \cdot 2H_2O$)	Kaolinite (PDF#75-1593) ($Al_2O_3 \cdot 2SiO_2 \cdot 2H_2O$)	Kaolinite (PDF#78-1996)
Minor phases ($(K_{0.86}Al_{1.94})(Al_{0.965}Si_{2.895}O_{10})((OH)_{1.744}F_{0.256})$)	Muscovite (PDF#86-1385) Quartz (SiO_2) possible	Muscovite (PDF#07-0042) (K, Na)(Al, Mg, Fe)$_2$ ($Si_{3.1}Al_{0.9}$)$O_{10}(OH)_2$ Quartz (SiO_2) Rutile (TiO_2)
Al:Si atom ratio	1:1.21	1:1.69
Total moisture* (wt%)	14.65%	10.6%
Particle size (wt% less than) 10% - 50% - 90%	1.83µm – 14.83µm – 57.1µm	1.34µm – 6.55µm –21.5µm

Particle density	2.74 gm/cc	2.73 gm/cc

* The total moisture content was determined based on total mass loss during a Loss on Ignition (LOI) analysis, during which the sample was heated to 700°C, and includes both moisture sorbed onto the clay and also water of hydration. Determining total moisture based on LOI analysis assumes that the only mass change upon heating to 700°C is due to volatilization of water.

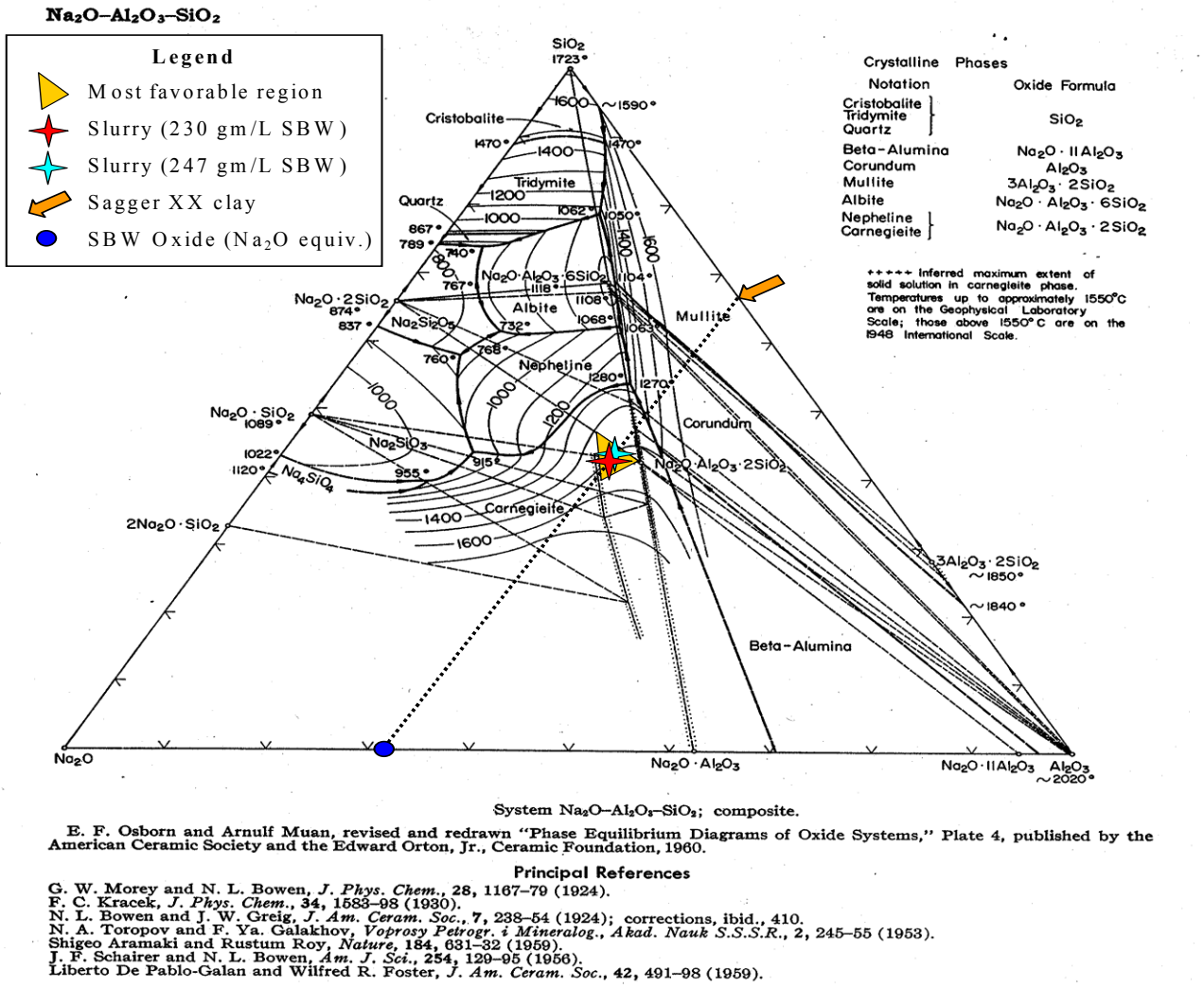

System Na_2O–Al_2O_3–SiO_2; composite.

E. F. Osborn and Arnulf Muan, revised and redrawn "Phase Equilibrium Diagrams of Oxide Systems," Plate 4, published by the American Ceramic Society and the Edward Orton, Jr., Ceramic Foundation, 1960.

Principal References

G. W. Morey and N. L. Bowen, *J. Phys. Chem.*, **28**, 1167–79 (1924).
F. C. Kracek, *J. Phys. Chem.*, **34**, 1583–98 (1930).
N. L. Bowen and J. W. Greig, *J. Am. Ceram. Soc.*, **7**, 238–54 (1924); corrections, ibid., 410.
N. A. Toropov and F. Ya. Galakhov, *Voprosy Petrogr. i Mineralog., Akad. Nauk S.S.S.R.*, **2**, 245–55 (1953).
Shigeo Aramaki and Rustum Roy, *Nature*, **184**, 631–32 (1959).
J. F. Schairer and N. L. Bowen, *Am. J. Sci.*, **254**, 129–95 (1956).
Liberto De Pablo-Galan and Wilfred R. Foster, *J. Am. Ceram. Soc.*, **42**, 491–98 (1959).

Figure 3.4-1. Ternary phase diagram showing clay and target feed compositions for the SBW test.

3.5.4 SBW Simulant

The SBW simulant used for this test was prepared from residual SBW simulants from previous experimental activities that were augmented with newly prepared simulant. The overall composition mimics that of the waste stored at the Idaho Nuclear Technology and Engineering Center (INTEC) in waste tank WM-180. The target and measured compositions are shown in Table 3.4-3.

Table 3.4-3. SBW simulant and slurry compositions.

Analyte		SBW Makeup (gm/L)	SBW Analysis (gm/L)	Δ%	Slurry (1) Makeup (gm/L)	Slurry Analysis (gm/L)	Δ%
Acid	H^+	1.1 *M*	---	---	0.99 *M*	---	---
Aluminum	Al	1.80E+1	1.86E+1	3%	5.14E+1	4.50E+1	-12%
Boron	B	1.20E-1	1.26E-1	5%	1.16E-1	3.41E-1	193%
Calcium	Ca	1.80E+0	2.13E+0	18%	2.16E+0	1.62E+0	-25%
Cesium	Cs	2.60E-1	2.31E-1	-11%	2.13E-1	3.98E-1	87%
Chloride	Cl	1.00E+0	1.17E+0	17%	1.08E+0	1.07E+0	-1%
Chromium	Cr	1.70E-1	1.51E-1	-11%	1.39E-1	1.99E-1	43%
Copper	Cu	4.40E-2	3.80E-2	-14%	3.50E-2	5.65E-2	61%
Fluoride	F	9.00E-1	<0.1	---	---	---	---
Iodide	I	1.50E-2	---	---	1.39E-2	---	---
Iron	Fe	1.20E+0	9.30E-1	-23%	2.11E+0	2.04E+0	-3%
Lead	Pb	2.70E-1	2.31E-1	-14%	2.13E-1	2.51E-1	18%
Magnesium	Mg	2.90E-1	3.49E-1	20%	6.51E-1	6.08E-1	-7%
Manganese	Mn	7.80E-1	6.62E-1	-15%	6.11E-1	6.47E-1	6%
Mercury	Hg	2.80E-1	---	---	2.51E-1	---	---
Nickel	Ni	8.60E-2	7.10E-2	-17%	6.55E-2	8.67E-2	32%
Nitrate	NO_3	3.30E+2	2.89E+2	-12%	2.67E+2	2.67E+2	0%
Phosphorus	P	8.80E-1	1.37E+0	56%	1.36E+0	1.22E+0	-10%
Phosphate	PO_4	2.70E+0	4.20E+0	56%	4.18E+0	3.75E+0	-10%
Potassium	K	7.70E+0	9.77E+0	27%	1.02E+1	9.74E+0	-5%

Rhenium	Re	1.20E-1	1.11E-1	-8%	1.02E-1	7.12E-2	-30%
Silicon	Si	---	---	---	6.03E+1	5.24E+1	-13%
Sodium	Na	4.70E+1	5.17E+1	10%	4.79E+1	4.89E+1	2%
Sulfur	S	2.24E+0	2.44E+0	9%	2.25E+0	1.89E+0	-16%
Sulfate	SO_4	6.70E+0	7.31E+0	9%	6.74E+0	5.65E+0	-16%
Titanium	Ti	---	---	---	3.35E+0	3.00E+0	-10%
Zinc	Zn	6.90E-2	---	---	6.51E-2	---	---

1. Estimate based on chemical analyses of the SBW simulant and Sagger XX clay.

3.6 Test Procedures and Operating Conditions

This section briefly describes general procedures and planned operating conditions for the test. Actual test events, and operating conditions parameter values experienced, are presented as a part of the test results in the following section 4 of this report.

Experimental activities were performed by Science Applications International Corporation (SAIC) personnel in accordance with documented operating procedures [SAIC, 2004]. SAIC personnel received experimental direction from BBWI personnel. Communication sheets detailing changes in operating parameters were prepared and initialed by TTT and BBWI personnel as documentation of experimental direction.

The FBSR system was ready for simulant feed operation after starting bed media was charged and preheating was completed beginning with nitrogen as the fluidizing gas, and then switching to steam following normal startup procedures. An initial inventory of carbon reductant was then established in the bed by adding about 1 kg of carbon. This was done by feeding carbon into the bed at a high rate, ~2 kg/hr, for about ½ hour. During this time the CEMS was monitored to verify the generation of H_2 and attainment of low O_2 concentrations, typically ~0-0.5% (dry, as measured). Water feed was then initiated at a minimum feed rate of about 2 kg/hr. The target O_2 concentration in the atomizing gas (~15 wt%) was then initiated. Bed temperatures were monitored to verify adequate, but not excessive wall heating, and heating from carbon oxidation.

The simulant feed slurry was initiated at 3 kg/hr when a carbon inventory was established in the bed, H_2 generation and low O_2 concentrations verified, and stable bed operation was observed. The system was then adjusted to achieve and maintain the planned operating parameter values listed in Table 3.5-1 while monitoring all key parameters for appropriate adjustment as the test proceeded.

Available spreadsheet tools were used for calculating fluidizing gas parameters, carbon stoichiometry, mineral stoichiometry, and simulant makeup parameters not directly provided via the system PLC. The spreadsheet tools were used as appropriate to monitor and recommend adjustments to the planned parameter values, based on experimental needs and operating conditions as the test progressed.

It was planned that the SBW demonstration testing would be performed during a one week period starting September 27, 2004. A total of 100 operating hours were available. This schedule provided the ability to operate and define acceptable ranges of key operating parameters, make minor adjustments, obtain product samples for onsite analyses and to send to SRNL for analysis.

Table 3.5-1. Key operating conditions for the September 2004 SBW FBSR test.

Parameter			Anticipated Range
Fluidizing Gas	Ratio (U/U_{mf})[a]		4 – 20 (based on particle density and HMPD)
	Velocity at distributor		0.08 -0.20 m/s
	Composition:		Steam initially, or steam and oxygen
	Fluidizing gas temperature		≤ 780°C
	Fluid gas distributor		THOR^{SM} proprietary.
	Distributor differential pressure		15 – 95 in WC (≥40 in WC during bed charging) Minimum distributor DP to be ≥100% total bed DP when product exceeds 70% bed mass
Feed & Additives	Slurry feed rate (total)		3.0 kg/hr after the switch from H_2O Otherwise 2.0 – 4.0 kg/hr
	K-T Sagger ball clay		230 gm/L SBW
	Berger Brothers P6 carbon addition		1.5 kg/hr for 30 minutes before slurry feed initiation. Nominally 0.8 ± 0.1 kg/hr after feed is started.
Atomizing Gas	NAR		>800 for the 0.079 ID Nozzle >1000 for the 0.100 ID Nozzle
	Atomizing gas flow rate		>2.0 kg/hr for the 0.079 ID Nozzle >3.0 kg/hr for the 0.100 ID Nozzle
	Composition:		N_2 and O_2 initially (N_2 flow varied to achieve desired atomization)
	Oxygen addition rate		0.40 kg/hr
Process Conditions	Bed temperature (from T3)		725 ± 5°C
	Freeboard temperature		715 ± 15°C
	Reactor wall temperature limit		≤780°C
Bed Parameters	Starting bed[b]	mass & medium	18 ± 1 kg white alumina
		particle size (HMPD)	0.14 mm (100 grit)
		particle density	3.8 gm/cc
	Fluidized bed depth		25 - 28 inches
	Reformer pressure at distributor		Atmospheric
Off Gas Parameters	Off-gas filter temperature		Nominally 400°C
	Oxidizer chamber temperature		1,000°C
	Partial quench outlet temperature		130°C
	Reheat outlet temperature		140°C
	Oxidizer outlet O_2 concentration		3%
	Carbon bed configuration		Stage 1: 3 inches (6 kg, ~0.15 s residence time) Stage 2: 9 inches (18 kg, ~0.45 s residence time) Stage 3: 12 inches (24 kg, ~0.6 s residence time)
	Carbon bed temperature		125 ± 3°C

(a)U_{mf} = Minimum fluidizing velocity, as calculated by the Wen and Yu correlation (Kunii and Levenspiel, 1991)

(b)Given that the alumina may be nearly twice as dense as the expected product, the size of the alumina was chosen to more closely match the fluidizing conditions needed for the product. (#100 grit [140µm] alumina fluidizes like 200µm product)

Some process conditions were expected to require adjustment in order to maintain stable bed operation. For example, as the bed particle density and size distribution was expected to change, the fluidizing gas flow rate would require adjustment in order to maintain the same ratio of fluidizing gas velocity compared to the minimum fluidizing velocity. Based upon previous experience, several other potential conditions and corrective actions guidelines were established:

- Detectable bed agglomerates in bed product. If higher than 10 wt% of the bed product or presence of granules >1/2" size, consider adjustments that might reduce the quantity of accretions/agglomerates. Adjustments to consider include (a) adjust fluidizing gas rate or nozzle atomizing gas to increase bed fluidization, feed atomization, and jet grinding activity, (b) change bed operating temperature, (c) lower the simulant slurry feed rate, or (d) recycle sieved bed materials to maintain adequate bed depth while increasing the frequency bed draining operations to remove larger agglomerates and nozzle accretions.

- Average bed particle size increasingly too large or excessive spread in the particle size distribution peaks. Same potential corrective actions as for bed agglomerates.

- Excessive fines elutriated to the filter. Reduce fluidizing gas flow rate, atomizing gas flow rate, and/or bed temperature.

- Off-gas H_2 levels too low or NO_x levels too high (NO_x reduction too low). Increase carbon additive rate or increase bed temperature.

- Excessive bed temperature gradient. Increase fluidizing gas flow rate, decrease bed temperature, decrease simulant slurry feed rate, decrease bed recycle, or change O_2 addition.

Several circumstances could dictate the need to shut down, cool down, remove the bottom distributor, and inspect or clean out the bed vessel or other equipment. These included bed defluidization, bed drain or feed nozzle restrictions, or failure of off-gas system components. Temperature, pressure, and flow instrumentation provided the on-line information that the operators used, along with periodic product samples (bed, cyclone, filter fines), to determine if any conditions were occurring that would make an unplanned shutdown necessary.

4. TEST RESULTS

The demonstration of TTT's mineralizing steam reforming process technology with simulated SBW was performed in the INEEL pilot scale fluidized bed test system at the STAR Center beginning on September 27 and continuing through October 1, 2004. Test operation commenced at 0900 on the first day when simulant slurry feed was initiated and was terminated when 100 hours of continuous operating time (COT) had been achieved. The SBW simulant slurry (a mixture of simulated SBW liquid solution and solid clay particles) contained 230 – 247 grams of K-T Sagger XX ball clay per liter of SBW simulant and feed rates ranged from 2 -3 kg/hr.

4.1 Test Conditions, Operations, and Performance

4.1.1 Test Conditions and Operations

The demonstration was intended to operate at the conditions described in Section 3.5, with provisions to modify the conditions as needed to respond to process changes, maintain a stable bed, and ensure satisfactory completion of the test. Actual test operating conditions and changes experienced in key parameters are shown in Figure 4.1-1 and Table 4.1-1.

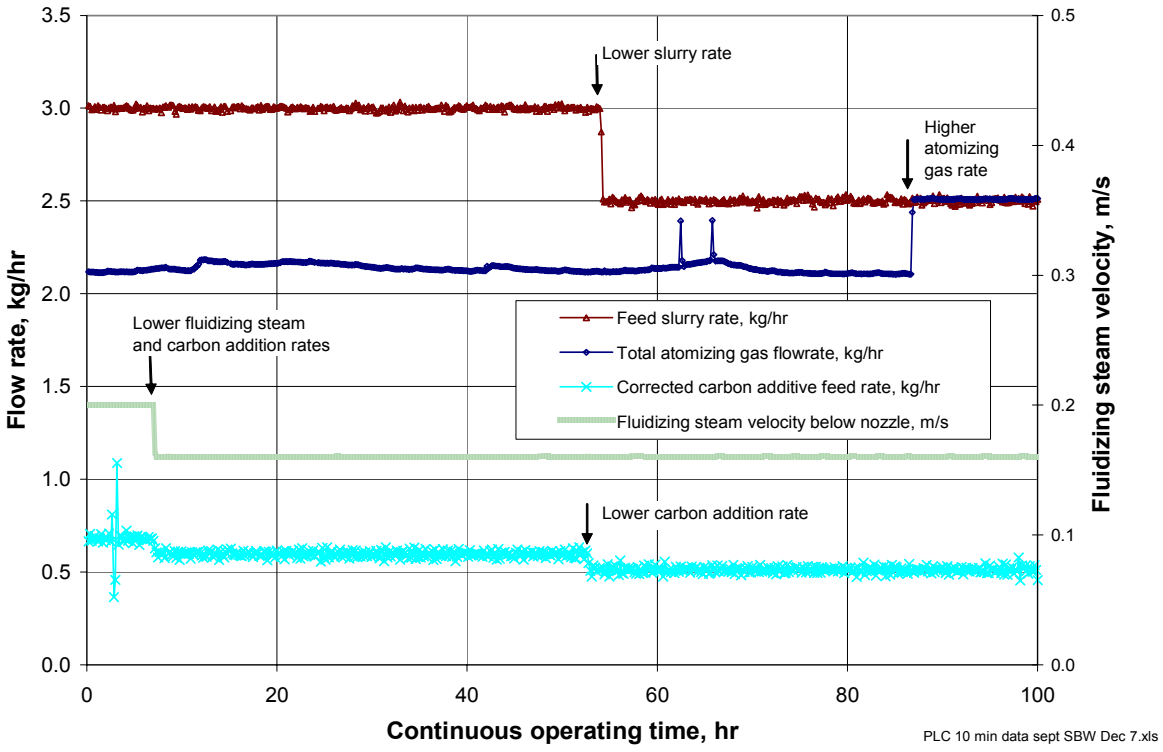

Figure 4.1-1. Process operating conditions.

Table 4.1-1. Process operating conditions.

Communication Sheet	Implementation Date and Time	Implementation COT (hr:mm)	Duration (hr:mm)	Process Input Streams						Slurry volumetric feed rate (L/hr) (SR1_F1A_VFR)	Slurry density (gm/mL) (SR1_D1A_VAL)	NAR (sL/L)	Bed temperature, T3 (°C) (SR1_T3_VAL)	Fluidized-bed density (kg/L) (BED_DENSITY)	Fluidizing velocity below feed (m/s) (FLUIDIZING_FV)
				Atomizing N_2 (kg/hr) (SR1_F1B_KGH)	Atomizing O_2 (kg/hr) (SR1_F3_KGH)	Total atomizing gas (kg/hr)	Fluidizing steam (kg/hr) (H1_F_PV)	Carbon feed rate setpoint (kg/hr) (LF2_FD_RATE)	Slurry mass feed rate (kg/hr) (SR1_F1A_VAL)						
1	27 Sep 04 09:00	0:00	7:00	1.72	0.40	2.12	2.5	0.80	3	2.21 - 2.22	1.35 - 1.36	800	729	1.13 - 1.26	0.20
2	27 Sep 04 16:00	7:00	45:40	1.74	0.40	2.14	**2.0**	**0.70**	3	2.21 - 2.28	1.32 - 1.36	800	730	0.68 - 1.13	0.16
3	29 Sep 04 14:15	52:40	1:27	1.72	0.40	2.12	2.0	**0.60**	3	2.21	1.36	800	730	0.68	0.16
4	29 Sep 04 15:37	54:07	11:58	1.72 - 1.90	0.40	2.12 - 2.30	2.0	0.60	**2.5**	1.84 - 1.90	1.32 - 1.36	**960**	729	0.65 - 0.74	0.16
5	30 Sep 04 06:35	66:05	20:35	1.72	0.40	2.12	2.0	0.60	2.5	1.83 - 1.89	1.32 - 1.37	960	729	0.64 - 0.70	0.16
6	1 Oct 04 03:10	86:40	13:25	2.11	0.40	2.51	2.0	0.60	2.5	1.83	1.37	**1150**	729	0.63 - 0.64	0.16
Shutdown	1 Oct 04 16:35	100:05													
Test averages				1.79	0.40	2.19	2.02	0.66	2.77	2.05	1.35	906	730	0.79	0.163

[SBW Mass Balances Dec 13.xls]Process parameter summary

The initial conditions were selected (see Section 3.5) and slurry feed was started at 3 kg/hr (communication sheet #1) at 9:00 am on September 27. The fluidizing steam velocity ratio was set at twenty times the minimum fluidizing velocity ($20*U_{mf}$, 2.5 kg/hr) and the carbon addition set point was 0.8 kg/hr. Rather than blending oxygen with the fluidizing steam, as has been done in previous tests, oxygen addition (0.4 kg/hr) was done via the atomizing gas (see Section 3.2.4.3).

A valve on the carbon feeder airlock jammed open at approximately COT 2:30. The FBSR pressure was increased to reduce air inleakage via the carbon addition port until the valve was freed and functioning again. Carbon addition was resumed after a 9-minute pause while the valve was repaired and the FBSR pressure was returned to normal (~12.4 psia at the distributor).

With hydrogen production around 6.5% (dry basis) and NO_x destruction over 97%, the decision was made to reduce the fluidizing steam velocity to $16*U_{mf}$ (2.0 kg/hr) and to decrease carbon addition set point to 0.7 kg/hr (Communication sheet #2) at COT 7:00. These changes were made to bring the fluidizing velocity more into the acceptable range ($4 – 20*U_{mf}$) and to reduce the carbon inventory in the bed because NO_x destruction was more than adequate. The reduction in fluidizing steam velocity can be seen in Figure 4.1-2 as a drop in steam distributor differential pressure (DP). The distributor was appropriately sized such that the distributor DP remained sufficiently high to ensure uniform steam distribution. The distributor DP remained constant during the run, except when the fluidizing steam was lowered or when particle data (density and diameter) were entered into the PLC, indicating that the distributor orifices did not become constricted.

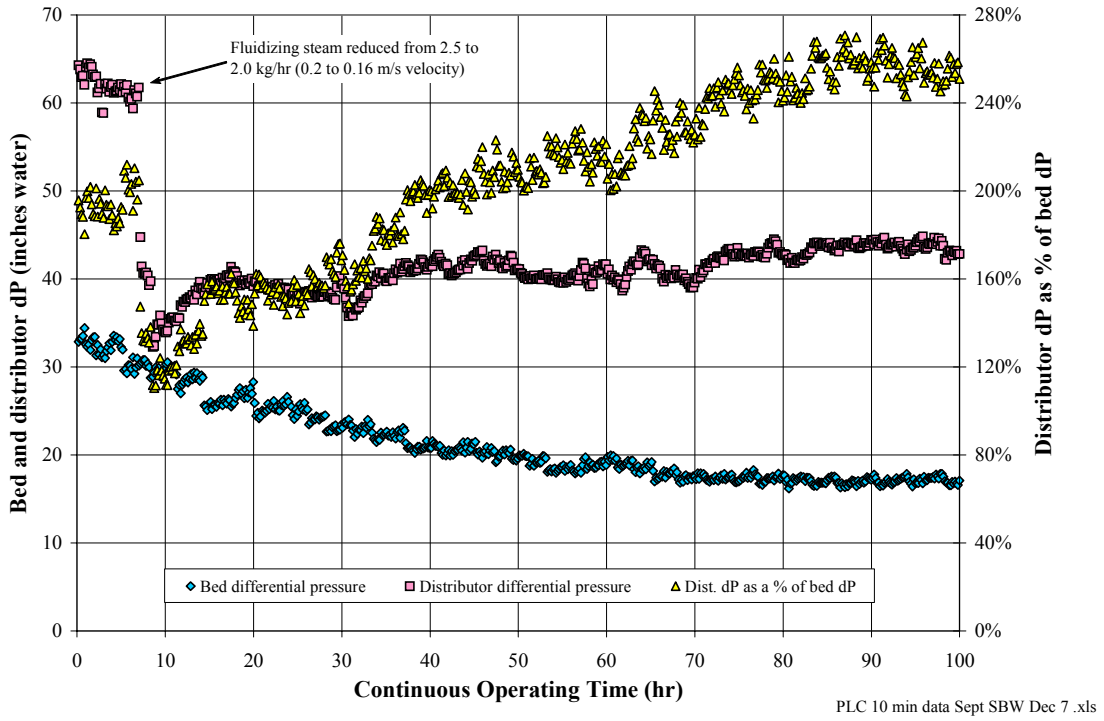

Figure 4.1-2. Bed and distributor differential pressures during the SBW FBSR test.

The decline in bed density as new product displaced the starting bed can be seen in the change in bed differential pressure in Figure 4.1-2. The rate of change after COT 54 is small because the slurry feed rate was reduced by 0.5 kg/hr and because the bed turnover was over 65%.

These set points established under communication sheet #2 were generally maintained for nearly two days of operation, except for four minor events, three of which caused short interruptions in slurry feed flow to the process and one which led to a minor adjustment to the slurry composition.

The first event (COT 8:20) resulted in a feed interruption and was precipitated by switching the main compressed air supply to the backup STAR Center compressor. A bulge was discovered in the main supply hose, which required replacement to address safety concerns. The momentary dip in air supply caused an automatic shutdown of power to the heaters and feed streams to the FBSR. Fluidization gas was switched to nitrogen. Systems were returned to normal operation and feed restarted after 25 minutes.

The second event was a pump seal failure that caused slurry to leak from the main feed recirculation pump into the secondary containment pan (COT 12:19). The feed slurry was transferred to another feed tank, flow from which was recirculated via another parallel recirculation pump, and there was no interruption in feed to the process. The transfer, however, caused a sudden small decrease in the slurry density (See Figure 4.1-3). The density change is believed to have resulted from air entrainment in the slurry when the transfer was made from one feed tank to another. At the time, the reduction in density was misinterpreted as a segregation of clay from the SBW simulant and 1.6 kg of clay was added to the remaining slurry (105 L) to compensate, effectively raising the clay concentration in the slurry from 230 gm to 247 gm clay/L SBW. This slightly higher clay concentration remained, however, well within the range for the desired product composition (see Figure 3.4-1), with negligible impact upon process product results.

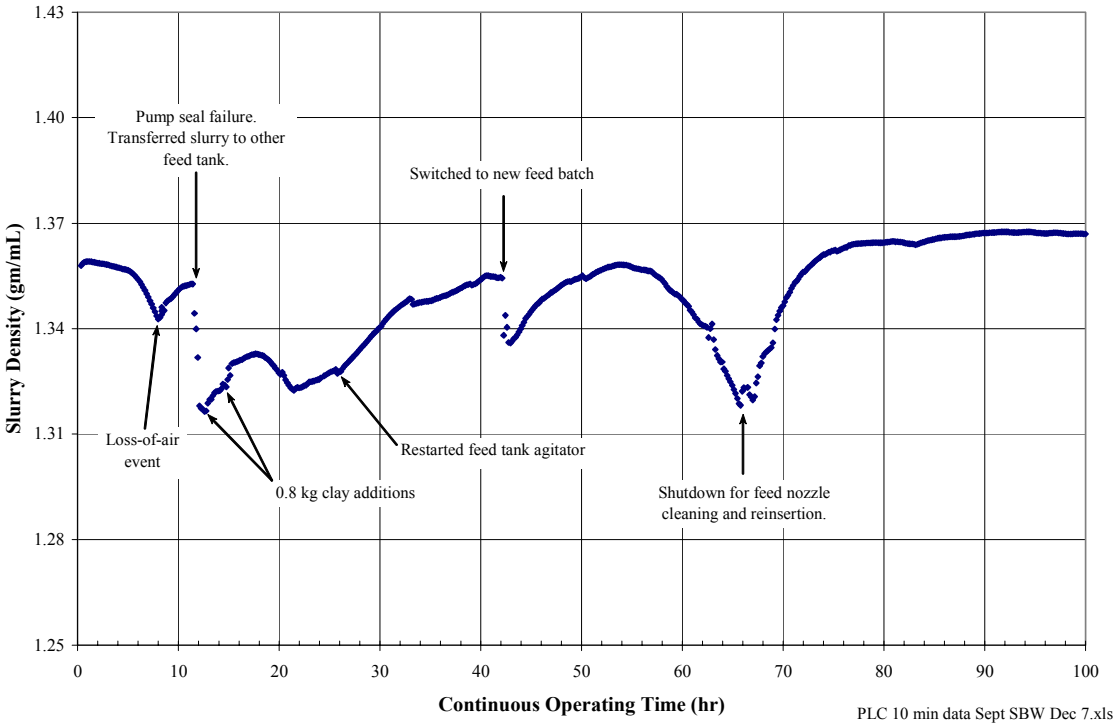

Figure 4.1-3. SBW slurry density as measured by the coriolis mass flow meter.

The slurry density routinely varied a small amount over time, presumably depending on the quantity of air that was entrained in the slurry, ranging from 1.32 to 1.37 gm/mL of slurry as measured by the coriolis mass flow meter. The most rapid changes in slurry density are associated with shutdowns and changes in feed tanks (Figure 4.1-3). In general, the density of the slurry feed would be expected to increase slightly over time in the feed tanks, as observed, as transient entrained air disengaged from the slurry mixture. Because slurry feed was controlled by mass, the density of the slurry had little impact on the operation. The only parameter affected by the small change in density was the quantity of atomizing nitrogen supplied, which was controlled volumetrically in proportion to the volume of feed. This impact was insignificant to the process.

In the third event (COT 14:52) a clump of undispersed clay, from the extra clay addition, may have restricted the feed injection nozzle. This resulted in a temporary (six minute) feed interruption while the liquid/slurry side of the nozzle was cleared and feed flow restored.

The final event, ordered under communication sheet #2, was a short feed interruption (95 seconds) during which slurry feed was switched to water feed to verify that the coriolis mass flow meter was giving reliable density readings (COT 24:04). This verification action was related to the second event noted above, since the slurry density continued to be lower than expected in spite of the extra clay addition. Passing water through the coriolis confirmed that the density readings were accurate.

The measured cyclone fines recycle rate was typically between 1.4 and 2.3 kg/hr, but suddenly decreased to less than 0.5 kg/hr at near COT 32. It was discovered that the lower recycle auger shaft had sheared and was not actually turning, leading to an inaccurate estimate of the fines recycle rate. Once the

shaft was repaired and excess accumulations of fines in the cyclone were returned to the bed, the recycle rate returned to normal (see Figure 4.1-8).

Some visual evidence of small nozzle accretions being formed and shed became noticeable about midway through the first day of operations, indicating they likely began even earlier. Small fragments of larger nozzle deposits/accretions were observed in product from the bed drain after about 20 hrs (bed drain of product was taken about every three to four hours to adjust bed height). No bed agglomerations were found, e.g., no large defluidized collections of bed granules were observed to have formed in the bed. A large intact nozzle accretion (approximately 1/2 inch diameter and 1 inch in length with centerline hole about 1/8 inch diameter) was first noted in a bed drain of product taken at about COT 32.

It was noted that nominal pressure in the atomizing gas line upstream of the nozzle had been increasing and fluctuating over time in a roughly step-wise manner, since soon after the test began. This pressure was about 6 psi at the beginning of the test and continually increased slowly with roughly ½ to 1 psi step-wise pressure increases/fluctuations (increase then drop back, but to the same or a net higher minimum level) until it reached about 10 psi just prior to the COT 32 bed drain. This generated some concern, but the pressure then dropped sharply back to 8 psi, which was thought to be a reasonable level.

This pattern of atomizing gas pressure behavior continued and the maximum pressures observed slowly increased to higher levels. A nozzle accretion of the size noted above was consistently observed, along with various fragments, in all subsequent bed drains over the next 18 hours. During this same time period, some concern was noted about the impact on bed fluidization/stability from potential buildup of accretions/agglomerations in the bottom receiver. Fluctuations in temperature measured by thermocouple T2, located just below the distributor, were observed to be increasingly erratic and of somewhat larger amplitude (10°C). Based on previous test experience, erratic T2 decreases meant accumulation of accretions/agglomerations below the distributor. Thermocouples positioned in the fluidized bed, however, continued to indicate good fluidization by their uniformity and consistency. Consequently no actions were taken at this time.

Communication sheet #3 was executed at COT 52.40 to reduce the carbon addition set point to 0.6 kg/hr while maintaining other process parameters unchanged. Hydrogen concentration in the off-gas was above 5 vol% and estimated NO_X destruction exceeded 98%, so the carbon addition set point was changed to reduce the weight fraction of excess carbon in the bed and filter products.

Continued erratic behavior of thermocouple T2, along with observations of nozzle accretions/fragments in the bottom bed drains, led to a decision to reduce the slurry feed rate to 2.5 kg/hr (communication sheet #4, COT 54:07), while maintaining the total atomizing gas flow rate at the level used throughout the test (NAR was increased). This was intended to reduce the size of the nozzle accretions. Further, purges of the bed drain port with 80 psig nitrogen gas before each bed drain operation were instituted to dislodge accretions/agglomerations that might be obstructing the drain line. The slurry feed rate was insufficient to produce bed product at a rate that would allow more frequent bed draining operations that would assure clearing of accretions/agglomerates from the bed. Consequently, the decision was made to screen bed material harvested near COT 51 and COT 53 and return the minus 50 mesh fraction to the bed. Screened bed media, totaling 709 gm, was returned to the bed and bed media was drained from the FBSR twenty minutes later (COT 57:35). Thermocouple T1, located below T2, showed an expected temperature spike when the bed was drained. T2 showed little change. Pulsing the drain line seemed to decrease the frequency of temperature dips on T2, but otherwise appeared to have little impact. No large agglomerations were observed in the drained bed product, just the typical nozzle accretions.

Near COT 62:30 the pressure of the atomizing gas upstream of the feed nozzle rapidly increased from 15 – 25 psig, indicating that the feed nozzle was becoming severely restricted, which indicated that appropriate feed slurry atomization was threatened. The nitrogen flow rate was increased briefly by substantially raising the NAR. This action cleared the restriction and restored the backpressure to normal levels.

The atomizing gas backpressure rose rapidly again at approximately COT 66, and increasing the NAR and water flushing of the liquid/slurry side of the nozzle did not clear the restriction. Feed was then purposely shut off for nearly three hours while the injector nozzle was cooled, removed, cleaned, and reinstalled. Approximately 50% of the air annulus was occluded. Restart was accomplished according to communication sheet #5, which was a continuation of the operating parameters and conditions established with communication sheet #4.

Because the bed drained at COT 65, prior to the shutdown for feed nozzle cleaning, contained several accretions, the decision was made to screen the drained media and return it to the FBSR so that more bed could be harvested in an attempt to drain out accretions that might remain in the reformer. A total of 759 grams of screened bed media were returned to the FBSR during the COT 66:10 shutdown. A subsequent bed drain recovered only one accretion.

Stable operation then continued for over 20 hours under the conditions of communication sheet #5. As expected, fewer accretions/fragments were harvested during the regular bed draining operations than were seen prior to cleaning the nozzle. Thermocouple T2 began tracking the behavior of T1 and responding as expected to bed draining operations. The bed mean particle size was slowly increasing over time, as had been the case essentially throughout the test.

At COT 86:40 the NAR was increased to 1150 in hopes of reducing the trend of continued gradual growth in the mean product particle size (communication sheet #6). The increased NAR led to a decreased rate of product accumulation in the bed and increased the rate at which fines were collected on the filter as determined by the masses of filter fines and bed product that were collected. These conditions were held until the completion of the test at COT 100. It was noted that atomization gas pressure began the stepwise increase pattern again during last five hours of the test and was at about 15 psi just prior to the test end. The COT 98 bed drain included two intact nozzle accretions and fragments of a third, while the sample drain included one intact nozzle accretion and considerable small accretion fragments. Prior to this time there had been only minor small accretions or fragments noted during bed drains and samples during the period of operation following the nozzle removal and cleaning. At the end of the run (COT 100), the bed drained well from the FBSR. Approximately 40 nearly intact medium to large nozzle accretions were noted in this final bed drain, and enough fragments to constitute another 10. Gentle prodding with a rod was required to complete a total bed draining. Two large nozzle accretions (3/4 inch diameter and 2 inch length) were found lying across part of the funnel drain entrance after the receiver and distributor were removed. No bed agglomerations were found. There was also a small ¼ inch deposit/accretion adhering to the exterior atomizing nozzle tip in the FBSR vessel.

Throughout the run, the slurry feed rate had been held conservatively low to assure that it did not exceed the capability of the system to transfer heat into the feed zone and to maintain bed temperature. As the alumina starting bed was displaced with newly formed mineralized SBW product, the thermal capacity and conductivity of the bed declined causing a slight increase in the differential temperature between the FBSR wall and the fluidized bed. Figure 4.1-4 shows the FBSR bed temperature (T3), wall temperature (T20), and the differential between the two. The differential temperature remained near 10°C, which is approximately half of the maximum acceptable operating limit for the FBSR equipment used in this test. A sudden increase in the differential can indicate a change heat transfer brought on by

sudden changes in the flow patterns within the bed as a result of impaired fluidization, fluidizing gas distributor restrictions, or a significant accumulation of defluidized accretions/agglomerates.

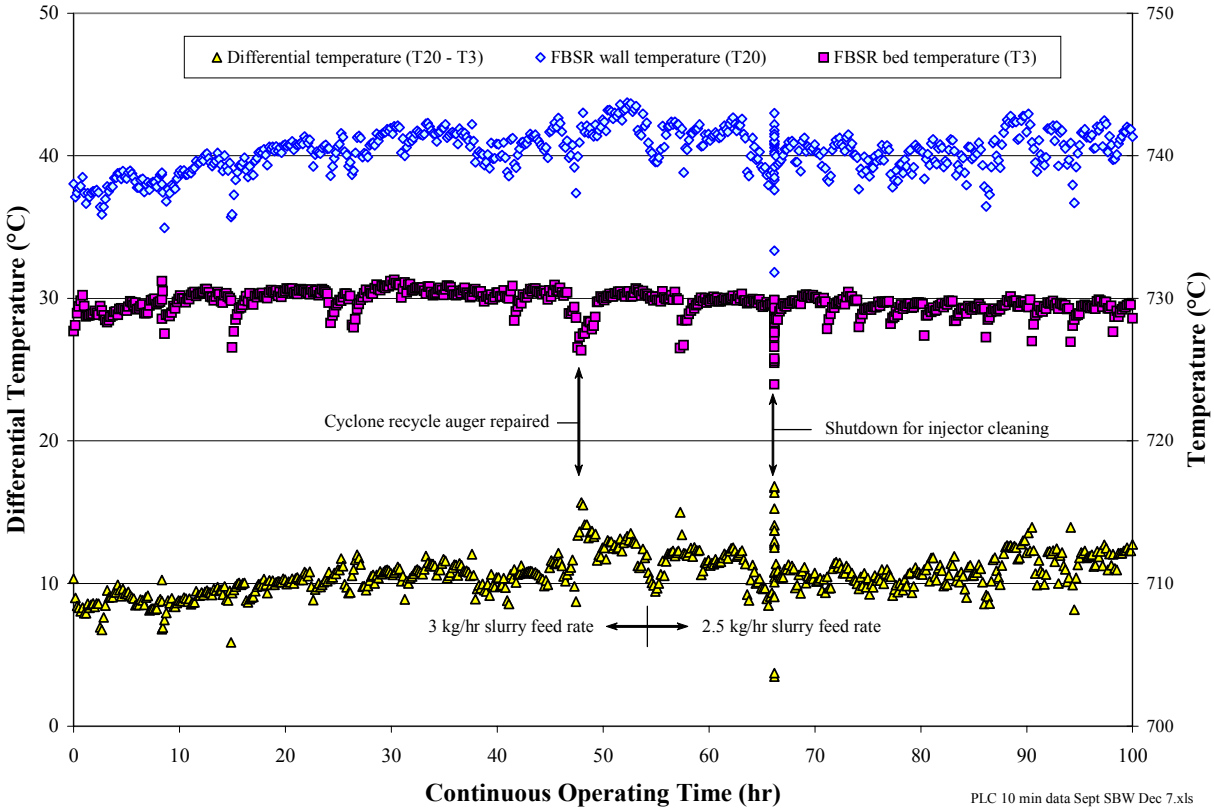

Figure 4.1-4. FBSR bed and wall temperature profiles.

4.1.2 **Fluidized Bed Performance**

One of the objectives of this test was to obtain stable, controlled, mineralizing process conditions and product material representative of longer-term steady operation. This, in turn, required establishing and maintaining appropriate stable bed fluidization operating conditions, and mineralizing reaction conditions, in the steam reformer vessel. Test process operating conditions, as described in the previous section, were adjusted appropriately as the bed characteristics changed gradually over time from those of the starting bed media (alumina grit) to those of the mineralized process product material (alkali-alumino-silicate).

The fluidized bed height, bed inventory, fluidized density, particle size, bulk density, and particle (true) density are key bed fluidization operating parameters and characteristics of the bed media/product. Bed height, bed inventory/mass, and fluidized density were continuously monitored and recorded by the PLC using differential pressures measured between a reference pressure tap location near the bottom of the bed (fluidizing gas distributor elevation), and pressure taps located at approximately 13 inches high in the bed, and in the upper disengaging section above the bed (see Figure 3.2-2).

Small amounts of bed product were periodically removed from the reactor to maintain the fluidized bed depth within an acceptable range and to obtain bed product samples for analyses. Bed product was removed either through a bottom drain orifice in the conical bottom receiver below the distributor and/or through a bed sample tube port that extends into the fluidized ("live") region of the bed at a location near centerline and 1.5 inches above the distributor elevation (see Figure 3.2-3). An interlock section consisting of two valves in series with an intervening pipe section is present in line below the sample tube, and another is present below the bottom receiver drain. The interlock valves are operated sequentially to collect "shots" of bed media from the selected location during operations. The interlocks collect a known volume "shot" of material during each cycle of actuation, equivalent to the pipe volume between the valves (approximately 150 ml), and prevent excessive air backflow into the vessel during the bed media collection.

Bed media collected through the bottom receiver is referred to as "bed bottom drain" or "bed drain" material. Bed media collected through the sample tube port are referred to as "bed samples", or "sample drains" and are expected to be more representative of the "active" fluidized bed media. These "bed samples" were regularly collected and used for fluidized bed media particle density and size determinations.

Bed media removed through the bottom receiver drain is bed media that has defluidized and collected in the bottom receiver (conical and drain tube sections) below the distributor. A static inventory of bed material, most of which would be fluidized if subjected to the flow conditions near or above the distributor, will collect in this "inactive bottom zone" up to an elevation approximately between one and two inches below the distributor (at or below the T2 thermocouple elevation and above the T1 thermocouple elevation). Initially this material will consist of starting bed material, but will be replaced with current active/fluidized bed media, which defluidizes in this "in-active" bottom receiver region following each bed drain collection activity. Bed particles and agglomerates, which grow too large to remain fluidized in the active bed zone above the distributor, will also fall-out and be collected on top of the static materials in the conical vessel bottom. If produced at a significant rate, these could build up and potentially impact the fluidizing gas distributor operations and bed fluidization. Regular bed drain collections were performed during the test operations to ensure that any such large unfluidized bed particles, accretions, or agglomerates collected would be removed and their presence/status evaluated.

Regardless of whether bed media was being collected through the sample tube or bottom drain, the activity involved three or more separate sequential "shots" (cycles of actuation of the interlock valves) for collection of bed media. In the sample tube case, the first two sequential "shots" were required to clear out the existing volume of "static" media collected earlier in the sample tube. The third, and any immediately subsequent "shots", are referred to as "dynamic shots" and considered to represent current active/fluidized bed media. Similarly, three to four shots from the bottom bed drain were considered to be necessary to remove all current static materials in the conical section and drain tube of the bottom receiver. Each valve, during a shot, is actuated in sequence and the maximum volume of the shot is the volume of the pipe between the two valves (approximately 150 ml). Depending on the bed media bulk density, the mass of each shot ranged from 0.3 kg at the test start, to about 0.15 kg at the end of the test.

The bed media bulk density was measured by pouring 20 – 30 cc of sampled bed media into a 100-ml graduated glass cylinder, settling the material by rapping the cylinder against the table or by setting the cylinder on a vibrator, and weighing the dry sample. The weighed sample was flooded with water to obtain an estimate of the void volume between the particles and an estimate of the particle density after recording the bulk density. The measurement was an estimate, because gas bubbles could form in the wetted bed media that might not be disengaged with tapping or vibrating, water might not fill into smaller particle voids, or the top of the water column might not always be exactly the same as the top

of the particle column. Nevertheless, the bulk and particle density tests were generally consistent with applicable density test methods (ASTM B 527, "Standard Test Method for Determination of Tap Density of Metallic Powders and Compounds", and ASTM C 128, "Standard Test Method for Density, Relative Density (Specific Gravity), and Absorption of Fine Aggregate"), and measured values for process monitoring and control during the test.

Bed product particle size distributions were measured during the test by obtaining about 15 – 35 grams of bed media sampled from the fluidized region and passing the material through a series of standard sieve screens, consistent with guidance in ASTM D 6913, "Standard Test Methods for Particle-Size Distribution (Gradation) of Soil using Sieve Analysis." The mass fraction of solids that accumulated on each screen (m_i) and the mean particle diameter of the size fraction (d_i) were used to compute the mass-mean and harmonic mean particle diameters (MMPD and HMPD). Process fluidizing calculations were based on the HMPD, which approximates the mean diameter of a sphere with an equivalent surface to volume ratio as the bed particles. The mass of fine particles influence the HMPD calculation more strongly than the masses of the larger particles.

$$\mathrm{MMPD} = \sum_{i=1}^{n} m_i d_i$$

$$\mathrm{HMPD} = \left[\sum_{i=1}^{n} \left(\frac{m_i}{d_i} \right) \right]^{-1}$$

The size fraction diameter (d_i) was defined as the geometric mean of the apertures for the sieve upon which the solids reside and the preceding, adjacent sieve ($d_i = \sqrt{a_i a_{i-1}}$). The diameter of the solids fraction that accumulated on the top screen was taken as the geometric mean of the sieve aperture and that of the next larger size sieve in the series. The fraction diameter for pan fraction of solids was taken as half of the aperture size of the last (preceding) sieve (a_n /2).

Figures 4.1-5 and 4.1-6 show how the bed operating conditions changed as the bed converted from the starting bed of alumina particles to a bed made primarily of mineralized product particles. The bed inventory decreased from an initial fluidized mass of about 15.5 kg at the start of the test to a mass of about 8 kg at the end of the test, before the final bed drain. These masses do not include about 19% more unfluidized mass in vessel receiver below the fluidizing gas distributor. The bed turnover had reached about 88% by the end of the test. The particle density, bulk density, and fluidized bed density also

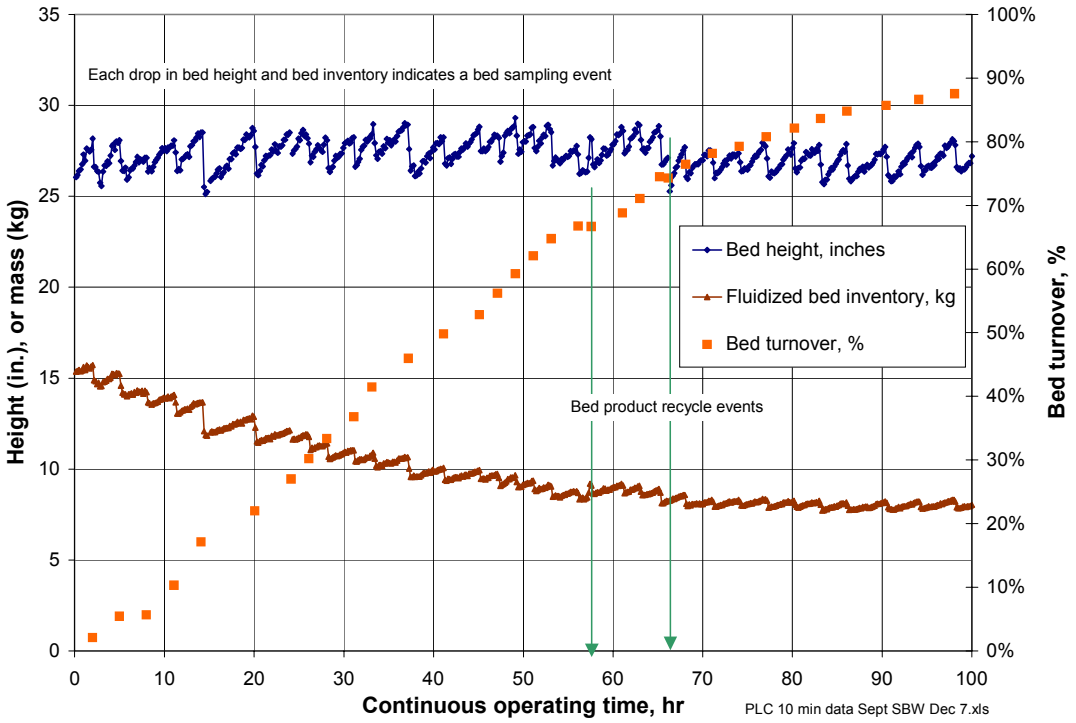

Figure 4.1-5. Bed height, inventory, and bed turnover.

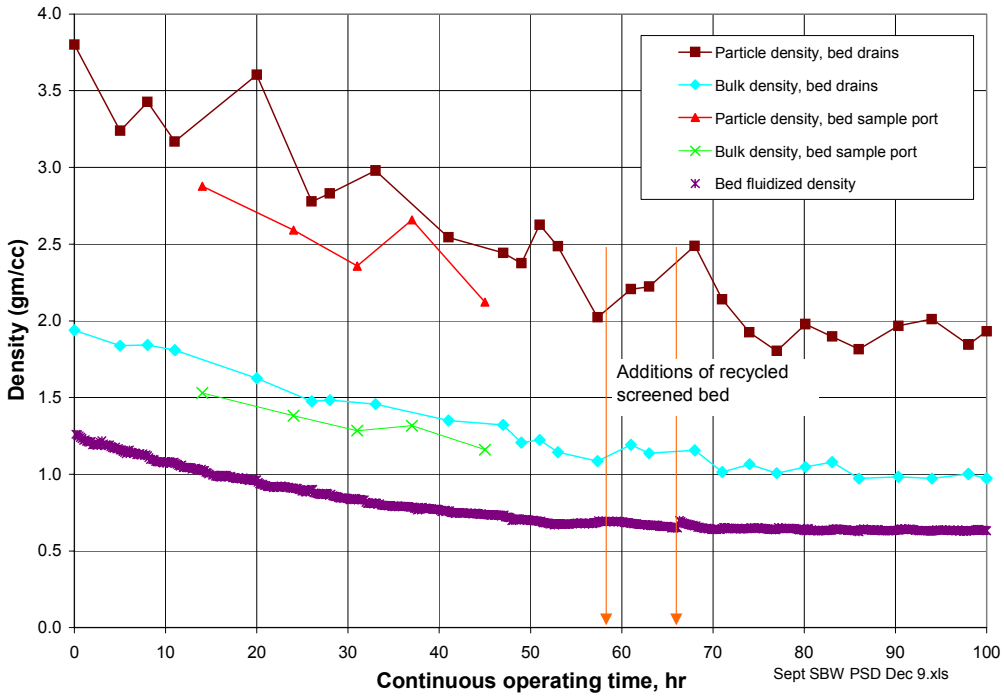

Figure 4.1-6. Bed particle density, bulk density, and fluidized density.

decreased by the end of the test to relatively stable values of about 1.9 gm/cc, 1.0 gm/cc, and 0.64 gm/cc respectively. Had the test continued until the bed turnover neared 100%, the bed density values would likely have been 5-10% lower, since the small amount of residual high density alumina starting bed material would have been completely replaced by the lower density product material.

Bed product was typically removed every 2-4 hours to successfully maintain the fluidized bed height within 26-29 inches. This maximized residence times of gas and particles in the bed, yet kept the bed height below the design maximum of 30 inches. Additionally, this kept the fluidized bed below the bottom flange of the transition section between the 6-inch diameter fluidized bed section and the 12-inch diameter particulate disengaging section of the reformer vessel.

The bed media density measurements for both bed drains and bed samples collected between COTs 14 and 45 indicate that both the particle density and bulk density ranged about 10% lower for bed samples (collected via the sample tube), as compared to material collected via the bottom receiver drain (bed drain). This difference in density was probably due to a higher concentration of the more dense starting bed material in the bed media collected through the bed drain port. Bed media was only collected through the bottom drain after COT 45, since the bed density values were earlier determined to be very close, regardless of which port was used, and because of the desire to ensure that any defluidized large bed particles/agglomerations or nozzle accretions were regularly removed from the fluidized bed and evaluated.

The trends in the average bed particle sizes are shown in Figure 4.1-7. Somewhat different trends were observed for the bed particle size distributions as the test proceeded, while the bed density values gradually decreased. The bed particle HMPD gradually increased from the starting bed HMPD of 0.128 mm to almost 0.2 mm at the end of the test. The trend gradually increased from about COT 10 to the end of the test. Whether or not the trend would have continued, or how soon the bed media might have reached an equilibrium HMPD for the operating conditions of the test, cannot be determined based on the test results.

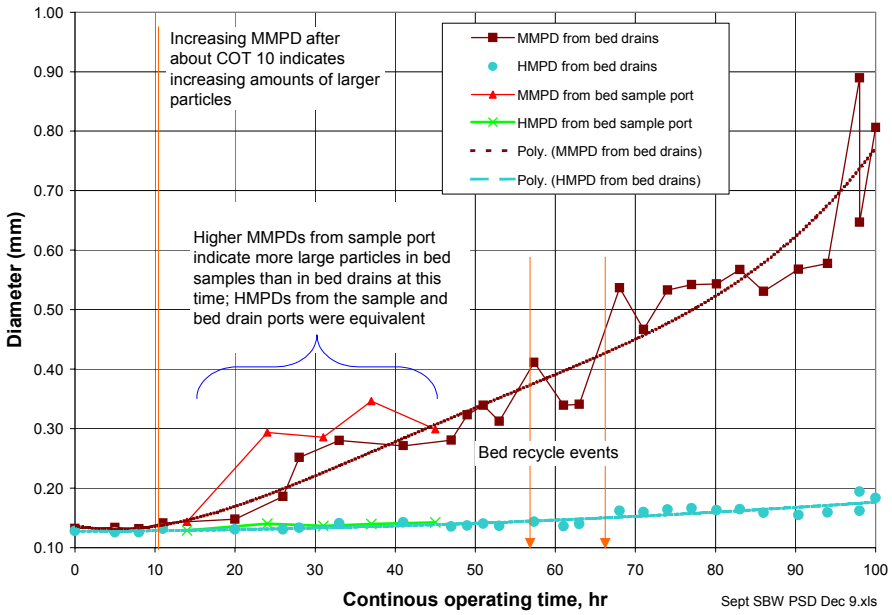

Figure 4.1-7. Bed media particle size trends over the course of the test.

The bed MMPD increased at an even higher rate during the test, ranging from 0.132 mm for the starting bed up to about 0.8 mm at the test end (for the final bed). Whether or not the trend would have continued, or how soon the bed media might have reached an equilibrium MMPD for the operating conditions of the test, cannot be determined based on the test results. Duplicate samples and particle size analyses for the COT 98 bed drain sample indicate potential extremes in the MMPD measurements, due to sampling and analysis artifacts. The measured MMPDs for these two duplicate samples were 0.65 mm and 0.89 mm, a relative percent difference of 31% from the average value of 0.77 mm.

Between COTs 14 and 45, when bed media was collected and analyzed both from the bed sample port and the bottom receiver drain, the bed media MMPD from the bed samples was slightly higher than that for the bed media from bed bottom drain. This small difference may have been due to a higher proportion of new bed product particles, including pieces of small nozzle accretions, being present in the fluidized bed, and consequently collected in the bed samples via the sample tube, or simply to various potential sampling errors (e.g. differences in sample collection timing, hang-up of larger materials in the bed drain, etc).

The bed operating conditions were not significantly affected by the two bed product recycle events (described in Section 4.1) that occurred at about COTs 57 and 66. At these times, or for a short time after these times, the bed turnover remained constant, and the bed fluidized density remained constant or slightly increased. Variations in other bed operating parameters remained within typical ranges.

The cyclone recycle rate measurement is a good indication of whether the recycle system is functioning properly. The rate at which fines are collected by the cyclone corresponds roughly with the fraction of the bed particles that are smaller than 100 µm (Figure 4.1-8). The recycle rate measurement was much lower than otherwise determined when the recycle auger was not functioning. Recycle was interrupted during the loss-of-air event that precipitated an automatic shutdown of the system and when the auger shaft broke. Some time after the system was brought back on-line after the automatic shutdown, the recycle auger was found de-energized. The second event took longer to discover, because

the motor was turning the broken end of the shaft. A depression in the measured recycle rate was recorded in both cases.

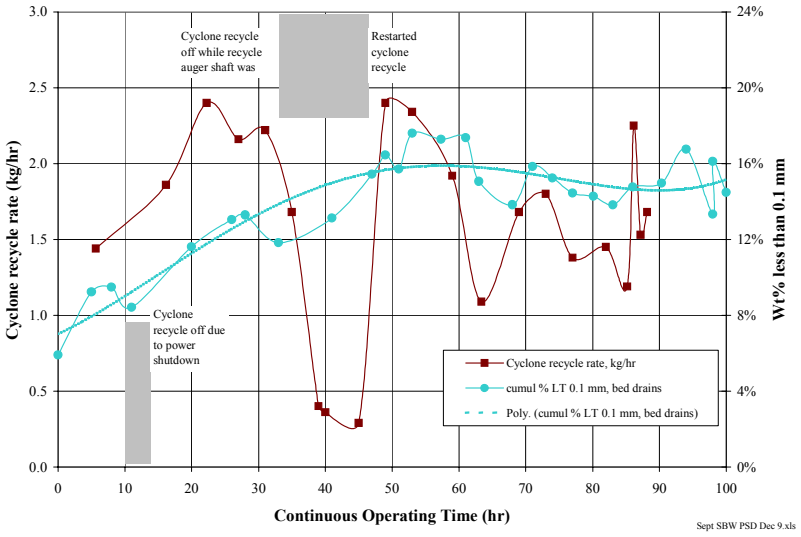

Figure 4.1-8. Cyclone recycle rate and bed fines fraction.

4.2

4.3 Solid Product and Fines Characterization

A sample of the fluidized bed material at COT 0 is depicted in an optical photograph shown in Figure 4.2-1. The starting alumina bed media appear like broken pieces of glass, all of fairly uniform size. The material is 100 "grit," average particle size of 140 μm, and a measured HMPD of 128 μm. These pieces have sharp edges and angular surfaces, and are nearly transparent. A 1 mm scale is visible in the background of this photograph. Additional optical photographs (Figures 4.2-2 through 4.2-4) show how the starting alumina bed was displaced over time with product bed. A few of the starting alumina bed particles are still visible by COT 86 (Figure 4.2-4). Individual product particles are more spherical in form and some have a popcorn-like appearance when compared to the alumina starting bed material.

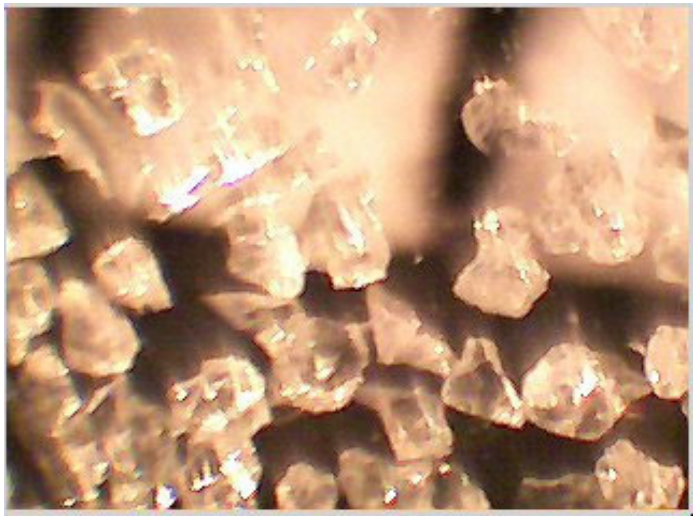

Figure 4.2-1. Photograph of the starting bed material.

Figure 4.2-2. Photograph of the bed material at COT 37.

Figure 4.2-3. Photograph of the bed material at COT 68.

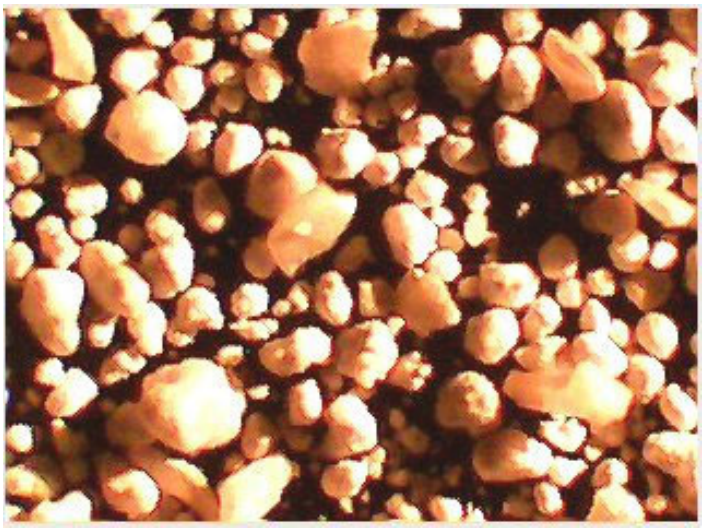

Figure 4.2-4. Photograph of the bed material at COT 86.

The alumina starting bed media had a very narrow particle size distribution (PSD), averaging 0.128 mm HMPD. Only about 5 wt% was less than 0.1 mm, 100 wt% was less than 0.2 mm. The narrow PSD for the starting alumina bed broadened during the test to include significant amounts of particles less than 0.1 mm, and significant amounts of particles greater than 0.3 mm, as shown in Figure 4.2-5. At the end of the test, almost 20 wt% of the bed mass was particles less than 0.1 mm in diameter, and over 40 wt% of the bed mass was particles greater than 0.3 mm.

Figure 4.2-5. Measured bed particle differential size distributions over the operating period.

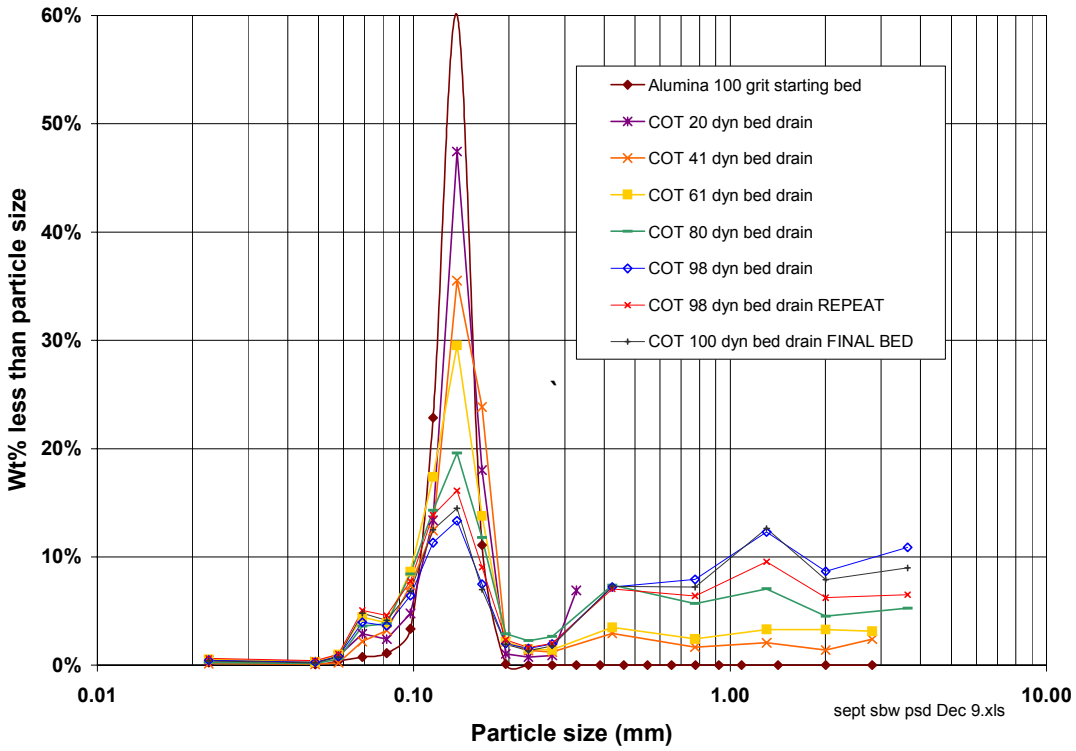

The end-of-test bed media had a nearly tri-modal distribution of particles. One group of particles, comprising about 30 wt% of the bed, had an average size near the original starting bed size, between 0.1 and 0.2 mm. A small mass, representing less than 5 wt% of the bed, is represented by smaller particles about 0.06 mm in diameter. A third group of larger particles comprises over 60 wt% of the bed, and has a very flat size distribution ranging from 0.4 to 4 mm.

The PSDs shown in this figure do not include larger fragments of nozzle accretions that were found in the bed media after the first few hours of test operation. Figure 4.2-6 shows a few of these fragments (appearing as lighter-colored, pieces [circled]) in the COT 24 bed media. The black particles are unreacted carbon additive. The finer gray material, comprising most of the sample, is the combined mineralized product and starting alumina bed.

The amounts and sizes of the nozzle accretion fragments had increased, as shown in Table 4.2-1, to represent between 3-6 wt% of the total mass of drained bed media by the end of the test. These pieces were screened from the bed media using a 3.5 mesh (5.6 mm) screen. Most of these pieces were smaller than 1 inch in size, but a few were larger than 2 inches. A few retained an intact tubular shape (Figure 4.2-7). When the nozzle accretion was attached to the nozzle, the atomized feed sprayed through the center hole. These nozzle accretions seemed to form and break off the nozzle continuously throughout the test. They did not cause any bed defluidization events, or any detectable operational problems, although they might have impacted the feed atomization performance.

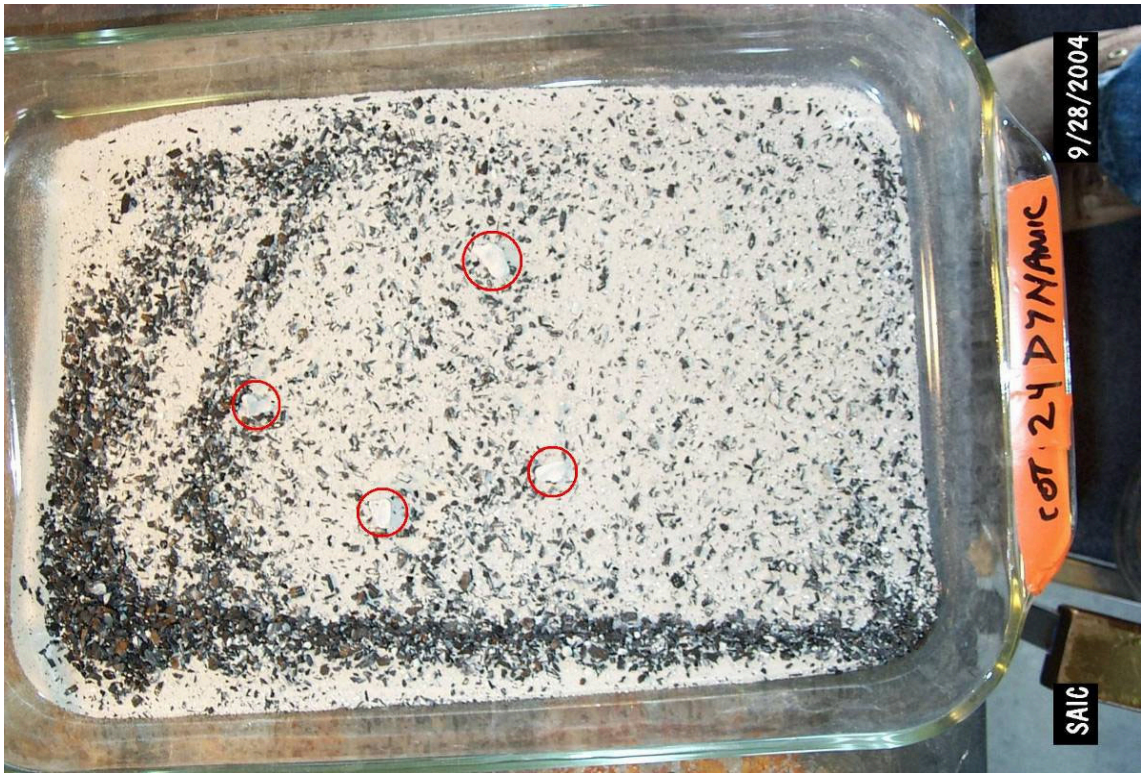

Figure 4.2-6. Nozzle accretion fragments (circled) in the COT 24 bed media.

Table 4.2-1. Properties of +3.5 mesh (+5.6 mm) nozzle accretion fragments found in dynamic bed drain samples.

COT	Approximate number of fragments	Weight % of total bed drain sample
77	9	1.4
80	13	0.8
83	15	4.6
86	14	4.6
90	13	2.8
94	Not recorded	2.8
98	~30	3
100	~100	6.3
Final bed drain	>100	3.2

Figure 4.2-7. An intact nozzle accretion recovered in the COT 51 static bed drain.

Figure 4.2-8 is a photograph showing the accretion remaining on the slurry feed atomization nozzle face in the reactor vessel at the end of the SBW test. This accretion was approximately 10 mm (0.4 inch) in diameter and 5 mm (0.2 inch) in length from the nozzle face. About half of the accretion broke off under light finger pressure and the majority of the remainder was easily removed using a small wire brush. A thin (< 0.5mm) film of hard material deposit remained on the nozzle face even after wire brush cleaning. This same type of residual film had been observed, and occasionally even more extensively, with different nozzles in previous experiments. It is hypothesized that this film is deposited on surface locations that are much cooler than other reactor surfaces that are at temperatures approaching the process operating temperature. The cooler surfaces appear to be subjected to liquid/slurry mist, due in part to close proximity to the cooler atomizing gas/feed flow. Once a film is in place it serves as a nucleation site for continued nozzle deposit/accretion growth. It has been visually observed that no hard film deposit is present on the majority of the hot vessel surfaces that are exposed to the process environment. Further, the area of residue film deposit appears to be much smaller with the modified nozzle design than that observed in similar, earlier tests with existing SprayCo® nozzle designs.

Although not obvious in Figure 4.2-8, the attached nozzle accretion/deposit had a clear cylindrical shaped channel at near the centerline through which the atomizing gas and atomized slurry mixture had been flowing. This is typical of the much larger tubular shaped accretions found in the bed, such as those shown in Figure 4.2-7, clearly indicating that they formed on the nozzle. The channel in the large accretion expands to a much larger diameter as the atomizing gas/slurry cone expands away from the nozzle face. The larger accretions also generally show a curvature, as they grow in length, consistent with what would be expected as the atomized feed bends upward due to the axial flow of fluidizing gas in the reactor vessel.

Figure 4.2-8. Nozzle accretion observed during vessel inspection at the end of the test.

Higher scanning electron microscope (SEM) magnifications of a bed particle are shown in Figure 4.2-9. This photograph is of the final bed product (COT 100) mounted in epoxy and then sectioned to allow for inspection of the interior of a bed particle. The "spots" noted in the photograph were analyzed for composition. Spot 1 is a calcium rich point with some oxygen, perhaps CaO. Areas noted by Spot 2 appear to be the desired nepheline product. The area noted by Spot 3 is rich in Al, Si, and O; and could be assumed to be aluminosilicate Sagger clay particles. Spots 4 and 6 are epoxy mounting material. Spot 5 appears to be mostly epoxy mounting material, but has some palladium. Non-conductive SEM samples need to be sputter coated with a conductive coating such that they can be examined. Typically, either carbon or Au/Pd coatings are used. The samples were carbon coated but the Pd is probably a contaminant from the sample handling and/or preparation process. Spot 7 appears to be a sodalite phase containing Cl. The information in this photograph indicates that the desired product material was being produced.

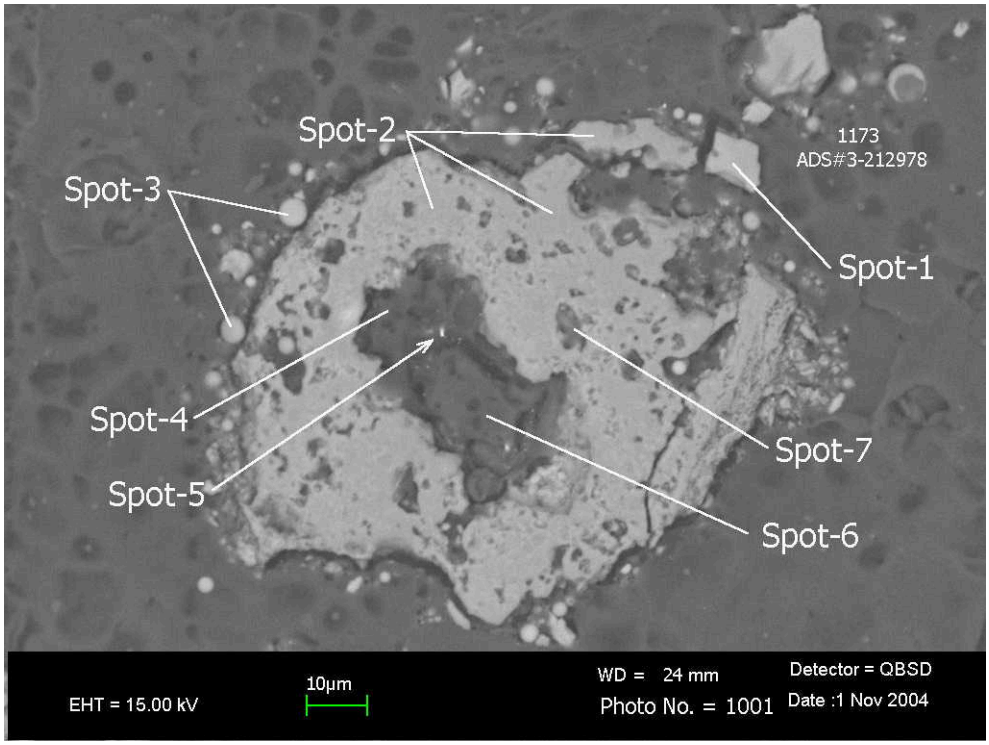

Figure 4.2-9. SEM photograph of the final bed (COT 100).

Voids are visible (Figure 4.2-9) within the larger product particle. This figure shows that the product particles do not generally consist of coatings of product that grew, onion-skin style, on the alumina particles (like typically occurs in SBW calcination and in SBW steam reforming to a carbonate product). Instead, the solid product granules appear to be formed by collections of many smaller particles and successive deposits of very small particles on the surface of existing larger product granules, much as what one might expect from successive rough/haphazard powder coating deposits of the very small clay particles contained in the atomized slurry droplets. Individual particles, on the surface of a larger particle, may range from less than 1 micron to several microns in diameter.

Fines elutriated from the bed and collected in the cyclone were continuously recycled back to the bed, except when the cyclone recycle rate was measured, cyclone catch samples were collected, or when the recycle auger shaft severed. Fines passing through the cyclone with the off-gas were collected by the heated sintered metal filters, and periodically removed from the test system. The filter fines have the consistency of fine powder or talc; individual particles tend to clump together, but are relatively easy to collect.

Differential particle size distributions of the cyclone and filter fines are compared to the end-of-test bed PSDs in Figure 4.2-10. The expanded scale shows how the test-end bed particle size measurements varied. The difference between the two COT 98 bed PSD measurements can be attributed to sampling and analysis artifacts. The final bed PSD leaned towards slightly smaller particle sizes than indicated by

the COT 98 bed media, probably because, during bed cool-down after COT 100, bed grinding attrited the particles. The cyclone and filter fines varied little during the test, as expected, since these fines are largely elutriated product, and the bed operating conditions were not significantly changed during the test.

Figure 4.2-10. Particle size distributions for the cyclone and filter fines.

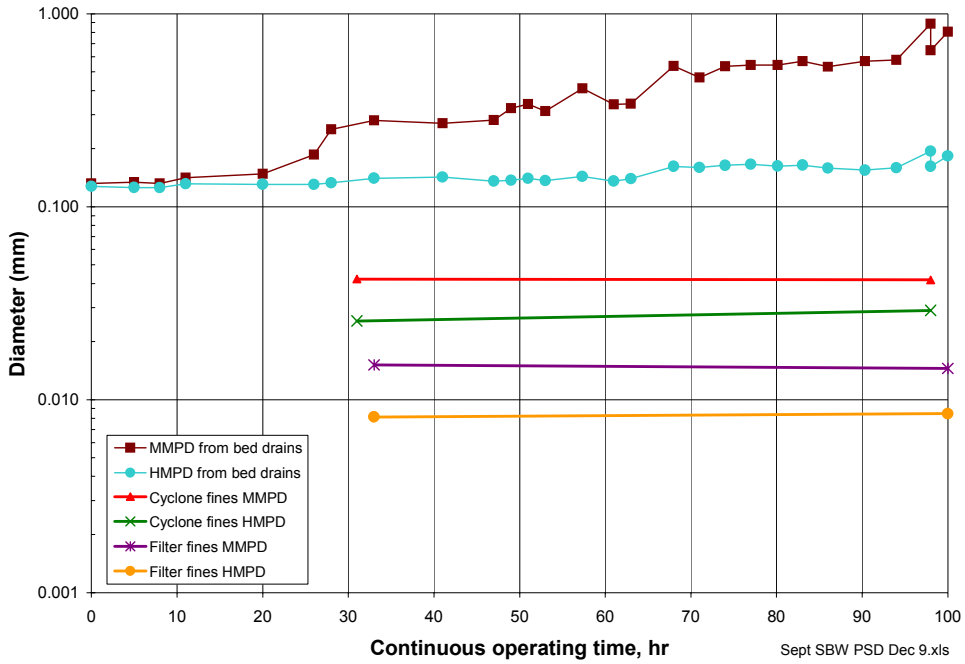

The average particle sizes are shown in Figure 4.2-11. The end-of-test MMPD of the cyclone particles (0.042 mm) was, on average, about 18 times smaller than the average COT 98 bed product (0.77 mm). The MMPD of the end-of-test filter fines (0.015 mm) was about 3 times smaller than the end-of-test cyclone fines.

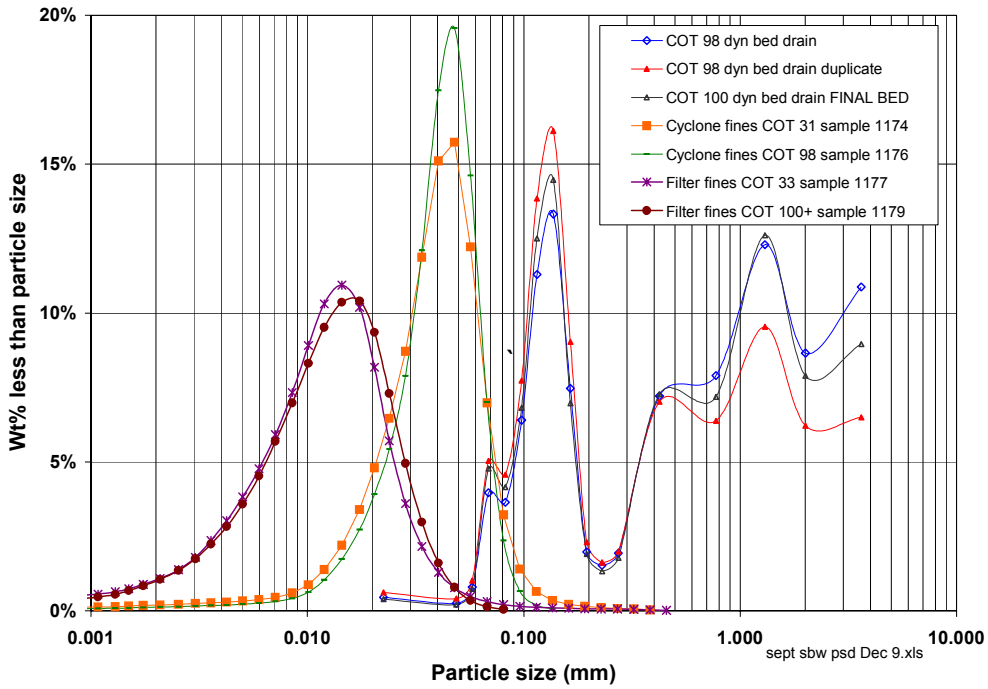

Figure 4.2-11. Average particle size measurements for the cyclone and filter fines.

The morphology of the cyclone fines can be seen in Figure 4.2-12. This SEM photograph indicates that the cyclone fines appear to be generally smaller versions of the bed product particles. Much smaller, sub-micron particles are visible on the surfaces of larger particles at this magnification. Individual particles range in size from 5-50 microns, consistent with the measured particle size distribution. The presence of carbon particles, as noted in the figure, indicates that the unreacted carbon in this size range was captured and recycled to the fluidized bed as desired.

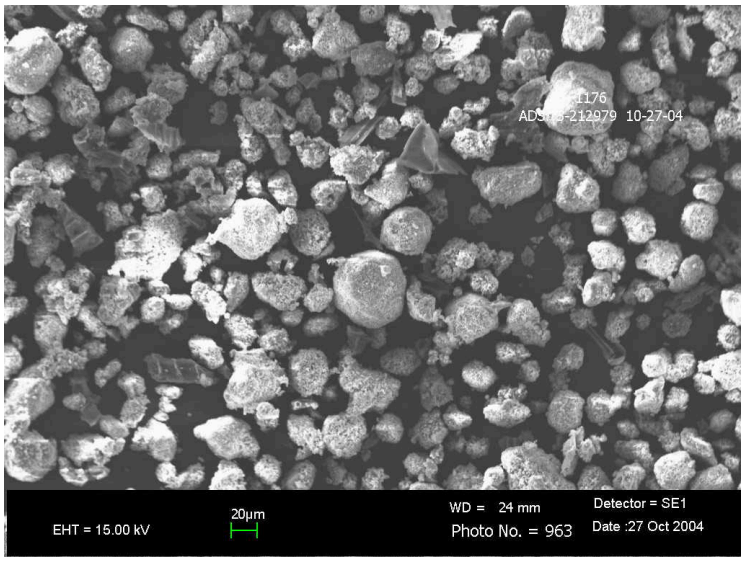

Carbon Particles

Figure 4.2-12. SEM photograph of cyclone fines sample at COT 98.

The morphology of the filter fines is shown in Figure 4.2-13. Particles ranging in size from 1-20 microns are visible, also consistent with the measured particle size distribution. The particles appear to be loose agglomerations of smaller particles.

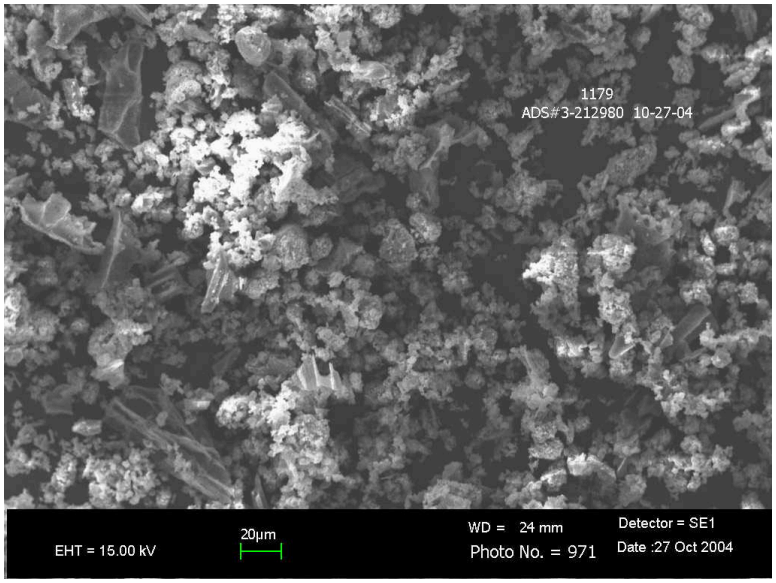

Figure 4.2-13. SEM photograph of filter fines sample at COT 100+.

The end-of-test bulk density of the cyclone and filter fines are shown in Table 4.2-2. Tapping the sample, consistent with ASTM B 527, significantly consolidates the sample, increasing the bulk density by about 43% and 60% respectively for the cyclone and filter fines.

Table 4.2-2. Bulk densities of the cyclone and filter fines.

Description	Bulk density (g/mL)	
	Untapped	Tapped
Cyclone Fines (including un-reacted carbon) at COT 98 (sample 1176)	0.534	0.765

Final Filter Fines (including un-reacted carbon) at COT 100+ (sample 1179)	0.300	0.480

Results of x-ray diffraction analyses on the solid products are summarized in Table 4.2-3. Inspection of the information in the table suggests the following. The alumina used for the starting bed depletes over time as the bed turns over and the desired nepheline product moves from a minor to major phase in the bed. Sodium aluminum oxide is seen as a trace phase in the bed; this is most likely a minor reaction between the feed and the starting bed material. Sodalite is a trace phase in all of the products. This is a desired product as it provides the cage-structured molecule for constituents such as Cl and SO_4. It is likely a trace phase since the concentrations of Cl and SO_4 are relatively small in the SBW. Anatase (TiO_2) is seen as a trace phase in the cyclone and filter products. This constituent is also a trace contaminant in the Sagger clay additive. Quartz (SiO_2) is seen as a trace or minor phase in all of the products. The Sagger clay contains up to 65 wt% SiO_2, and a minor portion is found as free SiO_2 (quartz) in the raw material. It is likely that this free silica (quartz) is not reacting during the steam reforming process. Previous FBSR experience has indicated that this constituent may contribute to defluidizing agglomerations [Soelberg, 2003], and may have contributed to the nozzle accretions/agglomerations noted in the bed product near the end of the demonstration. Sodium aluminosilicate is a major phase in the filter product. This phase is insoluble in acids, usually forming brittle, glassy crystals and is stable only at temperatures above 700ºC. It constitutes the sodium end-member of both the plagioclase and the alkali feldspar series. The phase does not appear to be detrimental, but may not afford the cage-structured molecule that would capture other metals or anions. Short residence times in the FBSR reactor may lead to the formation of this phase. This leads to the possibility that excessive atomization of the feed led to a "spray drying effect" for very fine droplets and the rapid formation of small particles of metastable minerals (e.g., carnegieite). The spray drying effect may have inhibited chemical reactivity, particle growth, and perhaps accounted in part for the morphology observed in the SEM photographs. In instances where particles did undergo particle growth (i.e. +70 mesh particles), the necessary reactions did occur to form the favorable sodalite or nosean phases.

A more detailed analysis of the solid products will be reported separately by SRNL. That analysis will include data regarding performance of the products when subjected to the Product Consistency Test (PCT) and the Single Pass Flow Through (SPFT) Test. Chemical composition of the solid products is detailed in Section 4.4.

Table 4.2-3. Summary of mineral phases observed in the FBSR solid products.

Description	Al_2O_3 Corundum PDF# 74-1081	$(K_{0.25}Na_{0.75})AlSiO_4$ Nepheline PDF# 74-0387	$Na_2Al_{22}O_{34}$ Sodium Aluminum Oxide PDF# 76-0923	$Na_{5.27}Ca_3(SiO_6O_{18})$ Combeite high	PDF# 78-1650	$Na_4Cl(Al_3Si_3O_{12})$ Sodalite PDF# 82-0517	SiO_2 Quartz PDF# 85-1053	TiO_2 Anatase PDF# 21-1272	$Na_{1.55}Al_{1.55}Si_{0.45}O_4$ Sodium Aluminum Silicate PDF# 49-0006	Bed
COT 31	Major	Minor	Trace	None	None	Trace	None	None	Bed	
COT 71	Minor	Major	Trace	Minor	Trace	Trace	None	None	Bed	
COT 100	Minor	Major	Trace	Minor	Trace	Trace	None	None	Cyclone	
COT 31	None	Major	None	Minor	Trace	Minor	None	None	Cyclone	
COT 71	None	Major	None	Minor	Trace	Minor	None	None	Cyclone	
COT 100	None	Major	None	Minor	Trace	Minor	Trace	None	Filter	
COT 33	None	Some	None	Trace	Trace	Minor	Trace	Major	Filter	
COT 71	None	Some	None	Trace	Trace	Minor	Trace	Major	Filter	
COT 100	None	Some	None	Trace	Trace	Trace	Trace	Major		

Off-Gas Characterization and Off-gas System Performance

The off-gas system downstream of the FBSR heated filter includes the thermal oxidizer for destroying H_2, CO, and total hydrocarbons (THC) from the FBSR, a water-spray partial quench to cool the hot oxidizer outlet off-gas, a reheater to ensure off-gas temperature control, and a carbon bed. The partial quench cooled the off-gas to about 130 ^oC, cool enough for the downstream carbon bed. The carbon bed was used in this test to capture Hg species and any halogen gases (HCl, Cl_2, etc) and SO_2 that may be in the off-gas for mass balance purposes.

4.4.1 Off-gas Composition at the Steam Reformer Heated Filter Outlet

The average off-gas composition (wet basis) at the outlet of the heated filter is shown in Table 4.3-1 for each test condition. The wet basis composition was calculated from the dry, as-measured composition by (a) correcting for zero and span calibration error/drift, and (b) normalizing the dry composition to a wet basis using the off-gas moisture content. The moisture content at the filter outlet location was not directly measured but was calculated from the fluidized bed input flow rates of fluidizing steam, evaporated water from the simulant, and water from oxidation of hydrogen-bearing species in the feed. The amount of water produced from the H^+ in the simulant was only 0.02 kg/hr, which was very small compared to the amount of fluidizing steam (2 kg/hr for most of the test), and the amount of total water in the simulant (1.7 kg/hr for a simulant slurry feed rate of 3 kg/hr).

The trends in the heated filter outlet off-gas composition are shown in Figure 4.3-1. This figure shows the continuously-monitored composition averaged over 10-minute time periods. Occasional gaps in the data trends occur when the instruments were off-line for calibrations. The carbon additive was fed to the FBSR, without any simulant feed, prior to COT 0. This established an initial inventory of carbon in the fluidized bed to ensure that FBSR conditions were sufficiently reducing when simulant feed was started. The trends over time indicate graphically how the gas composition varied during the test period. Concentrations of reduced gas species (H_2, CO, THC, and CH_4) were relatively high at COT 0.

After COT 0, when the simulant feed was started, off-gas concentrations of reduced gas species decreased when oxygen in the form of NO_3 in the feed and O_2 in the atomizing gas was started. Immediately following COT 0, the initially high NO_x levels gradually decreased, perhaps as the carbon inventory in the bed continued to increase at a relatively high carbon additive feed rate, or due to increasing catalytic effects as the inventory in the bed of potentially catalytic metals in the simulant increased. Apparent catalytic effects of simulant constituents were observed in prior SBW FBSR tests. The decreasing NO_x levels early in this test are consistent with trends in NO_x concentrations in prior tests.

A minor process upset occurred at COT 2:40, shortly after the test start, when one of the carbon addition valves stuck open, allowing some air inleakage every time the other carbon addition valve opened. This valve was rapidly repaired, but during the repair the carbon addition was momentarily turned off. The concentrations of reduced gas species significantly decreased, and the CO_2 and NO_x concentrations spiked, during this time. After the repair was complete and the carbon addition was restarted, the off-gas conditions returned to levels consistent with the trends prior to the process upset.

The carbon addition rate was decreased from 0.8 kg/hr to 0.7 kg/hr at COT 7, because NO_x levels had decreased sufficiently and NO_x destruction exceeded process objectives. The initial carbon input rate was no longer needed. Following this change, until about COT 40, NO_x levels slowly increased

simultaneously with a slow decrease in the H_2 concentration. This slow change in concentrations indicated that the carbon inventory in the bed slowly decreased following the decrease in the carbon feed rate.

Table 4.3-1. Off-gas composition (wet basis) at the outlet of the FBSR heated filter.

			FBSR outlet gas composition, wet basis											
			O_2, %	CO_2, %	CO, %	H_2, %	THC, ppm	CH_4, ppm	NO, ppm	NO_x, ppm	H_2O, %	N_2, %		
Test condition start date, time	COT	Test condition	AE1_A1_O2_WB_ADJ	AE1_A3_CO2_WB_ADJ	AE1_A5_CO_WB_ADJ	AE1_A2_H2_WB_ADJ	AE2_CST1_THC_WB_ADJ	AE1_A6_CHX_WB_ADJ	---	---	AE1_H2O_FRAC x100	AE1_N2_WB_ADJ	Total, %	Mole weight
9/27/04 9:00	0.0	1	-0.01	5.51	0.58	2.84	1,649	1,295	665	646	53.3	38.4	100.6	23.0
9/27/04 16:00	7.0	2	-0.01	5.67	0.44	2.30	1,532	1,186	587	556	50.3	41.8	100.4	23.4
9/29/04 14:15	52.8	3	-0.01	5.89	0.43	2.55	1,402	1,140	425	483	50.7	40.8	100.4	23.3
9/29/04 15:37	54.1	4	0.00	5.78	0.29	1.83	1,271	973	452	580	48.7	43.6	100.3	23.7
9/30/04 6:36	66.2	5	0.00	5.74	0.24	1.51	1,401	1,055	518	656	48.6	44.1	100.2	23.7
10/1/04 3:10	86.7	6	0.00	5.51	0.25	1.53	1,427	1,080	490	697	46.9	46.1	100.3	23.9
10/1/04 16:35	100.1	Feed off												
Test averages			0.00	5.69	0.37	2.02	1,454	1,118	562	589	49.7	42.6	100.4	23.5

Notes:

1. The CEMS data were recorded by the PLC, and automatically adjusted for zero, span error, and moisture content. All measurements were made on a dry basis.
2. PLC tag numbers in the column headers indicate the source of the data. No tag number indicates that the data was calculated from other PLC data.
3. The PLC calculations were checked by hand and compared with concentrations recorded on data sheets.
4. The THC analyzer sample gas was split from the other sample gas upstream of the CEMS 1 carbon filter, so the THC measurements were not affected by hydrocarbon sorption by the carbon filter.
5. The NO and NO_x results were corrected for 4x dilution of the sample gas (by air). The air dilution was required for chemiluminescent CEM operation to provide excess O_2 needed for operation of the NO_x converter. No sample gas dilution was performed for the other analyzers.
6. NO data is not available for some time periods. The NO_x analyzer was only in the NO_x mode during those times.
7. NO_x data is not available for some time periods. The NO_x analyzer was only in the NO mode during those times.
8. The moisture content and gas molecular weight were determined based on input mass flowrates and calculated gasified or reacted products.
9. The N_2 concentration was determined by difference on a dry basis and then converted to wet basis.
10. The N_2 flowrate determined from the calculated N_2 concentration (by difference) and the FBSR outlet gas flowrate averaged 5.1 kg/hr, which agrees well (within 7.8%) of the total N2 flowrate into the FBSR. The total N_2 flowrate into the FBSR averaged 5.8 kg/hr (from PLC tag V1_F1_VAL) less the average N_2 flowrate (0.30 kg/hr) into the oxidizer stage 2 (B1_F7_VAL).
11. The sum of the gas concentrations, near 100%, indicates good data quality.

[PLC 10 min data Sept SBW Dec 7.xls]CEM 1 table

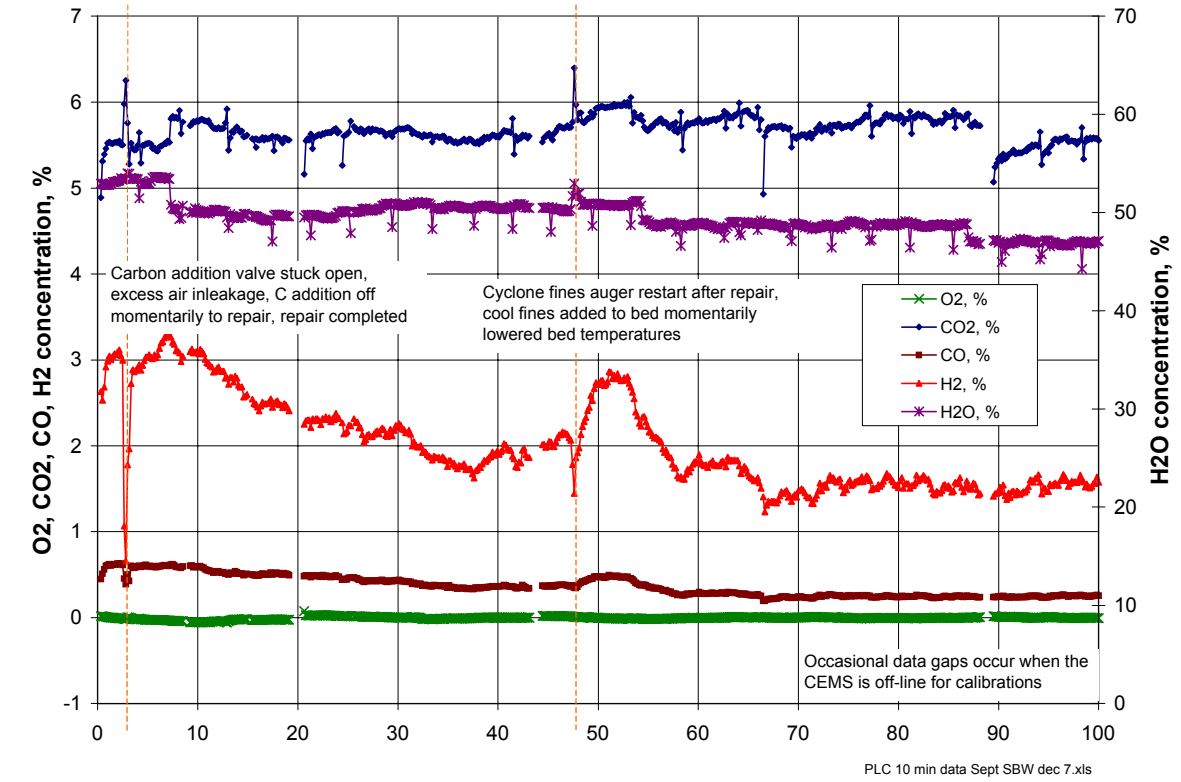
O2, CO2, CO, H2 concentration, %
H2O concentration, %
Carbon addition valve stuck open, excess air inleakage, C addition off momentarily to repair, repair completed
Cyclone fines auger restart after repair, cool fines added to bed momentarily lowered bed temperatures
O2, %
CO2, %
CO, %
H2, %
H2O, %
Occasional data gaps occur when the CEMS is off-line for calibrations
PLC 10 min data Sept SBW dec 7.xls

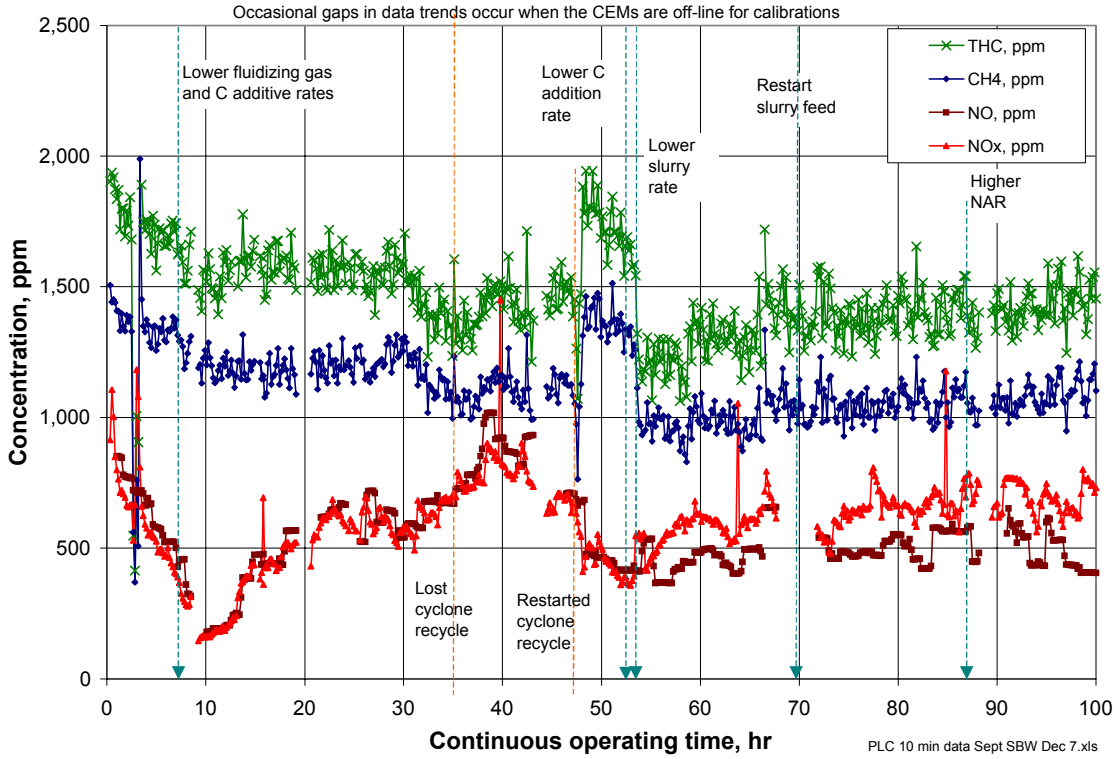
Occasional gaps in data trends occur when the CEMs are off-line for calibrations
Lower fluidizing gas and C additive rates
Lower C addition rate
Lower slurry rate
Restart slurry feed
Higher NAR
THC, ppm
CH4, ppm
NO, ppm
NOx, ppm
Lost cyclone recycle
Restarted cyclone recycle
Concentration, ppm
Continuous operating time, hr
PLC 10 min data Sept SBW Dec 7.xls

Figure 4.3-1. Wet basis off-gas composition at the FBSR heated filter outlet.

The cyclone recycle was impaired between about COT 35 and COT 47 when the recycle auger shaft was severed. During this time, starting at about COT 40, the NO_x concentration started to decrease, and the H_2 concentration started to increase. The carbon addition rate was again decreased, from 0.7 kg/hr to 0.6 kg/hr, at COT 52:40, because NO_x destruction was very acceptable. NO_x levels slowly rose, but the increase was limited because of the reduction in the slurry feed rate at COT 54:07. The off-gas composition was relatively constant during the remainder of the test, except for the ~3-hour time period when the feed rate was cut off at about COT 66.2, when the feed nozzle restricted and was cleared. The COT clock was turned off during this time. The off-gas composition during this time is not included in the test averages, nor it is shown in the off-gas trend, Figure 4.3-1.

4.4.2 Off-gas Composition Downstream of the Oxidizer

The average off-gas composition (wet basis) downstream of the thermal oxidizer, partial quench, and reheater is shown in Table 4.3-2 for each test condition. All of the CEMS 2 measurements, except for the O_2 measurement, were made on a dry basis, after condensing off-gas moisture from the off-gas. The O_2 measurement was made using a heated extractive ZrO_2 electrochemical sensor, on a wet basis, for thermal oxidizer process control. Except for the O_2 measurement, the wet basis composition was calculated from the dry, as-measured composition by (a) correcting for zero and span calibration error/drift and (b) normalizing the dry composition to a wet basis using the off-gas moisture content. The O_2 measurement required no calibration corrections and was measured on a wet basis. The moisture content downstream of the oxidizer and partial quench was not directly measured, but was calculated from the input flow rates of water into the process, and calculated amounts of water produced from oxidation reactions.

The CEMS 2 off-gas measurements were continuous, and recorded automatically by the PLC. Off-gas concentration trends in the oxidizer outlet off-gas composition are shown in Figure 4.3-2. This figure shows the continuously-monitored concentrations averaged over 10-minute time periods. The trends over time indicate graphically how the gas composition varied during the test series.

The O_2 concentration was very constant, controlled well by the oxidizer control system. Moisture and CO_2 concentrations were also very constant. The concentrations of these species were relatively insensitive to individual process changes considering the multiple sources of both H_2O and CO_2 in the oxidizer off-gas. Changes in FBSR operating conditions had little impact on the oxidizer outlet off-gas moisture content because much of the total off-gas moisture in the oxidizer outlet gas was the product of auxiliary fuel combustion and the partial quench water spray. The moisture content contributed at this point due to feed slurry content, fluidizing gas, and FBSR gas reactions (3.0 scfm average) was only about 12% of the total moisture (26 scfm average) in the off-gas downstream of the oxidizer and partial quench.

The oxidizer operated very efficiently to oxidize H_2, CO, THC, and CH_4 in the FBSR off-gas to CO_2 and H_2O. The average CO concentration measurement downstream of the oxidizer was 5 ppm. The high sensitivity CO analyzer experienced about 5 ppm positive zero drift following each calibration. The calibrated operating range of this nondispersive infrared (NDIR) analyzer was 0-300 ppm (wet basis). This bias is within the acceptable measurement error of up to 2% of the full-scale value. The gradual increases in the CO measurements for a few hours following each calibration result from this drift. The

reported CO values are biased a few ppm high because of this drift. The true CO concentration was probably between 0 and 6 ppm, considering a maximum measurement error range of $\pm$2% of the full-scale range. A maximum CO concentration of 6 ppm (wet basis), when converted to 7% O_2, dry basis, would be 9 ppm; well within the EPA Hazardous Waste Combustor (HWC) Maximum Achievable Control Technology (MACT) standard of 100 ppm for CO.

Table 4-3-2. Off-gas composition (wet basis) downstream of the oxidizer and upstream of the carbon bed.

Test condition start date, time	COT	Test condition	Oxidizer outlet gas composition, wet basis											Mole weight
			O_2, %	CO_2, %	CO, ppm	NO, ppm	NO_2, ppm	NO_x, ppm	SO_2, ppm	HCl, ppm	H_2O, %	N_2, %	Total, %	TOT_MW_AFTER_PQ x 1000
			B1_A1_O2_WB_ADJ	AE2_A1_CO2_WB_ADJ	AE2_A1A_CO_WB_ADJ	AE1_CST2_NO_WB_ADJ	AE1_CST2_NO2_WB_ADJ	AE1_CST2_NOX_WB_ADJ	AE1_CST2_SO2_WB_ADJ	AE2_A2_HCL_WB_ADJ	AE2_H2O_FRAC x 100	AE2_N2_WB_ADJ		
9/27/04 9:10	0.0	1	3.00	5.27	10	72	-2	70	1.1	0.1	39.2	53.2	100.7	25.0
9/27/04 16:10	7.0	2	3.00	5.43	7	79	-4	75	-0.6	0.1	37.7	54.6	100.7	25.1
9/29/04 14:15	52.8	3	3.00	5.52	3	81	-7	73	-1.0	0.1	37.4	54.8	100.7	25.2
9/29/04 15:37	54.1	4	3.00	5.53	3	80	-4	76	0.0	0.2	36.9	55.2	100.7	25.2
9/30/04 6:36	66.2	5	3.00	5.63	3	83	-4	79	-0.5	0.3	37.2	54.9	100.7	25.2
10/1/04 3:10	86.7	6	3.00	5.63	1	80	-4	76	0.8	0.3	37.6	54.4	100.7	25.1
10/1/04 16:35	100.1	Feed off												
Test averages			3.00	5.48	5	81	-4	76	-0.5	0.2	37.4	54.8	100.7	25.2

Notes:

1. The CEMS data were recorded by the PLC, and automatically adjusted for zero, span error, and moisture content. All measurements were made on a dry basis.
2. PLC tag numbers in the column headers indicate the source of the data. No tag number indicates that the data in that column was calculated after the test, from other PLC data, and not taken directly from the PLC.
3. The moisture content and gas molecular weight were determined based on input mass flowrates and calculated gasified or reacted products.
4. The N_2 flowrate determined from the calculated N_2 concentration (by difference) and the FBSR outlet gas flowrate averaged 66 kg/hr, which agrees reasonably well (within 18%) of the total N_2 flowrate into the oxidizer. The total N_2 flowrate into the oxidizer (including purge N_2, N_2 from oxidizer air, and N_2 from the feed nitrates) averaged 56 kg/hr.
5. The sum of the gas concentrations, near 100%, indicates good data quality.
6. The PLC calculations were checked with hand calculations and compared with concentrations recorded on data sheets during the test.

[PLC 10 min data Sept SBW Dec 7.xls]CEM 2 table

Figure 4.3-2. Wet basis off-gas composition downstream of the thermal oxidizer.

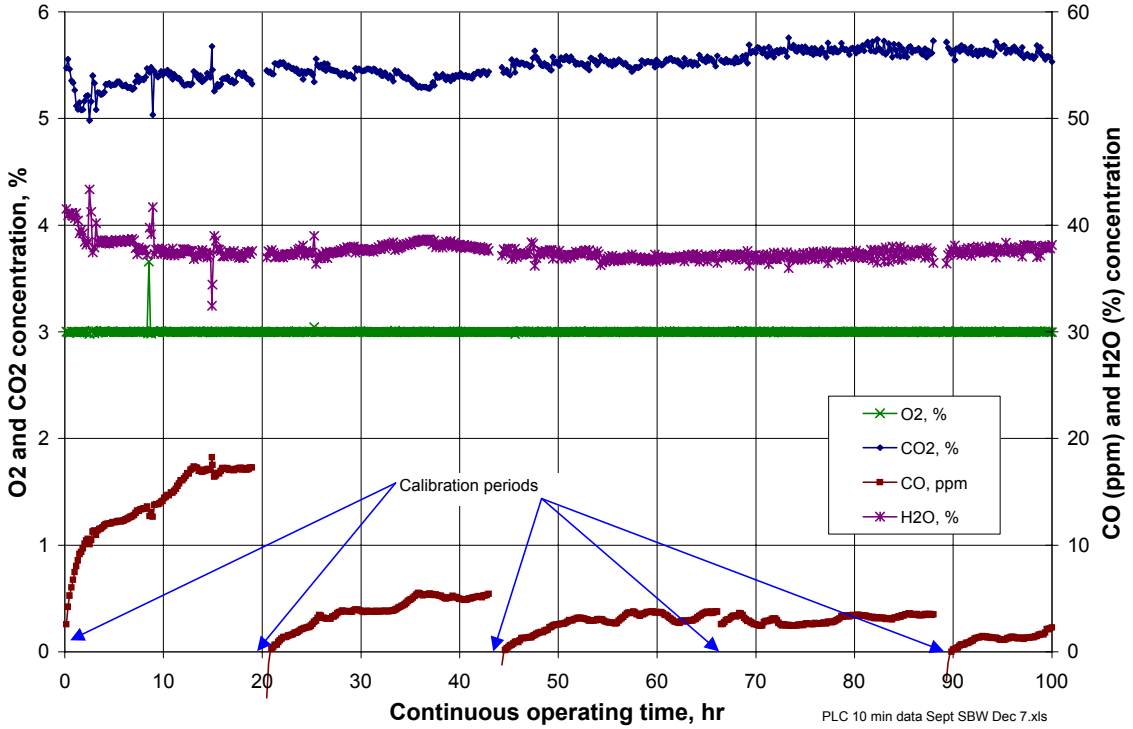

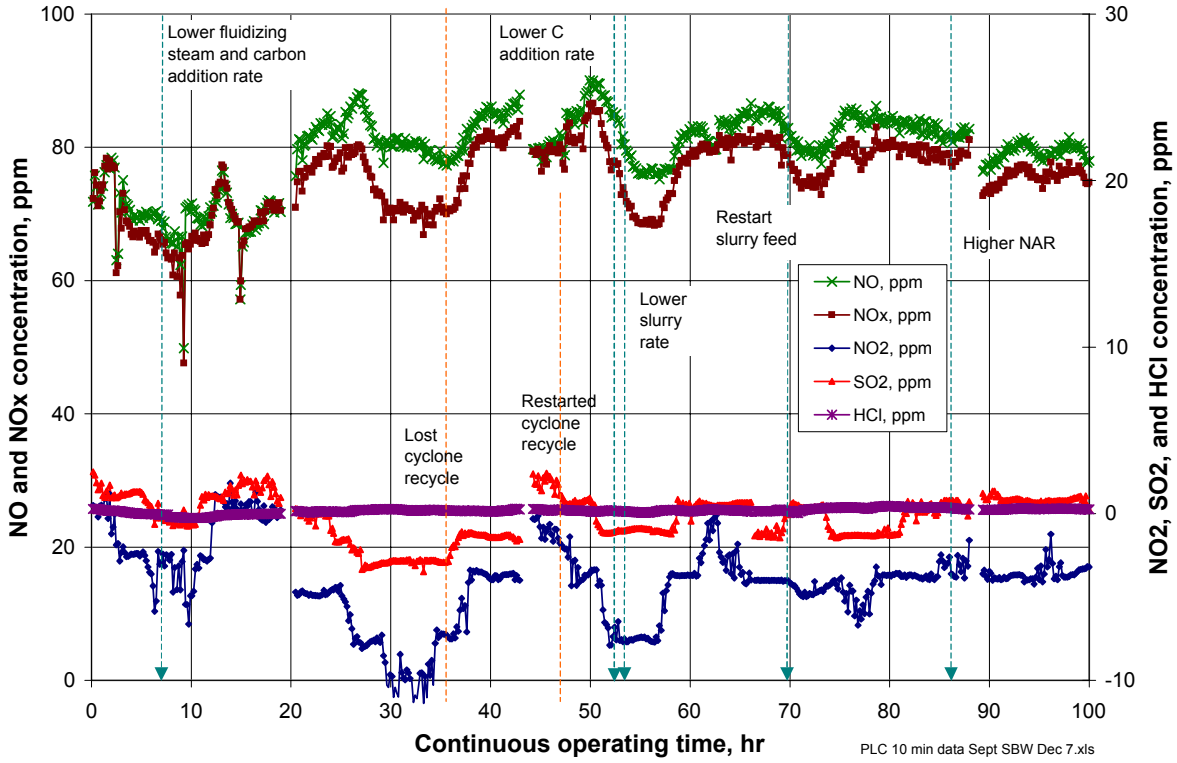

The HCl and SO_2 concentration measurements were also very low, averaging –0.5 ppm and 0.2

ppm, respectively. Ranges of maximum HCl and SO_2 concentrations were calculated based on typically acceptable instrument errors. Maximum HCl values could range to about 10 ppm (wet basis), based on a nominal 0-500 ppm range for this analyzer. This corresponds to a maximum concentration of about 15 ppm (dry, corrected to 7% O_2), still within the HWC MACT standard of 21 ppm for HCl.

The oxidizer outlet dispersive ultraviolet (DUV) NO_X analyzer directly measures both NO and NO_2, and then calculates the NO_X concentration by summing the NO and NO_2 measurements. The NO_2 measurement averaged –4 ppm during the test, causing the calculated NO_X measurement to average 4 ppm less than the NO measurement. The calibrated full-scale range for this analyzer was 0-500 ppm, so a 4 ppm bias in the measured data is only 0.8% of the full-scale range. No corrections were made to the NO_X data based on this small amount of bias.

4.4.3 NO_X Destruction

The nitrates and nitrites in the simulant react with the reductant in the FBSR, converting the N in the nitrates to predominantly N_2, and potentially other nitrogen gas species such as NO, N_2O, HCN, and NH_3. While only NO and NO_2 are measured by the FBSR outlet CEMS, grab samples in prior steam reformer tests have indicated the presence of both NH_3 and HCN in the FBSR outlet gas [Soelberg, 2003]. The presence of gas species such as NH_3 that, upon sorption in water form basic solutions containing such ions as NH_4^+ and OH^-, is confirmed by the pH measurements of the CEMS 1 condensate that averaged 9.2, even though the CEMS 1 condensate also contained sorbed nitrates and carbonate that would otherwise have driven the pH below 7. The pH of the CEMS condensate from the fully oxidized off-gas downstream of the oxidizer was typically less than 7 (averaging 3.3 for the CEMS 2 condensate) because of sorbed CO_2 (which forms carbonic acid) and trace amounts of other acid gas species. Species such as NH_3, if present in the FBSR off-gas, were efficiently destroyed by the oxidizer, and so did not impact the pH of the CEMS 2 condensate.

Table 4.3-3 shows NO_X destruction based on the amount of NO_X (NO and NO_2) measured in the off-gas compared to the amount of nitrate and nitrite in the feed. NO_X destruction trends during the test series are shown in Figure 4.3-3. The NO_X destruction results for this test easily met the test objective of at least 80% NO_X destruction. The calculated steam reformer NO_X destruction averaged 97.5% for the test series. Average NO_X destruction for specific test conditions ranged from 96.7% to 98.1%.

NO_X destruction started out lower, as low as 95%, in the first hour of test operation. It may have been lower than the test averages because of either unsteady-state carbon inventory conditions in the fluidized bed, or because, early in the test, the fluidized bed did not catalyze NO_X reducing reactions as much as later in the test. Components of the SBW simulant (such as Cr, Cu, Fe and Ni) are known catalysts under many conditions. Results of prior SBW FBSR tests have indicated catalytic effect by the fluidized bed on NO_X reduction reactions.

NO_X destruction during this SBW test was higher, averaging 97.5%, than NO_X destruction during the Hanford LAW FBSR test, when it averaged 92% [Olson, 2004]. The same carbon additive was used for both tests. The carbon:oxidant stoichiometry for the SBW test averaged 288%, while the carbon:oxidant stoichiometry for the Hanford LAW test was higher, averaging 412%. The higher NO_X destruction during the SBW test could have been due to the slightly higher FBSR operating temperature

of 729°C (for TC3), compared to 722°C for TC3 during the Hanford LAW test. A catalytic effect could also have contributed to the higher NO_X destruction during the SBW test, even though the carbon:oxidant stoichiometry was lower. The Hanford LAW simulant did not contain the potential catalytic components that the SBW surrogate contained.

Table 4.3-3. NO_X destruction for the SBW test series.

Test condition start date, time	COT	Test condition	FBSR carbon stoichiometry, %	At the FBSR filter outlet			At the oxidizer outlet		
				NO_x MTEC, ppm wet	NO_x, ppm wet	NO_x destruction, %	NO_x MTEC, ppm wet	NO_x, ppm wet	Total NO_x destruction, %
				---	AE2_CST1_NOX_WB_ADJ	---	---	AE1_CST2_NOX_WB_ADJ	---
9/27/04 9:00	0.0	1	297	23,256	646	97.2	2,322	70	97.0
9/27/04 16:00	7.0	2	249	24,858	556	97.8	2,540	75	97.1
9/29/04 14:15	52.8	3	202	24,933	483	98.1	2,525	73	97.1
9/29/04 15:37	54.1	4	240	21,885	580	97.3	2,169	76	96.5
9/30/04 6:36	66.2	5	240	21,676	655	97.0	2,079	79	96.2
10/1/04 3:10	86.7	6	240	20,832	697	96.7	1,922	76	96.0
10/1/04 16:35	100.1	Feed off							
Test averages			248	23,912	588	97.5	2,423	76	96.8

Notes:

1. The CEMS data were recorded automatically by the PLC, and automatically adjusted for zero, span error, and moisture content. All measurements were m

2. The NO_x Maximum Theoretical Emission Concentration (MTEC) is the calculated concentration in the off-gas that would exist if all NO_3 in the feed were gas, without any other NO_x formation or destruction.

3. PLC tag numbers in the column headers indicate the source of the data. No tag number indicates that the data in that column were calculated after the test not taken directly from the PLC.

4. Total NO_x destruction at the oxidizer outlet is calculated based on the oxidizer outlet NO_x concentration compared to the calculated NO_x MTEC at that loc includes thermal NO_x formed in the oxidizer in the NO_x destruction calculation.

5. The NO_x destruction in the oxidizer calculation is based on the difference between the FBSR NO_x destruction and the total NO_x destruction downstream o when the oxidizer actually reduces the amount of NO_x in the FBSR outlet gas.

[PLC 10 min data Sept S

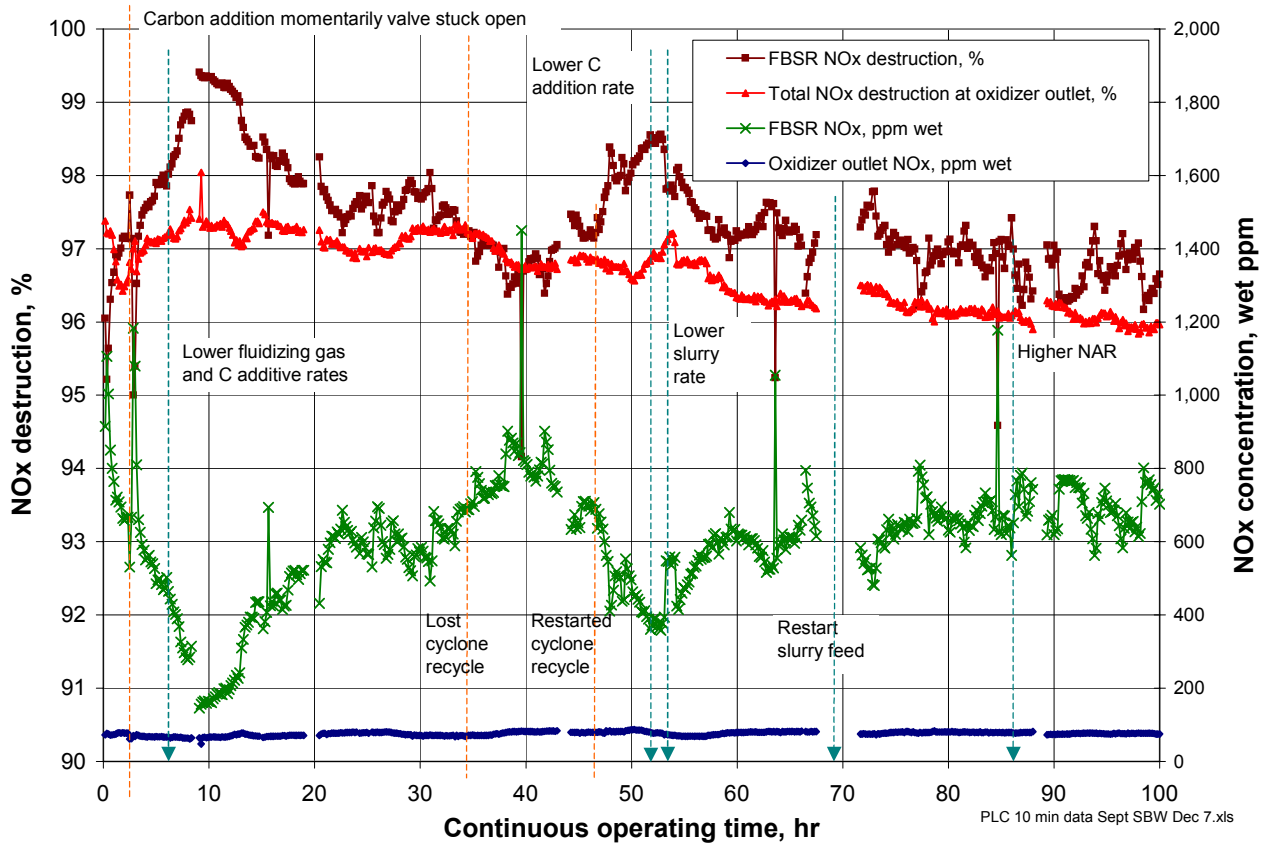

Figure 4.3-3. NO_X destruction trends for the SBW test series.

NO_X destruction was also determined for the entire steam reforming test system, using the NO_X measurements downstream of the thermal oxidizer. These NO_X destruction values show how a complete, integrated system performs to destroy nitrates in the feed and NO_X in the off-gas. The total system NO_X destruction ranged between 96.0–97.1% for the different test conditions, slightly lower than the NO_X destruction determined for the FBSR alone.

The nominal oxidizer NO_X concentration, prior to COT 0 when there was no NO_X in the FBSR off-gas, was about 50 ppm (wet basis). This was thermal NO_X formed in the oxidizer. The oxidizer will tend to generate thermal NO_X, or destroy NO_X contained in the entering gas, to reach its baseline of 50 ppm [ref?]. The FBSR off-gas NO_X concentration averaged 588 ppm (wet basis) for the test. That average concentration would be diluted about 10x to about 59 ppm, considering the dilution of the FBSR off-gas by the oxidizer input gases (natural gas and oxidizer air) and the evaporated partial quench water, but not including the oxidizer thermal NO_X. The total of the diluted FBSR NO_X and the thermal NO_X, at an average of 109 ppm, is higher than the measured oxidizer outlet NO_X concentration that averaged 76 ppm (wet). While the presence of NO_X in the FBSR off-gas depressed the formation of thermal NO_X, there was still enough thermal NO_X formation to cause the overall system NO_X destruction to be slightly lower than the FBSR NO_X destruction.

The NO_X destruction by the oxidizer averaged –36.6% for the test, because some thermal NO_X was

still formed. The amount of thermal NO_x was lower from the 50 ppm (wet) baseline for the oxidizer to about 17 ppm. This 17 ppm represented a negative NO_x destruction for the oxidizer. Several prior tests [Olson, 2004; Soelberg, 2004a; Soelberg, 2004b] have indicated that under some conditions, the oxidizer will tend to improve overall NO_x destruction when the oxidizer operation tends to lower the outlet NO_x concentration to near its baseline thermal NO_x concentration.

The FBSR NO_x destruction is compared to the C:oxidant stoichiometry in Figure 4.3-4. The stoichiometry was not purposefully varied during the test, because NO_x destruction was very acceptable. Trend lines generated by the spreadsheet software depicted in the figure are consistent with the expectation that higher carbon stoichiometries would cause higher H_2 concentrations and higher NO_x destruction. This is apparent even though the correlation between the C:oxidant stoichiometry, the H_2 concentrations, and the NO_x destruction seem poor because of the data scatter over a relatively narrow stoichiometry range.

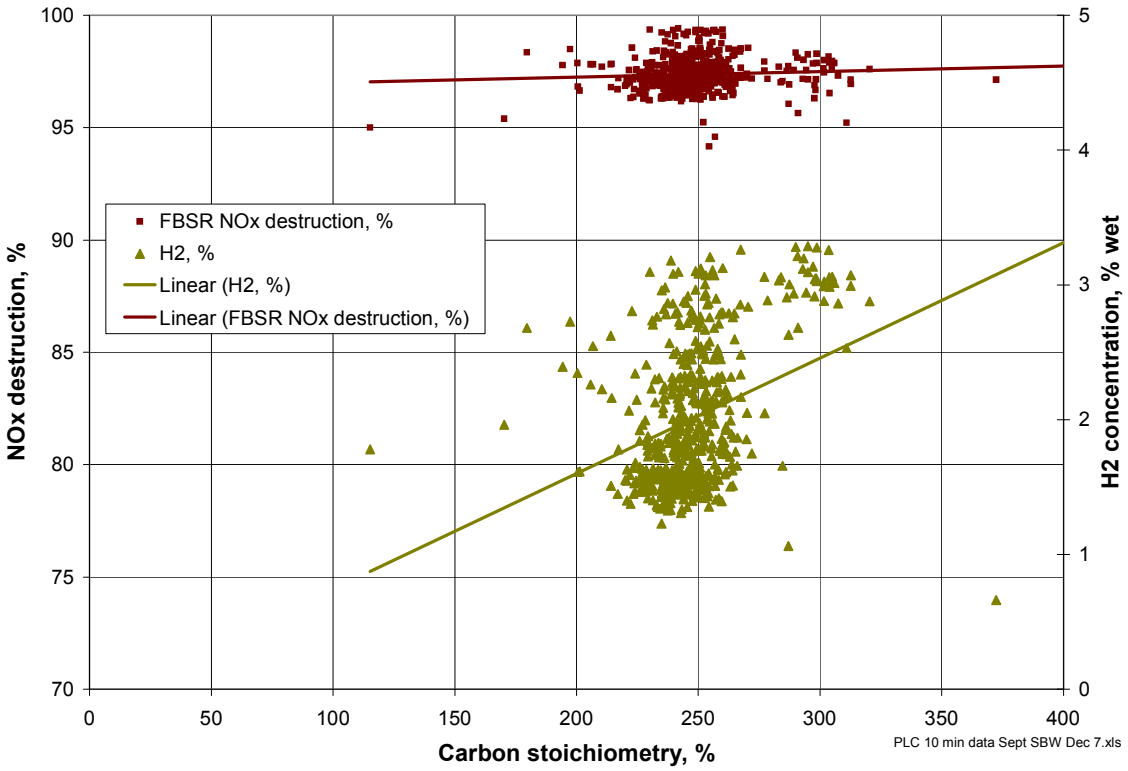

Figure 4.3-4. FBSR NO_x destruction and H_2 concentration compared to carbon stoichiometry.

Figure 4.3-5 shows a better correlation directly between NO_x destruction and H_2 concentration. For H_2 concentrations between about 1.5 – 3% (wet basis), NO_x concentrations decrease almost linearly, and NO_x destruction increases almost linearly. The best fits were obtained using a logarithmic regression for the NO_x destruction and a polynomial regression for the NO_x concentration, although other

correlations (linear, etc.) provide similar results.

Conditions during the SBW test (higher bed operating temperature or catalytic effects of components of the SBW simulant) resulted in increased H_2 formation and better NO_x destruction at lower carbon stoichiometries than were achieved in the Hanford LAW test. NO_x destruction almost always exceeded 96% whenever the H_2 concentration exceeded 1% (same as in the Hanford LAW FBSR test to achieve >90% NO_x destruction). These H_2 and NO_x conditions were achieved with carbon stoichiometries ranging down to 200%, about ½ of the carbon stoichiometry of 375% needed to achieve >90% NO_x destruction during the Hanford LAW test.

Figure 4.3-5. FBSR NO_x destruction compared to the FBSR off-gas H_2 concentration.

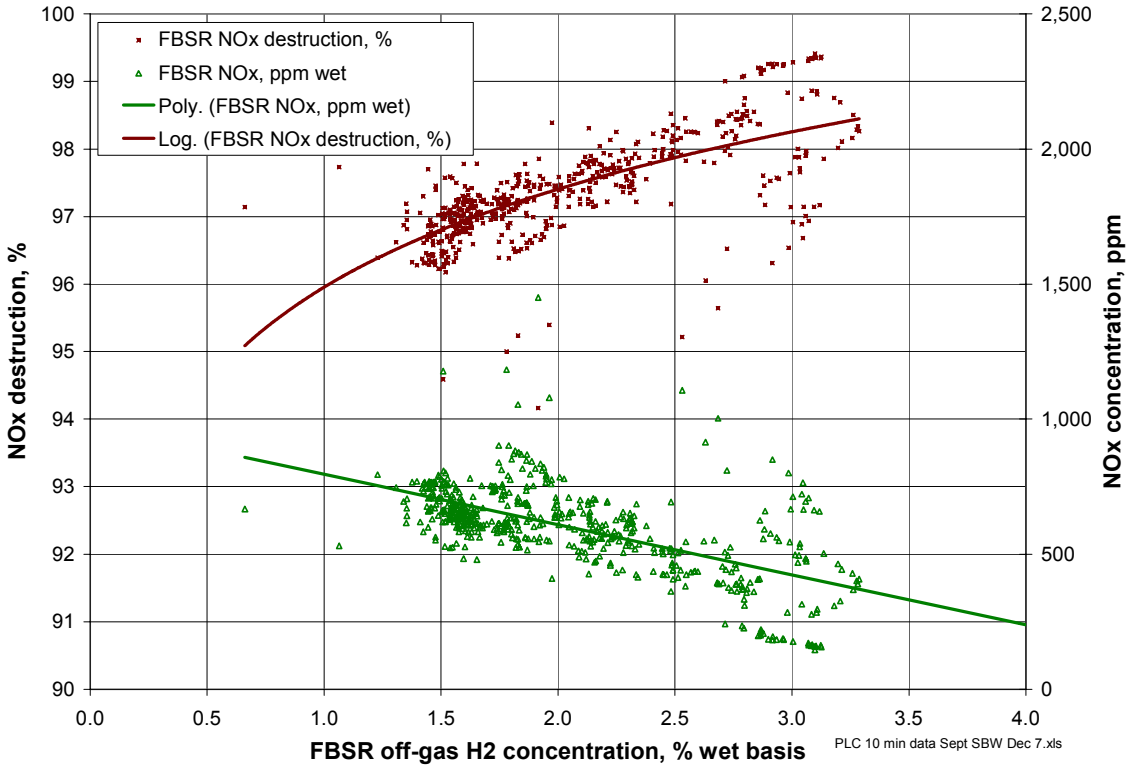

4.4.4 Off-gas Treatment Components Performance

Some FBSR operating parameters, and key off-gas system operating parameters, are shown in Table 4.3-4. The cyclone differential pressure averaged only 0.4 inches water column, which is much lower than a nominal cyclone differential pressure of about 5 inches water column for good cyclonic particle size separation. The cyclone in the FBSR test system was sized for a higher gas flow rate than was used during this test. However, the bed product, cyclone catch, and filter catch particle size data suggests that the cyclone did, in fact, remove elutriated fines with reasonable efficiency. The particle MMPD of the recycled fines averaged 0.042 mm, about 18 times smaller than the COT 98 bed product MMPD of 0.77 mm. The filter fines MMPD of 0.015 mm was about 3 times smaller in diameter than the cyclone fines. The average cyclone efficiency was about 82%, at a measured average cyclone recycle

rate of about 1.8 kg/hr (not including those times when the recycle was not operating) and an average filter fines capture rate of 0.40 kg/hr.

The heated, sintered metal filter bank performed very well to capture elutriated fines that passed through the cyclone. No fines were detected in downstream equipment such as the oxidizer, where fines might deposit out of the off-gas, or the carbon bed, where fines might be trapped in interstitial spaces in the bed, or in the CEMS filters.

The oxidizer is physically configured with three different stages to enable operation in a staged, non-selective, non-catalytic NO_X reduction (NSNCR) mode. The three-stage system was operated in a fully oxidizing mode, since NO_X was efficiently destroyed in the FBSR. Auxiliary fuel (natural gas) and air were added through a burner in stage 1. If other reduced gas species, such as THC, H_2, CO, H_2S, HCN, or NH_3, are formed in the FBSR, then those gas species are also oxidized in this stage. THC, CO, and H_2 would be oxidized to CO_2 and H_2O. H_2S would be oxidized to SO_2; HCN would be oxidized to H_2O, CO_2, and either N_2 or NO_X; and NH_3 would be oxidized to H_2O and either N_2 or NO_X.

This stage was operated in an oxidizing (rather than NO_X-reducing) mode, with approximately 105% stoichiometric air. Reduced gas species were fully oxidized in this stage at an operating temperature of 1,000°C. The hot stage 1 off-gas passed through stage 2, designed for NSNCR operation to quench the stage 1 gas to a temperature below 800°C, and through stage 3, designed for NSNCR operation as an oxidizer to fully oxidize the NSNCR off-gas. No quench water was added in stage 2, and only a small amount of air (to cool the air nozzles) was added in stage 3. The O_2 content in the stage 3 off-gas averaged 3.0% (wet basis).

The stage 1 temperature was controlled at 1,000°C, and no temperature control was required in stages 2 and 3. The stage 3 off-gas averaged 742°C. The stage 1 residence time was 3.0 seconds, conservatively high for good engineering practice, to efficiently oxidize organic materials. The total residence time in stages 1-3 was 5.9 seconds. The low CO content of the oxidizer outlet off-gas, averaging 5 ppm (wet basis), confirms highly efficient oxidation of organic compounds. The calculated combustion efficiency of the oxidizer was 99.99% using a CO concentration of 5 ppm and an average CO_2 concentration of 5.48% (wet basis).

The partial quench used water spray evaporation to cool the oxidizer off-gas to a temperature cool enough for the downstream carbon bed. A mist eliminator downstream of the partial quench was designed to capture any residual water mist in the event that an upset of the partial quench resulted in excessive off-gas cooling and un-evaporated water droplets in the off-gas. The partial quench operated within its control range for the duration of the test, and cooled the off-gas to an average temperature of 130°C. An electric reheater was used to slightly reheat the off-gas to an average of 139°C so that, after some minimal heat losses, the carbon bed operating temperature averaged 124°C.

4.4.5 Off-gas Mercury Emissions Control

Fluidized bed test results have repeatedly shown that mercury, a toxic hazardous metal that is included in the SBW simulant, quantitatively volatilizes to the off-gas and is not retained in the solid bed product or fines [Boardman, 2004, Marshall, 2003, Soelberg, 2004a and 2004b]. Continuous off-gas mercury measurements, which were performed in prior FBSR tests, were not performed during the September SBW test because the Hg analyzer was not available during the test time period. Instead, the

amount of Hg volatilized to the off-gas was captured in the 3-stage granular activated carbon bed to perform mass balance calculations and to determine the performance of the carbon bed for Hg capture.

The carbon bed was configured to be as consistent as possible (considering the size of the pilot-scale test system) with full-scale granular activated carbon bed design parameters for efficient mercury capture. The inside diameter of the bed, at 17.6 inches, was sized so that the off-gas superficial (empty-bed) velocity in the carbon bed was near the nominal design maximum limit of 1 ft/s. The actual superficial gas velocity for the SBW Sagger clay test was about 1.2 ft/s, slightly higher than the limit. The carbon bed contained 1.5 mm sized NUCON Mersorb sulfur-impregnated activated carbon granules in 3 levels as noted in Table 3.5-1. The total superficial gas residence time in all three stages was 1.2 s, close to the nominal design minimum of 2 s. The bed operating temperature averaged 124 ^{o}C, within the maximum operating temperature limit of about 150 ^{o}C.

Table 4.3-4. Key operating parameters for the FBSR and off-gas system.

Test condition start time	COT	Test condition	Feed slurry rate, kg/hr	Atomizing N_2 flowrate, kg/hr	Atomizing O_2 flowrate, kg/hr	Total atomizing gas flowrate, kg/hr	Fluidizing steam flowrate, kg/hr	Fluidizing steam velocity below nozzle, m/s	Uncorrected carbon additive feed rate, kg/hr	Corrected carbon additive feed rate, kg/hr	Total N_2 gas input flowrate, kg/hr	Final H3 super-heater steam outlet temp, C	Cyclone diff pressure, inches water	Cyclone outlet gas temp, C
			SR1_F1A_VAL	SR1_F1B_KGH	SR1_F3_KGH	---	H1_F_PV	FLUIDIZING_FV	LF2_FD_RATE	0.852	V1_F1_VAL	H4_T2_VAL	C1_PD_VAL	C1_T3_VAL
9/27/04 9:00	0.0	1.0	2.99	1.72	0.40	2.12	2.48	0.20	0.80	0.68	5.79	806	0.3	517
9/27/04 16:00	7.0	2.0	3.00	1.74	0.40	2.14	1.99	0.16	0.70	0.60	5.83	776	0.4	494
9/27/04 14:15	52.8	3.0	3.00	1.72	0.40	2.12	1.99	0.16	0.60	0.52	5.67	777	0.3	501
9/29/04 15:37	54.1	4.0	2.50	1.75	0.40	2.15	1.99	0.16	0.60	0.51	5.71	776	0.4	493
9/30/04 6:36	0.0	5.0	2.50	1.72	0.40	2.12	1.99	0.16	0.60	0.51	5.71	791	0.3	497
10/1/04 3:10	86.7	6.0	2.50	2.10	0.40	2.50	1.99	0.16	0.60	0.51	6.12	798	0.4	500
10/1/04 16:35	100.1	Feed off												
Averages			2.77	1.79	0.40	2.19	2.02	0.16	0.66	0.56	5.83	784	0.4	497

Test condition start time	COT	Test condition	Filter diff pressure, inches water	Filter outlet gas temp, C	FBSR filter outlet H_2O flowrate, kg/hr	Calculated FBSR filter outlet gas flowrate, kg/hr	FBSR filter outlet gas flowrate, scfm	Natural gas flow to oxidizer, kg/hr	Air flowrate to oxidizer stage 1, kg/hr	Air flow to oxidizer stage 3, kg/hr	N_2 purge flow to oxidizer stage 2, kg/hr	Oxidizer stage 1 temp, C	Oxidizer stage 2 temp, C	Oxidizer stage 3 temp, C
			F1_PD_VAL	F1_T2_VAL	H2O_BEFORE_OXI_KGH	TOTAL_KGH_BEFORE_OXI	---	B1_F1_VAL	B1_F2_VAL	B1_F5_VAL	B1_F7_VAL	B1_T1_VAL	B1_T2_VAL	B1_T3_VAL
9/27/04 9:00	0.0	1.0	9	411	4.39	10.48	6.48	2.71	59.7	6.44	0.30	1,000	845	723
9/27/04 16:00	7.0	2.0	8	384	3.93	10.06	6.14	2.66	58.5	5.71	0.30	1,000	847	723
9/27/04 14:15	52.8	3.0	6	370	3.90	9.88	6.04	2.68	58.9	5.50	0.30	1,000	854	728
9/29/04 15:37	54.1	4.0	7	372	3.60	9.57	5.81	2.70	59.3	5.04	0.30	1,000	859	738
9/30/04 6:36	0.0	5.0	7	384	3.59	9.55	5.79	2.79	61.4	4.62	0.30	1,000	878	762
10/1/04 3:10	86.7	6.0	7	376	3.57	9.94	5.99	3.00	66.1	4.54	0.30	1,000	903	789
10/1/04 16:35	100.1	Feed off												
Averages			7	383	3.80	9.91	6.03	2.74	60.3	5.30	0.30	1,000	862	742

Table 4.3-4. Key operating parameters for the FBSR and off-gas system (continued).

Test condition start time	COT	Test condition	Partial quench water flowrate, kg/hr	Partial quench outlet gas temp, C	Reheater outlet gas pressure, psia	Reheater outlet gas temp, C	Total input gas flowrate, kg/hr	Total input gas flowrate, scfm	Measured total off-gas flowrate, k/hr	Measured total off-gas flowrate, scfm	Ratio, measured/ calculated total off-gas rates	Carbon bed diff pressure, inches water	Carbon bed temp, C
			PQ1_F1_VAL	PQ1_T1_VAL	AJ1_P2_VAL	AJ1_T1_VAL	TOTAL_KGH_ AFTER_PQ	SCFM_AFTER _PQ	AJ1_F1_VAL	AJ1_F1_SCF M	AJ1_F1_OG MR_CALC	GAC1_PD _VAL	GAC1_T_ VAL
9/27/04 9:00	0.0	1.0	16.8	130	10.8	138	96.4	54.6	115	65.0	1.19	9	123
9/27/04 16:00	7.0	2.0	15.0	130	11.1	139	92.2	51.8	107	60.2	1.16	8	123
9/27/04 14:15	52.8	3.0	14.7	130	11.4	140	91.9	51.6	106	59.6	1.15	8	124
9/29/04 15:37	54.1	4.0	14.4	130	11.3	140	91.3	51.2	105	58.6	1.14	8	123
9/30/04 6:36	0.0	5.0	15.0	130	11.4	140	93.7	52.6	107	60.1	1.14	8	124
10/1/04 3:10	86.7	6.0	16.8	130	11.4	139	100.7	56.6	116	65.0	1.15	9	124
10/1/04 16:35	100.1	Feed off											
Averages			15.3	130	11.2	139	93.8	52.7	108	61.0	1.16	8	124

1. PLC tag numbers indicate the source of the data. No tag number indicates that the datawas calculated after the test, from other PLC data, and not taken directly from the PLC.
2. Standard temperature is 68°F, standard pressure is 1 atmosphere. N_2 was used to atomize the quench water.
3. The superficial volume, velocity, and residence time are calculated from the bed volume assuming 100% void space.
4. Residence time calculations were made using the average oxidizer outlet offgas flowrate less the average partial quench water flowrate, which is 51.4 scfm.
5. The average residence time in Stage 1 was 3.1 seconds. The volume of Stage 1 is (14.8 ft3) was based on a inside diameter of 21 inches and a length of 74 inches, not including the conical reducing section at the inlet of the quench section.
6. The average residence time in Stage 2 was 0.3 seconds. The volume of the quench stage (1.1 ft3) was based on the volume of the frustum (8 inches long), the throat length (10 inches), and the throat inside diameter (8 inches).
7. The avg residence time in Stage 2 was 2.4 seconds. The volume of the oxidizing stage (9.22 ft3) was based on an inside diameter of 21 inches and a length of 46 inches.

[PLC 10 min data Sept SBW Dec 7.xls]flowrate table

Figure 4.3-6. Measured Hg concentrations and removal efficiencies for the carbon bed.

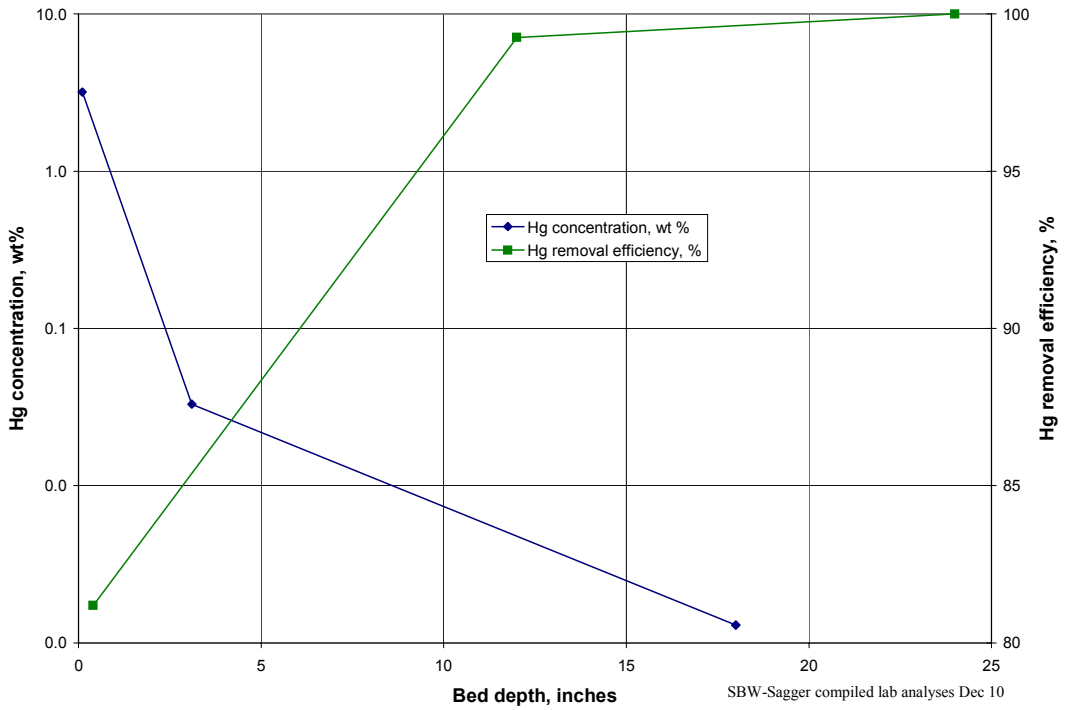

The leachability of the sample collected at the top of the first stage was measured using the Environmental Protection Agency Toxicity Characteristic Leachability Procedure (TCLP) test. These results are shown in Table 4.3-6. The leached Hg was near, but still below, the TCLP limit for Hg. Even though the amount of Hg in the leachate was near the TCLP limit, the carbon strongly retained the Hg present in the sample. Only 0.0068% of the Hg in the carbon was leached. The low concentrations of Ba and Ni detected in the TCLP leach solution are probably from trace levels in the carbon, from contamination, or trace amounts in the off-gas that were captured in the carbon bed.

Table 4.3-6. Carbon bed TCLP leach test results.

Element	Concentration in TCLP extract, mg/L			Measured value, % of TCLP limit	Normalized concentration in the sample, wt%	Portion in the sample that leached during TCLP, %
	Detection limit	Measured	TCLP limit (40 CFR 261 Subpart C)			
As	0.021	U	5	---	---	---
Ba	0.034	0.052	100	0.052	NA	---
Cd	0.0016	U	1	---	---	---
Cr	0.084	U	5	---	---	---
Pb	0.031	U	5	---	---	---
Ni	0.0016	0.14	20	0.7	NA	---
Se	0.073	U	5	---	---	---
Ag	0.003	U	6	---	---	---
Hg	0.001	0.133	0.2	66.5	3.9	0.0068
U = Undetected NA = Not available						

[SBW-Sagger compiled lab analyses Dec 10.xls]Hg TCLP

4.6 Process Mass Balance & Elemental Partitioning

The feed slurry, when sprayed into the bed, dries and undergoes evaporation, thermal decomposition, and other reactions that denitrate and solidify the solid forming feed constituents. The cumulative masses of slurry feed, carbon additive, and calculated solid product from the slurry are shown in Figure 4.4-1. The input mass flow rates were very consistent and controlled, with slight changes in the slope of the cumulative feed when a feed rate change was made during the test. The total output masses are shown in Figure 4.4-2.

4.6.1 Overall Mass Balance and Product Distribution

The total input solid masses were the starting bed media, solid forming constituents from the SBW-clay slurry feed, and the carbon reductant. Total output solid masses were the mineralized bed product, the mass of the cyclone recycle samples (not returned to the bed), and the filter fines catch. The output bed product was the sum of the mass of the bed removed at the end of the test and the mass of the bed material removed at discrete times during the test from either the bed drain port or the bed sample port. Bed media was removed during the test to control the bed height as solidified feed added to the bed mass, to obtain samples for analyses, to periodically inspect the bed media for appearance, and accretions/agglomerations, and to provide a pathway for such agglomerations, if they occurred, to be removed from the bed.

The cumulative solid product feed and cumulative total outputs were zero at the test start. No significant alumina fines collected and drained from the filter vessel prior to initiating SBW slurry feed at COT 0. The input solids sum to 90.4 kg, which include the starting alumina bed (18 kg) and about 1.5 kg of recycled bed media. By the end of the test, the measured cumulative output (including the final bed dump) was 87.9 kg.

The solid product distribution and mass balance closure are shown in Table 4.1-1. The solid mass balance closure, the total output mass of 87.9 kg as a percentage of the total input mass of 90.4 kg, of 98% is very good. The error (~2%) is within reasonable error bounds for the various measurements used to provide data for the mass balance calculations – slurry feed rate, calcine mass per unit of slurry, carbon additive residues, and recovery and measurement of the bed, cyclone, and filter product masses.

Samples of the top of each of the three stages, and also the bottom of the third stage, were analyzed for Hg and S concentrations (Table 4.3-5). Each sample was collected by vacuuming a layer of approximately 0.2 inches from the bed at the specified bed depth. The Hg analyses included hot acid (HF, aqua regia, boric acid) extraction consistent with the extraction procedures specified in ASTM D6784 ("Standard Test Method for Elemental, Oxidized, Particle-Bound, and Total Mercury in Flue Gas Generated from Coal-Fired Stationary Sources [Ontario Hydro Method]"). A single extraction of carbon used in carbon bed Hg sorption might not quantitatively remove all of the sorbed Hg, and multiple extractions can more quantitatively recover sorbed Hg [Del Debbio, 2003]. Triplicate extractions have recovered about 1.5 times as much Hg and S from Hg-laden Mersorb than did a single extraction [Boardman, 2004]. A single extraction was used in the carbon bed sample analyses for the SBW Sagger clay test, so the reported Hg concentrations should be considered minimum values.

Table 4.3-5. Hg and S measurement results for the carbon bed.

Stage	Sample number	Sample location	Average sample bed depth, inches	Hg concentration, wt %	S concentration, wt%	Total mass of carbon represented by that sample, kg	Cumulative bed depth, inches	Total mass of Hg, g	Total mass of Hg normalized for 100% Hg mass balance closure, g	Normalized Hg concentration, wt %	Hg removal efficiency at the cumulative bed depth, %
1	1180	Top of stage 1	0.1	3.2	10.7	1.1	0.4	34	41	3.9	81.2
2	1181	Top of stage 2	3.1	0.033	13.8	23	12	7.6	9.2	0.040	99.3
3	1182, 1183	Average for stage 3	18	0.0013	10.8	24	24	0.3	0.4	0.0016	100.0
Average S concentration			---	---	11.8	---	---	---	---	---	---
Totals for all 3 stages			---	---	---	48	24	42	51	---	100

Notes:

1. The Hg concentrations in the stage 3 samples are so low that they were averaged to provide a single average concentration for stage 3.
2. The assumed mass of carbon represented by sample 1180 is twice the depth of the sample collected, 0.4 inches.
3. The assumed mass of carbon represented by sample 1181 is the bottom of stage 1, not represented by sample 1180, and all of stage 2.
4. The average Hg concentration for stage 3 represents the entire mass of carbon in stage 3.
5. The total input Hg from the SBW slurry feed is 51 g. The total mass of Hg calculated in the carbon bed is 82% of the input mass, perhaps due to the use of only a single rather than multiple extractions during sample analysis. The concentrations and masses of Hg captured in the carbon bed were normalized to to equal the total input Hg, assuming that (a) negligible Hg partitioned to other effluent streams, and (b) the carbon bed capture efficiency was 100%.

[SBW-Sagger compiled lab analyses Dec 10.xls]Hg in C bed

Figure 4.3-6 shows how the concentration of Hg in the carbon bed was initially high at the top of the first stage (the 0.1 inch average bed sample depth) but rapidly decreased by about 100x at the top of stage 2 (3.1 inches average bed depth). The average stage 3 concentration, representing a depth of 18 inches, was about 2,700x lower than at the top of stage 1. The results show that most of the Hg was captured within the first inch of the carbon bed. The mass transfer zone (the layer in the bed in which most of the Hg is actively being sorbed) under these conditions was under 3 inches, because the concentration of Hg at the 3.1-inch bed depth was so low compared to the Hg concentration at the 0.1 inch bed depth. The expected maximum Hg capacities for Mersorb operating at the conditions of this test are at least 10-20 wt%. The greatest normalized Hg concentration, at 3.9 wt%, was much lower than this maximum range, suggesting that even at the front end of the bed, the carbon had not reached its sorption capacity. The measured S concentrations, averaging 11.8%, ranged nearly identical to the expected S concentration of 12%, indicating that S was not volatilized from the carbon during this test.

Table 4.4-1 shows two mass flow rates for the carbon reductant additive. The mass of carbon added to the carbon feed hopper is the difference between the masses of the total additions and the mass recovered from the hopper at the end of the run, and represents an accurate measure of the total carbon additive used in the process. The cumulative carbon feed based on the PLC is less accurate because it is determined by the sum of small differences between relatively large numbers. Furthermore, the carbon feeder set point is at the low end of the controller's calibration and linear range. Consequently, the carbon additive flow rate computed by the PLC is about 17% higher than indicated by the actual net amount of carbon added to the feed hopper.

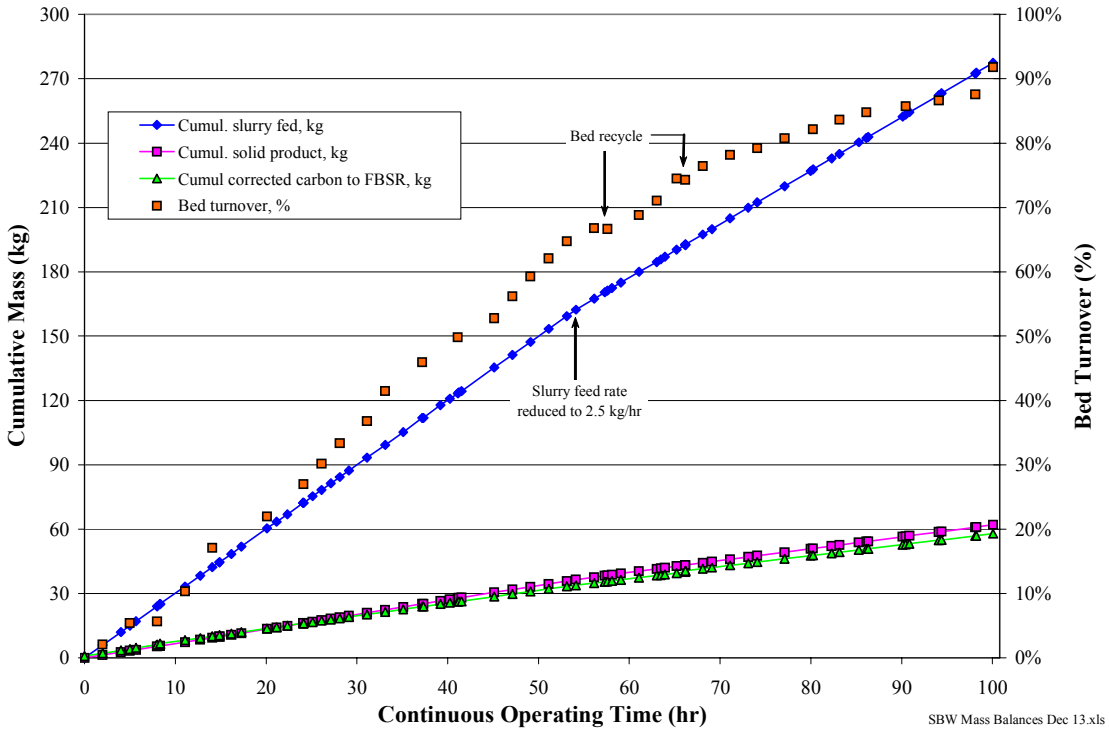

Figure 4.4-1. Cumulative input feed masses.

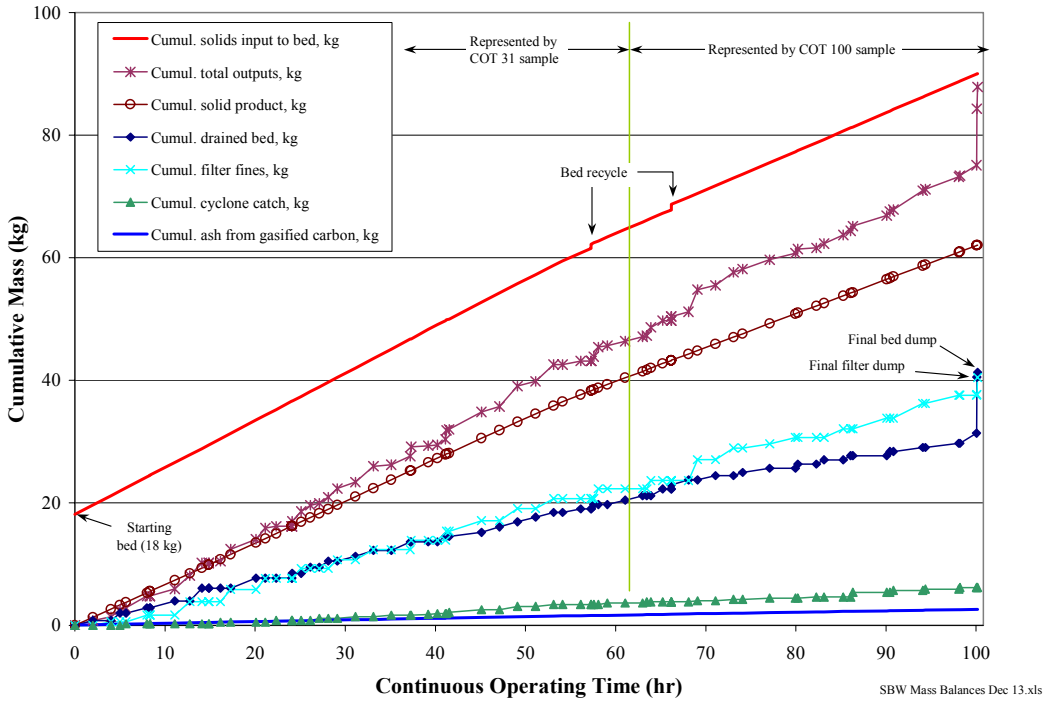

Figure 4.4-2. Cumulative product masses.

Table 4.4-1. Solid product distribution and overall mass balance closure for the SBW FBSR test.

FBSR input masses		
Input streams	Wt frac. or wt%	Input mass, kg
Starting alumina bed, kg:	---	18.0
Total feed slurry input from PLC, kg:	---	277.6
kg solid product/kg slurry:	0.221	---
Total steam reformed solid product: [1]	---	62.1
Recycled bed media	---	1.47
Mass of carbon added to the carbon feed hopper, kg:	---	58.0
Ash content of carbon additive, wt % as received:	5.0%	---
Percent of carbon additive that was gasified (calculated from total carbon input and residual unreacted carbon):	89.8%	52.1
Total solids (ash) from carbon additive (calculated from carbon ash content, total carbon additive, and % gasified carbon), kg:	---	2.6
Total unreacted carbon determined from product sample analyses		
Average unreacted carbon in bed product:	3.0%	1.2
Average unreacted carbon in cyclone catch:	4.9%	0.3
Average unreacted carbon in filter fines:	10.9%	4.4
Total unreacted carbon:	---	5.9
Total input solids, kg (sum of steam reformed feed, recycled bed, ash from gasified carbon additive, and unreacted carbon additive):		90.1
Total input solids excl. starting bed and unreacted carbon, kg:	---	64.7
Solids mass balance closure		
Solid mass balance closure, total output mass/total input mass:	98%	---
Solid product distribution excluding starting bed		
Percent to bed product & cyclone recycle (incl. unreacted C)	44%	---
Percent to filter fines (incl. unreacted C)	56%	---
Carbon feed rate check	---	---
Mass of carbon added to the carbon feed hopper, kg:	---	58.0
Cumulative carbon fed based on PLC, kg:	---	68.1
Accuracy of cumulative carbon added from PLC (feeder) compared to cumulative gravimetric carbon input, % error:	17.4%	---

FBSR output masses	
Output streams	Output mass, kg
Cumulative drained bed, kg:	41.3
Cumulative cyclone catch, kg:	6.1
Cumul. filter fines, kg:	40.4
Total output solids, kg:	87.9
Drained bed excluding starting bed and unreacted carbon, kg	22.1
Cyclone catch excluding unreacted carbon, kg:	5.8
Mass of filter fines not including organic carbon, kg:	36.0
Total output solids excluding starting bed and unreacted carbon, kg:	64.0

[SBW Mass Balances Dec 13.xls]Gross mass balance table

1. Includes 1.6 kg extra clay added on 9/29.

The product to fines ratio ranged from about 0.6 to 1.3 by mass (0.78 based on masses for entire test), well below the desired ratio of 3.5 to 1 noted in the test objectives. No emphasis was placed on the process parametric or configuration changes to improve the product to fines ration other than recycling the cyclone catch to the bed. The distribution of FBSR product appears in Figure 4.4-3 to have been strongly influenced by the decrease in slurry feed rate and increase in NAR that took place at COT 54. The increased atomization and longer product residence time in the bed (increased attrition) are the likely contributors to the increased fines fraction in the second half of the run. Improved cyclone efficiency could reduce the quantity of fines that escape recycle to the bed, but more extensive changes in the process (mechanical or chemical) will likely be necessary to achieve the desired ratio. This may include changing the mechanism and location of fines re-introduction or improvements to the mineralizing chemistry and kinetics to improve cohesion of the product particles, shorten residence time needed to convert metastable mineral phases to thermodynamically stable forms (e.g., carnegieite to nepheline), and controlling attrition resistance and particle size growth.

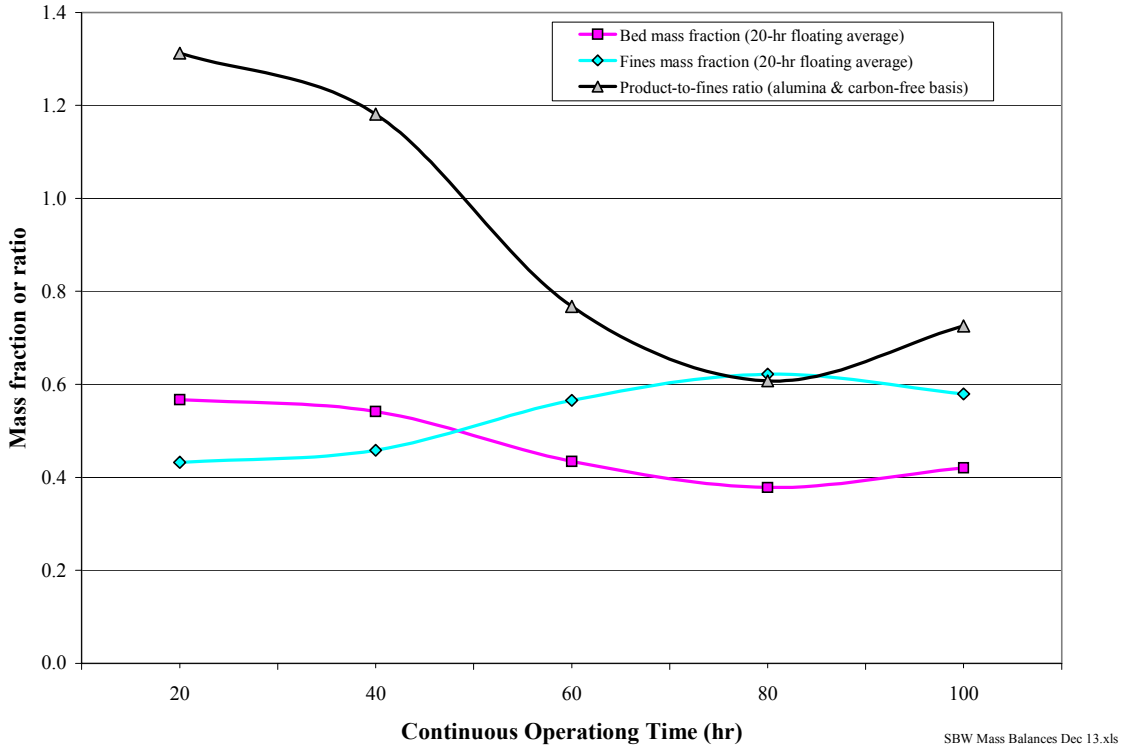

Figure 4.4-3. Product to fines ratio (alumina and carbon-free basis).

4.6.2 Elemental Mass Balance and Distribution

A mass balance and distribution of key feed elements was accomplished by numerically integrating the bed turnover estimate to account for the fractions of starting bed and mineralized product in both bed samples. The bed turnover at COT 31 was approximately 43%. The measured composition of the COT 31 sample was assigned to all of the bed material harvested between COT 0 and COT 61, because the average estimated turnover for the first 61 hours was 42%. The bed media harvested after COT 63 were assigned compositions based on the COT 100 sample mineralized SBW and starting bed alumina phase compositions, weighted according to the estimated bed turnover at the time the material was harvested. The COT 100 mineralized SBW phase composition was determined by subtracting out the mass and element contribution of the residual starting bed, based on the estimated bed turnover at COT 100. Compositions of the influent and effluent samples are given in Table 4.4-2 and the elemental mass balance computations are shown in Table 4.4-3.

Table 4.4-2. FBSR influent and effluent stream elemental compositions.

	Sample number	Sample date	Sample description	Units	Al	B	Ca	Cl	Cr	Cs	Cu	F	Fe	Hg	I	K	Mg	Mn
Input	1154	27-Sep	INEEL SBW simulant	g/L	18.6	0.13	2.1	1.17	0.15	0.23	0.04	0.10	0.93	0.27	0.02	9.8	0.35	0.66
	1156	27-Sep	INEEL SBW slurry - 1st batch	g/L	45.0	0.46	1.6	1.07	0.19	0.40	0.06	0.14	2.0			9.9	0.60	0.64
	1162	29-Sep	INEEL SBW slurry - 2nd batch	g/L	45.0	0.22	1.6	1.06	0.21	0.39	0.05	0.14	2.1			9.6	0.61	0.65
	na	---	Sagger XX kaolin clay (anhyd.)	wt%	wt%		16.30						0.09			0.59	0.58	
	na	---	Berger Bros. P6 carbon ash	wt%	0.16		48.2						0.30			2.8	1.48	
	1100	2-Aug	Starting bed COT 0	wt%	53.0		0.10		< 0.01				0.10			< 0.01	< 0.01	
Products	1171	28-Sep	Bed product COT 31	wt%	37.7		1.15	0.055	0.031	0.034	0.014	<0.1	0.36			1.34	0.11	0.13
	1173	1-Oct	Bed product COT 100 (final bed)	wt%	20.3		2.71	0.092	0.068	0.031	0.011	<0.1	0.71			3.29	0.24	0.28
	1174	28-Sep	Cyclone fines COT 31	wt%	12.9		3.65	0.18	0.056	0.065	0.018	<0.1	0.64			3.05	0.22	0.23
	1176	1-Oct	Cyclone fines COT 98	wt%	13.0		3.31	0.18	0.055	0.062	0.031	<0.1	0.64			3.40	0.23	0.24
	1177	28-Sep	Filter fines COT 33	wt%	15.4		3.70	0.36	0.054	0.15	0.021	<0.1	0.60			2.69	0.27	0.24
	1179	4-Oct	Filter fines COT 100+	wt%	15.1		3.65	0.39	0.056	0.17	0.019	<0.1	0.62			2.88	0.26	0.24
Effluents	1163	29-Sep	CEMS 1 condensate 1710	mg/L				<10				<10						
	1164	29-Sep	CEMS 2 condensate 1710	mg/L				<10				<10						
	1169	1-Oct	CEMS 1 condensate 1630	mg/L	0.067	0.19	0.050	<10	<0.01		0.016	<10	<0.01			0.197	<0.01	<0.01
	1170	1-Oct	CEMS 2 condensate 1630	mg/L	0.084	0.27	0.042	<10	<0.01		0.050	<10	<0.01			0.196	<0.01	<0.01
GAC	1180	5-Oct	Carbon bed top of top layer	wt%										3.2				
	1181	5-Oct	Carbon bed top of middle layer	wt%										0.033				
	1182	5-Oct	Carbon bed top of bottom layer	wt%										0.0008				
	1183	5-Oct	C bed bottom of bottom layer	wt%										0.0018				

	Sample number	Sample date	Sample description	Units	Na	Ni	NO_2	NO_3	P	Pb	Re	S	Si	Ti	Zn	TIC (1)	TOC	pH
Input	1154	27-Sep	INEEL SBW simulant	g/L	51.7	0.071		289	1.4	0.23	0.11	2.4			0.07			
	1156	27-Sep	INEEL SBW slurry - 1st batch	g/L	48.8	0.084		269	1.2	0.25	0.07	1.9	51.8	3.0				
	1162	29-Sep	INEEL SBW slurry - 2nd batch	g/L	49.1	0.090		265	1.2	0.25	0.08	1.9	52.9	3.0				
	na	---	Sagger XX kaolin clay (anhyd.)	wt%	1.59				0.16				0.0	28.7				
	na	---	Berger Bros. P6 carbon ash	wt%	0.14				0.46			0.27	0.70	0.01				
	1100	2-Aug	Starting bed COT 0	wt%	< 0.01				< 0.01			< 0.01	0.40	< 0.01				
Products	1171	28-Sep	Bed product COT 31	wt%	5.09	0.017		<0.1	0.17	<0.01	0.004	0.045	7.86	0.30		3.52		
	1173	1-Oct	Bed product COT 100 (final bed)	wt%	12.3	0.040		<0.1	0.38	<0.01	0.005	0.041	17.6	0.71		2.42		
	1174	28-Sep	Cyclone fines COT 31	wt%	14.5	0.028		<0.1	0.30	<0.01	0.017	0.14	22.0	0.95		5.92		
	1176	1-Oct	Cyclone fines COT 98	wt%	15.3	0.031		<0.1	0.32	<0.01	0.016	0.13	22.1	0.96		3.42		
	1177	28-Sep	Filter fines COT 33	wt%	14.7	0.026		<0.1	0.41	<0.01	0.041	0.82	18.1	1.05		11.4		
	1179	4-Oct	Filter fines COT 100+	wt%	15.5	0.030		<0.1	0.42	<0.01	0.038	0.72	18.8	1.05		9.61		
Effluents	1163	29-Sep	CEMS 1 condensate 1710	mg/L			11.8	<10										9.2
	1164	29-Sep	CEMS 2 condensate 1710	mg/L			<10.0	<10										3.2
	1169	1-Oct	CEMS 1 condensate 1630	mg/L	<0.01	<0.01	11.5	<10	<0.01	<0.02		245	0.089	<0.01		6010	<850	9.2
	1170	1-Oct	CEMS 2 condensate 1630	mg/L	<0.01	<0.01	<10.0	<10	<0.01	<0.02		3.6	0.012	<0.01		3.03	<5	3.3
GAC	1180	5-Oct	Carbon bed top of top layer	wt%								10.7						
	1181	5-Oct	Carbon bed top of middle layer	wt%								13.8						
	1182	5-Oct	Carbon bed top of bottom layer	wt%								10.5						
	1183	5-Oct	C bed bottom of bottom layer	wt%								11.0						

1. Total inorganic carbon (TIC) analysis on bed, cyclone, and filter products determined by Loss-on-ignition at 525°C.

[SBW-Sagger compiled lab analyses Dec 10.xls]Influent - Effluent Table

Table 4.4-3. Elemental mass balance.

Material description	Qty [1]	Al (kg)	Ca (kg)	Cl (kg)	Cr (kg)	Cs (kg)	Cu (kg)	F [2] (kg)	Hg [2] (kg)	I [2] (kg)	Fe (kg)	K (kg)
SBW-Sagger XX slurry	277.6 kg	9.1	0.33	0.22	0.040	0.081	0.011	0.02	0.1	0.003	0.41	2.0
Carbon ash	2.60 kg	0.002	1.3	---	---	---	---	---	---	---	0.004	0.1
Starting alumina bed	18.0 kg	9.5	0.01	---	---	---	---	---	---	---	0.01	---
Total Input	298.2 kg	18.7 kg	1.6 kg	0.22 kg	0.040 kg	0.081 kg	0.011 kg	0.02 kg	0.1 kg	0.003 kg	0.43 kg	2.0 kg
Harvested bed (COT 0 - COT 61) [3]	19.7 kg	7.43	0.23	0.01	0.01	0.01	0.003	< 0.02	---	---	0.07	0.26
Harvested bed (COT 63 - COT 100) [4]	20.4 kg	5.12	0.47	0.02	0.01	0.01	0.002	< 0.02	---	---	0.12	0.57
Cylcone samples (COT 0 - COT 61)	3.4 kg	0.44	0.12	0.006	0.002	0.002	0.001	< 0.3	---	---	0.02	0.10
Cylcone samples (COT 63 - COT 100)	2.4 kg	0.32	0.08	0.004	0.001	0.001	0.001	< 0.2	---	---	0.02	0.08
Filter catch (COT 0 - COT 61)	19.7 kg	3.04	0.73	0.071	0.011	0.030	0.004	< 2.0	---	---	0.12	0.53
Filter catch (COT 63 - COT 100)	16.4 kg	2.48	0.60	0.064	0.009	0.028	0.003	< 1.6	---	---	0.10	0.47
Total Output	82.1 kg	18.8 kg	2.2 kg	0.17 kg	0.035 kg	0.074 kg	0.013 kg	< 4.2 kg	---	---	0.45 kg	2.0 kg
Recovery		101%	140%	80%	86%	92%	116%	---	---	---	106%	99%

Material description	Qty [1]	Mg (kg)	Mn (kg)	Na (kg)	Ni (kg)	NO_3 [5] (kg)	P (kg)	Pb (kg)	Re (kg)	S (kg)	Si (kg)	Ti (kg)
SBW-Sagger XX slurry	277.6 kg	0.12	0.13	9.9	0.018	54.3	0.25	0.05	0.014	0.38	10.6	0.61
Carbon ash	2.60 kg	0.04	---	0.002	---	---	0.01	---	---	0.01	0.02	0.0002
Starting alumina bed	18.0 kg	---	---	---	---	---	---	---	---	---	0.07	---
Total Input	298.2 kg	0.16 kg	0.13 kg	9.9 kg	0.018 kg	54.3 kg	0.25 kg	0.05 kg	0.014 kg	0.39 kg	10.7 kg	0.61 kg
Harvested bed (COT 0 - COT 61) [3]	19.7 kg	0.02	0.03	1.00	0.003	< 0.02	0.01	< 0.00	0.001	0.01	1.5	0.06
Harvested bed (COT 63 - COT 100) [4]	20.4 kg	0.006	0.05	2.14	0.007	< 0.02	0.07	< 0.002	0.001	0.01	3.1	0.12
Cylcone samples (COT 0 - COT 61)	3.4 kg	0.007	0.01	0.50	0.001	< 0.3	0.010	< 0.03	0.001	0.005	0.75	0.033
Cylcone samples (COT 63 - COT 100)	2.4 kg	0.006	0.01	0.37	0.001	< 0.2	0.008	< 0.02	0.000	0.003	0.54	0.023
Filter catch (COT 0 - COT 61)	19.7 kg	0.053	0.05	2.90	0.005	< 2.0	0.080	< 0.2	0.008	0.16	3.6	0.21
Filter catch (COT 63 - COT 100)	16.4 kg	0.043	0.04	2.54	0.005	< 1.6	0.069	< 0.2	0.006	0.12	3.1	0.17
Total Output	82.1 kg	0.14 kg	0.17 kg	9.5 kg	0.022 kg	< 4.2 kg	0.24 kg	< 0.4 kg	0.017 kg	0.30 kg	12.6 kg	0.62 kg
Recovery		84%	132%	95%	125%	---	94%	---	116%	77%	117%	101%

1. Product masses are on a carbon free basis.
2. Shaded values are calculated from makeup components.

[SBW Mass Balances Dec 13.xls]Elemental Balance

3. Sample 1171 (COT 31) has the approximately the same turnover as the composite bed product from COT 0 - COT 61.
4. Sample 1173 (COT 100) was used for the composite bed product from COT63 - COT 100, corrected for the average turnover for the time period.
5. Product denitration exceeds 92%.

The mass balance closure for all of the alkali metals, aluminum, phosphorus, titanium, and iron are excellent and the closures for silicon and a few other elements are good. Cesium concentration in the simulant is sufficiently high that tramp cesium in the wood-based carbon and clay additives did not adversely impact the computation.

The only component with a total mass in excess of 1.0 kg that did not have reasonable mass balance closure was calcium. The slurry concentration for calcium was measured 24% lower than expected based on the SBW makeup target concentration and the clay composition. The difference, however, would only reduce the recovery to 130%. The majority of the calcium in the process is introduced in the carbon. Variations in the calcium concentration of the carbon, analytical error, and uncertainty in the quantity of gasified carbon are the most likely causes of low mass balance closure.

Closures for chlorine and sulfur are low, but this may be due to the formation of gaseous species. Only 77% of the total input sulfur was accounted for in the solid products. SO_2 was not detected in the FBSR off-gas downstream of the oxidizer. While other gaseous sulfur species such as COS or CS_2 might have existed upstream of the oxidizer, these would probably have been oxidized to SO_X in the oxidizer.

Table 4.4-4 shows the distribution of elements between the bed product and filter fines. The masses for the powders and for the elements do not include the elemental or gravimetric contributions of the starting alumina bed or elemental (organic) carbon. The masses are representative of the ash and

mineralized product according to analytical results. The starting bed and elemental carbon were subtracted out mathematically because they comprised about half of the total mass of product and would have significantly biased the Al results (i.e., alumina, being non-volatile and mechanically resistant to attrition, would bias the aluminum distribution in favor of the bed product if not subtracted).

Only elements for which analyses were performed and that were found in concentrations in excess of lower detection limits are given in the table. A fines-to-product concentration ratio between about 0.8 and 1.2 indicates that the element in question was nearly evenly distributed between the fines and bed media. Ratios significantly >1.2 indicate that the element was more prevalent in the fines, and ratios <0.8 suggests that the element was more prevalent in the bed product. Ranges for the partitioning factors are used because several factors could have biased the partitioning results. These factors include the representativeness of the samples collected, number of samples analyzed, recovery (dissolution) of the element from the mineralized sample matrix for analysis, and analytical accuracy of the analysis.

Table 4.4-4. Key element partitioning.

	Powder		Re			Cs			Re/Cs
	Mass	%Mass	Mass	%Mass	Conc.	Mass	%Mass	Conc.	w/w
Bed + cyclone products [1]	27.9 kg	44%	2.6E-3 kg	15%	0.009%	1.6E-2 kg	21%	0.057%	0.16
Filter fines	36.2 kg	56%	1.4E-2 kg	85%	0.039%	5.9E-2 kg	79%	0.162%	0.24
Fines-Product ratio	1.29	---	5.5	---	4.3	3.7	---	2.9	---

	Al [1]			Na			Si [1]		
	Mass	%Mass	Conc.	Mass	%Mass	Conc.	Mass	%Mass	Conc.
Bed + cyclone products [1]	3.8 kg	40%	13%	4.0 kg	42%	14%	5.8 kg	47%	21%
Filter fines	5.5 kg	60%	15%	5.4 kg	58%	15%	6.7 kg	53%	18%
Fines-Product ratio	1.47	---	1.1	1.4	---	1.0	1.1	---	0.9

	Ca [1]			Cl			Cr		
	Mass	%Mass	Conc.	Mass	%Mass	Conc.	Mass	%Mass	Conc.
Bed + cyclone products [1]	0.9 kg	40%	3.2%	0.04 kg	22%	0.13%	1.5E-2 kg	43%	0.053%
Filter fines	1.3 kg	60%	3.7%	0.14 kg	78%	0.37%	2.0E-2 kg	57%	0.055%
Fines-Product ratio	1.5	---	1.1	3.6	---	2.8	1.4	---	1.0

	Cu			Fe [1]			K		
	Mass	%Mass	Conc.	Mass	%Mass	Conc.	Mass	%Mass	Conc.
Bed + cyclone products [1]	6.0E-3 kg	45%	0.022%	0.22 kg	50%	0.79%	1.0 kg	50%	3.7%
Filter fines	7.3E-3 kg	55%	0.020%	0.22 kg	50%	0.61%	1.0 kg	50%	2.8%
Fines-Product ratio	1.2	---	0.9	1.00	---	0.8	0.98	---	0.8

	Mg			Mn			Ni		
	Mass	%Mass	Conc.	Mass	%Mass	Conc.	Mass	%Mass	Conc.
Bed + cyclone products [1]	4.0E-2 kg	29%	0.14%	8.6E-2 kg	50%	0.31%	1.2E-2 kg	54%	0.043%
Filter fines	9.6E-2 kg	71%	0.27%	8.7E-2 kg	50%	0.24%	1.0E-2 kg	46%	0.028%
Fines-Product ratio	2.4	---	1.9	1.0	---	0.8	0.84	---	0.6

	P			S			Ti		
	Mass	%Mass	Conc.	Mass	%Mass	Conc.	Mass	%Mass	Conc.
Bed + cyclone products [1]	0.09 kg	38%	0.32%	0.02 kg	8%	0.08%	0.24 kg	39%	0.85%
Filter fines	0.15 kg	62%	0.41%	0.28 kg	92%	0.77%	0.38 kg	61%	1.05%
Fines-Product ratio	1.6	---	1.3	12	---	9	1.6	---	1.2

1. Excludes mass and element contributions of the alumina starting bed and residual carbon.

[SBW Mass Balances Dec 13.xls]Elemental Balance

The elemental partitioning results are generally similar to partitioning results from the Hanford LAW mineralization test and the Phase 2 SBW mineralization test [Olson, 2004 and Soelberg, 2004b]. Sulfur partitioned more to the fines than any other element, 9 times more by concentration than to the bed product. A 1.4 fines-to-product partitioning ratio for sulfur was reported for the Hanford LAW and Phase 2 SBW mineralization tests. Possible explanations for this distribution may be that the analytical analyses performed did not successfully detect all of the sulfur present in the bed product, the samples analyzed were not sufficiently representative, or that sulfur did partition to the fines for an unexplained process or chemical phenomenon.

Other elements with fines-to-product partitioning factors greater than 1.2 were rhenium (surrogate for technetium), cesium, chlorine, magnesium, and phosphorous. Conversely, nickel partitioned more to the bed product. The primary constituents (aluminum, sodium, and silicon), calcium, chromium, copper, iron, potassium, and manganese distributed nearly equally between the bed product and fines.

4.6.3 Reductant Utilization

Solid carbon was used as a reductant to provide sufficiently reducing conditions to convert nitrates and nitric acid in the simulant to N_2. The carbon was fed through a series of lock-out valves that alternated opening and closing, allowing discrete amounts of carbon into the fluidized bed at a relatively high frequency, while preventing any air influx into the bed, or fugitive emissions from the bed. The valves were purged with a small quantity of N_2 that entered the bed with the carbon.

Sufficient carbon was added to ensure an excess of carbon relative to the amount needed to (a) react with the added O_2 in the atomizing gas, (b) react with the nitrates in the simulant feed, and (c) react with steam. FBSR off-gas measurements that show practically zero O_2, excess H_2 and THC, and averaged 97.5% NO_x destruction, confirm that the carbon added to the steam reformer produced overall reducing conditions, and that the carbon:O_2 and carbon:NO_x reactions almost quantitatively remove the O_2 and NO_x in the system. Some of the solid carbon fed to the steam reformer remained unreacted and was removed from the steam reformer in the bed product, in cyclone fines samples, and in the filter fines.

The carbon:oxidant stoichiometry was defined, in the context of this test, as the ratio of available carbon compared to the total available O_2 and NO_x, assuming that carbon would react first with available O_2 according to the theoretical equation

$$C + O_2 \rightarrow CO_2$$

CO is an expected reaction byproduct of the carbon reaction with O_2 in the FBSR. Carbon can also react with other species, especially H_2O, to produce H_2, C_nH_m, and additional CO and CO_2. But the ratio of CO and total hydrocarbons (THC) compared to CO_2 measured in the FBSR off-gas indicates that on average 92% of the C is oxidized to CO_2 rather than CO and THC.

The 100% stoichiometric amount of C required to react with the O_2 (to form CO_2) is mathematically subtracted from the total C additive input. The remaining C is the amount available to

react with NO_x from the feed simulant according to the assumed theoretically efficient reactions to form N_2 and CO_2:

$$5C + 4MNO_3 \rightarrow 2M_2O + 2N_2 + 5\ CO_2$$

$$3C + 4\ MNO_2 \rightarrow 2M_2O + 2N_2 + 3CO_2$$

In reality, a variety of byproducts (such as NO, CO, THC, and H_2) can result from reactions of the carbon reductant with O_2, NO_x, and H_2O. Residual amounts of these byproducts in the off-gas represent process inefficiencies in the conversion of C to CO_2 and the conversion of NO_x to N_2. The target carbon:oxidant stoichiometry is generally set to be considerably higher than 100% for this reason. The difference between the stoichiometry during the FBSR test and 100% stoichiometry represents the sum of "gasification inefficiencies", which includes (a) the amount of C that gasified to CO and THC instead of CO_2, (b) the amount of C that reacted with H_2O and produced intermediate products like H_2 that were not completely used to convert nitrates and nitrites to N_2, and (c) solid carbon that exits the FBSR unreacted in the bed product, cyclone fines samples, and the filter fines.

The stoichiometric amount of carbon added during the test period, relative to the amount of carbon needed to react with the O_2 and NO_x, is shown in Table 4.4-5 for each test condition. The stoichiometry changed whenever the carbon feed rate was changed, or when the simulant feed rate was changed. The overall stoichiometry was always reductant-rich to ensure sufficiently reducing conditions in the fluidized bed for efficient NO_x destruction.

Table 4.4-5. Calculated carbon:oxidant stoichiometry during test operation.

Test Condition	Start Date, Time	COT	FBSR Carbon Stoichiometry, %
1	9/27/04, 9:00	0.0	297
2	9/27/04, 16:00	7.0	249
3	9/29/04, 14:15	52.8	202
4	9/29/04, 15:37	54.1	240
5	9/30/04, 6:36	66.2	240
6	10/1/04, 3:10	86.7	240
Feed Off	10/1/04, 16:35	100.1	
		Test Average	248

The equation used to calculate the carbon:oxidant stoichiometry is:

Stoich, % = (corrected reductant feed rate – 0.408 x O_2 feed rate)/(0.0580 x slurry feed rate) x 100%

The coefficients 0.408 and 0.0580 are stoichiometric coefficients from the above C, O_2, and nitrate equations, converted to a mass basis, accounting for the amount of carbon in the carbon additive (91.9 wt%), the corrected reductant feed rate, and the target concentration of total nitrate in the feed slurry. The

units of the reductant, O_2, and slurry feed rates are kg/hr.

The carbon mass balance closure and distribution to the output streams are shown in Table 4.4-6. All of the input carbon was from the carbon in the solid carbon additive. Carbon outputs included carbon in the solid output streams (the bed product, the cyclone fines samples, and the filter fines), carbon in the measured CO_2, CO, and THC concentrations in the FBSR off-gas, carbon in the CEMS 1 condensate, and carbon captured in the CEMS 1 carbon filter. Carbon in the CEMS 1 condensate includes carbon in carbon-bearing species that were in the FBSR off-gas, but were scrubbed from the off-gas with the water condensate upstream of the CEMS 1 analyzers, and so were not included in the CEMS 1 analysis. Carbon-bearing species captured in the CEMS 1 carbon filter were also removed from the CEMS 1 sample gas upstream of the CEMS 1 analyzers (except for the THC analyzer, which was located upstream of the carbon filter).

Table 4.4-6. Carbon distribution for the SBW FBSR mineralization test series.

		Carbon mass inputs, kg			Carbon mass outputs, kg C							
					Solid outputs					C in off-gas at the filter outlet		
		Total solid carbon additive	Carbon from solid carbon additive	Carbon from simulant	Bed product	Cyclone samples	Filter catch	C in the CEMS 1 condensate	C captured in the CEMS 1 carbon filter	CO_2	CO	THC
Totals of individual streams	Total organic (reduced) carbon (TOC)	58.0	51.6	0.0	1.2	0.3	4.3	2.4	0.0	0.0	2.0	0.8
	Total inorganic (fully oxidized) carbon (TIC)	0.0	0.0	0.0	0.0	0.0	0.0	0.3	2.7	30.3	0.0	0.0
Input or output	TOC	51.6			5.8			5.1				
	TIC	0.0			0.0			33.4				
Total input or output		51.6			44.3							
Total carbon mass balance closure, %		85.9										

	Distribution of C amoung the FBSR effluent streams, weight % of total output C							
	Solid outputs			C in the CEMS 1 condensate	C captured in the CEMS 1 carbon filter	C in off-gas at the filter outlet		
	Bed product	Cyclone samples	Filter catch			CO_2	CO	THC
TOC	2.8	0.6	9.7	5.4	0.0	0.0	4.5	1.7
TIC	0.0	0.0	0.0	0.8	6.1	68.4	0.0	0.0
TOC	13.1			11.6				
TIC	0			75.3				
Totals	100.0							

Notes:

1. The mass of total solid carbon additive fed to the fluidized bed used for carbon mass balance calculations was determined gravimetrically from the mass of carbon added to the feeder hopper, not the amount determined by the PLC. The gravimetric amount is more accurate than the total amount fed based on the PLC.
2. The carbon content of the carbon reductant was estimated at 88.9%, determined from the SRNL moisture and loss-on-ignition analyses (3.1% and 95%, respectively), and allowing for 1% each residual H, N, and O that may be present in this wood-based carbon.
3. No organic or inorganic carbon was present in the simulant.
4. Prior analyses have shown that negligible inorganic carbon is present in any of the FBSR mineralized effluents.
5. The organic carbon content of the bed product was determined using two bed sample analyses (a) sample 1171, 3.52% C, for the 20.4 kg bed product from COT 0 to COT 61, and (b) sample 1173, 2.42% C, for the 20.9 kg bed product from COT 61 to COT 100. The C content was determined using the bed sample LOI values at 525°C, assuming the entire LOI mass loss is from organic C.
6. The organic carbon content of the cyclone samples was determined using 4.7 wt% average organic C concentration in 6.2 kg from samples 1174 and 1176. The C content was determined using the cyclone fines sample LOI values at 525°C, assuming the entire LOI mass loss is from organic C.
7. The organic carbon content of the filter fines was determined using (a) sample 1177, 11.4% C, for the 22.3 kg filter fines from COT 0 to COT 61, and (b) sample 1179, 9.6% C, for the 18.2 kg bed product from COT 61 to COT 100. The C content was determined using the filter fines sample LOI values at 525°C, assuming the entire LOI mass loss is from organic C.
8. Organic carbon was detected in the CEMS 1 condensate samples. Inorganic carbon was not detected, indicating minimal sorption of CO_2 in the CEMS 1 condensate. The TIC detection limit was used in the C mass balance calculations. This TIC and TOC represents TOC that was not detected as CO_2 or CO by the CEMS 1, and so is accounted for separately in addition to the total C determined based on CO_2, and CO recorded by CEMS 1.
9. TIC or TOC captured in the carbon filter includes carbon in carbon-bearing species that passed through the CEMS 1 chiller, but were captured in the CEMS 1 carbon filter used to protect the CEMS 1 analyzers from fouling by condensible hydrocarbons. The THC analyzer was located upstream of the carbon filter to avoid capture of THCs prior to THC analysis, but both CO and CO_2 analyzers were downstream of the carbon filter. The amount of TIC and TOC captured by the carbon filter was not measured. The amount of TOC captured in the carbon filter was assumed to be zero; the amount of TIC captured in the carbon filter was estimated to be equivalent to the amount of total carbon captured in the CEMS 1 condensate.
10. The C measured in the FBSR offgas was determined using the average filter outlet off-gas flowrate and concentrations of CO_2, CO, and THC. THC is reported as CH_4.

[PLC 10 min data Sept SBW Dec 7.xls]carbon MB

The overall carbon mass balance closure, at about 86%, indicates reasonably good accounting of carbon in the FBSR, considering that the combined accuracy of all of the different flow rate and concentration measurements and estimates was approximately plus or minus 10%.

Most of the effluent carbon (about 87%) was in the off-gas CO_2, CO, or THC, including both the measured concentrations of these species in the off-gas, and also the amounts of organic and inorganic carbon detected in the CEMS 1 condensate, and carbon captured in the CEMS 1 carbon filter. Only 13% of the carbon was found as organic carbon (residual unreacted carbon additive) in the solid products. About 75% of the organic carbon input to the fluidized bed was converted to fully oxidized CO_2, even though the C:oxidant stoichiometric ratio averaged 248%, over 2 times as much carbon as was needed to stoichiometrically react with the atomizing O_2 and nitrates in the feed to produce CO_2 and N_2. This was because the C:oxidant stoichiometry was based on the C:O_2 and C:NO_x overall reactions, and did not account for the amount of carbon gasified to CO and other gas species through reactions with O_2, nitrates, and steam. While over 2 times as much carbon was added than was needed to stoichiometrically react with O_2 and NO_x, much of the "extra" carbon was utilized in other steam reforming reactions, and was necessary to provide adequately reducing conditions to efficiently destroy NO_x.

5. CONCLUSIONS/RECOMMENDATIONS

The INEEL's pilot scale fluidized bed test system at the STAR facility was successfully operated during the last week of September 2004 to conduct a continuous 100-hour experiment demonstrating THOR Treatment Technologies mineralizing steam reforming process with simulated waste material representative of INEEL's SBW.

A large amount of real-time process operating conditions data and process materials data was generated. These data have been compiled and undergone considerable analysis leading to the test results presented herein. Considerable further analyses are, however, possible and warranted to generate increased understanding of the technology and response to changes in key process parameters.

Further analyses of existing test data, coupled with additional controlled process technology tests such as bed thermal profile tests and nozzle studies, would be extremely valuable to determine reactor/bed responses to key input parameter changes for future process optimization and improved test diagnostic capabilities. Several different, important FBSR mineralizing process mechanisms and complex interactions cannot be well understood from currently available data and analyses alone. Considerable additional controlled testing and model-based evaluations of both local and global heat transfer, fluid dynamics, and reaction rate driven chemistry conditions are needed to provide predictive means for process/system scaling and optimization.

The following are key conclusions and recommendations from the pilot scale fluidized bed SBW mineralized steam reforming process technology test results.

1) The pilot scale test successfully achieved the planned total of 100 hours of cumulative/continuous stable processing operations, at an average feed rate of 2 L/hr. A sufficient quantity of mineralized product material was produced under stable process conditions for performance and durability testing. The process achieved about 90% bed turnover (replacement of the starting bed with mineralized product solids) and operated essentially within desired process conditions. This met the desired test objective of operating for 100 hours, but was slightly short of the test objective average feed rate of >3 L/hr. Fluidized bed operations were stable and controlled; bed height, fluidized density, pressure drop, and axial temperature differences were all within expected control ranges. No defluidizing bed agglomerations were experienced and the test was terminated as planned after reaching 100 hours of operation.

2) The pilot scale test produced a significant quantity of representative FBSR mineralized solid product materials, samples of which have been analyzed for chemical/physical properties, and can be used to compare/validate equivalency with small lab-scale batch equilibrium mineralizing chemistry studies/tests by SRNL. The total amount of simulated SBW feed and additives processed was approximately 354 kg and the total solid product mass collected was approximately 88 kg (64 kg of total product solids excluding starting bed and unreacted carbon solids, consisting of about 28 kg of bed product [22 kg of bed and 6 kg of cyclone samples] and 36 kg of filter fines). This represents a total mass reduction within the process of 266 kg, or about 75%. The total input of solids includes 58 kg of carbon and about 47 kg clay. Therefore, about 230 kg of SBW surrogate resulted in about 88 kg of solid product, a waste mass reduction of about 62%. An overall solids mass balance closure of near 98% was achieved. The net solid waste product material mass and volume are, of course, interesting for any subsequent processing or direct handling and disposal activities.

3) The bed product to fines collected mass ratio ranged from 0.6 to 1.3, and for the entire test

averaged 0.78 (44 wt% to the bed product and 56 wt% to the fines). Although this result did not satisfy a test objective of obtaining a product to fines ratio greater than 3.5 to 1 (approximately 80% bed product), no emphasis had been placed upon process parameter or system configuration changes other than utilizing cyclone recycle, to attain this objective. Rather, the focus of this test was primarily upon achieving stable operation over the planned operating period and representative product material for use in subsequent determination of product performance/durability properties.

4) The mineralized product materials in the bed at test end had a particle density of approximately 1.9 g/cc and an average MMPD of 0.77 mm, and 0.22 mm HMPD, as compared to the starting bed (alumina, 100 grit) particle density of approximately 3.8 g/cc and average size of 0.132 mm MMPD and 0.128 HMPD. The product particles in the cyclone had an average MMPD of 0.042 mm (18 times smaller than the bed product granules), while the filter product (fines) had an average size of 0.016 mm (3 times smaller than the cyclone product). Although the bed product average particle size clearly grew throughout the test, the cyclone and filter fines size distribution remained essentially constant.

5) The bed product particle size distribution shows a strongly bi-modal (or almost tri-modal) distribution with peaks at 0.140 mm (range 0.02 to 0.30 mm) and 1.03 mm (range 0.30 to 3.5 mm). It is suspected that the larger size bed particles may in fact be present largely as a result of the regular formation and drop off of various material deposits from the atomization nozzle tip. These relatively large nozzle accretions were of various sizes and many were generally broken up into smaller pieces by action of the bed, thus providing larger seed particles for subsequent deposit of atomized slurry and particle growth. The smaller particle size peak and range may be indicative of the likely process product size in the absence of nozzle accretions.

6) The mineralized product materials (fluidized bed/vessel and cyclone) consisted primarily of small, somewhat rounded, granular solid particles with a bumpy and porous surface appearance. They are easily distinguished from the sharp, jagged “glass like” appearance of the alumina starting bed material. The product granules appear to be formed by collections of many smaller particles and successive deposits of very small particles on the surface of existing larger granules, much as what one might expect from successive “rough/haphazard powder coating layer deposits” of the very small clay particles contained in the atomized simulant slurry droplets. This is generally consistent with the appearance of bed product from the previous FBSR mineralized test with Hanford LAW, and is contrasted to the very smooth onion skin layered deposit appearance of earlier carbonate products from “non-mineralized” fluidized bed steam reforming experiments. The appearance of the cyclone product particles is similar to those of the bed product, with much smaller particles observed on the surfaces. The filter fines, however, appear to be somewhat similar but with a much more porous and jagged assemblage/collection of particles, indicating potentially other formation mechanisms are present.

7) The mineralized steam reforming process is intended to destroy the nitrates and immobilize the SBW metals as oxides in a stable product solid consisting largely of alkali aluminosilicate target mineral phases of various structures. Test results show that nitrates and nitrites in the waste feed were effectively eliminated and that the mineralized product in the bed and cyclone and fines consisted of desired target mineral phases or likely pre-cursors. Nepheline was a major phase in the bed and cyclone product and present to some extent in the filter product. Sodalite was a trace mineral in the bed and cyclone product. A sodium aluminosilicate was a major phase in the fines, which may or may not be an effective mineral, and may be a result of some very rapid spray

drying of small droplets/particles.

8) The elemental mass balance closure for sodium, potassium, aluminum, phosphorus, titanium, and iron are excellent (within 94%) and the closures for the remainder are good (within 80%). The mass balance closure for carbon was about 86%, reasonable accounting for that element. Closures for S and Cl are lower than expected, 77% and 80% respectively, but perhaps can be attributed to the formation of gaseous species not detected. Elemental analyses indicate that Re (Tc surrogate) and Cs strongly partitioned to the fines, as did Cl and S, while the other metals generally partitioned evenly between the bed and fines. The amount of radionuclide surrogates and hazardous metals and acid gas anions is notably very small. Elemental analyses for product phase partitioning evaluations could be considerably improved if somewhat larger "spiked" amounts were utilized in any future testing.

9) NO_X was very satisfactorily destroyed throughout the SBW mineralized steam reforming process test. The average NO_X destruction based on measurements upstream of the thermal oxidizer was 97.5% well beyond the minimum test objective of 80%, and considerably better than the 92% achieved in the preceding Hanford LAW test with the same carbon additive. The higher destruction efficiency in the SBW test maybe due to the slightly higher temperature (729 vs. 722 °C) in the SBW test and/or the presence of various catalytic metals in the SBW that were not present in the LAW.

10) The off-gas treatment system components performed very well. The cyclone performed well despite being sized for much higher gas flow rates than experienced in this SBW mineralized steam reforming test (the cyclone differential pressure was only 0.4 inches water column, as compared to the nominal design value of 5 inches water column). The average cyclone efficiency was about 82% at an average cyclone recycle rate of 1.8 kg/hr and an average hot filter fines capture rate of 0.4 kg/hr. No fines were detected in equipment downstream of the hot filter. The multi-stage thermal oxidizer performed well in its single stage oxidizing mode, as per design, effectively destroying all residual reduced gas species and maintaining low NO_X levels. The partial quench, mist eliminator, and GAC bed performed as expected.

11) The waste feed atomization nozzle appears to have performed effectively throughout the test in providing slurry atomization, while minimizing formation of localized nozzle deposits and accretions as compared to pre-demonstrational functional equipment tests and the initial SBW experiment in July. There were, however, also clear indications that regular small growth and shedding of product/deposit materials were likely occurring from the nozzle tip. The upstream gas pressure for the atomizing nozzle regularly increased and decreased, and nozzle tip accretions in sample and bed drain products regularly appeared. Several larger nozzle tip accretions were observed over the course of the test operations, and the atomizing gas annulus on the nozzle became nearly occluded just after midway through the test, requiring a brief halt to the demonstration for removal, cleaning, and replacement of the nozzle. The nozzle deposit and accretion behavior gradually began again and atomizing gas pressure was again reaching high levels just before the test end. A small nozzle deposit was noted on the extended anti-bearding tip at the end of the test. This area around the nozzle is thought to be cooler that the rest of the vessel and bed, perhaps contributing to the deposits. Although all large nozzle accretions were managed satisfactorily with the bottom drain, further work is clearly needed to understand and provide for atomization nozzle characteristics that favor the process.

12) The overall operations and performance of the fluidized bed test system equipment was good. Several minor incidents occurred which required operator actions/interventions. These were,

however, generally corrected rapidly and had no significant discernible impacts upon the mineralized steam reforming process. The particular system/equipment incidents have been discussed in the results section and noted for potential modifications for improving future test operations. Briefly, the notable incidents, other than the atomizing gas nozzle occlusion, all occurred within the first day of operations and were: a) the upper carbon feed valve on the interlock section failed open which allowed small amounts of atmospheric air to enter with carbon feed during process operation (operations continued, 1 hour to restore), b) an air compressor hose problem led to inadequate air supply for plant operations which triggered an automatic trip of the thermal oxidizer, as designed, and cutoff of reformer process feed with a switch of fluidizing steam to nitrogen (30 minutes to restore and return to processing), c) bearing seals failed on the slurry mixture recirculation pump and recirculation flow was switched to the alternate pump without process interruption, d) cyclone recycle interrupted for a few hours due to a sheared auger, but process operations were continued (repaired and restarted auger within about 2 hours once noted) e) the atomizing nozzle orifice became partially occluded (processing halted for 3 hours to remove, clean, and replace nozzle).

6.

7.**REFERENCES**

Addison, C. C, 1964, and Logan, N., "Anhydrous Metal Nitrates," *Adv. Inorg. Chem. Radiochem.*, 6, 71.

Antal, M. J., 1979, et al., *A Study of the Steam Gasification of Organic Wastes*, Final Progress Report to the U.S. Environmental Protection Agency, Princeton University, Princeton, NJ.

Barrer, R. M., 1959, J. W. Baynham, F. W. Bultitude, and W. M. Meier, *Hydrothermal Chemistry of the Silicates. Part V23I, Low-Temperature Crystal Growth of Aluminosilicates, and of Some Gallium and Germanium Analogues***,** 195-208.

Bartos, H. R., 1956, and Margrave, J. L., *J. Phys. Chem.*, 160, 256.

Berry, L. G., 1959, and Mason, B., *Mineralogy Concepts, Descriptions, Determinations***,** W.H. Freeman & Co., San Francisco, CA, 630pp.

Boardman, R. D, 2004, B. H. O'Brien, N. R. Soelberg, S. O. Bates, C. P. St. Michel, R. A. Wood, and B. J. Ward, "High-Temperature MACT Calcination Test," INEEL/EXT-04-01625, February.

Bradley, R. F., 1972, Goodlett, C. B., *Denitration of Nitric Acid Solutions by Formic Acid*, DP-1299, Savannah River Laboratory, Aiken, SC.

Bray, L. A. 1963, *Denitration of Purex Wastes with Sugar,* HW-76973; Hanford Atomic Products Operation, Richland, WA.

Brookins, D. G, 1984, *Geochemical Aspects of Radioactive Waste Disposal***,** Springer-Verlag, New York, 347pp.

Brown, R. W., 1975, Lippiat, J. H., Price, D., Izod, D. C. A., *Intl. J. Mass Spect. Ion Phys.*, 16, 101.

Cheng, I. F., 1997, Muftikian, R., Fernando, Q., Korte, N., *Chemosphere*, 35, 2685.

Cox, J. L., 1994, Hallen, R. T., Lilga, M. A., *Environ. Sci. Technol.*, 28, 423.

Dana, E. S., 1932, *A Textbook of Mineralogy*, John Wiley & Sons, Inc., New York, 851pp.

Deer, W. A., 1963, Howie, R. A., and Zussman, J., *Rock-Forming Minerals, Vol IV***,** John Wiley & Sons, Inc., New York, 435pp.

Del Debbio, J. A, 2003, T. L. Watson, and J. B. Heintzelman, *Long-Term Performance of Sulfur-Impregnated, Granulated Activated Carbon (GAC) for Mercury Removal from NWCF Off-Gas*, INEEL/EXT-03-01102, September.

Dotson, J. M., 1975, Peters, T. E., U. S. Patent 3,862,296.

Elliott, M. A., 1981, Wiley, Ed, *Chemistry of Coal Utilization, 2nd Suppl. Vol.*, Interscience, New York, p. 1500.

Freeman, E. S., 1956, *J. Phys. Chem.*, 60, 1487.

Gunderloy Jr., F. C., 1968, Fujikawa, C.Y., Dayan, V.H., Grid, S., *Dilute Solution Reactions of the*

Nitrate Ion as Applied to Water Reclamation, Technical Report No. TWRC-1; FWPCA: Cincinnati, OH.

Gunderloy Jr., F. C., 1970, Wagner, R. I., Dayan, V. H., *Development of a Chemical Denitrification Process*, Technical Report No. EPA 17010EEX/10/70; U.S. Environmental Protection Agency, Water Quality Office: Washington, DC.

Hayhurst, A. N., 1992, and Lawrence, A. D., *Prog. Energy Combust. Sci.*, 18, 529.

Jantzen, C. M., 1982, Clarke, D. R., Morgan, P. E. D., and Harker, A. B., "Leaching of Polyphase Nuclear Waste Ceramics: Microstructural and Phase Characterization," *J. Am. Ceram. Soc.*, 65[6], 292-300.

Jantzen, C. M., 2002, *Engineering Study Of The Hanford Low Activity Waste (LAW) Steam Reforming Process (U)*, WSRC-TR-2002-00317, REV. 0, July 12.

Jantzen, C. M., 2003, *Disposition of Tank 48H Organics by Fluidized Bed Steam Reforming (FBSR)*, WSRC-TR-2003-00352, September.

Jantzen, C. M., 2004, J. C. Marra, and J. M. Pareizs, *Analysis of Raw Materials for Fluidized Bed Steam Reforming (FBSR)*, SRNL-ITB-2004-0004, June 30.

Kirk-Othmer, 1995, *Encyclopedia of Chemistry*, Vol. 16.

Klingenberg, R. 1986, and Felsche, J., "Interstitial Cristobalite-type Compounds, $(Na_2O)_{0.33}Na[AlSiO_4]$)," *J. Solid State Chemistry*, 61, 40-46.

Kramer, C. M., 1983, et al., *High Temperature Science*, 16, 257.

Kunii, D. 1991, and Levenspiel, O., *Fluidization Engineering*, 2nd Edition, Butterworth-Heinemann, Newton, MA.

Kuo, Kenneth Kuan-yun, *Principles of Combustion*, John Wiley & Sons, 1986, p. 372

Mattus, A. J., 1993, Lee, D. D., *The Nitrate to Ammonia and Ceramic (NAC) Process – A Newly Developed Low-Temperature Technology*, CONF-930873-18; Oak Ridge National Laboratory, Oak Ridge, TN.

McCarthy, G. J., 1976, and M. T. Davidson, "Ceramic Nuclear Waste Forms: I," *Am. Ceram. Soc. Bull.*, 54, 782-786 (1975) and "Ceramic Nuclear Waste Forms: II," *Am. Ceram. Soc. Am. Ceram. Soc. Bull.*, 55[2]190-194.

Meile, L. J., January 1984, and Johnson, A. J., *Waste Generation Reduction - Nitrates FY 1982 Status Report*, Rockwell International, RFP-3465, DOE/TIC-4500 (Rev. 72).

Morgan, P. E. D., 1981, Clarke, D. R., Jantzen, C. M., and Harker, A. B., "High-Alumina Tailored Nuclear Waste Ceramics," *J. Am. Ceram. Soc.*, 64 [5] 249-58.

Murphy, A. P., 1991, *Nature*, 350, 223.

Nimlos, M., 1990, and T. Milne, *Preliminary Screening of Steam-reforming Efficacy of Rhodium*

Catalysts for Destroying Halon 1301 (CF_3Br), Letter Report to Sandia from SERI dated June 28, 1990.

Nimlos, M. R., 1992, and T. A. Milne, *Environ. Sci. Technol.*, 26, 545.

Olson, A. L. 2004, N. R. Soelberg, D. W. Marshall, and G. L. Anderson, *Fluidized Bed Steam Reforming of Hanford LAW Using THOR^{SM} Mineralizing Technology*, INEEL/EXT-04-02492, November.

Rusin, J. M., 1979, M. F. Browning, G. J. McCarthy, "Development of Multibarrier Nuclear Waste Forms," *Sci. Basis for Nucl. Waste Mgt. I*, G. J. McCarthy (Ed.), Plenum Press, New York, 169-180.

Ryan, J. L., 1995, *Redox Reactions and Foaming in Nuclear Waste Glass Melting*, PNNL-10510, August.

SAIC, 2004, *Steam Reformer Operating Instructions*, SAIC-SR-OI-01, Current revision.

Seymour, R. G., 1995, *Development of the High-Level Waste High-Temperature Melter Feed Preparation Flowsheet for Vitrification Process Testing,* WHC-SD-WM-SP-008, February.

Soelberg, N. R., 2003, D. W. Marshall, S. O. Bates, D. D. Siemer, *SRS Tank 48H Waste Steam Reforming Proof-of-Concept Test Results*, INEEL/EXT-03-01118, September.

Soelberg, N. R., 2004a, D. W. Marshall, D. D. Taylor, and S. O. Bates, *Phase 2 TWR Steam Reforming Tests for Sodium-Bearing Waste Treatment*, INEEL/EXT-04-01494, January 30.

Soelberg, N. R., 2004b, D. W. Marshall, S. O. Bates, and D. D. Taylor, *Phase 2 THOR^{sm} Steam Reforming Tests for Sodium-Bearing Waste Treatment*, INEEL/EXT-04-01493, January 30.

Appendix A

Hydraulic Similarity Tests

D. W. Marshall

Appendix A

HYDRAULIC SIMILARITY TESTS

Introduction To Hydraulic Similarity

At times it is desirable to model a fluidized bed system using smaller equipment or parameters that are more conducive to getting the data needed for making judgments about the system. It is important to select bed media and operating parameters such that the hydraulic behavior of the model is representative of the actual system when such physical models are used. The bed recirculation, convection cell geometry, and fluidization mode may not match that of the actual system if hydraulic similarity is not achieved.

Direct observations of the bed convection cells or fluidization mode cannot be made of the 6-inch fluidized-bed steam reformer (FBSR) when it is operating at temperature. It was desirable, therefore, to model the FBSR using a Plexiglas tube and suitable bed material so that the convection could be photographically documented during tests of the INEEL ring distributor and compared to the THOR SM Treatment Technologies proprietary distributor. The objective was to monitor fluidization of bed material and flow patterns resulting from the gas injection points and the of distributor geometries rather than to evaluate distributor pressure drop. Efforts were made to select distributors, from the existing stock, that have similar pressure drops during the experiment.

Methodology

Hydraulic similarity can be satisfactorily achieved when scaling parameters are matched between the actual system and the physical model, which operates at less harsh conditions. Horio, et al., proposed the use of two scaling parameters based on the square root of the Froude numbers. Fitzgerald and Crane proposed the use of more restrictive scaling parameters that include the Reynolds number, solid-gas density ratio, Froude number, geometric similarity of the reactor and bed medium. These two sets of scaling parameters were tested by Roy and Davidson, who found that the simpler set proposed by Horio was best suited for particle Reynolds numbers less than 30 and the Fitzgerald & Crane parameters were better suited for particle Reynolds numbers over 30. A concise summary of physical models and these parameters has been provided by Kunii and Levenspiel.

The particle Reynolds number is less than 10 at FBSR operating conditions (see Table A-1), and the scaling parameters proposed by Horio, et al. are appropriately used. These are the Froude number for the minimum fluidization velocity and the difference of the square roots of the Froude numbers at the operating parameters and that at minimum fluidization velocity:

$$Fr_{mf} = \frac{u_{mf}^2}{g \cdot d_p}$$

Parameter (1)

$$\sqrt{Fr} - \sqrt{Fr_{mf}} = \frac{u - u_{mf}}{\sqrt{g \cdot d_p}}$$

Parameter (2)

Table A-1. Hydraulic similarity test operating conditions.

Reference Case		Physical Model		
Reactor diameter	6.065 in.	Reactor diameter		5.75 in.
Bed medium	alumina	Bed medium		silica sand
Particle density	3.95 g/cc	Particle density		2.63 g/cc
Particle size (HMPD)	245μm	Particle size (HMPD)		214 μm
Reactor temperature	720°C	Reactor temperature		~27°C
Min. fluidizing velocity (U_{mf})	0.038 m/s	Min. fluidizing velocity (U_{mf})		0.038 m/s
Particle Reynolds No. (Re_{mf})	0.05	Particle Reynolds No. (Re_{mf})		0.49
Velocity ratio U/U_{mf}	6	Velocity ratio U/U_{mf}		5.4
Bed pressure (0" elevation)	12.3 psia	Bed pressure (0" elevation)		13.4 psia
Bed differential pressure	45 in.WC	Bed differential pressure		30 in.WC
Fluidizing gas	steam	Fluidizing gas		air
Fluidizing gas rate	2.8 kg/hr	Fluidizing gas rate		13.9 kg/hr
Instrument purge flow	1.0 kg/hr			
Froude number at U_{mf} (Fr_{mf})	5.96e-4	Froude number at U_{mf} (Fr_{mf})	6.95e-4	Ratio = 1.17
Fluidized without feed - Reference		*Fluidized without feed - Model*		
SBW+clay feed rate (UTB or lower nozzle)	0 kg/hr	Air injection (lower or UTB nozzle)		24.0 kg/hr
SBW+clay slurry NAR	0			
SBW+clay water fraction	0.67	Simulated instrument purge (upper nozzle)		3.0 kg/hr
Particle Reynolds No. (Re_{top})	0.4	Particle Reynolds No. (Re_{top})		3.8
$\sqrt{Fr_{bottom}} - \sqrt{Fr_{mf}}$	0.122	$\sqrt{Fr_{bottom}} - \sqrt{Fr_{mf}}$	0.117	Ratio = .96
$\sqrt{Fr_{middle}} - \sqrt{Fr_{mf}}$	0.130	$\sqrt{Fr_{middle}} - \sqrt{Fr_{mf}}$	0.122	Ratio = .93
$\sqrt{Fr_{top}} - \sqrt{Fr_{mf}}$	0.144	$\sqrt{Fr_{top}} - \sqrt{Fr_{mf}}$	0.129	Ratio = 0.90
Lower or UTB feed nozzle – no spare		*Lower or UTB feed nozzle – no spare*		
SBW+clay feed rate (UTB or lower nozzle)	6 kg/hr	Air injection (lower or UTB nozzle)		24.0 kg/hr
SBW+clay slurry NAR	500			
SBW+clay water fraction	0.67	Simulated instrument purge (upper nozzle)		3.0 kg/hr
Particle Reynolds No. (Re_{top})	0.9	Particle Reynolds No. (Re_{top})		7.8
$\sqrt{Fr_{bottom}} - \sqrt{Fr_{mf}}$	0.122	$\sqrt{Fr_{bottom}} - \sqrt{Fr_{mf}}$	0.117	Ratio = 0.96
$\sqrt{Fr_{middle}} - \sqrt{Fr_{mf}}$	0.463	$\sqrt{Fr_{middle}} - \sqrt{Fr_{mf}}$	0.458	Ratio = 0.99
$\sqrt{Fr_{top}} - \sqrt{Fr_{mf}}$	0.527	$\sqrt{Fr_{top}} - \sqrt{Fr_{mf}}$	0.519	Ratio = 0.98
Lower or UTB feed nozzle – with idled spare		*Lower or UTB feed nozzle – with idled spare*		
SBW+clay feed rate (UTB or lower nozzle)	6 kg/hr	Air injection (lower or UTB nozzle)		24.0 kg/hr
SBW+clay slurry NAR	500			
SBW+clay water fraction	0.67	Simulated instrument purge (upper nozzle)		3.0 kg/hr
Spare nozzle purge	1.4 kg/hr	Spare nozzle purge		4.7 kg/hr
Particle Reynolds No. (Re_{top})	1.0	Particle Reynolds No. (Re_{top})		8.7

$\sqrt{Fr_{bottom}} - \sqrt{Fr_{mf}}$	0.122	$\sqrt{Fr_{bottom}} - \sqrt{Fr_{mf}}$	0.117	Ratio = 0.96
$\sqrt{Fr_{middle}} - \sqrt{Fr_{mf}}$	0.488	$\sqrt{Fr_{middle}} - \sqrt{Fr_{mf}}$	0.510	Ratio = 1.05
$\sqrt{Fr_{top}} - \sqrt{Fr_{mf}}$	0.581	$\sqrt{Fr_{top}} - \sqrt{Fr_{mf}}$	0.573	Ratio = 0.99

The first parameter, Fr_{mf}, is essentially uniform throughout the bed and was computed only once. The second parameter, however, varies depending on where atomizing gases, aqueous feed, and other gases are introduced or generated. For simplicity (and for the lack of reliable mixed-gas property data) the gases were assumed to behave as ideal gases, gas generation beyond water vaporization was neglected, and all gases were assumed to have the same physical properties of the fluidizing gas. These assumptions should not have introduced large errors into the calculations since water vapor is the dominant species in the FBSR and air is the only species in the physical model.

Options exist to inject feed at one or more of three levels; 1) through the uniaxial-tube Bernoulli-effect (UTB) nozzle that extends through the reactor receiver plate into the distributor region, 2) through a horizontal nozzle located about four inches above the distributor, and 3) through a horizontal nozzle located about 13 inches above the distributor. The small elevation difference between the UTB nozzle and the lower horizontal nozzle prompted another assumption to treat these points as being the same elevation. This divides the reactor into three distinct regions, which are:

1. Between the distributor and the lower feed nozzle elevations,
2. Between the lower and upper feed nozzle elevations, and
3. The surface of the fluidized bed.

The elevations are taken at the distributor (0”), just below the upper feed nozzle elevation (+12”), and at the mean elevation of the bed surface (+30”) for the hydraulic similarity calculations.

Test Conditions

The reference case conditions were selected to be representative of the conditions to be used during the mineralizing flowsheet demonstrations. The feed rate was not expected to exceed 6 kg/hr and the nozzle atomizing ratio was expected to remain relatively low to maximize residence time and minimize feed plume penetration through the bed. The bed media was assumed to be white alumina with an average particle size of 245µm (60-grit). Fluidizing gas velocity was assumed to be six times the minimum fluidizing velocity because this is needed with the virgin bed to maintain adequate pressure drop in the distributor.

The sum of instrument purges is assumed to be 1 kg/hr in the reactor section during actual tests. The flow is adjusted to satisfactorily match the scaling parameters and divided equally between the lower and upper gas injection (feed) points in the physical model to achieve hydraulic similarity.

Silica sand for the bed in the physical model was available at the SAIC STAR Center. The sand, as received, had a mass-mean particle diameter (MMPD) of 270µm and a harmonic-mean particle diameter

(HMPD) of 216μm. For hydraulic similarity, it is desirable to have an HMPD of 0.203μm, which could have been achieved with the available sand if a 40-mesh sieve screen had been available to screen out the larger particles. A 35-mesh sieve was used, which reduced the HMPD to approximately 0.214μm, based on a previous sand sample. Because the sand HMPD was larger than desired, the Froude number at minimum fluidization could not be strictly matched with the reference case. The second matching parameter (difference in the square roots of the Froude numbers) matched reasonably well, despite the initial calculations being based on the ideal particle size. The larger particle size resulted in the fluidizing gas flow in the physical model being 5.4 times the minimum fluidizing velocity rather than 6 times the minimum in the reference model.

The experiment consisted of several tests intended to represent different modes of operation. These tests are designated in numerical order (e.g., 1, 2, 3, etc.). Several ad hoc tests were also conducted because the desired conditions were easily configured and achieved. The ad hoc tests are designated alphanumerically (1a, 1b, etc.). Table A-2 shows the conditions planned and tested. Two other tests were planned that would have simulated operation with feed entering two feed nozzles (upper and lower or lower and UTB), rather than just one, but limitations on the equipment prevented the investigators from achieving the desired flow rate of air.

Quarter-inch tubing was used to represent the feed nozzles located at the 4"and 13" datum lines and the UTB nozzle. Although gas velocities in the immediate vicinity of the nozzles differ from the actual gas flows, the matching parameters are meant to show representative behavior of the bulk emulsion phase

Table A-2. Summary of the physical model test conditions.

Test	Distributor	Air flow rates				
		Fluidizing	UTB	Lower nozzle	Upper nozzle	Total
1	THOR^{SM}	13.9 kg/hr 6.3 scfm	---	---	---	13.9 kg/hr 6.3 scfm
1a	THOR^{SM}	13.9 kg/hr 6.3 scfm	---	24.0 kg/hr 11.0 scfm	3.0 kg/hr 1.4 scfm	40.8 kg/hr 18.6 scfm
1b	THOR^{SM}	13.9 kg/hr 6.3 scfm	24.0 kg/hr 11.0 scfm	---	3.0 kg/hr 1.4 scfm	40.8 kg/hr 18.6 scfm
1c	THOR^{SM}	13.9 kg/hr 6.3 scfm	16.0 kg/hr 7.3 scfm	---	3.0 kg/hr 1.4 scfm	32.8 kg/hr 15.0 scfm
2	Ring	13.9 kg/hr 6.3 scfm	---	---	---	13.9 kg/hr 6.3 scfm
3	Ring	14.0 kg/hr 6.3 scfm	---	24.0 kg/hr 11.0 scfm	3.0 kg/hr 1.4 scfm	40.9 kg/hr 18.6 scfm
3a	Ring	13.9 kg/hr 6.3 scfm	---	16.1 kg/hr 7.3 scfm	3.0 kg/hr 1.4 scfm	32.9 kg/hr 15.0 scfm
4	Ring	14.0 kg/hr 6.3 scfm	24.0 kg/hr 11.0 scfm	---	3.0 kg/hr 1.4 scfm	40.9 kg/hr 18.6 scfm
4a	Ring	13.9 kg/hr 6.3 scfm	16.0 kg/hr 7.3 scfm	---	3.0 kg/hr 1.4 scfm	32.8 kg/hr 15.0 scfm
5	Ring	13.9 kg/hr 6.3 scfm	24.0 kg/hr 11.0 scfm	4.7 kg/hr 2.1 scfm	3.0 kg/hr 1.4 scfm	45.6 kg/hr 20.8 scfm
5a	Ring	13.9 kg/hr 6.3 scfm	15.7kg/hr 7.2 scfm	4.7 kg/hr 2.1 scfm	3.0 kg/hr 1.4 scfm	37.3 kg/hr 17.0 scfm
6	Ring	13.9 kg/hr 6.3 scfm	4.7 kg/hr 2.1 scfm	24.0 kg/hr 11.0 scfm	3.0 kg/hr 1.4 scfm	45.6 kg/hr 20.8 scfm

Test Observations

Each of the test conditions was recorded using a digital video camera so that the emulsion flow and elevation of bubble/slug formation could be documented. Datum lines were drawn on the Plexiglas tube to denote the 4" and 13" elevations (relative to the bottom flange face) corresponding to the elevations of the feed ports in the actual process.

Overall bed level dropped during the course of the testing because elutriated bed particles were swept away by the ventilation system. The bed level would not have dropped as much had the Plexiglas model been fitted with an expanded freeboard and a cyclone catch recycle, as the actual system. Approximately 20-25% of the bed mass had been lost by the conclusion of the tests.

Test 1 showed the fluidization of the sand using the THOR^{SM} distributor. Bubbles in the emulsion were observed near the bottom flange, in the vicinity of the distributor, but not along the flange or walls positioned at right angles to the distributor. This is evidence that the gas is not uniformly distributed in the immediate vicinity of the distributor in spite of efforts to space orifices such that the gas would be more evenly distributed. The jet plumes reached the exterior walls of the reactor only near the distributor ends. The emulsion was fluidized, however, over the entire observable cross section of the bed. The emulsion was observed to descend along the wall orthogonal to the distributor. Slugs were generally symmetrical and tended to flow up the center of the column. All slugging was observed above the lower feed nozzle elevation, beginning approximately 7" above the distributor. Slugs were mostly axial with an occasional "flat" slug near the top of the bed (bubble filled the full cross section of the reactor).

Some Berger Brothers activated carbon was added to the fluidized bed to trace bulk emulsion flow. The carbon remained near the surface of the bed and did not get carried down the sidewalls with the emulsion.

Test 1a was conducted with the THOR^{SM} distributor and the addition of gas through the upper feed nozzle to represent the addition of instrument purge gases and gas through the lower side feed port to represent slurry feed evaporation and atomization. Some bubbles were observed impinging on the reactor wall opposite of the feed nozzle, indicating that the bed was being penetrated by the nozzle jet. It should be noted that the quarter-inch tubing used to inject the gases is not representative of the feed nozzle in terms of gas quantity or velocity at the nozzle. Hydraulic similarity is achieved approximately eight inches above the injection point. Nonetheless, this observation is consistent with observed fouling and accretions on the wall opposite the feed nozzle from past reactor operation, especially when a light-weight product replaces the starting bed. Low density bed media allow for deeper penetration of the gas plumes. Some gross recirculation of the bed was induced by injection of the gas at the lower feed port, resulting in somewhat more upward flow of the emulsion along the opposite wall and down flow of the emulsion above the feed port and cyclone catch recycle injection. Flat slugs were frequently observed. The activated carbon mixed in the top portion of the bed, but was not observed below the upper side port.

Test 1b was conducted with the THOR^{SM} distributor and the addition of gases to represent instrument purges, feed, and feed atomization. The feed and atomizing gas surrogate air was injected through the UTB instead of the lower feed port. The addition of the gas through the UTB caused gross recirculation of the bed emulsion with down flow dominating on the side of the reactor behind the UTB injector, which is angled upward from the bottom such that it passes through the distributor zone. The gross recirculation (i.e., "gulf streaming") of the bed was more pronounced than in Test 1a when the feed was introduced through the lower side feed port. The UTB jet plume was observed against the opposing reactor wall. As slugs passed the upper feed nozzle (13") elevation, the bulk flow of the emulsion would

reverse directions, as evidenced by the observable plume from the purge injection. Slugs tended to be less centered in the bed; forming more "wall slugs" than axial slugs. The bed surface was more violent and elutriated particles were more prevalent in the freeboard. Activated carbon was mixed in because of the violent bed surface, but was not observed below the upper side port.

The gross circulation of the bed causes the emulsion phase to flow downward, toward the distributor, at the elevation where cyclone catch recycle is introduced. This places the fine carbon particles in the bottom of the bed, near the vicinity of the distributor (and oxygen). Furthermore, the circulation of the emulsion sweeps recycled product fines into the feed zone where they may be captured and help form seed particles. The velocity of the emulsion phase past the cyclone catch recycle injection point seems to be higher than when the lower side feed port is used.

Test 1c was an unplanned test condition selected purely for the visualization of the bed at a reduced feed rate. Hydraulic similarity conditions had not been computed nor intentionally set. The air injection rate in the UTB nozzle was decreased from 24 to 16 kg/hr. This action caused the impingement of the air jet plume to be more intermittent and smaller than at the higher feed rate. The bed surface was also less violent.

Test 2 was conducted with the ring distributor installed and the bed fluidized at approximately $5.4*U_{mf}$. Bubbles were observed around the perimeter of the reactor wall in the vicinity of the distributor. The distribution appears to be more uniform than the THOR ^{SM} distributor, which only exhibited bubbling near the reactor walls where the distributor terminated. This result was not unexpected because the mean free path between the ring and the reactor wall is generally less than it is from the orifices of the THOR^{SM} distributor to the reactor wall except near the edge of the distributor. Slugs formed at about the same level as in Test 1, approximately 7" above the distributor. Slugs were predominately axial. Beyond a few inches above the distributor, the emulsion flow was indistinguishable from that induced by the THOR^{SM} distributor. Activated carbon was observed on the surface of the bed and appeared to mix in the top couple of inches of the bed.

Test 3 was conducted with conditions the same as during Test 1a, except that the ring distributor was used. Feed surrogate air was injected through the lower side port at 24 kg/hr and a surrogate instrument purge was added at 3 kg/hr through the upper side port. Some bubbles were observed impinging on the wall opposite of the lower side port, indicating full penetration of the bed by the jet plume. Gross bed recirculation patterns and slug formation was the same as in Test 1a. Carbon mixed in the top inches of the bed, but has not been observed descending the sides of the reactor with the emulsion phase.

Test 3a was conducted with reduced feed surrogate air (reduced from 24 to 16 kg/hr), but otherwise configured the same as Test 3. Feed jet plume penetration of the bed was reduced. More carbon was observed on the surface of the bed than in Test 3.

Test 4 was conducted with the same conditions as Test 3, except the feed surrogate air was directed through the UTB nozzle. The air jet plume impinged on the wall of the reactor and gross bed recirculation was more pronounced when using the UTB nozzle than a side mounted nozzle. The UTB discharged at an elevation just above the distributor and well below the point where bubble coalescence resulted in slugs.

Test 4a was conducted to visualize decreased feed while using the ring distributor. The air flow rates and injection points match that of Test 1c. Gross bed recirculation patterns appear to be the same except in the immediate region of the distributor. The ring distributor has a more uniform distribution of

bubbles that are visible around much of the reactor perimeter, except where the down flow of the induced emulsion recirculation is most pronounced.

Test 5 was conducted to simulate a condition where the UTB nozzle was used for feed injection and the lower side port was fitted with an idled feed injector as a backup to the UTB. Air flow to the UTB was 24 kg/hr and to the lower nozzle injected 4.7 kg/hr. The combined gas flows caused a significant amount of bed to be ejected into the freeboard. Although the UTB and lower side ports are not coplanar, but have common radial vector components that may have increased the bed recirculation rate. The UTB plume impinged on the opposing reactor wall. No side nozzle bubbles were observed on the opposing wall, but this may have been obscured or captured by the UTB plume.

Test 6 was similar to Test 5 except that the feed surrogate air was injected through the side nozzle and the UTB was idled. The bed remained violently stirred, but elutriation was reduced because the bed surface was less violent than when the UTB was used.

Tests 7 and 8 were intended to simulate conditions where a clay slurry and liquid feed were fed through separate nozzles. The desired flows could not be achieved due to limitations in the air manifold used for the tests.

Conclusions

The THOR^{SM} and ring distributors adequately fluidize the bed. The emulsion phase was observed to be in motion at all points in the bed and around the bottom flange at the elevation of the distributor. The bubbles emanating from the THOR^{SM} distributor were visible near the edge of the supporting flange, but not along the reactor wall orthogonal to the distributor. The ring distributor bubbles were seen at the reactor wall around most of the reactor circumference. By all appearances, the ring distributor seems to distribute the gases more uniformly in the immediate vicinity of the distributor than the THOR^{SM} distributor. The movement of the emulsion phase appears to be independent of the distributor configuration at the elevation of the lower side port.

Carbon pieces mixed into the upper portion of the fluidized bed, but did not become distributed throughout the bed to a significant extent. None of the pieces were observed descending the reactor wall with the emulsion phase when about 500 cc of activated carbon added to the bed. This suggests that a small percentage of the carbon is distributed in the bed during normal operation. The quantity of carbon normally extracted from the process through bed sampling and bed draining activities suggests that a large inventory of carbon must normally exist in the bed.

The UTB nozzle induces greater bed recirculation because the nozzle was at an angle upward from the bottom with a ~20° radial component. This resulted in greater wall slugging occurring, which in turn caused the bed surface to be more violent and more particles to be elutriated from the bed.

References

T. J. Fitzgerald and S. D. Crane, in *Proc. 6th Int. Conf on Fluidized Bed Combustion*, vol.3, p. 815, Atlanta, GA, 1980.

M. Horio et al., in *Fluidization V*, K. Østergaard and A. Sørensen, eds., p. 151, Engineering Foundation, New York, 1986; *AIChE J.*, **32**, 1466 (1986).

D. Kunii and O. Levenspiel, *Fluidization Engineering*, 2nd Ed., Butterworth – Heinemann, 1991, pp 152 – 153.

R. Roy and J. F. Davidson, in *Fluidization VI*, J. R. Grace Et al., eds., p. 293, Engineering Foundation, New York, 1989.

Appendix B

Nozzle Atomization And Slurry Viscosity Test Results

Nicholas R. Soelberg

Douglas W. Marshall

Appendix B

NOZZLE ATOMIZATION AND SLURRY VISCOSITY TEST RESULTS

Introduction

Mineralizing clay was blended with sodium-bearing waste (SBW) and Hanford low activity waste (LAW) simulants to perform the fluidized bed steam reforming (FBSR) tests. High-quality atomization of the liquid waste/slurry as it is injected into the FBSR reactor is essential to maintaining long-term FBSR operation and achieving the desired FBSR products. Sufficient atomization is necessary to avoid excessively large droplets (poor local dispersal of slurry over the bed region/surface being sprayed) which may lead to localized overcooled granules and possible formation of larger agglomerations of bed particles that could cause defluidization of the bed and failure of the operation.

Conversely, increased atomization can produce a finer distribution of spray over the bed region; but if excessive, this may lead to undesirable fine particles that elutriate from the bed. Increased atomization gas also adds to the total gas flow effectively fluidizing the bed. The total fluidizing gas flow must be controlled within a desired range to avoid additional elutriation of small particles. Elutriation of fine particles from the bed process is mitigated to some extent by cyclone capture and recycle of elutriated fines to the bed for further potential incorporation into bed product.

Avoiding persistent nozzle accretions is necessary to prevent the formation of solids attached to the nozzle tip that can impair nozzle atomization performance. Small nozzle accretions that form and break off of the nozzle might not impair nozzle atomization, but accretions that persist and grow on the nozzle can contribute to poor atomization and bed defluidizing agglomerations.

Several different nozzle sizes and designs were evaluated prior to, during, and after the FBSR tests leading up to the SBW mineralizing demonstration documented in this report. This activity was performed in an effort to improve longer-term atomization performance and minimize the chance of defluidizing agglomerations during FBSR operation because of nozzle accretions or other forms of nozzle anomalies. As new nozzle configurations were considered and developed, the performance of each nozzle type was tested by pumping slurries through the nozzles under selected atomizing conditions and observing the results.

Liquid atomization depends on, among other factors, the liquid viscosity. Viscosities of various radioactive waste simulants used in fluidized bed steam reforming (FBSR) testing can vary widely, especially when clay, a mineralizing additive, is slurried with the simulant. Viscosity measurements were made for slurries of the SBW simulant in conjunction with the nozzle atomization tests. The viscosity measurements were used to determine relative viscosities for slurries with different clay concentrations, for evaluating the results of the nozzle atomization tests, and to provide assurance prior to FBSR test operations that the selected feed slurry compositions would not have feed-related problems due to viscosity.

The nozzle atomization tests were designed to provide comparative performance data for different nozzles under the selected liquid feed and atomizing gas conditions. Results from the nozzle atomization tests are qualitative, in that the tests enable visual and photographic observation of what the atomized spray patterns appear like under the selected test conditions. The qualitative results reported here, including digital particle size analyses, do not provide actual quantification of droplet particle size distributions produced by the nozzles. However, they are useful as a guide for determining how the

atomization performance of one nozzle compares to another nozzle under the selected flow conditions. Droplet particle size measurements were not performed for all of the nozzle atomization tests that were done. The atomization tests were done at ambient temperature, without the presence of a fluidized bed, and so did not provide a valid representation of what happens to individual droplets or to the spray pattern in an actual heated fluidized bed. The atomizing gas and the atomized feed droplets experience rapid heat transfer, the droplets quickly begin to evaporate (especially upon reaching boiling temperatures), and quickly begin to impact hot bed particles that are in the droplet flight paths in a heated, fluidized bed with hot fluidizing gas flowing upward and hot, circulating bed particles located nearby.

Liquid droplets that impact bed particles are heated even more quickly by the heat conducted from the particle, but conversely, that bed particle is quickly cooled to a lower temperature by the relatively cool liquid droplet. The cooled bed particle remains relatively cool until the remaining liquid in the droplet is evaporated, and heat is transferred from the fluidized bed to the particle. The droplet flight paths and the atomized spray pattern are affected by the fluidizing gas flow and the impingement of the atomizing gas and mass of atomized droplets on the bed media, as momentum is exchanged between the atomizing gas, atomized droplets, fluidizing gas, and bed media. This impingement can tend to propel the bed particles and fluidizing gas away from the tip of the feed nozzle, depending on the atomizing gas and liquid flow rates and velocities.

None of these heat, momentum, and mass transfer phenomena, which are inherent to spraying a liquid slurry into a hot fluidized bed, are modeled by the ambient temperature nozzle atomization tests. The nozzle atomization tests that were performed are not applicable for determining the optimum droplet size or slurry feed rate. However, the nozzle atomization tests were used to visualize the atomized spray pattern and to select nozzle and atomizing conditions that appeared to provide appropriate atomization of the feed, without dripping or spitting from the nozzle, and provided sufficient atomizing energy to overcome gravity effects on atomized droplets.

Sequence of Testing

Several different nozzle atomization tests were performed, on May 6, June 7, June 22, July 30, and September 13, all prior to the SBW mineralization test performed during the period of September 27 through October 1, 2004.

Qualitative, investigatory nozzle atomization tests were performed on May 6 (prior to the May functional equipment test) and June 7, 2004. The May 6 test was performed primarily to determine appropriate Troy clay – water slurry atomization conditions for the May functional equipment test.

Additional, qualitative nozzle atomization tests were performed on June 7, after the May functional equipment test, to determine what sizes of nozzles, and atomizing gas flow rates, were appropriate for feed slurries of Troy clay mixed with SBW lite simulant and OptiKast clay mixed with Hanford LAW lite simulant.

Slurry atomization tests were performed on June 22, 2004. These tests were more quantitative and less subjective than the prior nozzle atomization tests. These tests were performed to:

- Visualize the atomized spray of simulant slurry from feed nozzles under selected operating conditions.
- Determine if the uniaxial-tube Bernoulli (UTB) waste injection nozzle atomized the slurry similarly to the SprayCo® nozzle when operated under similar conditions, but using more

quantitative measurements than performed in prior nozzle atomization tests.

- Qualitatively measure the atomized spray droplet particle size.

- Provide data needed to select the feed nozzle operating conditions (nozzle size and configuration, simulant slurry feed rate, atomizing gas flow rate, and nozzle atomizing ratio [NAR]) for the initial SBW mineralizing FBSR experimental demonstration.

The atomization performance of a modified nozzle was tested on July 30, prior to the Hanford LAW FBSR test. This nozzle incorporated modifications to the standard SprayCo® nozzle to prevent or minimize the formation of deposits on the nozzle surfaces exposed to the fluidized bed. These qualitative tests were performed to verify if the atomization performance was still comparable to the standard, same-sized SprayCo® nozzle.

Nozzle atomization tests were performed on September 13, 2004 preparatory to the planned September SBW FBSR test. Two different-sized nozzles were tested. These tests were performed to:

- Visualize the atomized spray of simulant slurry from feed nozzles under selected operating conditions

- Determine how two different sizes of the modified nozzle atomized the SBW simulant mixed with the amount of clay expected to be used in the September SBW FBSR test.

- Qualitatively measure the atomized spray droplet particle size as a function of slurry flow and atomizing gas flow rate.

- Provide data needed to select the feed nozzle operating conditions (nozzle size and configuration, atomizing gas flow rate, and NAR) for the September SBW FBSR test.

- Measure backpressure on the nozzles as a function of slurry feed and atomizing gas flow rates.

It was postulated that the best atomization performance occurs when the atomizing gas, at the nozzle discharge point, reaches sonic velocity. At sonic velocity, the atomizing gas momentum is higher than for lower atomizing gas velocities. Feed nozzle atomization might be optimized by operating the nozzle with an atomizing gas backpressure approximately twice the nozzle outlet pressure, thereby providing sufficient pressure drop across the nozzle for the atomizing gas to reach sonic velocity.

Experimental Setup

A simplified open spray booth was set up in the FBSR enclosure at the SAIC STAR Center. The spray booth is shown in Figure B-1. The atomizing feed nozzles were mounted on a temporary stand so that the atomized slurry from the nozzle could be directed into a ventilated duct. The spray was drawn into the ventilation duct to prevent excessive and hazardous mist from forming in the enclosure. An open space of about 1-2 feet between the nozzle tip and the inlet to the ventilation duct enabled visual observation of the spray, photography, and droplet sampling. Air was used at the atomizing gas. Air was adequately representative of the N_2 gas used for atomization during FBSR tests and the O_2/N_2 mixture used for atomizing gas during the September SBW test. The O_2 concentration in the atomizing gas used

in the September SBW test ranged between 14 – 17 volume% O_2.

Figure B-1. The spray test setup in the FBSR enclosure, with a UTB nozzle mounted to spray into the ventilation hood.

Diagnostics

Two different techniques were used to document the tests and attempt to determine the particle size range of the atomized droplets for each nozzle under different nozzle operating conditions. High-speed photography provides photographic records of each spray condition. The photography was done using a film camera, 400 ASA film, and a 1/40,000th second flash. The camera was aimed at a 90^{o} angle to the spray, at a distance of 1-2 ft from the spray. The flash was directed at a 90 ^{o} angle to spray, and also at 90 ^{o} to the camera. A black background behind the spray enabled the white slurry droplets to stand out from the background in the photos.

Samples of the atomized droplets were collected on glass microscope slides for subsequent microscope and particle size analysis. The slides were first numbered and coated with a thin film of oil. The oil caused the water-based droplets to bead up separately rather than run together on the glass. Droplet samples were collected by swiping the oil-coated slides through the spray pattern. Optical

microscope analysis, including collection of digital photos, was performed on the slide samples. The digital photos were analyzed to determine the droplet particle size distribution using Image Pro Plus computer software for counting and sizing particles.

Nozzles Tested

The nozzle types included (a) commercially available SprayCo® nozzles of different sizes (with and without the SprayCo® antibearding configuration), (b) a uniquely modified version of the SprayCo® nozzle, and (c) uniaxial-tube Bernoulli-effect nozzles of different sizes and configurations. The UTB nozzles were modeled after the nozzle design used in prior THOR^{sm} demonstration testing. The UTB nozzle atomizes feed co-axially with the flow of the FBSR fluidizing gas.

Two SprayCo® nozzle types and sizes were tested (see Figure B-2). The nozzles essentially consist of two concentric tubes, an inner liquid flow tube and an outer concentric gas flow tube. The SprayCo® nozzle designator indicates the size of the liquid and air orifices, e. g., a 100150 nozzle and 180 cap, indicating that the liquid orifice inside diameter was 0.100 inches, the liquid tube outside diameter was 0.150 inches, and the atomizing gas flowed through the annulus formed between the 0.150 inch liquid tube and the 0.180 inch gas orifice.

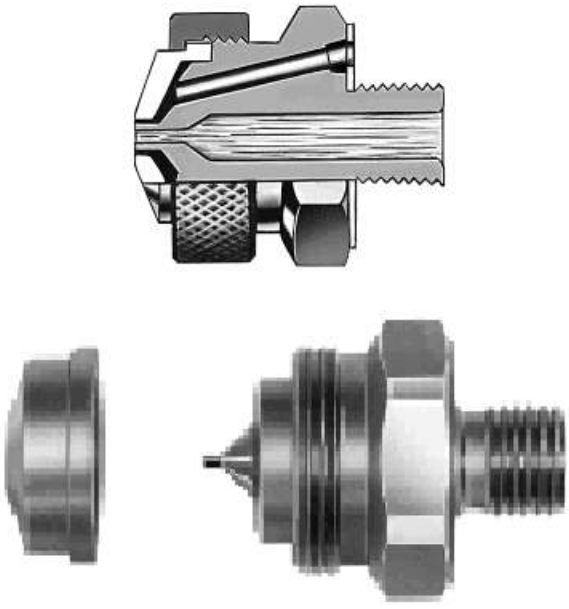

Figure B-2. SprayCo® nozzle.

The SprayCo® nozzles tested were:

- A standard SprayCo® nozzle with a 0.100 inch ID and 0.150 inch OD liquid tube, and a 0.180 inch ID air cap. The 0.100 nozzle is not available in the antibearding design.

- A SprayCo® nozzle with a 0.060-inch ID liquid tube. This was an antibearding nozzle, i.e., the liquid tube extends from the air cap a few thousandths of an inch.

The UTB nozzle uses the same principle. Liquid/slurry flows within the inner tube, while an atomization gas flows in the concentric gap formed between the ID of the larger outer tube and the OD of the inner tube (the liquid flow tube). The UTB nozzles were fabricated by SAIC according to dimensions supplied by TTT. The following nozzles were tested.

- A smaller UTB nozzle with a 0.125 inch OD liquid tube, and a 0.25 inch OD atomizing gas tube

- A larger UTB nozzle with a 0.1175 inch ID x 0.1875 inch OD liquid tube, and a 0.2145 inch ID x 0.3125 inch OD atomizing gas tube.

Two different-sized modified (Marshall/Eldredge design) spray nozzles were tested. These nozzles incorporated modifications to the standard SprayCo® nozzle to prevent or minimize the formation of deposits on the nozzle surfaces exposed to the fluidized bed.

The larger nozzle's dimensions were 0.100-inch ID and 0.150-inch OD liquid tube and a 0.170-inch ID air tube which yields a 0.010-inch concentric gap for atomizing gas flow and an atomizing gas cross sectional area of 0.0050 in^2, consistent with the original SprayCo® nozzle dimensions. The smaller nozzle used smaller diameter concentric tubes with liquid tube dimensions of 0.071-inch ID and 0.120-inch OD and a 0.141-inch ID air tube; which yields a 0.011-inch concentric gap for atomizing gas flow and atomizing gas cross sectional area of 0.0043 in^2. The smaller nozzle dimensions were designed to accommodate a range of anticipated lower SBW slurry flow rates while providing for similar or higher atomization gas flow rates and relatively higher gas velocities. A higher gas velocity provides increased atomization energy for a given gas flow rate.

These nozzles were designed with smaller atomizing gas cross-section areas than were used in the August 2004 Hanford LAW test, in order to increase the velocity of the atomizing gas as it exited the nozzle. This was done based on the premise that, for the same atomizing gas flow rate, better atomization could be accomplished if the atomizing gas could be accelerated to sonic velocity, enabling a higher gas momentum that would more efficiently shear the atomized liquid into smaller droplets. The gas would reach sonic velocity when the nozzle backpressure reached at least twice the downstream pressure of about 12.5 psia.

Test Solutions

Troy clay – water slurry solution was used for the May 6 tests. Concentrations were 40 wt% clay-water and 33.3 wt% clay water.

The June 7 tests were performed with Troy clay mixed in SBW "lite" simulant, at a concentration of 323 g Troy clay per liter of the lite simulant. The lite simulants were prepared using the exact proportions of the major chemical constituents, leaving out minor (especially hazardous) constituents such as lead, nickel, mercury, and cesium. These minor constituents were not expected to contribute significantly to the slurry rheology or atomization characteristics. Slurry viscosity tests showed that viscosities of the SBW lite simulant, with and without clay, were similar to the viscosities of the actual

SBW simulant with and without clay.

The June 22 atomization tests were performed with SBW lite simulant mixed with Troy clay and Hanford LAW lite simulant mixed with OptiKast clay. The OptiKast clay had a smaller average particle size (about 4 μm mass mean particle diameter [MMPD]) in comparison to the Troy clay (about 15 μm MMPD). Representative amounts of clay were used. The SBW simulant was blended with 291 g Troy clay (as received) per liter of SBW simulant. The Hanford LAW simulant was blended with 784 g OptiKast (as received) per liter of Hanford LAW simulant.

The July 30 tests were performed with 635 g OptiKast clay mixed with 1 liter of Hanford LAW lite simulant.

The September 13 tests were performed with two different slurry mixtures 217 and 250 g Sagger clay (as received) per liter of SBW Lite.

Test Results

May 6, 2004 Tests

The 40 wt% clay-water slurry rapidly (within 1 minute of operation) plugged the SprayCo® nozzle with a 0.060 inch ID liquid tube. The restrictions could not be removed and prevented by normal nozzle cleaning activities such as rodding out the feed tube. This size nozzle was used in the Phase 2 THOR mineralizing test, when the feed was slurried with SnoBrite clay that had a smaller particle size (about 5 um mass mean diameter). Apparently, the larger particle size of the Troy clay affected the nozzle performance. Nozzles with 0.060 ID liquid tubes were considered too small for feeding simulant slurries in the forthcoming FBSR tests based on this result.

The 0.060-inch nozzle was replaced with a 0.100-in ID SprayCo® nozzle. The 40 wt% slurry also plugged the 0.100 nozzle, so the 40 wt% slurry was modified with added water to lower the concentration to 33.3 wt%. This slurry atomized without plugging with the 0.100 nozzle and an average NAR of at least 1,000. Pulsing of the peristaltic pump caused the liquid flow to oscillate, which caused the NAR to oscillate as the atomizing gas flow was controlled at a constant flow rate. The actual instantaneous NAR varied above and below 1,000 with the liquid oscillation. This may have caused the NAR to be higher than necessary, to ensure that atomization was maintained as the liquid flow rate pulsed to a higher than average flow rate.

The nozzle was switched back to the 0.060-inch nozzle at the end of this test to determine if the 33.3 wt% slurry could be fed through this nozzle. The 0.060-inch ID nozzle rapidly and repeatedly restricted again, so the SprayCo® nozzle with a 0.100 inch ID liquid tube was selected for feeding the clay-water slurry in the May functional equipment test.

The atomizing gas backpressure, used to indicate when the atomizing gas velocity at the nozzle discharge reaches sonic velocity, was not measured during these tests.

June 7, 2004 Tests

Additional, qualitative nozzle atomization tests were performed on June 7. A pulse dampener installed after the May functional equipment test significantly reduced pulsing caused by the peristaltic pump, potentially improving feed atomization at lower NARs.

The degree of atomization and atomization pattern was observed subjectively at different slurry and

atomizing gas flow rates. Atomization tests were performed with slurry rates at 3.5 and 7 kg/hr, with atomizing air rates between 1.4 and 3.6 kg/hr, and NAR between 200-800. Regardless of nozzle size or type, the slurry was not fully atomized, without visible "spitting" and non-uniform spray patterns, until the NAR was at least 450 NAR and the atomizing gas rate was at least 1.8 kg/hr. Lower NARs and atomizing gas flow rates could subject the bed to larger droplets that over-wet bed particles.

The air gap of the UTB nozzle gradually became occluded, probably because of a small amount of droplet recirculation that attached to the tips of liquid and atomizing gas tubes. This finding indicated that the UTB, if used, should be beveled to sharpen the edges of the nozzle tubes to reduce the surface area to which feed slurry droplets could adhere. After this nozzle atomization test, the UTB design was modified to bevel the tube tips. The liquid tube was beveled on the inside, and the air tube was beveled on the outside. These sharp edges were postulated to minimize the amount of surface on which liquid could attach, while maintaining the velocity and momentum of the atomizing gas at the nozzle discharge.

The atomizing gas backpressure, used to indicate when the atomizing gas velocity at the nozzle discharge reaches sonic velocity, was not measured during these tests.

June 22, 2004 Tests

The nozzle sizes were determined based on spray tests that were done in May. During those tests, nozzle sizes that were too small rapidly plugged with slurry. The minimum nozzle sizes were determined from these tests.

The SprayCo® nozzle had a 0.100 inch diameter liquid nozzle, a 0.150 outer dimension, and a 0.180 inch air cap, the same dimensions as the SprayCo® nozzle used in prior tests. The SBW atomization test results are shown in Table B-2. The UTB nozzle was tested at two different flow rates at NARs ranging from 50 to 750. The SprayCo® nozzle was tested at two different flow rates at NARs ranging from 100 to 750.

Atomization Patterns

High speed photos showing atomization by the SprayCo® nozzle are shown in Figures B-3 through B-5. At lower NARs and atomizing gas flow rates, the liquid was not atomized, but merely flowed out of the nozzle. At higher NARs, the liquid was atomized. At the highest NARs tested, the liquid was atomized with the highest energy.

The degree of atomization was high for the SprayCo® nozzle with an atomizing air flow rate of 3.6 kg/hr and a NAR at 750 as shown in Figure B-3 for a slurry feed rate of 7 kg/hr. As the NAR decreased, the energy of atomization decreased. At a NAR of 300 (1.8 kg/hr atomizing air flow rate), the SBW slurry was less atomized than at higher NARs. The spray was clearly less atomized at 150 NAR (0.9 kg/hr atomizing air flow rate), affected by gravity, and was considered to be unsatisfactory for FBSR operation.

The slurry was well atomized at high NARs (450-750, 1.4-2.3 kg/hr atomizing air) as shown in Figures B-4 and B-5 for a slurry feed rate of 3.5 kg/hr, but starting with a 300 NAR (0.9 kg/hr atomizing air), the effect of gravity on the atomized spray was apparent. At a 150 NAR (0.45 kg/hr atomizing air), droplets were clearly not well atomized. At a 100 NAR (0.3 kg/hr atomizing air) no atomization was accomplished. Based on this visual analysis, the lowest reasonable NAR for a slurry feed rate of 3.5 kg/hr was 450, and the lowest reasonable atomizing gas flow rate was about 1.4 kg/hr.

The atomized spray for the UTB and SprayCo® nozzles was similar, except that (a) the SprayCo®

nozzle produced a slightly narrower total spray cone pattern of around 30 °, and (b) a slight asymmetry in the spray pattern from the UTB was not apparent in the SprayCo® spray pattern. The SprayCo® and UTB nozzles produced similar atomization at similar slurry and atomizing gas flow rates except for those differences.

Based on these observations, and without supporting particle size data that was not yet available at the time of the June functional equipment test, the June functional equipment test was operated with a minimum NAR of 300 and a minimum atomizing gas flow rate of 1.8 kg/hr.

Table B-1. June 22 nozzle atomization test results.

291 g Troy clay per L SBW simulant								
Nozzle	Simulant slurry rate, kg/hr	Atomizing air rate, kg/hr	NAR	Photo film roll	Photo frame number	Slide number	Droplet MMPD from slides, mm	Observations
UTB	7	3.64	600	3	16	16,17,18	---	
UTB	7	2.72	450	3	20	19	---	
UTB	7	1.82	300	3	21	20	0.569	
UTB	7	0.91	150	3	22	21	0.892	coarse
UTB	7	0.61	100	3	25	25	2.803	very coarse
UTB	7	0.31	50	3	---	---	---	Slurry dribble from tip
UTB	3.5	2.27	750	3	31	22	0.285	
UTB	3.5	1.82	600	3	34	23	0.268	
UTB	3.5	1.36	450	3 and 4	36, 1	24	0.631	
UTB	3.5	0.91	300	4	2	26	1.727	very coarse
UTB	3.5	0.45	150	4	4	---	---	Slurry dribble from tip
Sprayco	7	3.63	600	5	4	35	0.218	
Sprayco	7	2.72	450	5	1	34	0.268	
Sprayco	7	1.82	300	4	22	33	0.242	Looks good
Sprayco	7	0.91	150	4	20	32	1.616	
Sprayco	3.5	2.27	750	4	7	27	0.319	
Sprayco	3.5	1.82	600	4	9	28	0.201	
Sprayco	3.5	1.36	450	4	11	29	0.308	
Sprayco	3.5	0.91	300	4	14	30	0.954	
Sprayco	3.5	0.45	150	4	16	31	2.090	very coarse
Sprayco	3.5	0.31	100	4	18	---	---	Slurry dribble from tip

[Slurry spray particle Sizes 02.xls]SBW slurry spray test summary

Figure B-3. NAR decreasing from 600 to 150 for the SprayCo® nozzle at an SBW slurry feed rate of 7 kg/hr.

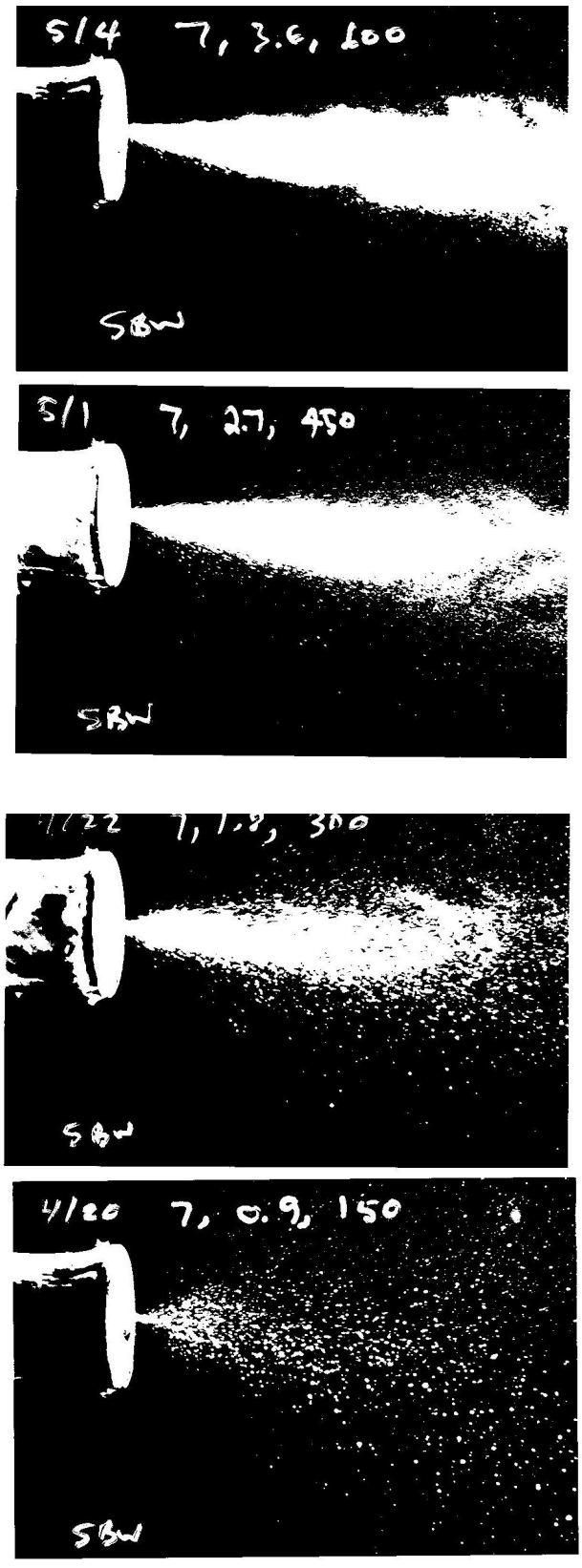
5/4 7, 3.6, 600
SBW
5/1 7, 2.7, 450
SBW
SBW
4/20 7, 0.9, 150
SBW

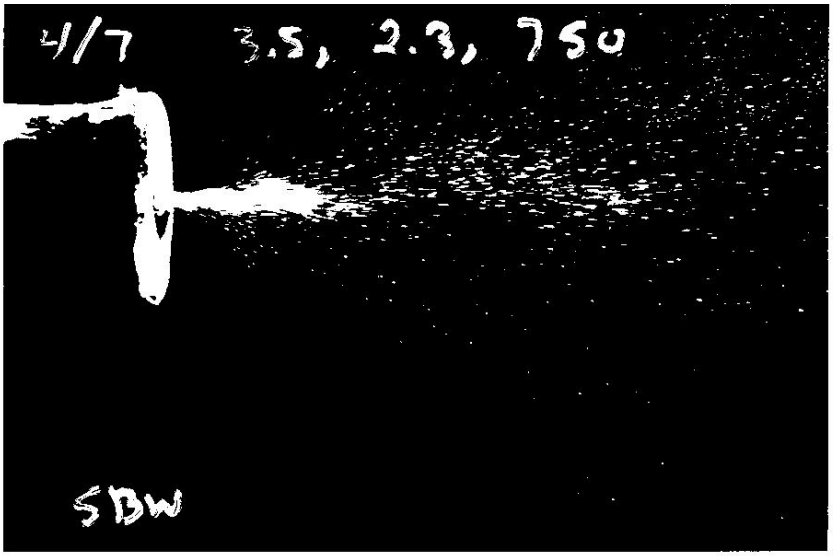
4/7 3.5, 2.3, 750
SBW

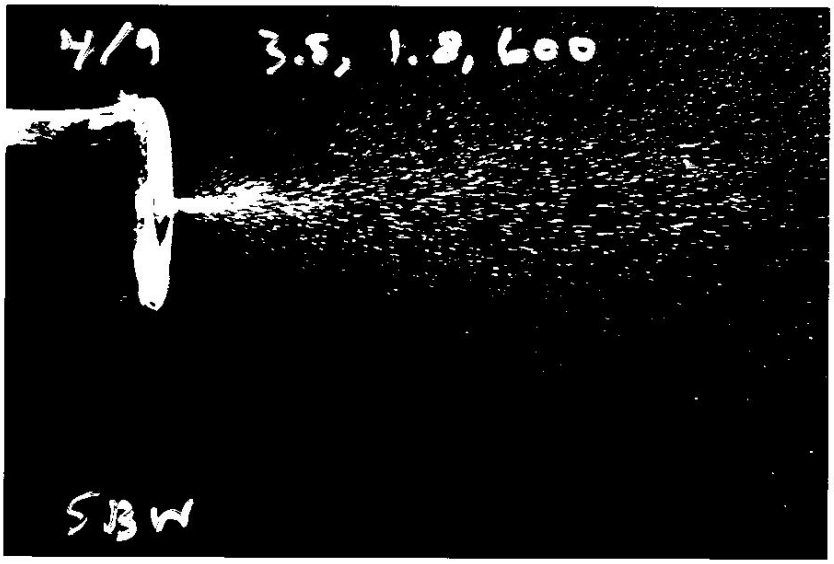
4/9 3.5, 1.8, 600
SBW


4/11 3.5, 1.4, 450

Figure B-4. NAR decreasing from 750 to 450 for the SprayCo® nozzle at an SBW feed rate of 3.5 kg/hr.

Figure B-5. NAR decreasing from 300 to 100, SprayCo® nozzle at an SBW slurry feed rate of 3.5 kg/hr.

Droplet Particle Size Distribution Measurements

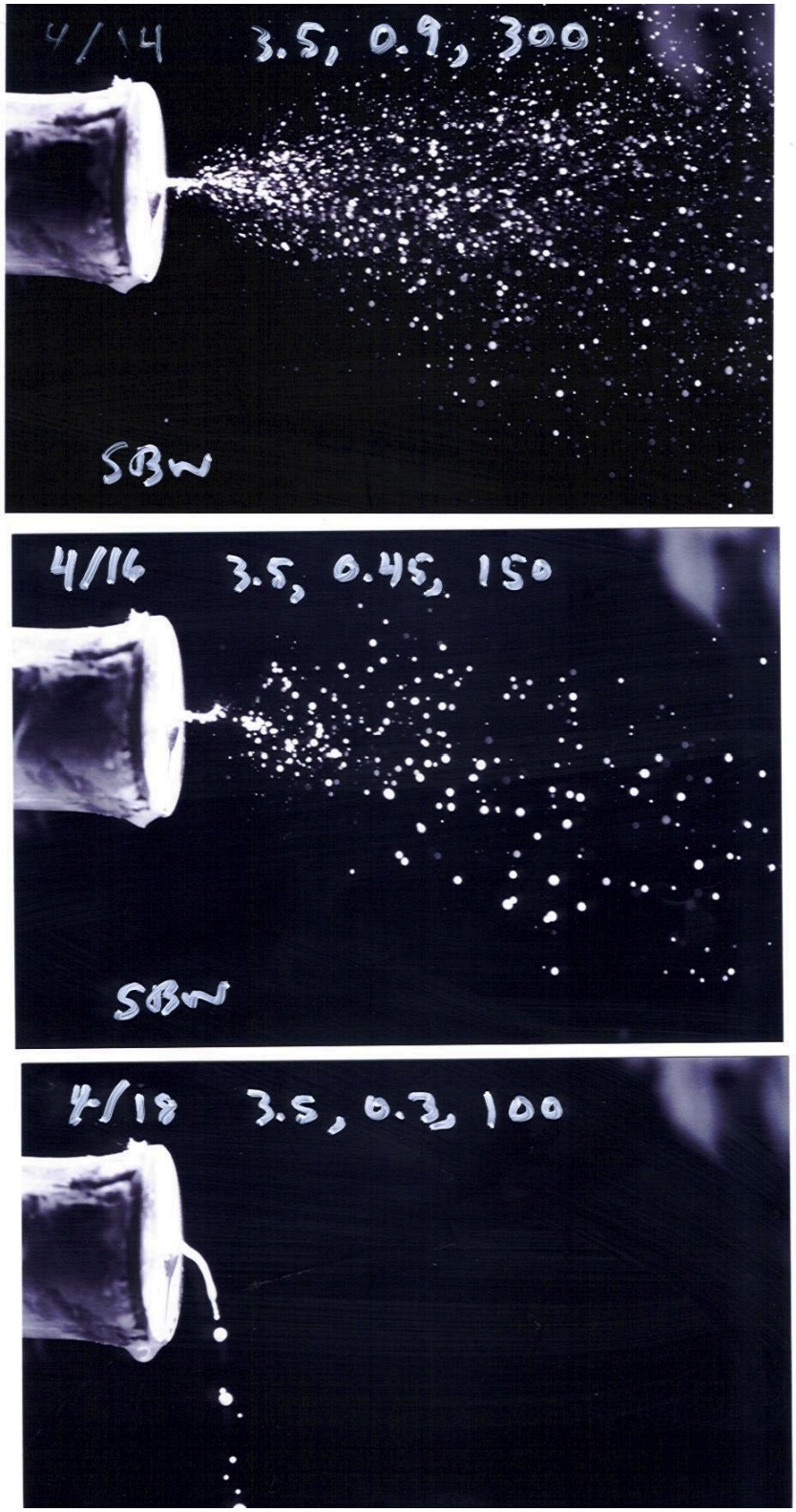

Figures B-6 and B-7 show example photographs of droplets collected on microscope slides. An oil

coating on the slides caused the droplets collected on the slides to bead up rather than run together. However, after sample collection, the larger droplets tended to flatten onto the glass, making a disc on the glass that was larger than the original spherical droplet. This tendency was more visible with the larger droplets. If the smaller droplets had the same tendency, it was not noticeable to the naked eye during sample collection. The droplet size measurements for at least the larger droplets (and maybe the smaller droplets too) were larger than the actual spherical droplets because of this tendency. The droplet size measurements may be up to 10-50% larger than the true droplet sizes. The measured sizes are not adjusted for this observed bias.

Table B-1 summarizes the average droplet particle sizes for the SprayCo® nozzle. While NAR has been used as a feed nozzle operating parameter, the comparison of the measured MMPDs show that, at NARs below about 600, the MMPDs are significantly affected not only by the NAR but also by the slurry feed rate and the atomizing gas flow rate, which, at constant NAR, varies with the slurry feed rate. At a NAR of 300, the average droplet size for the SprayCo® nozzle was about 0.242 mm, slightly larger than the average bed particle size for the June FBSR functional equipment test. The droplet size quadrupled to about 0.954 mm for the same nozzle at 300 NAR and 3.5 kg/hr slurry feed rate, because although less slurry was being fed, the atomizing gas flow rate was also lower. The same trend occurred for the UTB nozzle.

The UTB nozzle was used during the June FBSR functional equipment test. The slurry feed rate was ramped up to 7 kg/hr with a NAR of 300 over a period of about 25 minutes. Even at lower simulant feed rates during initial startup, the minimum atomizing gas flow rate was set at 1.8 kg/hr because these atomization tests indicated that lower atomizing gas flow rates might not adequately atomize the feed slurry. At the nominal operating conditions, an average droplet size of 0.569 mm was about 2.6 times higher than the average bed particle size. Such large droplet sizes might have contributed to the defluidizing agglomeration that occurred during the approximately 4.5 hour operating time of the FBSR test. The agglomeration was located just above the UTB nozzle, where the feed droplets would have impacted bed media, and nearly blocked the entire cross-section of the FBSR.

Figure B-8 shows a correlation of droplet size compared to NAR. This correlation suggests that the atomizing gas flow rate affects the droplet size as much or more than the NAR. Both Figures B-8 and B-9 show that, at a NAR above 600 and an atomizing gas flow rate above 2.5 kg/hr, the maximum feed slurry atomization is achieved, at an average droplet size of about 0.250 mm. Smaller droplet sizes were not achieved over the ranges of NAR (up to 750) and atomizing gas flow rate (up to 3.6 kg/hr) that were tested.

These data suggest that the best nozzle operating conditions for achieving the smallest average particle size are a NAR of at least 500 and an atomizing gas flow rate of at least 2 kg/hr, regardless of SBW slurry feed rate.

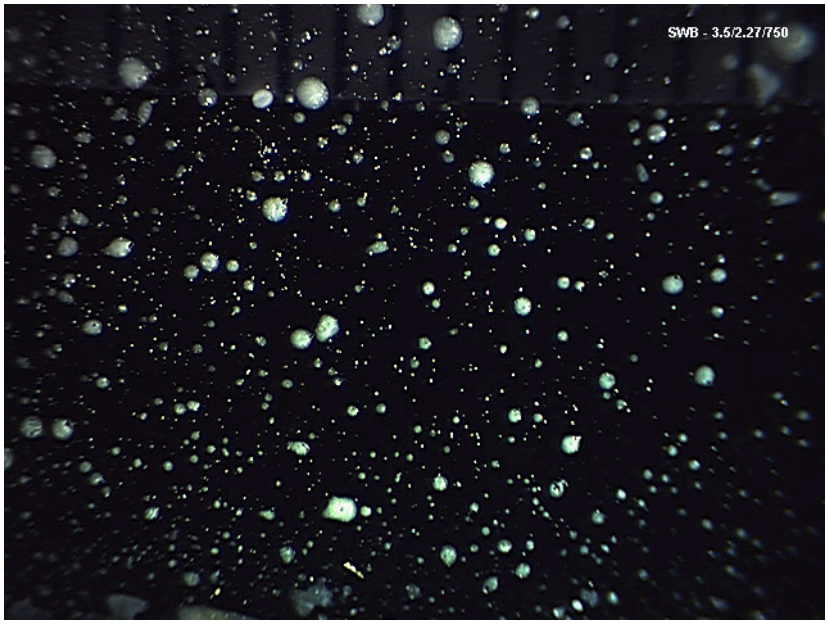

Figure B-6. Atomized droplets collected on an oil-coated slide for the UTB nozzle operated at a SBW slurry feed rate of 3.5 kg/hr, an atomizing gas flow rate of 2.27 kg/hr, and a NAR of 750. At the top of the photo is a faint millimeter scale. The larger droplets are about 0.5 mm in size.

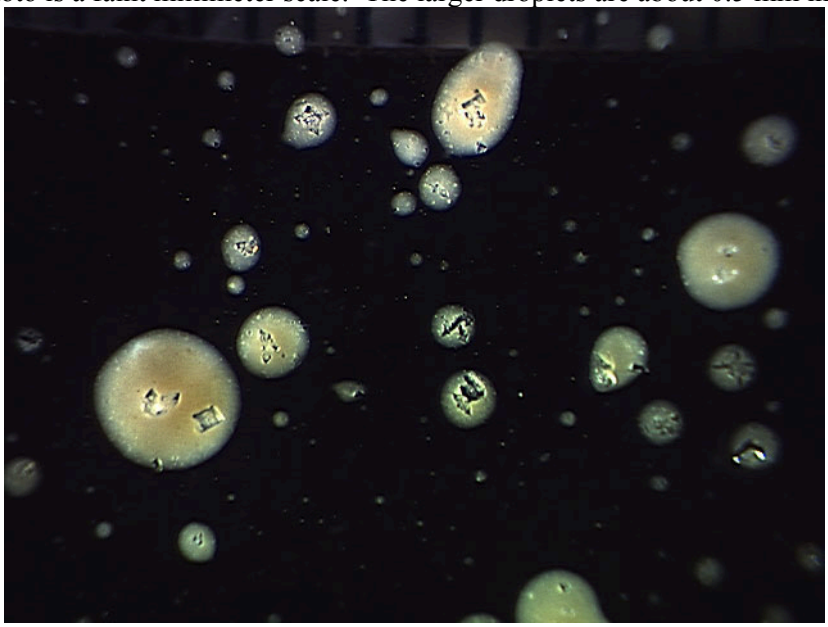

Figure B-7. The droplet pattern collected on an oil-coated slide for the UTB nozzle operated at a SBW slurry feed rate of 3.5 kg/hr, an atomizing gas flow rate of 0.91 kg/hr, and a NAR of 300. At the top of the photo is a faint millimeter scale. This figure has the same magnification as Figure B-6. The largest droplet range exceeded 2.6 mm in size. The discoloration inside the larger droplets is due to water drying during the few hours after the slide was collected and when the microscope photo was taken.

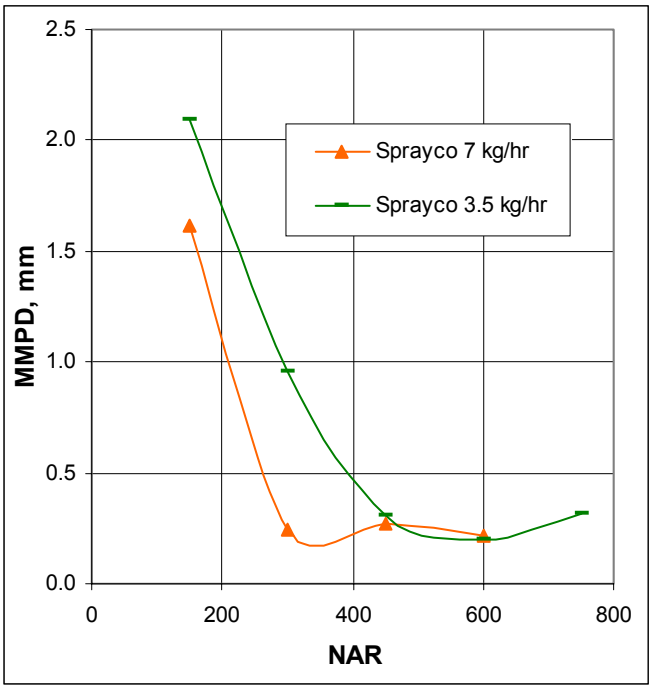

Figure B-8. Average atomized droplet size compared to NAR for the SBW slurry.

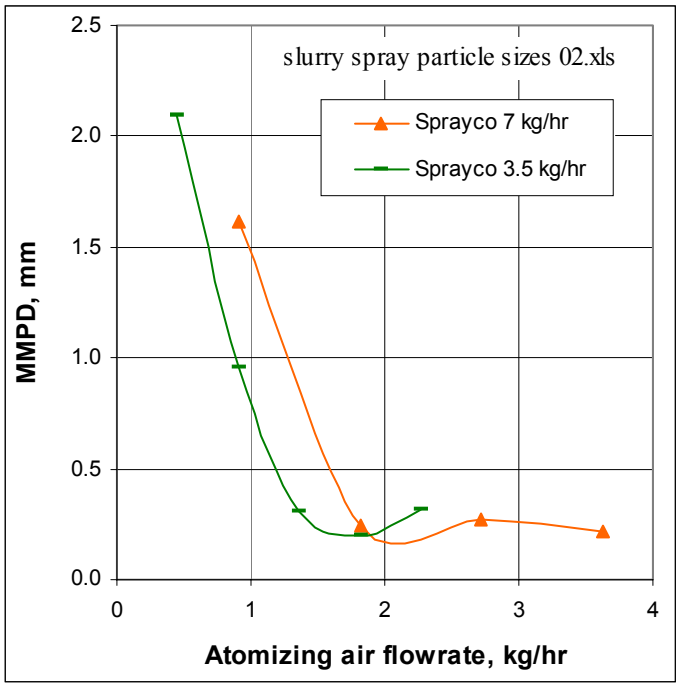

Figure B-9. Average atomized droplet size compared to atomizing gas flow rate for the SBW slurry.

The SprayCo® droplet particle size distribution measurements are shown in Figure B-10. The very best atomization (providing the smallest droplets) occurred for both 3.5 and 7 kg/hr slurry feed rates when the NAR was at least 600 and the atomizing gas flow rate was at least 1.8 kg/hr. Even under these conditions, the largest droplets collected on the slides were about 0.3 mm, larger than the starting bed media for the past several FBSR tests.

Another grouping of particle size distributions resulted from several atomization tests when the NAR was at least 300, and the atomizing air flow rate was at least 1.4 kg/hr. The largest collected droplets from these conditions exceeded 0.6 mm.

When the NAR was less than 300, or when the atomizing gas flow rate was less than 1.4 kg/hr, then the sizes of atomized droplets increased considerably, ranging up to over 2.6 mm for the largest collected droplets produced when the slurry feed rate was 3.5 kg/hr, the atomizing gas flow rate was 0.45 kg/hr, and the NAR was 150.

Figure B-10. Measured cumulative particle size distributions for the ranges of nozzle operating conditions of the SBW slurry spray tests.

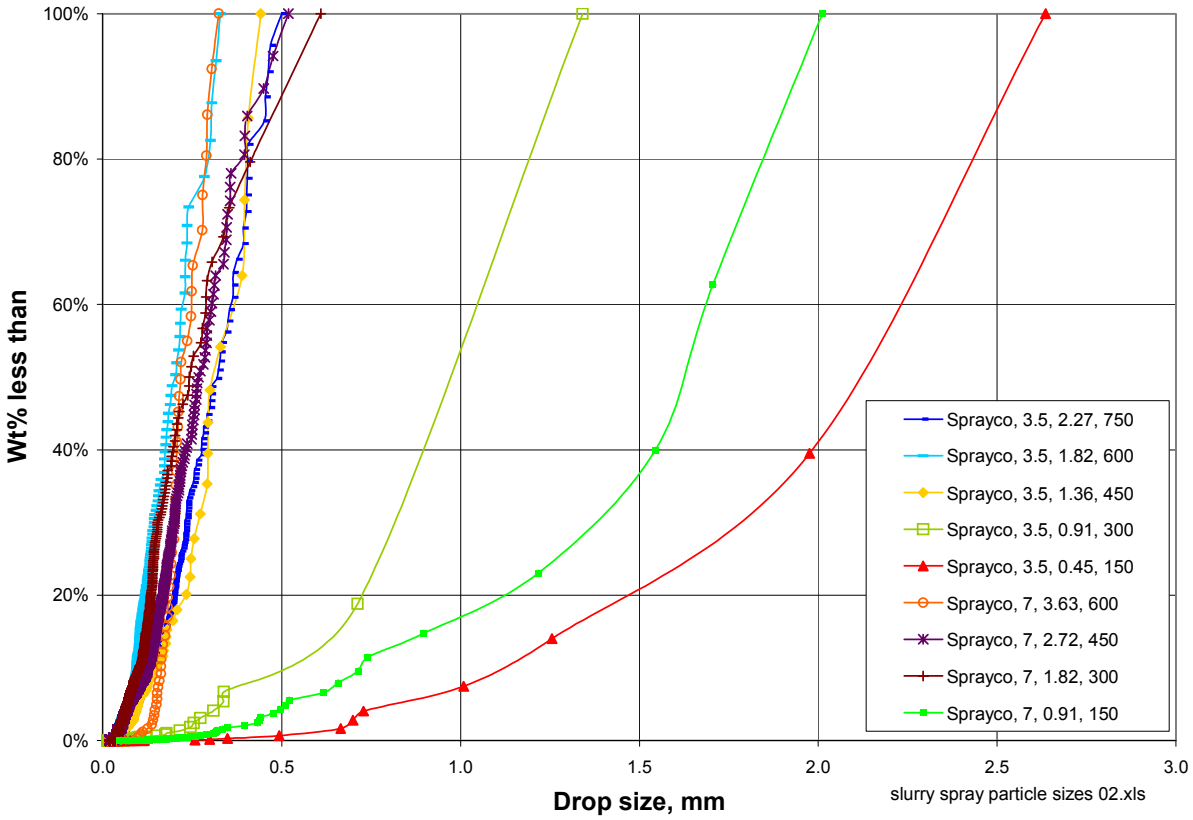

July 30, 2004 Nozzle Atomization Tests

Following the May and June slurry atomization tests, the May and June functional equipment tests, and the July SBW FBSR test, the modified the Marshall/Eldredge nozzle with the 0.100 inch ID liquid tube was selected for the Hanford LAW FBSR test. The atomization performance of this newly modified nozzle was tested on July 30, prior to the Hanford LAW FBSR test, to verify if the atomization performance was still comparable to the standard, same-sized SprayCo® nozzle. Qualitative, real time visual observations were made, which indicated that the atomized spray patterns and behavior of the new nozzle effectively matched those observed for the SprayCo® nozzle. No aberrant behavior was noted. No attempt was made to obtain quantitative spray droplet size data, as had been done in the earlier SprayCo® test, and project schedule and cost constraints did not allow for further work in this area. A limited qualitative photographic record of the tests was made.

September 13 Tests

Slurry atomization tests were performed on September 13, 2004 preparatory to the planned September SBW FBSR test. Two different-sized Marshall-Eldredge spray nozzles were tested.

Digital photographs were taken to document each test condition. Spray droplets were also collected on microscope slides, photographed, an analyzed digitally to determine droplet particle size distributions. As expected, better atomization (smaller atomized droplets) was achieved at higher NARs and higher atomizing gas flow rates. The nozzle with the smaller atomizing gas cross section area (providing a higher atomizing gas velocity) achieved better atomization (smaller droplets) without restricting than did the larger nozzle. Both nozzles achieved better atomization than did nozzles used in prior FBSR tests with higher concentrations of clay in either SBW or Hanford LAW simulants.

The slurries were fully atomized, with no roping, liquid buildup on the nozzle, or dripping, for all test conditions. At lower atomizing gas flow rates, a bimodal spray pattern was produced. A central spray pattern that contained almost all of the slurry droplets had a total spray angle of about 20 ^{o} (at low atomizing gas rates) that increased as the atomizing gas rate increased. A second, fainter, spray pattern

that contained few droplets, had a total spray angle of about 80 ^{o}, increasing to 110-120^{o} and almost disappearing at the higher atomizing gas rates.

The atomizing air induced sufficient suction on the liquid stream that the tubing downstream of the slurry feed pump was under negative pressure. This negative pressure encouraged some gas bubbles to form, which were separated in the gas vent tube.

The test results are summarized in Tables B-2 and B-3. Both nozzles atomized the 217 g/L slurry to 0.1 – 0.2 mm MMPD. The small nozzle produced smaller slurry droplets than did the larger nozzle at lower atomizing gas flow rates. The droplet size increased rapidly for the larger nozzle at atomizing gas rates below 3 kg/hr. The droplet size increased rapidly for the smaller nozzle at atomizing gas rates below 2 kg/hr.

The large nozzle was not tested with the 250 g/L slurry. The few test conditions with the 250 g/L slurry showed that atomization for this higher slurry concentration is nearly identical to that the 217 g/L slurry. The smaller nozzle atomized the 250 g/L slurry to 0.1 – 0.2 mm MMPD when the slurry flow rate was 4 kg/hr, the atomizing gas ranged from 2 – 3 kg/hr, and the NAR was 700 – 1,000. The 250 g/L slurry at 4 kg/hr was atomized using the smaller nozzle almost as well as the 217 g/L slurry at the same flow rate.

The atomized droplet MMPDs are very similar for both nozzles at similar NARs as shown in Figures B-11 and B-12. These figures show that, at the same NAR, the droplet MMPDs are smaller for higher slurry flow rates. This occurs because, for the same NAR, the higher slurry flow rates have higher atomizing gas flow rates. While the higher slurry flow rate is more difficult to atomize, the higher atomizing gas flow rate improves the atomization effectiveness.

Table B-2. September 13 SBW atomization test results for the larger nozzle.

217 g Sagger per L SBW simulant, 1.35 gm/mL slurry			Large nozzle: 0.100 x 0.150 liquid, 0.170 air cap				0.00502 sq. in. gas orifice area		
Nozzle	Simulant slurry rate, kg/hr	Atomizing air rate, kg/hr	Atomizing air rate, scfm	Nozzle back-pressure, psig	Atomizing gas velocity, f/s	NAR	Slide number	Measured droplet MMPD from slides, mm	Observations
Large	2	1.67	0.82	4.8	459	960	1	0.183	Bimodal spray pattern
Large	2	2.33	1.14	8.3	641	1,340	2	0.110	
Large	2	3.00	1.47	12.5	825	1,725	3	0.039	Outer cone fading
Large	2	3.33	1.63	14.4	916	1,915	4	0.045	Almost no drops hitting light
Large	3	2.00	0.98	6.2	550	765	5	0.337	
Large	3	2.67	1.31	9.9	734	1,025	6	0.121	
Large	3	3.33	1.63	14.4	916	1,270	7	0.042	
Large	4	2.68	1.31	9.8	737	768	8	0.182	Very little mist hitting light
Large	4	3.66	1.79	16.0	1006	1,050	9	0.084	
Large	5	3.66	1.79	16.0	1006	840	10	0.120	

[sept 13 large nozzle psds.xls]summary for report

Table B-3. SBW atomization tests using the smaller nozzle.

217 g Sagger per L SBW simulant, 1.35 gm/mL slurry			Small nozzle: 0.079 x 0.120 liquid, 0.141 air cap				0.00430 sq. in. gas orifice area		
Nozzle	Simulant slurry rate, kg/hr	Atomizing air rate, kg/hr	Atomizing air rate, scfm	Nozzle back-pressure, psig	Atomizing gas velocity, f/s	NAR	Slide number	Measured droplet MMPD from slides, mm	Observations
Small	2	1.67	0.82	4.8	536	960	11	0.178	No bimodal spray pattern
Small	2	2.00	0.98	6.8	642	1,160	12	0.099	
Small	2	3.33	1.63	13.2	1069	1,925	14	0.024	
Small	3	1.67	0.82	4.8	536	640	20	0.237	Visibly coarser spray
Small	3	2.00	0.98	6.2	642	765	15	0.160	
Small	3	3.33	1.63	14.1	1069	1,270	19	0.082	
Small	4	1.00	0.49	4.4	321	288	26	0.300	
Small	4	1.67	0.82	6.4	536	480	25	0.249	
Small	4	3.00	1.47	13.8	963	865	23	0.107	Bimodal spray visible with coarser drops
Small	4	3.66	1.79	16.0	1175	1,050	24	0.106	Feed pulses less severe at higher NARs
Small	5	1.33	0.65	5.4	427	305	30	0.496	Large bimodal spray
Small	5	2.00	0.98	8.1	642	460	29	0.204	
Small	5	3.66	1.79	15.7	1175	840	27	0.124	
250 g Sagger clay per L SBW simulant									
Small	4	2.00	1.01	8.0	661	575	31	0.196	Visible bimodal spray
Small	4	3.00	1.51	13.4	992	865	32	0.120	Faint bimodal spray
Small	4	3.67	1.85	17.0	1214	1,060	33	0.123	Almost no bimodal spray

[Sept 13 spray tests sheet 2.xls]summary for report

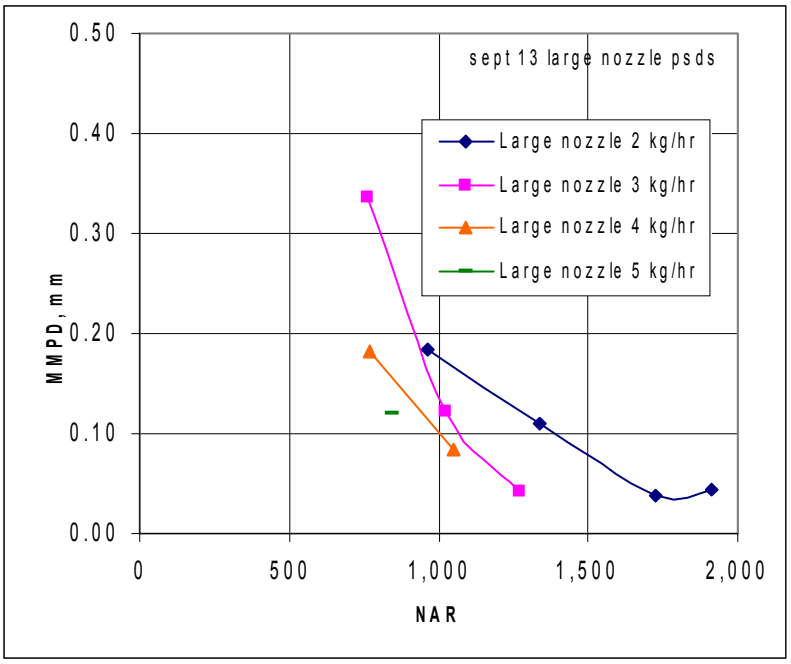

Figure B-11. Atomized slurry mass mean particle diameter compared to NAR for the large nozzle, 2 – 5 kg/hr slurry flow rate.

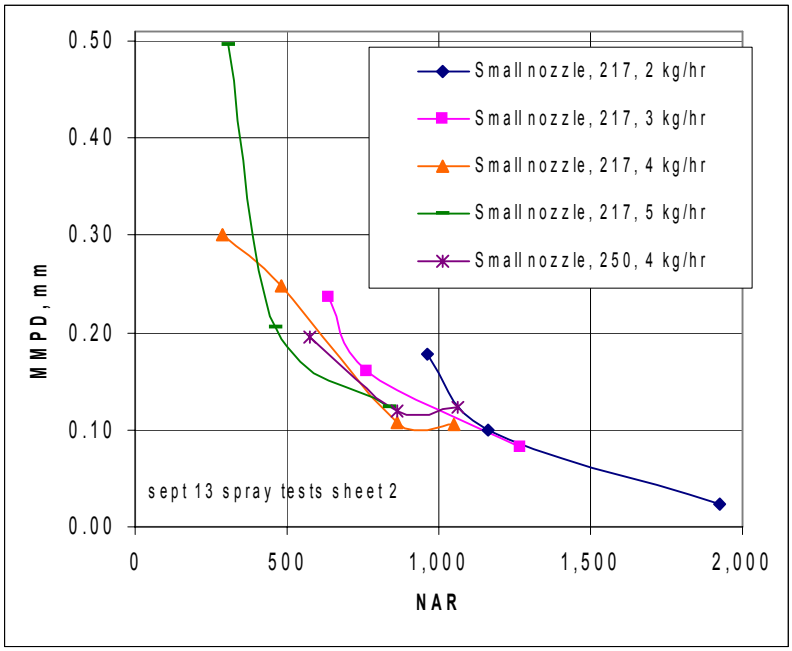

Figure B-12. Atomized slurry mass mean particle diameter compared to NAR for the small nozzle, 2 – 5 kg/hr slurry flow rate.

Figures B-13 and B-14 show that, compared to the atomizing gas flow rate, the droplet MMPD produced by the two nozzles was similar, except at lower atomizing gas flow rates. The small nozzle produced smaller slurry droplets at lower atomizing gas flow rates than the larger nozzle did. This was because the smaller nozzle, with a smaller open cross-section area for the atomizing gas, resulted in a higher atomizing gas velocity at the nozzle tip. The average droplet size increased rapidly at atomizing gas rates below 3 kg/hr for the larger nozzle. The average droplet size increased rapidly at atomizing gas rates below 2 kg/hr for the smaller nozzle.

A minimum NAR of 800 (for the small nozzle) and 1,000 (for the large nozzle), and a minimum atomizing gas rate of 2 kg/hr (for the small nozzle) and 3 kg/hr (for the large nozzle) were recommended operating limits for the September SBW FBSR test in order to best control the atomized spray particle size at average particle sizes near or below the bed particle size. If these operating conditions resulted in excessive fines elutriation to the off-gas filter, or if the bed particle size was not readily controlled, then decreasing the atomizing gas rate and NAR might produce larger droplets and reduced the amount of fines generation. If excessive particle agglomeration occurred, then increasing the NAR and atomizing gas rate might reduce particle agglomeration.

The calculated gas velocity reached about 1,000 – 1,100 f/s when the atomizing backpressure gauge reached about 13-16 psig, approximately the speed of sound in air at 70 ^{o}F [1,128 f/s, De Nevers, Noel, 1977, “Fluid Mechanics,” Addison-Wesley Publishing Company, Reading, Massachusetts, Page 176

263].

The small nozzle was recommended as the first choice nozzle for the September SBW FBSR test, since best atomization performance was provided by the smaller nozzle, without any apparent restrictions during over 1 hour of nozzle operation.

Droplet Particle Size Distributions

The droplet cumulative particle size distributions (PSDs) are shown in Figures B-15 and B-16. The smallest particle sizes were obtained with the highest atomizing gas flow rates and NARs for a given slurry feed rate. The PSDs are consistent with the nozzle operating condition recommendations determined from the MMPD analyses. Whenever the larger nozzle was operated with at least 1,000 NAR and at least 3 kg/hr, 60 wt% or more of the atomized mass was in droplets less than 0.1 mm, and the largest measured droplets were under 0.2 mm. Whenever the larger nozzle was operated with less than 1,000 NAR or less than 3 kg/hr, the mass of droplets less than 0.1 mm ranged between 3 – 40 wt%, and the largest measured droplets exceeded 0.4 mm.

When the smaller nozzle was operated with at least 800 NAR and at least 2 kg/hr, 35 wt% or more of the atomized mass was in droplets less than 0.1 mm, and the largest measured droplets were under 0.2 mm [except for one test condition (3 kg/hr slurry, 2.67 kg/hr atomizing air, and 1,025 NAR), that appears to be an anomalous condition]. Whenever the smaller nozzle was operated with less than 800 NAR or less than 2 kg/hr, the mass of droplets less than 0.1 mm ranged between 2 – 30 wt%, and the largest measured droplets ranged to 0.7 mm.

Example digital photos that were used to determine the particle size distributions and MMPDs are shown in Figures B-17 and B-18. The faint blue marks at the bottom of the photos indicate 1 mm marks. The number of particles per photo varied according to droplet size, slurry flow rate, and sampling variations, but typically ranged between 500 – 1,500.

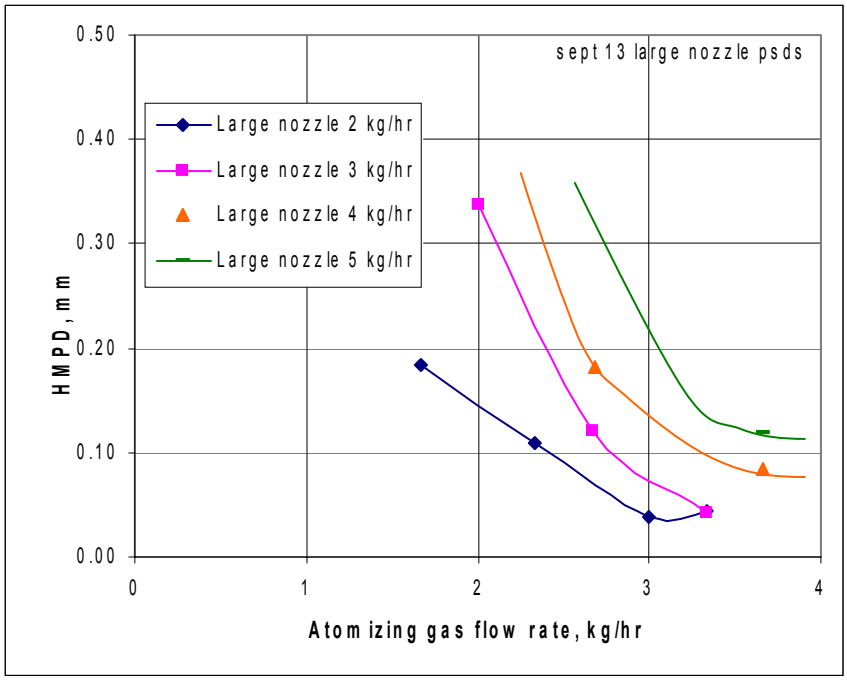

Figure B-13. Atomized slurry mass mean particle diameter compared to atomizing gas flow rate for the large nozzle, 2 – 5 kg/hr slurry flow rate.

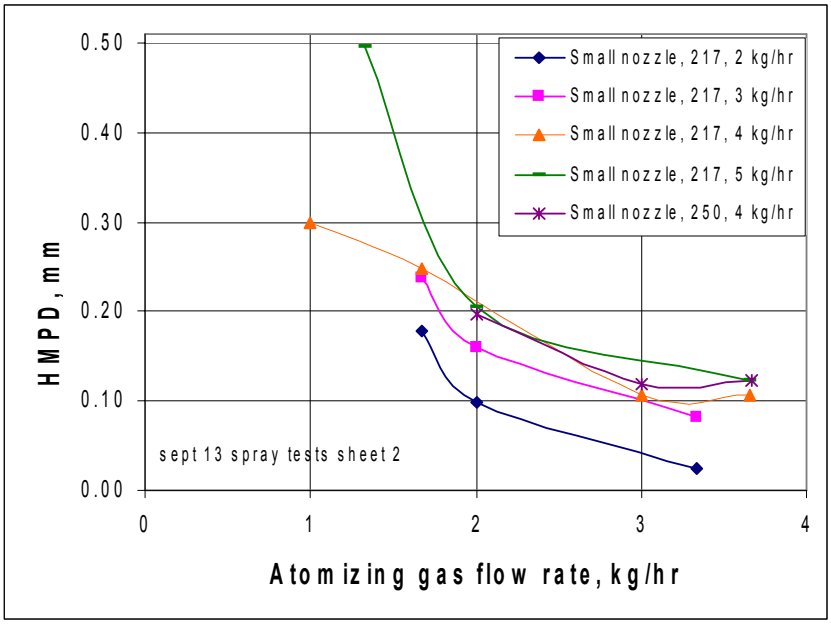

Figure B-14. Atomized slurry mass mean particle diameter compared to atomizing gas flow rate for the small nozzle, 2 – 5 kg/hr slurry flow rate.

Figure B-15. Cumulative particle size distributions for the large nozzle.

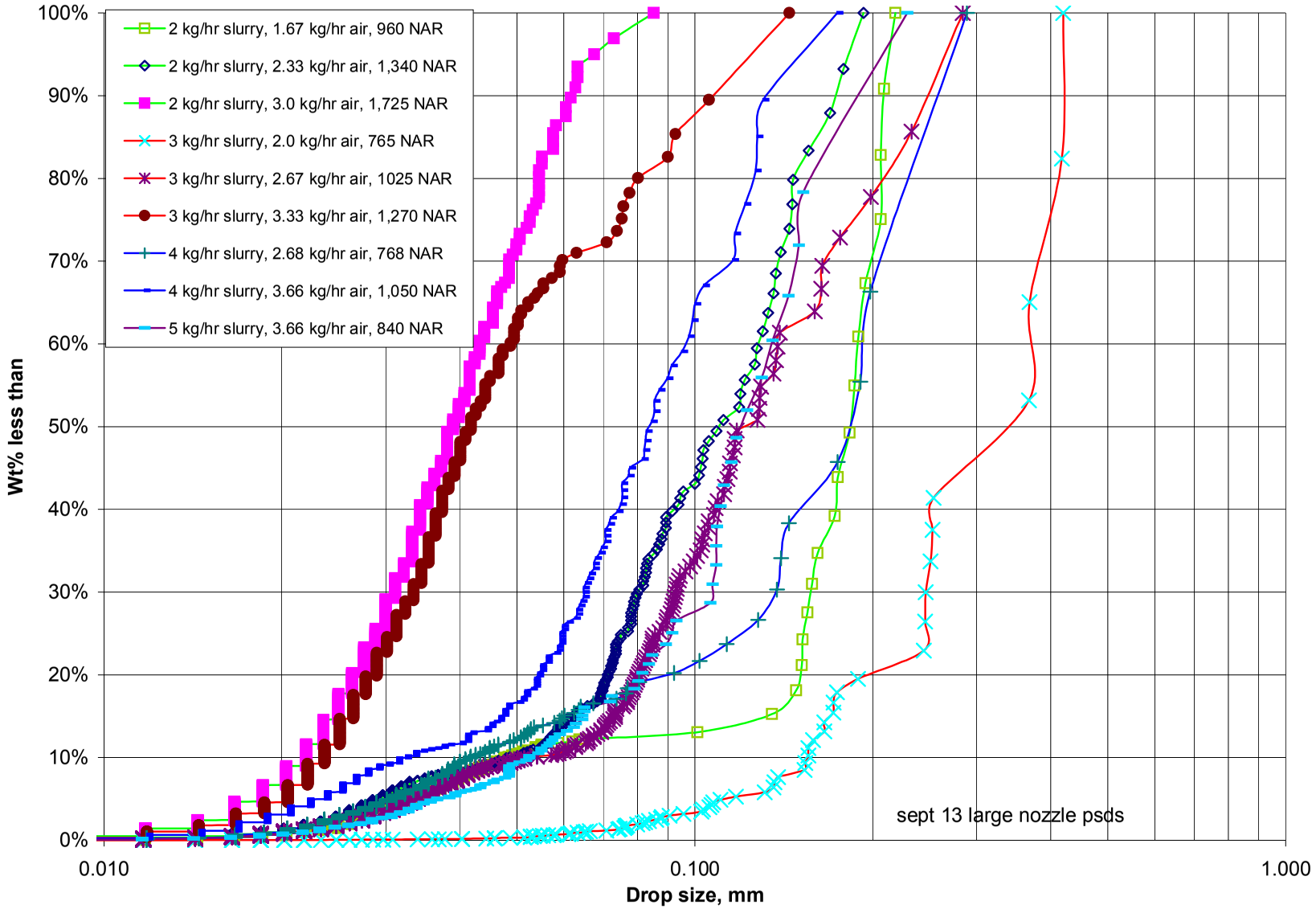

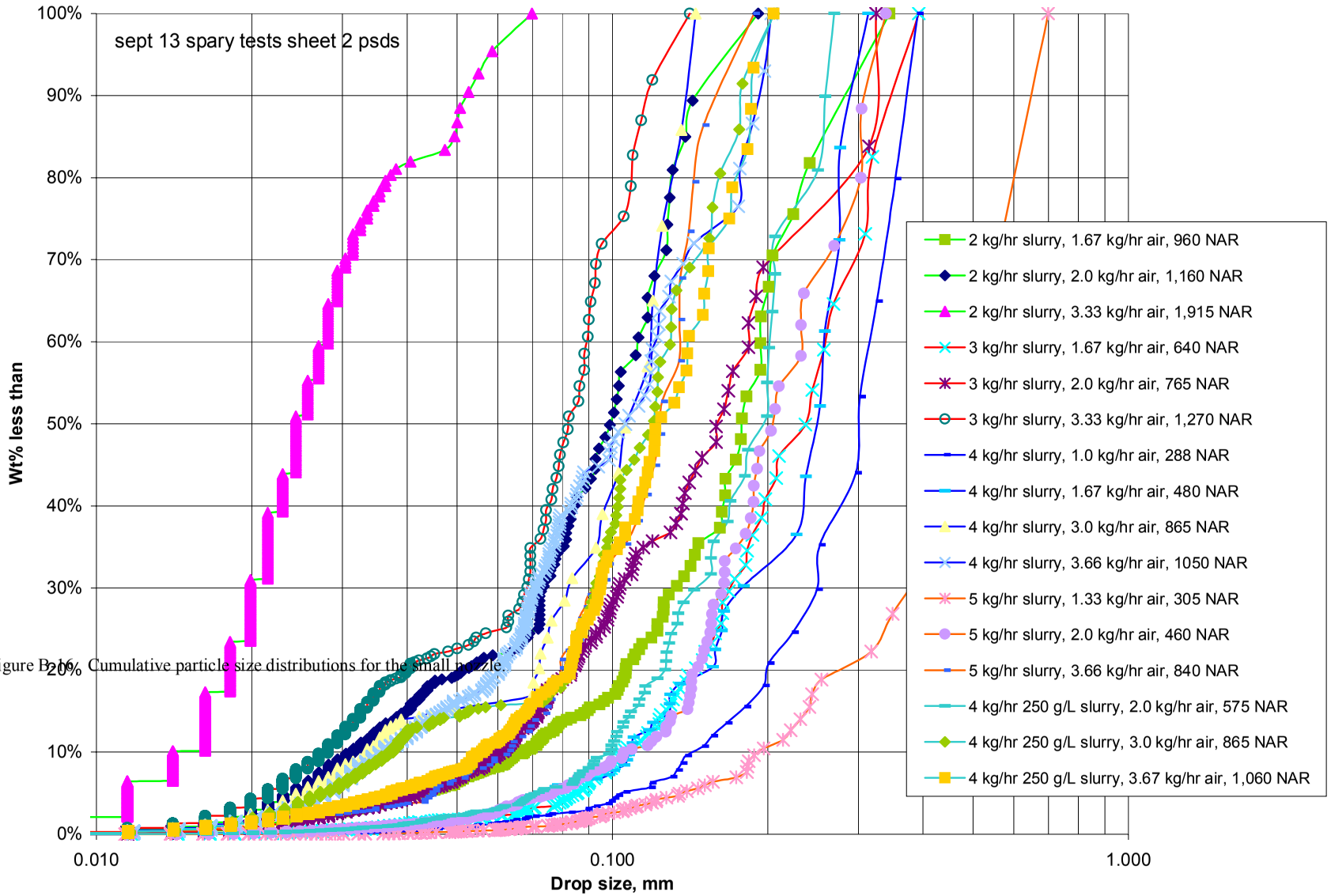

Figure B.16. Cumulative particle size distributions for the small nozzle.

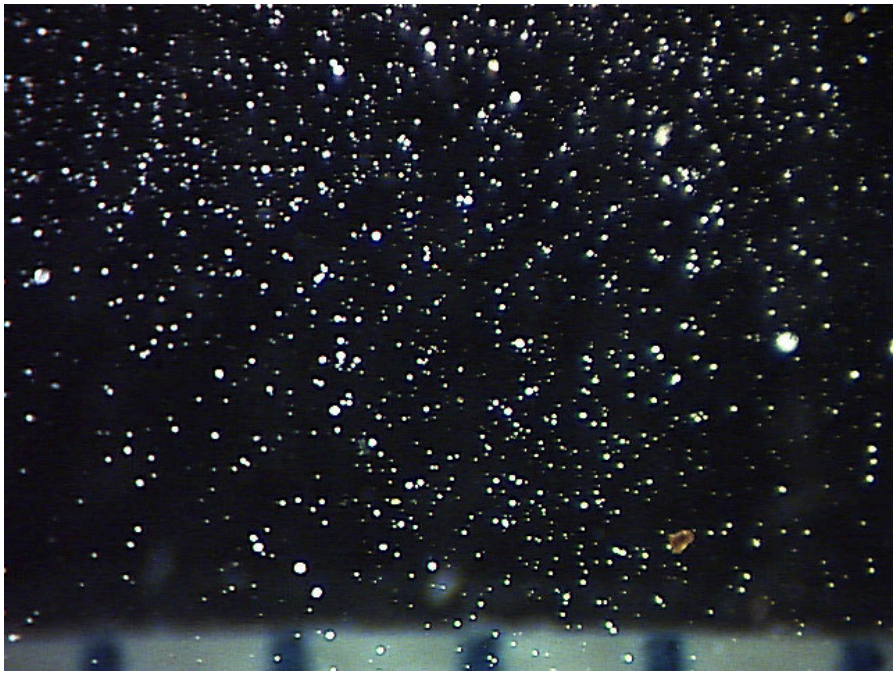

Figure B-17. Large nozzle, test 1f, 2 kg/hr slurry, 3.33 kg/hr atomizing gas, 1,915 NAR.

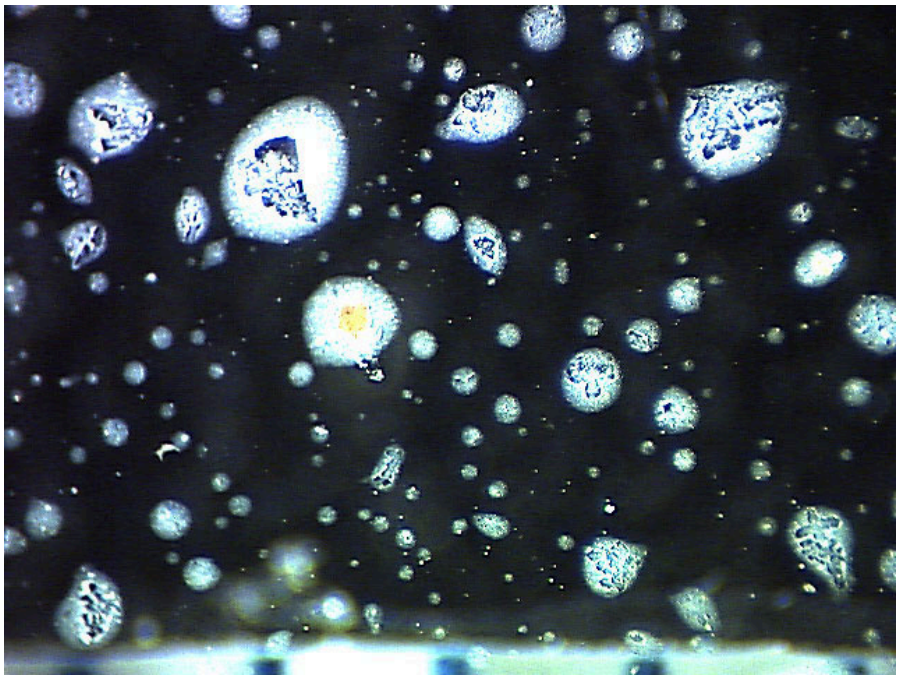

Figure B-18. Small nozzle, test 7g, 5 kg/hr slurry, 1.33 kg/hr atomizing gas, 305 NAR. These droplets are much larger due to the low atomizing gas rate, higher slurry rate, and lower NAR. The mottled appearance of the larger droplets may be from the separation or drying of clay particles.

Nozzle Backpressure Test Results

The atomizing gas backpressure during the August Hanford LAW FBSR test ranged around 6 psig, too low to have caused the atomizing gas to reach sonic velocity during that test. The two new Marshall-Eldredge nozzles, designed for use in the September 2004 SBW FBSR test, were both sized with smaller atomizing orifice total cross sectional areas so that for similar atomizing gas flow rates they would induce higher atomizing gas velocities, even reaching sonic velocities.

The nozzle backpressure was measured during the September 13 nozzle atomization tests at the same slurry and gas flow rates, and for several intermediate gas flow rates. These measurements were made to provide data that was used to verify the values of atomizing gas backpressure, measured using the test apparatus, that resulted in sonic velocity for the atomizing gas. Some baseline nozzle backpressure measurements were also made with atomizing gas flowing through the nozzles, but without any slurry flow. Backpressure measurements were made for three nozzles – the two Marshall-Eldredge nozzles used in the nozzle atomization tests, and also, for reference, the larger nozzle used in the August 2004 Hanford LAW test. Air was used as the atomizing gas. In order to most accurately measure the backpressure over a relatively wide range, two pressure gauges were used; one with a 0-15 psig range and the other with a 0-100 psig range.

The atomizing gas flow rates and backpressure results for the dry (no slurry) backpressure tests are shown in Table B-4. The bolded values indicate the conditions at which sonic gas velocities were reached, because the absolute backpressure is greater than twice the ambient pressure. As observed during the August 2004 Hanford LAW FBSR test, the Marshall-Eldredge nozzle used during that test did not reach sonic flow conditions for atomizing air rates up to 4 kg/hr. The atomizing gas flow rate for that test ranged between 2.6 and 3.5 kg/hr, so the atomizing gas velocity did not reach sonic conditions during that test. The two new nozzles reached sonic flow conditions by about 3.25 kg/hr during the nozzle backpressure test, when the measured backpressure exceeded twice the pressure downstream of the nozzle (assumed to be ambient pressure in this case).

Surprisingly, the smallest of the two new nozzles exhibited backpressures similar to the larger of the new nozzles, even though the smallest nozzle was designed with 14% less atomizing gas cross sectional flow area. The nozzle with the smaller atomizing gas orifice cross sectional area should have caused higher backpressures for the same atomizing gas flow rate. The fact that the measured backpressures for the two nozzles were so similar suggests that either (a) the backpressure measurements had some bias or measurement error for the different nozzles, (b) the actual atomizing gas cross-section area for at least one nozzle was different from the design value, or (c) the pressure drop on the atomizing gas due to the tortuous path of the atomizing gas in the nozzle is significant compared to the pressure drop induced by the design atomizing gas cross section area at the nozzle discharge.

	Nozzle		
	Original (used in the August 2004 Hanford LAW test)	"Large" new nozzle, 35% smaller than the original nozzle	"Small" new nozzle, 45% smaller than the original nozzle
Nozzle ID	0.100 in.	0.100 in.	0.079 in.
Nozzle OD	0.150 in.	0.150 in.	0.120 in.
Cap ID	0.180 in.	0.170 in.	0.141 in.
Atomizing air rate (kg/hr)	Backpressure (psig)		
1.50	2.1	4.25	4.1

1.67	2.4	5.0	4.8
2.00	3.3	6.4, 6.5	6.4
2.25	4.0	7.8	7.6
2.50	4.6	9.4	8.9
2.75	5.1	10.75	10.6
3.00	6.0	12.2, 12.0	12.25
3.25	6.6	**13.6**	**14.0**
3.50	7.4	**15.1**	**15.5**
3.75	8.2	**16.7**	**17.0**
4.00	8.8	**18.0, 18.2**	**19.0**

The bolded values indicate backpressures that are greater than the ambient pressure of about 12.5 psig. The gas velocity through the nozzle, when the downstream (ambient) pressure is less than ½ of the upstream pressure, is at the sonic velocity for these conditions.

Table B-4. Dry nozzle backpressure data.

Nozzle backpressure was recorded during the nozzle atomization tests. The backpressure results are shown in Table B-5, which contains all the test conditions that are listed in Tables B-2 and B-3, but also more test conditions that did not have photographic or PSD measurements. As shown in Figures B-19 and B-20, regressions of the data are consistent with conventional knowledge that (a) the gas flow rate is proportional to the square root of the upstream pressure (approximated by the backpressure measurement) during subsonic flow, (b) the gas flow rate is proportional to the backpressure for sonic flow, (c) the condition where sonic flow is reached is where the square root and linear correlations of flow rate to backpressure meet, and (d) sonic flow is reached when the backpressure is approximately twice the downstream pressure (assumed to be ambient pressure in this case).

The smaller nozzle was sensitive to the presence of slurry at the nozzle tip. Figure B-20 shows that the impact varied with the slurry mass flow rate. The backpressures were reduced compared to the dry nozzle backpressures at the same atomizing gas flow rates, when slurry was fed at 2 kg/hr. At slurry flow rates of 4 – 5 kg/hr, the backpressures significantly increased compared to the dry nozzle backpressures. The data, including the particle size distributions, suggest that two differing regimes exist in the operation of the smaller Marshall-Eldredge nozzle, as can be seen by the data regressions. For the smaller nozzle, some data sets near 12-13 psig were used for regressing the subsonic and the sonic curves so that the two would intersect. For both nozzles, the subsonic flow rate was proportional to the square root of the backpressure, as expected for subsonic flow.

Table B-5. Nozzle backpressure during the nozzle atomization tests.

Test	Clay Concentration g/L	Slurry Rate kg/hr	NAR	Air Flow rate kg/hr	Backpressure psig
1.a	217	2.0	960	1.67	4.8
1.b	217	2.0	1150	2.00	6.2
1.c	217	2.0	1340	2.33	8.3

1.d	217	2.0	1530	2.66	10.4
1.e	217	2.0	1725	3.00	12.5
1.f	217	2.0	1915	3.33	14.4
2.a	217	3.0	765	2.00	6.2
2.b	217	3.0	890	2.33	7.9
2.c	217	3.0	1025	2.67	9.9
2.d	217	3.0	1150	3.00	12.4
2.e	217	3.0	1270	3.33	14.4
3.a	217	4.0	666	2.32	7.7
3.b	217	4.0	768	2.68	9.75
3.c	217	4.0	865	3.00	12.5
3.d	217	4.0	955	3.33	14.25
3.e	217	4.0	1050	3.66	16
3.f	217	5.0	840	3.66	16
4.a	217	2.0	960	1.67	4.75
4.b	217	2.0	1160	2.00	6.8
4.c	217	2.0	1340	2.33	8.2
4.d	217	2.0	1530	2.66	9.2
4.e	217	2.0	1725	3.00	11.5
4.f	217	2.0	1915	3.33	13.2
5.a	217	3.0	765	2.00	6.2
5.b	217	3.0	890	2.33	8.4
5.c	217	3.0	1025	2.67	10.2
5.d	217	3.0	1150	3.00	12.1
5.e	217	3.0	1270	3.33	14.1
5.f	217	3.0	640	1.67	4.8
6.a	217	4.0	666	2.32	8.3
6.b	217	4.0	768	2.67	11.6
6.c	217	4.0	865	3.00	13.75
6.d	217	4.0	955	3.32	15.5
6.e	217	4.0	1050	3.66	17
6.f	217	4.0	575	2.00	7.8
6.g	217	4.0	480	1.67	6.4
6.h	217	4.0	288	1.00	4.4
6.i	217	5.0	840	3.66	15.7
7.a	217	5.0	765	3.32	14.8
7.b	217	5.0	690	3.00	13.1
7.c	217	5.0	615	2.67	11.4

7.d	217	5.0	537	2.33	9.6
7.e	217	5.0	460	2.00	8.1
7.f	217	5.0	385	1.67	-
7.g	217	5.0	305	1.33	5.4
8.a	250	4.0	575	2.00	8
8.b	250	4.0	670	2.33	10
8.c	250	4.0	768	2.67	11.5
8.d	250	4.0	865	3.00	13.4
8.e	250	4.0	956	3.33	15.2
8.f	250	4.0	1060	3.67	17

Figure B-19. Large nozzle backpressure during the spray tests.

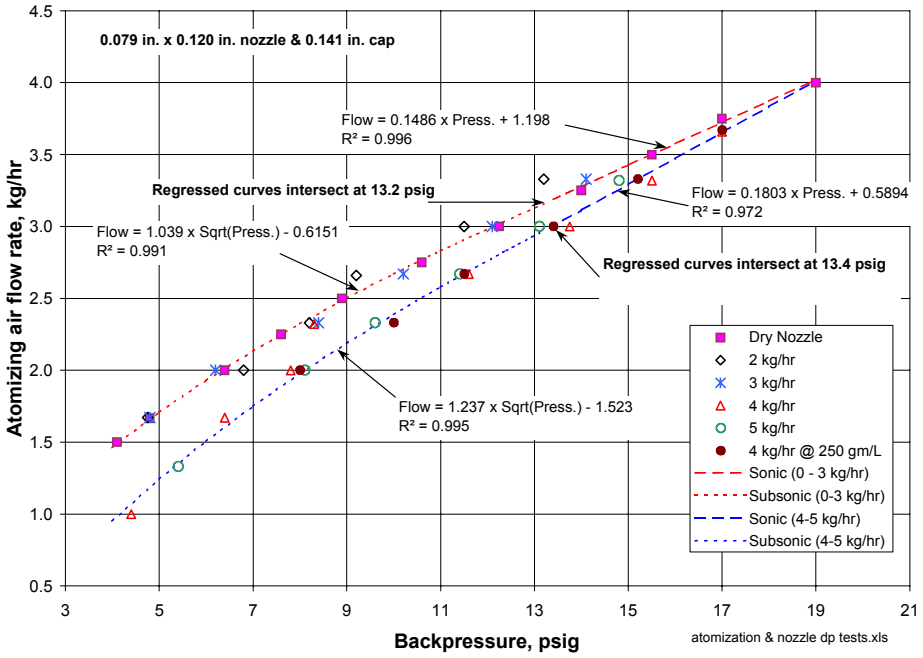

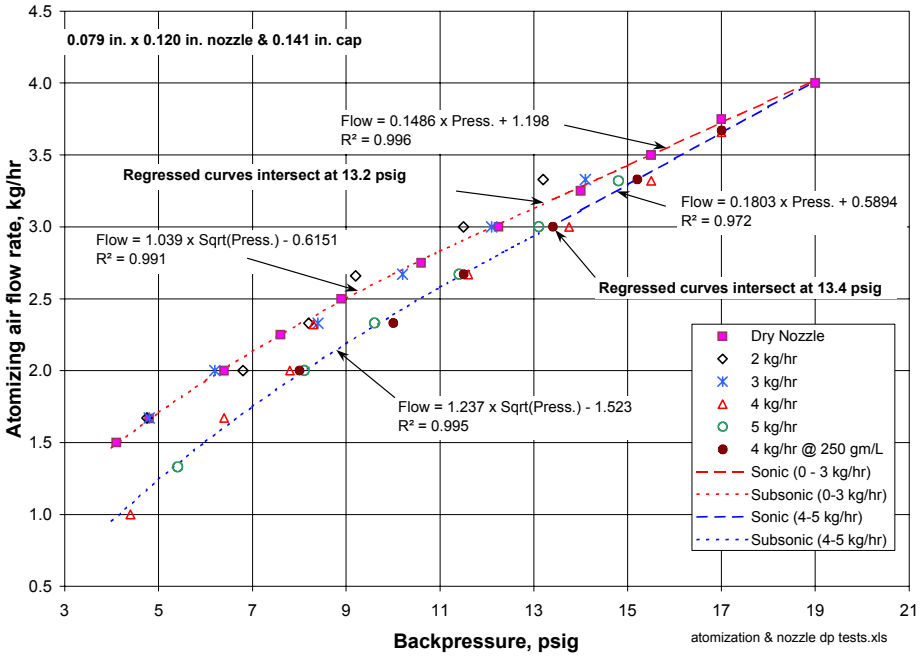

Figure B-20. Small nozzle backpressure during the spray tests.

Slurry Viscosity Measurements

Viscosity measurements were made using a Brookfield Model LVDV-1+ viscometer. This viscometer measures viscosity at different shear rates by measuring the torque on a rotating spindle immersed in the sample fluid. Different spindles were used to provide viscosity results at spindle torques within 10-100% of the instrument full-scale torque (674 dyne-cm), for a range of spindle revolutions per minute (between 0.3-100 rpm) allowed by the instrument. The best spindles for the Hanford simulant slurries had a disk that rotated in the sample fluid. The use of a disk spindle rather than a cylindrical spindle prevented calculations that relate the measured viscosity (in centipoise, cp) to a specific shear rate (in seconds^{-1}).

Viscosity measurements prior to the FBSR test were made using a lite version of the SBW simulant. The lite simulant was prepared using the exact proportions of the major chemical constituents of these simulants, leaving out minor (especially hazardous) constituents such as lead, nickel, and mercury. These minor constituents were not expected to significantly affect the simulant viscosity. The lite surrogates were blended with various concentrations of clay that were anticipated to provide a range of viscosity results that would bracket the clay selection and concentration for the FBSR test. The viscosity of a sample of the actual SBW simulant and clay slurry used in the FBSR test was subsequently measured for comparison to the pretest measurements.

Figure B-21 shows results of the SBW simulant slurry viscosity measurements done prior to the September SBW FBSR test. As expected, these slurries were much more viscous than water (which has a nominal viscosity of 1 cp), the SBW simulant, and the SBW lite simulants without clay. The viscosities of water and the SBW simulants (without clay) were too low for accurate measurement using the test apparatus, but the measurements showed that the viscosities of the SBW and SBW lite simulants were within about a factor of 2 of water viscosity under the tested conditions.

The SBW lite – Sagger clay slurry viscosities ranged between 20 – 6,000 cp. The slurries of SBW simulant and SBW lite simulant mixed with Troy clay were less viscous at similar shear rates, even when the Troy clay concentration was higher. Slurries with higher concentrations of the same kind of clay exhibited higher viscosities at the same shear rate.

The slurries were shear-thinning at all conditions but the very lowest shear rates and higher clay concentrations. This finding, in combination with results of the nozzle atomization tests, provided confidence prior to the FBSR test that the feed slurry would not cause feed atomization problems because of high viscosities, since shear rates during slurry atomization are known to be very high [Alderman, N. J. and N. I. Heywood, "Improving Slurry Viscosity and Flow Curve Measurements," Chemical Engineering Progress, April 2004]. The range of shear rates during pumping, mixing, and stirring processes is typically 10 – 1,000 s^{-1}, while shear rates during spraying and atomization typically range between 10^5 – 10^6 s^{-1}. Shear rates in the slurry sample during the viscosity tests were not greater than 10 – 1,000 s^{-1}, considering the degree of fluid agitation during the viscosity tests compared to typical fluid agitation during pumping, mixing, and stirring processes.

Figure B-21. Measured viscosities for SBW simulant slurries.

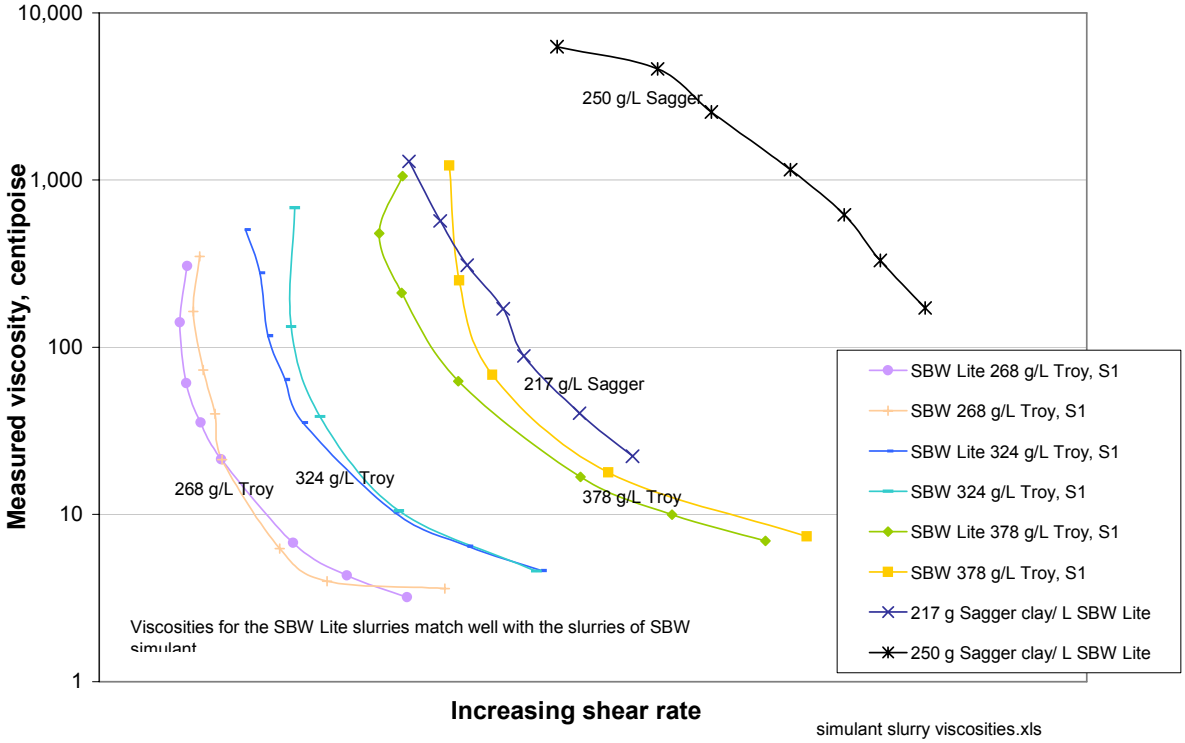
10,000
1,000
100
10
1
Measured viscosity, centipoise
250 g/L Sagger
217 g/L Sagger
378 g/L Troy
324 g/L Troy
268 g/L Troy
Viscosities for the SBW Lite slurries match well with the slurries of SBW simulant
SBW Lite 268 g/L Troy, S1
SBW 268 g/L Troy, S1
SBW Lite 324 g/L Troy, S1
SBW 324 g/L Troy, S1
SBW Lite 378 g/L Troy, S1
SBW 378 g/L Troy, S1
217 g Sagger clay/ L SBW Lite
250 g Sagger clay/ L SBW Lite
Increasing shear rate
simulant slurry viscosities.xls

Appendix C

Carbon Reductant Selection

Nicholas R. Soelberg

Appendix C

CARBON REDUCTANT SELECTION

An evaluation of different potential carbon reductants was performed during the third quarter of FY2004, to select the carbon reductant(s) to be used in the fluidized bed steam reforming tests. Several different candidate carbons were evaluated. This evaluation was performed using the results of laboratory analyses performed at Savannah River National Laboratory[1,2], and results of the evaluation are summarized below.

Carbon Reductant Ranking Criteria

The candidate carbons were evaluated and ranked according to the following criteria:

- *Mass loss during a thermal gravimetric analysis (TGA) oxidation stage*: The higher the mass loss, the more reductant is available per mass of additive. The difference between this mass loss and 100% is the total moisture and ash, both undesired in the carbon additive. The moisture or ash content alone were not considered separate ranking criteria, since they are included in this criterion. The high moisture content of the BS-NB carbon (C1) causes a low ranking for this carbon for this criterion.

- *Temperature at start of oxidation during TGA*: This criterion indicates initial carbon reactivity.

- *Slope of mass loss during oxidation*: This criterion indicates how rapidly the oxidation can occur. Since the temperature at the end of oxidation is included in the slope calculation, it is not listed as a separate criterion.

- *Carbon particle size distribution*: Larger particles are desirable, as long as they can (a) be fed in the carbon reductant feed system, and (b) stay fluidized or "floated" on the smaller bed particles, because more mass will be utilized in the bed before the size is so small that it passes on through the cyclone. Large amounts of fines are undesirable, because these would tend to be elutriated out of the fluidized bed before the particles have had sufficient residence time for efficient reaction completeness.

Other criteria were considered but not included in this analysis:

- *Particle toughness*: Hardness of particles could be good (indicating toughness) or bad (indicating brittleness). Tests considered were Ball-Pan hardness (ASTM D 3802) and the Hardgrove Grindability Index test (ASTM D-409).

- *Particle density*: A lower particle density indicates easier fluidization of the typically larger particles. This is desirable because it minimizes the amount of the carbon particles removed with bed product.

- *Specific surface area/porosity*: More surface area is desirable, and is probably related to the slope of mass loss during TGA oxidation.

Particle toughness was excluded from the analysis due to lack of readily available data, even though particle toughness (resistance to attrition in the fluidized bed) was desired. Particle density could

have been readily available through simple laboratory analysis, but was discarded as a criterion because it was not considered to be a very significant discriminator. Specific surface area/porosity was excluded as a separate criterion because (a) additional laboratory analyses would have been necessary to provide these data, and (b) the slope of mass loss during oxidation, which was included in the evaluation, was considered to be an adequate, representative surrogate for this criterion.

Carbon Thermal Gravimetric Analysis

Results of TGA analyses performed by SRNL are tabulated in Table C-1. Data for several key criteria related to carbon reactivity are provided by the TGA results. Tabulated data taken from the TGA charts include (a) the mass loss at temperatures up to about 100 ^{o}C, due largely to sorbed H_2O and possibly other more volatile sorbed species, (b) mass loss during the oxidation stage at temperatures ranging from about 250-850^{o}C, (c) the total mass loss (100% minus the total mass loss indicates the residual ash content), (d) the starting and ending temperatures for the oxidation stage, and (e) the slope of mass loss during oxidation. All of this data was from TGAs performed in an air atmosphere. Since the FBSR design uses steam as the fluidizing gas and the FSBR is operated in an O_2-deficient atmosphere, the air-TGA results may not entirely represent FBSR conditions. TGAs performed in a steam atmosphere may have better represented the carbon reactivities and performance in an FBSR environment. Efforts to modify the commercially available TGA equipment to operate in a steam atmosphere were not successful within available time and cost constraints, and so was not performed.

The moisture loss ranged below 10 wt%, consistent with vendor product data, except for the BS-NB sample, which had almost 20 wt% moisture loss. Perhaps this amount of moisture loss was from a non-representative sample. Mass loss during oxidation ranged above 90% for the wood-based carbons (except for the BS-NB sample, affected by the high moisture loss). The coke and anthracite-based carbons exhibited lower mass loss, indicating less useable reactive mass for denitrating the FBSR feeds. The wood-based carbons also exhibited lower temperatures at which oxidation mass loss started, lower oxidation end temperatures, and faster oxidation rates as indicated by the slope of the mass loss during oxidation.

Carbon Particle Size Distribution

Carbon particle size distribution data from the sieve tray measurements at SRNL are shown in Figures C-1 and C-2. The original data was converted to particle size distribution in terms of cumulative wt% less than each size cut, a graph of typically Gaussian differential particle distributions, and a single mass mean diameter (MMD) for each carbon. Three of the carbons (C5, C6, and C3) had significant mass fractions greater than the largest screen (4 mesh, 4.75 mm) used in the sieve analyses, so the actual MMD for these carbons is subject to some error. The sieve analyses for these carbons only captures the smaller half of the typical Gaussian particle size distributions.

The MMD calculation required that the average particle size of the >4 mesh mass be estimated. A maximum particle size for any carbon of 10 mm, and an average particle size of the >4 mesh mass of 7.4 mm was assumed. Even if appreciable error is introduced by the >4 mesh assumptions, the relative ranking of carbons is not changed, so further particle size analyses of the C5, C6, and C3 carbons was not warranted.

Table C-1. Results of carbon reductant TGA analyses in an air atmosphere.

Sample	ID	Type/size	Manufacturer	TGA mass loss, wt% (air atmosphere)			TGA t
				25 < T < 200 to 500 C (attributed to mainly sorbed H2O, etc)	During oxidation stage, between 250-500 C and 430-700C	Total (100-ash)	T at star of oxida tion, C
C1	BS-NB	Wood base, 4x12 mesh	Barneby-Sutcliffe, Columbus, OH	19.7	76.8	96.5	350
C2	GC-CBM	Coal base, low density, 6x12 mesh	General Carbon, Paterson, NJ	3	94.6	97.6	480
C3	BS-WBC	Wood base, ~minus 0.5 inch	Barneby-Sutcliffe	3.6	94.9	98.5	250
C4	GC-CRB	Wood base, 4x6 mesh	General Carbon	4.7	91.8	96.5	470
C5	BB-NWC	Wood base, ~minus 0.7 inch	Berger Brothers, Chicago, IL	2.1	94.5	97.7	300
C6	MC-DRC	Coke, "dry rice size"	Mid-Continent Coal and Coke, Clairton, PA	0.82	86.7	87.5	460
C7	AI-776	Anthracite coal, ~minus 0.2 inch	Anthracite Industries, Sunbury, PA	5.1	88.2	93.3	530
C8	BS-AD	Wood base, 4x8 mesh	Barneby-Sutcliffe	6.9	91.2	98.1	400
C9	BS-VS	Anthracite coal, ~minus 0.4 inch	Barneby-Sutcliffe	4.5	77.9	82.4	530

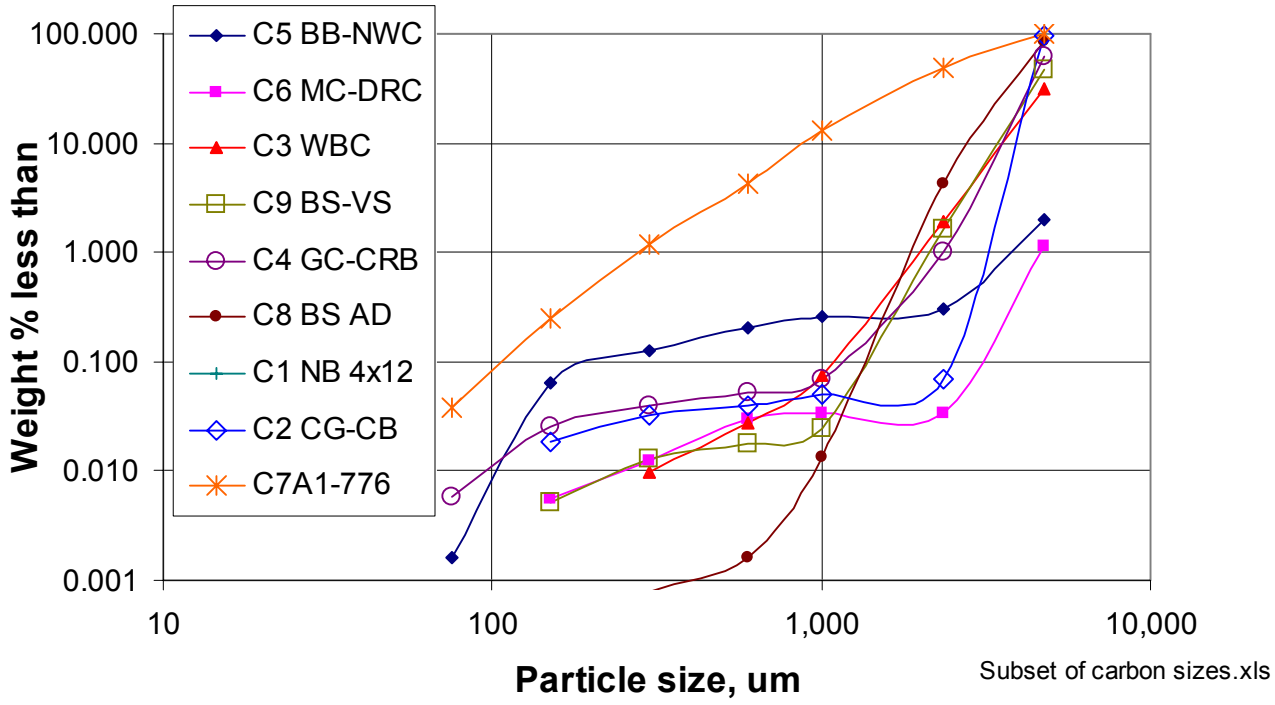

Figure C-1. Cumulative carbon reductant particle size distributions.

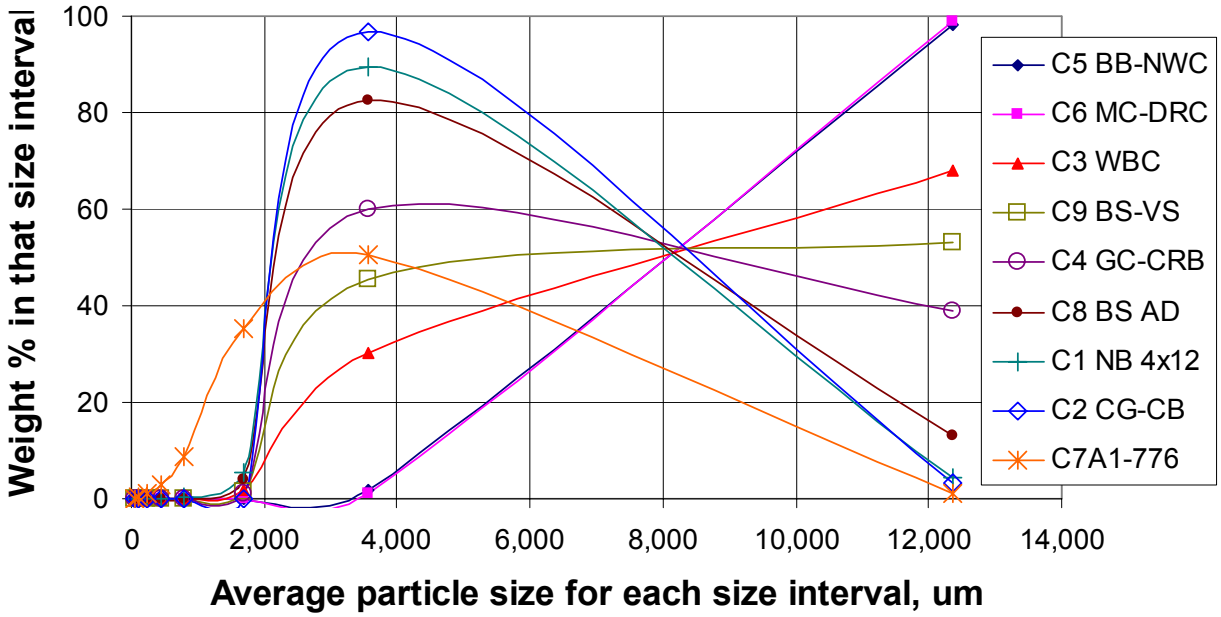

Figure C-2. Differential carbon reductant particle size distributions.

The MMDs for the 9 carbons ranged between 1.7 mm to 7.2 mm. How particle size impacts the performance of a carbon additive in a fluidized bed steam reformer (FSBR) is not entirely clear, but for this evaluation, independent of other criteria (such as specific surface area, ability to feed, and ability to fluidize), the larger particle size was considered desirable. More of the mass of larger particles would tend to stay in the bed and be reacted before the particle attrits or is reacted to a size small enough to be elutriated from the bed and cyclone. However, it is not desirable that the carbon particles are so large that (a) they cannot be fed through the carbon reductant feed system, or (b) they are so large that they cannot remain fluidized and are appreciably removed from the bed during sampling or harvesting of product.

Even particles significantly larger than the size that would be fluidized by the fluidizing gas tend to be buoyed up by, or float on, the mass of fluidized particles. Visual observations in the room-temperature 6-inch fluidized bed model at the SAIC STAR Center indicate that many of the carbon particles in the 2-4 mm size range tend to float near the top of the fluidized portion of alumina bed particles.

The carbon particle density and shape, in combination with the particle size, indicates the ability to be appropriately fluidized. However, these data were not readily available and were excluded from this analysis. Perhaps the ideal carbon would have a relatively large particle size, able to provide more of its mass in steam reforming reactions before the particle elutriates from the bed, an irregular shape, and a lower particle density, allowing the particle to be more easily fluidized in the bed and not drained from the bed.

Carbon Reductant Rankings And Selection

Results of this evaluation are summarized in Table C-2. The lowest numerical total ranking indicates the best carbons based on the criteria. All of the ranking criteria were equally weighted.

The top two carbons stand out from the rest based on their numerical rankings.

1. C5 BB-NWC Wood base, ~minus 0.7" Berger Brothers, Chicago, Illinois (Score of 8)

2. C3 BS-WBC Wood base, ~minus 0.5" Barneby-Sutcliffe. (Score of 9, almost same as C5)

The C5 carbon was selected for the FBSR tests, because it ranked highest and was available at a significantly lower cost. The C5 carbon (also referred to as “P3” carbon by Berger Brothers) was procured and tested in the reductant feeder, and found to restrict the feeder. A smaller particle-size range C5-type carbon (referred to as “P6”) was procured for feeder testing. This carbon could be reliably fed

and so was procured for FBSR testing.

There were several carbons in the next tier, although their scores were all similar:

3. C8	BS-AD	Wood base, 4x8	Barneby-Sutcliffe. (Score of 17)
4. C6	MC-DRC	Coke, "dry rice size"	Mid-Cont. Coal and Coke, Clairton, PA. (Score 19)
5. C4	GC-CRB	Wood base, 4x6	General Carbon. (Score of 20)
6. C2	GC-CBM	Coal base, low density, 6x12	General Carbon, Paterson, NJ. (Score of 22)
7. C1	BS-NB	Wood base, 4x12	Barneby-Sutcliffe, Columbus, OH. (Score of 23)

The BS-NB carbon, ranked 7th, was the carbon most highly recommended by THOR^{SM} Treatment Technologies for prior tests. Four other wood-based carbons, one coke-based carbon, and one coal-based carbon may perform as well as the BS-NB carbon according to this ranking. The BS-NB carbon was ranked lower because of the unexpectedly high moisture content. Another moisture analysis performed on the BS-NB carbon might confirm if the high moisture content indicated by the first analysis was correct.

The C6 coke-based carbon was included in the second-tier group because it ranked first (largest) for particle size, although it did not rank high in other criteria. The C2 coal-based carbon was included in the second-tier group because it had a high mass loss during TGA oxidation, although it did not rank high in other criteria. All the other high-ranked and medium-ranked carbons are wood-based. Based on the TGA analyses, wood-based carbons seem to be more reactive than the coke and coal-based carbons, confirming TTT's recommendations that the wood-based carbons are more reactive.

The two anthracite-based carbons ranked lowest, mainly because they were less reactive than the other carbons based on the TGA analyses.

The rankings could change if data were included for the particle toughness, particle density, ash composition, and steam TGA criteria.

Table C-2. Numerical rankings of carbon reductants.

Sample	ID	Type/size	Manufacturer	Mass loss during TGA oxidation stage, between 250-500°C and 430-700°C	Temp. at start of oxidation, °C	Slope of oxidation step, %mass loss/°C	Particle size, MMD, mm	Totals	Overall Rank
C1	BS-NB	Wood base, 4x12 mesh	Barneby-Sutcliffe, Columbus, OH	9	3	3	8	23	7
C2	GC-CBM	Coal base, low density, 6x12 mesh	General Carbon, Paterson, NJ	2	7	7	6	22	6
C3	BS-WBC	Wood base, ~minus 0.5 inch	Barneby-Sutcliffe	1	1	4	3	9	2
C4	GC-CRB	Wood base, 4x6 mesh	General Carbon	4	6	5	5	20	5
C5	BB-NWC	Wood base, ~minus 0.7 inch	Berger Brothers, Chicago, IL	3	2	1	2	8	1
C6	MC-DRC	Coke, "dry rice size"	Mid-Continent Coal and Coke, Clairton, PA	7	5	6	1	19	4
C7	AI-776	Anthracite coal, ~minus 0.2 inch	Anthracite Industries, Sunbury, PA	6	8	8	9	31	9
C8	BS-AD	Wood base, 4x8 mesh	Barneby-Sutcliffe	5	4	2	6	17	3
C9	BS-VS	Anthracite coal, ~minus 0.4 inch	Barneby-Sutcliffe	8	8	9	4	29	8

[carbon tga results.xls]ranking

[1] Jantzen, C. M., 2004, J. C. Marra, and J. M. Pareizs, *Analysis of Raw Materials for Fluidized Bed Steam Reforming (FBSR),* SRNL-ITB-2004-0004, June 30.

[2] Marra, Jim, "Carbon Source Data," personnal communication to A. L. Olson, March 16, 2004.